The mode of action of the HIV protease inhibitor lopinavir against HPV

A thesis submitted to the University of Manchester for the degree of Doctor of Philosophy in the Faculty of Medical and Human Sciences

2011

Gavin Batman

School of Medicine

Contents Page

Figure List

Tables

Word Count (excluding appendices) – 61,152

Abstract

The University of Manchester
Gavin Batman, February 2011
Degree of Doctor of Philosophy in the Faculty of Medical and Human Sciences

The Mode of Action of the HIV protease inhibitor against HPV

Human papillomavirus (HPV) related cervical cancer is still the most common gynaecological malignancy in developing countries and, as yet, there is no alternative to surgery for the treatment of HPV-associated pre-malignant lesions. HPV 'hijack's' the host-cell ubiquitin-proteasome system to degrade the p53 and Rb tumour suppressor proteins which in turn, leads to the development of cancer. Previous studies have shown that the HIV protease inhibitor lopinavir selectively inhibits the chymotryptic-like activity of the 26S proteasome which stabilises p53 and induces the apoptosis of HPV positive cervical carcinoma cells. Based on this it was hypothesised that lopinavir treatment of HPV positive cervical carcinoma cells would produce changes in the levels of a wide range of cellular proteins that are dis-regulated by HPV-related activation of the proteasome. In order to address this, antibody microarray screening was carried out on lopinavir treated and control untreated HPV positive SiHa cervical carcinoma cells. This showed lopinavir induced alterations in 51 proteins including the cellular antiviral defence protein RNase L. Lopinavir induced both a dose and time dependent increase in RNase L which was subsequently confirmed by western blotting. Transient siRNA silencing of RNase L expression reduced the lopinavir-dependent toxicity in SiHa cells, suggesting an important role for this protein in the toxicity of lopinavir in HPV infected cells. SiHa cells were much more sensitive to lopinavir than CaSKi cervical carcinoma cells which had much higher levels of the E6 protein and did not up regulate RNase L. Furthermore, lopinavir treated HPV16 E6/E7 immortalised keratinocytes were also shown to up regulate RNase L protein expression and these cells were much more sensitive to lopinavir induced apoptosis than mortal control keratinocytes. In addition, transient expression of RNase L in RNase L-deficient C33A cells and the same cells stably transfected with HPV16 E6 (C33AE6) demonstrated that E6 protected these cells from RNase L-induced cell death. Surprisingly, analysis of RNase L protein levels in these cells demonstrated that E6 did not induce the degradation of the RNase L protein. Instead it was found that E6 stabilised the interaction between RNase L and its endogenous inhibitor protein, ABCE1, and that lopinavir de-stabilised this interaction. Given that C33A tumour cells, E6/E7 immortalised keratinocytes and hTert immortalised keratinocytes are all sensitive to lopinavir, this implies that this compound does not specifically target HPV immortalised cells but rather targets immortalised cells in general, regardless of how this was achieved. The optimum concentration of lopinavir for all these effects was 25 µM, which is 15-fold higher than is observed in cervico-vaginal secretions following oral dosing with the drug Kaletra. In conclusion these results have confirmed the potential of lopinavir to treat HPV related pre-cancerous cervical lesions and provided at least part of the mode-of-action. Indeed they strongly support the use of lopinavir as a low-cost, self-applied topical alternative to surgery for this disease which will be of particular benefit in low-resource countries. Finally, the ability of lopinavir to induce apoptosis of non-HPV related immortalised cells merits further investigation since this indicates this drug may be useful for the treatment of other non HPV related pre-malignant conditions.

Declaration

No portion of this work has been submitted in support of an application for another degree or qualification of this or any other university or other institute of learning.

Copyright Statement

i. The author of this thesis (including any appendices and/or schedules to this thesis) owns certain copyright or related rights in it (the "Copyright") and s/he has given The University of Manchester certain rights to use such Copyright, including for administrative purposes.

ii. Copies of this thesis, either in full or in extracts and whether in hard or electronic copy, may be made **only** in accordance with the Copyright, Designs and Patents Act 1988 (as amended) and regulations issued under it or, where appropriate, in accordance with licensing agreements which the University has from time to time. This page must form part of any such copies made.

iii. The ownership of certain Copyright, patents, designs, trade marks and other intellectual property (the "Intellectual Property") and any reproductions of copyright works in the thesis, for example graphs and tables ("Reproductions"), which may be described in this thesis, may not be owned by the author and may be owned by third parties. Such Intellectual Property and Reproductions cannot and must not be made available for use without the prior written permission of the owner(s) of the relevant Intellectual Property and/or Reproductions.

iv. Further information on the conditions under which disclosure, publication and commercialisation of this thesis, the Copyright and any Intellectual Property and/or Reproductions described in it may take place is available in the University IP Policy (see http://www.campus.manchester.ac.uk/medialibrary/policies/intellectual-property.pdf), in any relevant Thesis restriction declarations deposited in the University Library, The University Library's regulations (see http://www.manchester.ac.uk/library/aboutus/regulations) and in The University's policy on presentation of Theses

Acknowledgements

I would firstly like to thank my supervisors, Dr Ian Hampson and Dr Lynne Hampson, for all their guidance, expertise and support they have given me throughout my PhD. I would also like to thank Professor Henry Kitchener and Professor Nalin Thakkar for their support and advice.

This project was funded by the Humane Research Trust, and I would like to acknowledge this support.

I would also like to thank all the lab members, past and present, in particular, Dr Anthony Oliver and Dr Xiaotong He for all their technical guidance and support.

I would like to give special thanks to my parents and my sisters for all their support, both financial and moral!

Finally I would like to say thank you to Lucy for her unending support, and for always making me smile, and to all my friends for keeping me sane!

Abbreviations

2-5A	2'-5' oligoadenylates
ab	Antibody
AIDS	Acquired Immuno-Deficiency Syndrome
BSA	Bovine serum albumin
CaSKi	HPV positive cell line
C33A	HPV negative cervical cancer cell line
cDNA	complementary deoxyribonucleic acid
CIN	cervical intraepithelial neoplasia
DDT	dithiothreitol
DMSO	dimethylsulphoxide
dNTP	deoxyribonucleotide triphosphate
dsDNA	double stranded deoxyribonucleic acid
dsRNA	double stranded ribonucleic acid
ECL	enhanced chemiluminescence
EDTA	ethylenediamenetetraacetic acid
FBS	foetal bovine serum
FRET	fluorescence resonance energy transfer
GAPDH	Glyceraldehyde- 3-phosphate dehydrogenase
GFP	Green fluorescent protein.
HAART	highly active antiretroviral therapy
HCV	Hepatitis C virus
HHV-8	Human Herpes Virus 8
HIV	Human Immunodeficiency Virus
HPV	Human Papillomavirus
HTLV	Human T-cell Leukaemia virus type 1
IFN	Interferon
Kb	kilo base pairs
kDa	kilo Daltons
LBC	Liquid Based Cytology screening
LCR	long coding region
MG-132	A synthetic proteasome inhibitor
MODC	mouse ornithine decarboxylase
mRNA	messenger ribonucleic acid
nm	nanometres
OAS	Oligoadenylate synthetase
OD	optical density
ORF	open reading frame
pap	Papanicolaou staining
PI	Protease inhibitor
p53	tumour suppressor protein p53
PAGE	polyacrylamide gel electrophoresis
PBS	phosphate buffered saline
PCR	polymerase chain reaction
PFA	paraformaldehyde
Rb	retinoblastoma protein
RNA	ribonucleic acid
RNase L	ribonuclease L protein

RNASEL	Approved gene name for RNase L
RT-PCR	reverse transcription polymerase chain reaction
SCC	Squamous cell carcinoma
SDS-PAGE	sodium dodecyl sulphate polyacrylamide gel electrophoresis
SiHa	HPV positive cervical cancer cell line
siRNA	small interfering RNA
TE	Tris-EDTA
ub	ubiquitin
URR	upstream regulatory region
V	volts
X-Gal	5-bromo-4-chloro-3-indolyl-b-D-galactopyranoside

1. Cervical Cancer and the Human Papillomavirus

Globally, it is estimated that there were 529,409 new cases of cervical cancer in 2008, leading to 274,883 deaths [1] making cervical cancer the 2nd most common malignancy affecting women worldwide [2].

While the infectious nature of the common wart was identified as early as 1907 [3], the transmissible agent was not identified as human papillomavirus (HPV) until 1949 [4]. The significance of these findings were not truly appreciated until the work of Harald Zur Hausen proposed a link between persistent HPV and the development of squamous cell carcinoma of the cervix [5]. Research has now shown that infection with specific types of HPV (e.g. 16 or 18 – see section 1.1.1) is associated with over 99% of cervical carcinoma cases, unequivocally implicating HPV as a causative agent in the development of cervical cancer [6].

1.1. High-risk HPV and Cervical Carcinogenesis

1.1.1. Transmission of HPV and Associated Risk Factors

HPV is a sexually transmitted infection and as such, the transmission route of ano-genital HPV infection is primarily as a result of mucosa-to-mucosa contact through penetrative sex [7] and concurrent infections with multiple HPV types is not uncommon [8, 9]. Accordingly, the risk factors associated with HPV infection relate to an individuals' sexual practices namely; an early age of first sexual contact, a high number of sexual partners and exposure to high-risk contacts including prostitutes and promiscuous sexual partners [10].

1.1.2. Environmental Cofactors for Carcinogenic Progression

Whilst HPV DNA has been detected in up to 99% of cervical carcinomas [6], it is also known that during the ages of greatest sexual activity, the prevalence of HPV DNA in sub-clinical infections (i.e. presence of viral DNA with normal cytology) can be as high as 40% in the female population [10]. In sexually active women up to the age of 30, the annual rate of infection with HPV is estimated to be 10-15% [10]. However, it is estimated that for every 1,000,000 women infected with HPV only ~100,000 women will develop pre-cancerous changes in cervical tissues [11]. Assuming no therapeutic intervention, of these 100,000 women, approximately 8,000 (8%) will go on to develop carcinoma *in situ* [11], which is <1% of those women originally infected with the virus. This observation suggests that infection with HPV is necessary yet it is insufficient to cause cervical cancer in isolation. This has led to the identification of alternative additional co-factors that are now known to play a role in tumorigenesis such as immunosuppression, smoking and use of oral contraceptives. HIV positive individuals or patients under induced immunosuppression (e.g. renal transplant patients) demonstrate increased levels of both HPV infection and cervical cancer

(reviewed in [12] and [13-18]. The metabolic by-products of cigarette smoke have been detected in cervico-vaginal fluids, and this is thought to increase the risk of cervical cancer through a number of mechanisms - directly through mutagenic effects on cervical cells, and also by mediating a reduction in antigen presenting Langerhans cells which impairs local immunity [12]. Whilst the risks associated with the use of oral contraceptive are low, there is evidence to suggest that 16α-hydroxyestrone, a metabolite of oestrogen, is associated with DNA damage that may lead to mutations acting synergistically with HPV to bring about carcinogenesis [11].

1.1.3. Human Papillomavirus Classification and Genomic Variation

The papillomaviruses belong to a distinct taxonomic grouping, the *Papillomaviridae* [19]. Examples of papillomaviruses have been found in a wide range of mammalian and avian hosts, and they are extremely species specific [20]. Regardless of host species, the papillomaviruses have strikingly similar structures; they are small, non enveloped viruses with an icosahedral capsid of approximately 55 nm diameter which contains a dsDNA genome 8kb in size [21]. HPVs demonstrate specific tropisms for squamous epithelial cells where they induce a state of hyperproliferation at HPV type-specific anatomical sites [22].

There are over 100 known papillomaviruses which are split into numerous genera (Figure 1.1, from [19]) and further grouped by sequence similarity. Changes in HPV DNA sequences occur, as in many viruses, through point mutations, deletions and insertions. Unlike RNA viruses, the HPV genome is much more stable due to the proofreading capabilities of DNA polymerases [23]. However, selective pressures can allow chance mutations to become established in a population and in conjunction with the process of genetic drift, allow variants, types and subtypes to evolve [23].

The classification of HPV types depends on the L1 open reading frame (ORF) of the HPV genome (L1 is discussed in Section 1.2.1.2). The L1 ORF which codes for the major capsid protein is highly conserved between HPV types, and as such, nucleotide sequence analysis of L1 is a suitable marker by which new HPV types are defined. A new HPV type is defined as having DNA sequence for the L1 ORF that differs by >10% when compared to its closest match. A subtype is defined by an L1 ORF difference of between 2% and 10%, and an HPV variant is defined by an L1 ORF difference of less than 1%, when compared to its closest match [19].

Figure 1.1 - Phylogenetic Classifications of Papillomaviruses.

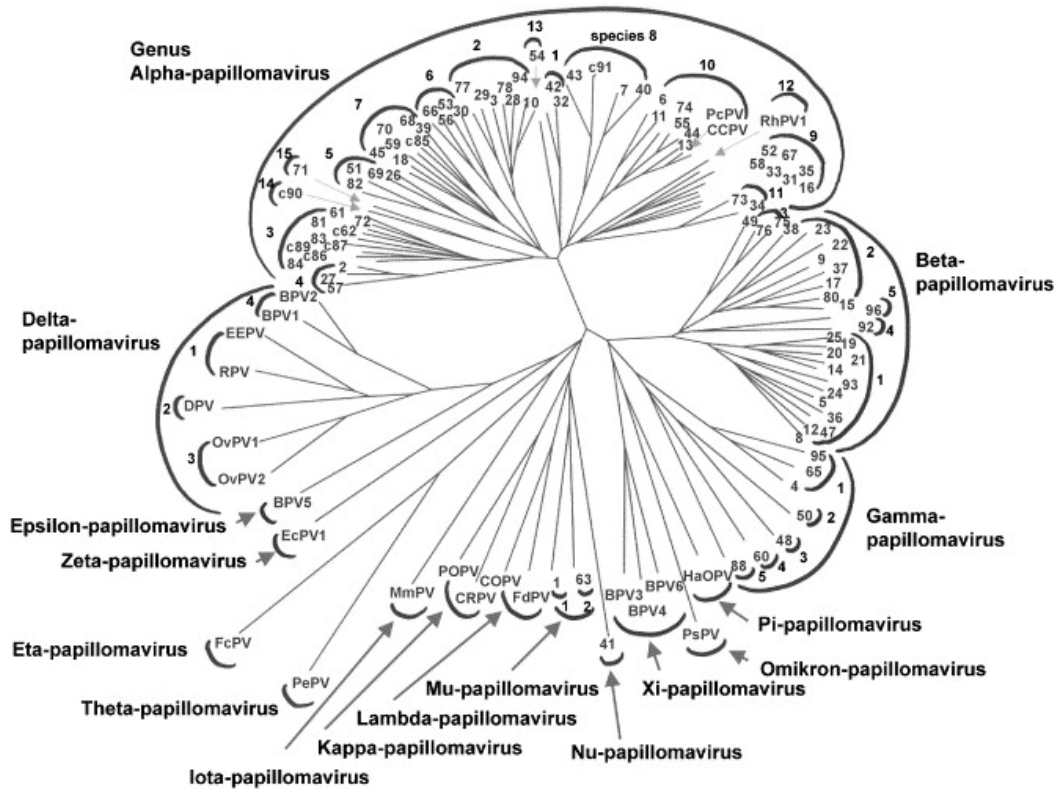

Figure 1.1 - Phylogenetic classifications of known human papillomaviruses (HPVs). HPVs are split into 5 evolutionary genus groups, alpha, beta, gamma, mu and nu and further grouped into separate species within each genus. The alpha and beta subgroups encompass 90% of the known HPV types that are implicated in cervical infection, including the high-risk types HPV16 and HPV18. Figure from [19].

The known HPVs can be broadly split into two groups based on their specific tropisms [10]:

- **Cutaneotropic types** (e.g. HPV 1, 2, 3, 8, 41, 48, 60, 63 and 65) frequently isolated from plantar warts, in cutaneous lesions of patients with verruciform epidermodysplasia and common skin warts.
- **Mucosotropic types** (e.g. 6, 11, 16, 18, 26, 30, 31, 32, 33, 34, 35, 39, 42, 44, 45, 51, 52, 53, 54, 55, 56, 58, 59, 64, 66, 67, 68, 69, 70, 73) are associated with both benign and malignant infections of the anogenital tract of both sexes .

HPV types can be further sub-classified as being either high-risk (HR) or low-risk (LR) based on their propensity to induce malignant transformation in infected cells. The HPV α-genus contains many mucosotropic HPV types of clinical importance including several low-risk types associated with benign common skin warts (e.g. HPV-2) [23]. However, of more clinical importance, the α-genus also contains 15 HPV types associated with cervical neoplasms termed

high-risk types (e.g. types 16 and 18). There are also three potential high-risk types and 12 low-risk HPV types which are rarely associated with malignant progression [24]. Along with cervical neoplasia, the high-risk types are also associated with vulval, vaginal, penile, anal and oropharyngeal neoplasias [24].

Phylogenetic analysis of the known HPV variants demonstrates that these tend to cluster within specific geographical regions and within specific ethnic groups (reviewed in [23]). Due to its association with malignant progression, intratypic sequence heterogeneity within the high-risk HPV type 16 has been most extensively studied [23]. To date, 5 distinct Phylogenetic branches of HPV-16 have been identified; European (E), which contains the prototype HPV-16 type, Asian (As), Asian American (AA), and two African variants (Af-1/Af-2). The most studied variants are the Asian-American (AA), the L83V and the European variant (E). The AA variant is predominantly found in North and South America and studies have shown that HPV type 16 (AA) is detected in almost a quarter of cervical cancers diagnosed in Mexico. When compared to HPV type 16 infection with a European (E) variant, epidemiological evidence suggests that the AA variant possesses an increased oncogenic capability. Secondary to this, when compared to the E variant, infection with the AA variant is associated with an increased risk of progression to cervical cancer, and is found in younger women, who present with a more aggressive carcinoma [25, 26].

The L83V variant falls within the larger European variant group and a nucleotide substitution at position 350 (350G) produces a leucine to valine amino acid change. The presence of HPV type 16 is associated with viral genome integration and disease progression and it has also been demonstrated that further to this, when compared to the prototype HPV type 16, infection with the L83V variant increases the risk of viral persistence and disease progression [27].

1.1.4. Site of Infection

The cervical canal is lined with two cell types: squamous cells and columnar cells. Squamous cell carcinomas (SCC) develop at sites of active squamous metaplasia, which occur at the boundary between these two cell types [28]. This is labelled the cervical transformation zone (Figure 1.2) and is a region of active squamous metaplasia wherein the squamous cells of the ectocervix gradually envelop and replace the columnar cells of the endocervix. This makes the region particularly susceptible to HPV-related malignancy.

Figure 1.2 – The cervical transformation zone

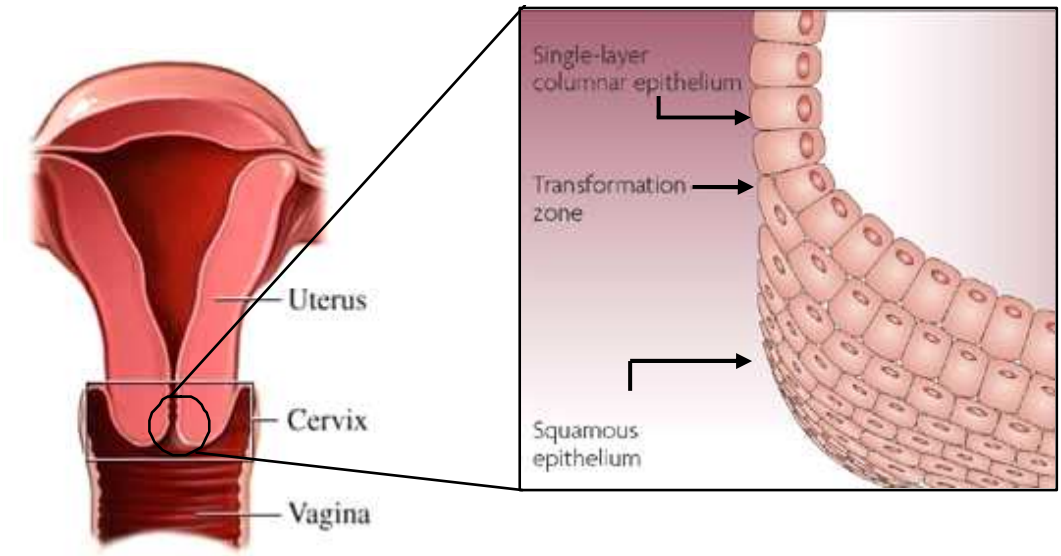

Figure 1.2 – The cellular boundary between the columnar cells of the endocervix and the squamous cells of the ectocervix form the cervical transformation zone. The transformation zone is the location from which cervical cancer is thought to develop.

1.1.5. HPV and malignant progression

HPV infection leads to a deregulation of the normal cell cycle control, leading to uncontrolled cellular proliferation. The process from initial HPV infection through to cervical carcinoma follows a clearly defined path consisting of 4 distinct stages; HPV infection, viral persistence, progression of a clone of persistently infected cells towards precancerous lesions, and invasion leading to malignancy [28]. Cervical squamous cell carcinomas originate from non-invasive, premalignant precursor lesions termed Cervical Intraepithelial Neoplasia (CIN) [29]. There are varying degrees of CIN, labelled I, II and III, which correlate with the degree of atypia observed – CIN I refers to mild dysplasia, CIN II to moderate dysplasia whilst CIN III refers to severe dysplasia leading to carcinoma *in situ*. The progressive development of CIN and the development of cervical cancer along with the associated cellular atypia are depicted in Figure 1.3. This shows the cytology, assessed by Papanicolaou (Pap) staining (top row), and also lesions as viewed by colposcopy (bottom row).

Figure 1.3 – PAP staining and colposcopy imaging of cervical cancer progression

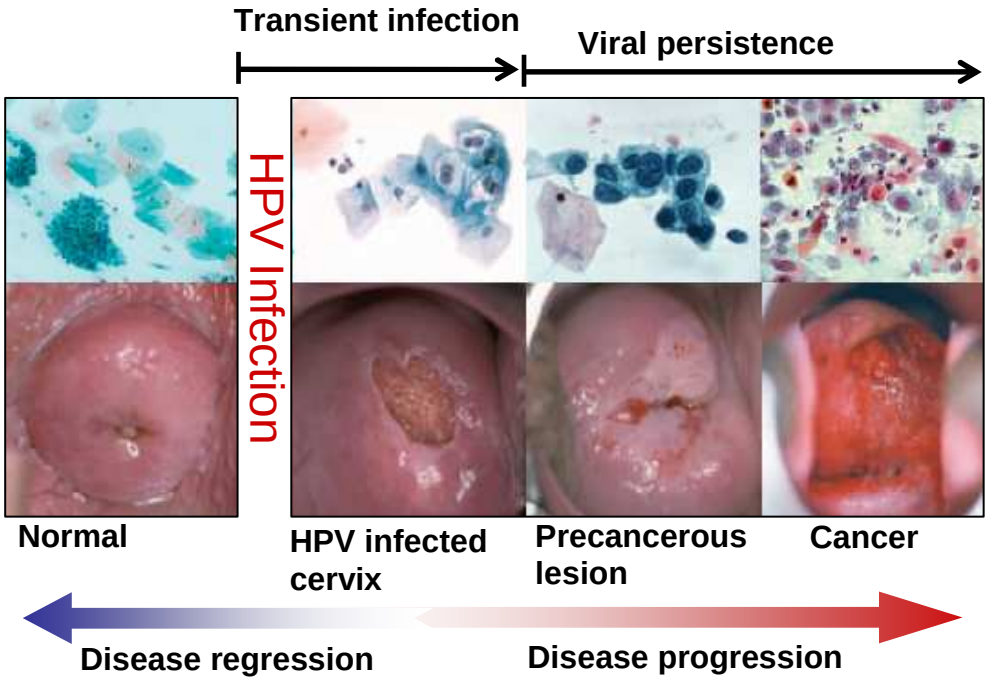

Figure 1.3 - The progressive development of cervical cancer and the associated cellular atypia is depicted, shown both in terms of cytology by PAP staining (top row) and also colposcopy (bottom row). Diagram adapted from [28].

1.2. Cervical HPV infection and the molecular basis of carcinogenesis

1.2.1. HPV Genome

The HPV genome is split into eight open reading frames (ORF) that are transcribed as one polycistronic message from a single strand of the dsDNA genome (as reviewed in [20, 30]). Figure 1.4, (adapted from [31]) is a schematic representation of the circular dsDNA genome of HPV 16, which is representative of the known HPVs. The genome can be split into three sections; the early region (E), which is approximately 4kb in size and codes for the non structural E1-E7 proteins, the late region (L) which is approximately 3kb and codes for the viral capsid proteins L1 and L2, the major and minor capsid proteins respectively, and finally the non-coding long control region (LCR). The latter is approximately 1kb, and contains *cis* elements that govern viral replication and gene expression.

Figure 1.4 – Schematic diagram of HPV type-16 genome

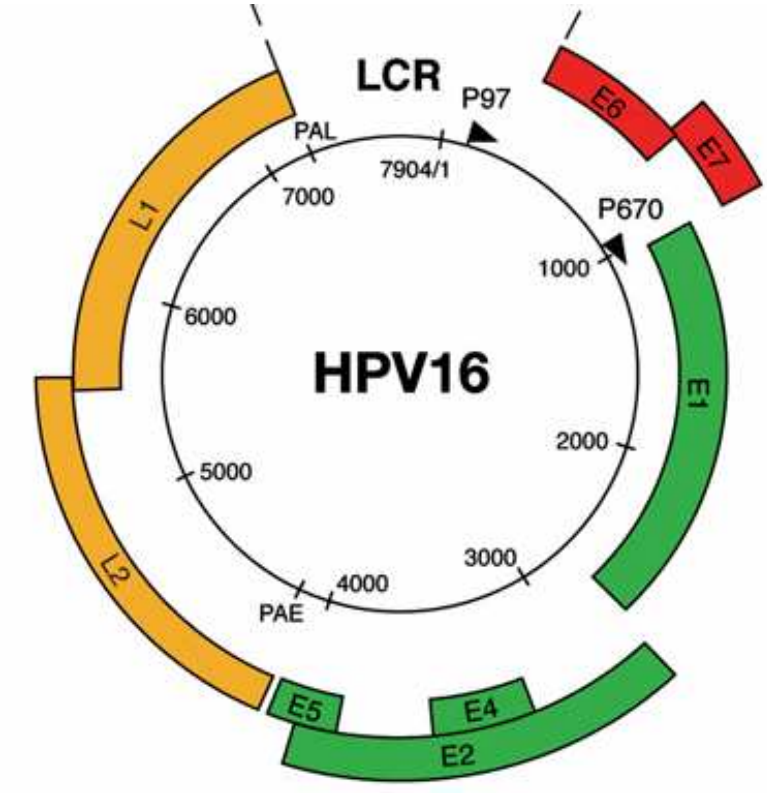

Figure 1.4 - Schematic diagram of HPV type-16 genome. The genome of HPV type 16 is approximately 8kb in size, and codes for 8 genes (LCR, long coding region). The expression of the viral early proteins (E6 & E7) is directed by the p97 promoter, whilst expression of the remaining early proteins and late structural proteins is directed by the p670 promoter (diagram adapted from [31]).

1.2.1.1. HPV Early Proteins

The E6 and E7 proteins are the first viral proteins, and their transcription is driven by the early p97 promoter. The specific roles of E6 and E7 in carcinogenesis are discussed in greater detail in subsequent sections (1.2.2.3 and 1.2.2.4 respectively).

The E2 protein is a DNA binding protein which interacts with $ACCN_6GGT$ motifs within the viral LCR and its expression is controlled by the p670 promoter [32]. E2 is 360 amino acids and contains three functional domains, a C-terminal DNA binding domain, an N-terminal transcription activation/DNA replication domain, and a central domain which forms a flexible hinge [33]. Upon binding, E2 forms a complex with the E1 protein which possesses ATP-dependent helicase capabilities promoting the unwinding of the viral DNA [34, 35]. The E2 protein is also responsible for viral genome segregation during cell division, carrying this out by tethering the viral genome to mitotic chromosomes by interaction with the bromodomain protein, Brd4 [36] [37]. One final role is

that of a repressor activity on the viral early promoter, which limits expression of the E6 & E7 early proteins [21, 30, 38] a key factor in the carcinogenic process.

The E4 ORF is translated from spliced transcripts with the first five amino acids of the E1 protein to generate an E1^E4 fusion protein [39]. The viral E1^E4 protein is the most highly expressed of all HPV proteins [29]. It is expressed in the later stages of replication in the upper layers of the differentiating epithelia, however little is known about its function. *In vitro* over expression studies have demonstrated that the E4 fusion protein interacts with the cellular cytokeratin network to facilitate its collapse, which suggests that the E4 protein plays a role in viral egress [29].

The E5 protein of HPV is a small hydrophobic protein made up of 83 amino acids [29]. It is found primarily in the golgi apparatus, the endoplasmic reticulum and also in the plasma membrane [29]. E5 is the primary transforming protein of bovine papillomavirus (BPV) however, the E5 protein of HPV possesses only weak transforming abilities on its own. Indeed, the E5 ORF is often deleted in cervical carcinomas, suggesting that it is not essential for viral maintenance and malignant progression in HPV infection [40].

Since the E6 and E7 proteins are the key transforming proteins of high-risk HPV types their structure and function are summarised in greater detail in sections 1.2.2.3 and 1.2.2.4 respectively.

1.2.1.2. The HPV Late Proteins and Viral Entry

Expression of the structural late viral proteins, L1 and L2, is driven by the late viral promoter, p670. The HPV capsid is composed of 360 copies of L1 and 12 copies of the L2 protein, arranged into an icosahedral lattice composed of 72 pentamers of L1 protein with L2 proteins located at the vertices [41]. Whilst L1 forms the major structural protein, L2 is located internally, and is a multifunctional protein, with roles in genome encapsidation, L1 interaction and capsid stabilisation, endosomal escape of virions and nuclear transport of the HPV genome [42].

In order for HPV virions to infect proliferating basal cells there must first be a break or microtrauma in the epithelia. Viral attachment is achieved through heparin sulphate proteoglycans (HSPG) and requires the L1 major capsid protein [42-48]. Binding with HSPG induces a conformational change in both L1 and L2 proteins resulting in the exposure of the L2 amino terminus and internalisation of the HPV genome [47].

1.2.2. The High-risk HPV E6 and E7 Proteins and the Ubiquitin-proteasome System

Within cells, proteins undergo a constant cycle of synthesis and degradation. There are two systems by which cells bring about this constant turnover of proteins; the lysosomal system and the ubiquitin-proteasome system.

The ubiquitin-proteasome system is responsible for the rapid degradation of damaged, abnormal or incorrectly folded proteins. The system is also responsible for the tightly regulated

control of a wide range of proteins, including those involved with transcription (reviewed in [49]), cell cycle progression [50, 51], IkB which regulates NFkB mediated transcription [52], antigen presentation [53, 54], cell surface receptors and apoptosis [54].

However, the ubiquitin-proteasome system also plays a role in diseases such as cystic fibrosis [55] and tumour development, as highlighted by the virally induced degradation of p53 through interaction with the E6 protein of HPV [56, 57].

1.2.2.1. Ubiquitination

Aharon Ciechanover and Avram Hershko are credited with the discovery of a heat-stable polypeptide that was shown to play an essential role in the recently discovered non-lysosomal pathway of protein degradation [58]. That polypeptide was later termed ubiquitin - a 76 amino acid protein, and its covalent attachment to a particular target protein is one of many essential steps that must occur prior to proteasomal degradation [59]. Prior to entering the proteasome, proteins become targeted for degradation by covalent attachment of multiple ubiquitin units, in what is known as the ubiquitination cascade. Initially, the E1 enzyme activates ubiquitin, creating a high-energy intermediate [60-62]. Following this step, the activated ubiquitin is transferred to an E2 ubiquitin conjugating enzyme [63]. The ubiquitin is then transferred to the target protein, which is conjugated to an E3 ubiquitin-ligase enzyme [54, 62, 64]. This process is repeated, with each ubiquitin polypeptide acting as the substrate for the attachment of further ubiquitin polypeptides. Attachment of four or more ubiquitin molecules is required before the proteasomal degradation can occur [65, 66]. Ubiquitinated products are recognised by the 19S regulatory subunits of the proteasome, at which point they are de-ubiquitinated and unfolded before being transferred to the 20S catalytic core of the proteasome, where they are degraded in an ATP-dependent manner [54].

1.2.2.2. The Proteasome complex

Research into degradation of abnormal proteins led to the discovery of an ATP-dependent, non-lysosomal proteolytic system in *Escherichia Coli* [67], a system which was also later identified in rabbit reticulocytes [68]. Hough et al later identified the main catalytic complex within this system [69], which was later termed the proteasome [70].

The proteasome (extensively reviewed in [71]) is a 2.5 MDa complex composed of several interacting units: the tubular 20S active core unit, which is flanked by two 19S regulatory subunits [72], which are capable of recognising poly-ubiquitinated proteins. Upon complete ubiquitination, protein substrates are translocated into the core of the proteasome through a gated channel consisting of seven α-units. In its native state, this gated channel is too narrow to allow passage of folded proteins [73]. Upon binding with 19S regulatory subunits, there is a conformational change in the 20S core, which widens the entry channel, and together, they are referred to as the 26S proteasome [70]. The 20S core subunit, contains two inner rings consisting of seven β units that have a range of activities – β1 expresses caspase-like activity, β2 expresses tryptic-like activity and

β5 expresses chymotrypsin-like activities [74], splitting peptide bonds after acidic, basic and hydrophobic amino acid residues respectively [73]. Following degradation within the core of the proteasome, peptides of 2-25 amino acid residues in length are released [75].

1.2.2.3. The HPV E6 Protein

The E6 protein is the first gene expressed by HPV and along with E7, is a key protein responsible for the increased malignant transformation following infection with high-risk HPV types. The E6 protein is 150 amino acids in size and contains two Cys-x-x-Cys motifs arranged into two zinc binding domains [76] and its expression is driven by the P97 early promoter [30].

The association of E6 protein with malignancy was initially investigated by two independent research groups. These authors speculated that the link between high-risk HPV types and cervical cancer was associated with an innate ability to modulate or alter the activity of cellular pathways or proteins that govern the cell cycle [57]. They concluded that it was directly related to the association of the HPV E6 protein with cellular p53 that played a role in modulating cellular control [56, 57].

The 'guardian of the genome', p53, is a site specific DNA binding protein that is expressed following DNA damage or aberrant initiation of the cell cycle (as defined in [30]). It can induce the expression of negative regulators of the cell cycle such as the cyclin-dependent kinase inhibitor $p21^{CIP}$ and trigger the apoptosis of damaged cells [77, 78]. Normal p53 turnover, however, is also regulated by the ubiquitin-proteasome pathway (see section 1.2.2.1), and this process is regulated by the MDM2 protein, which functions as a physiological ubiquitin-ligase (E3) enzyme [79].

The transforming capabilities of high-risk HPV types are linked with the ability of E6 to completely abrogate the regulatory functions of p53. This is achieved through binding of the E6 protein with an E6 accessory protein (E6-AP) [80] which is a member of the 'homology to E6 C terminus' (HECT) family of E3 ubiquitin ligases [81]. This forms a complex with p53 that produces the poly-ubiquitination of lysine residues on p53 [82], inappropriately targeting p53 for rapid degradation by the cellular proteasome [82, 83].

Studies have shown that the E6 protein of high-risk HPV type 16 is able to bind E6-AP more efficiently than low-risk HPV types which produces greater effects on p53 than low-risk types. As a consequence, HPV 16 E6 is able to bring about the degradation of p53 much more rapidly than other HPV types [84]. In the absence of p53-mediated cell cycle control, the cell is free to undergo successive rounds of unhindered replication. During this unchecked proliferation, the viral oncogenes promote genetic instability, which promotes errors in replication fidelity that may eventually lead to malignant transformation [21]. The E6 protein is crucial for this process since it abolishes, misdirects and degrades the cellular proteins in order to redress the vast stoichiometric imbalance between viral and cellular proteins. It is noticeable that E6 from low-risk types can still bind p53 but with a much weaker bond, and as such, fails to target p53 for improper degradation [85].

1.2.2.4. The HPV E7 Protein

The E7 protein, driven by the viral early promoter, is 98 amino acids in size and is divided into three conserved domains termed CR1, CR2 and CR3, all showing homology to the adenovirus E1A protein [77]. The CR1 domain contains the amino terminus; the CR2 domain contains an L-X-C-X-E region that allows for binding of the retinoblastoma tumour suppressor protein (Rb) and CR3 consists of two zinc finger motifs, similar to that of E6 [29]. The actions of the E7 protein, in some respects, are the primary mechanisms involved in the immortalisation process. E7 is able to interact with cellular members of the retinoblastoma (Rb) tumour repressor proteins, and like E6, facilitates the progression of otherwise quiescent cells into the S phase of cell cycle [86]. The retinoblastoma protein (Rb) is a nuclear phosphoprotein [87, 88] and was the first tumour suppressor protein to be identified [89]. Its physiological role is to control elements of the cell cycle [90], more specifically, the transition of the cell between the G1 and S phase of the cell cycle, and achieves this through the repression of transcription of genes required to overcome the G1/S checkpoint [91]. Within the uninfected cell, Rb exists in an unphosphorylated form in the G1 phase. In its hypophosphorylated state, Rb is able to bind to members of the E2F transcription factor family of proteins [92], repressing transcription of genes directed by E2F factors. Phosphorylation of Rb inactivates it, and removes its ability to bind E2F which allows transcription to proceed. This sequential phosphorylation is carried out by cyclins and cyclin-dependent kinases, namely cyclin-D and Cdk-4 and Cdk-6 [93] and also cyclin-E and Cdk-2 [94, 95]. At the peak of phosphorylation, Rb releases E2F, which is then free to promote the transcription of factors essential for S phase transition.

E7 is also able to completely compromise the activity of Rb by incorrectly targeting it for proteasomal-mediated degradation [96]. It has been shown that E7 facilitates ubiquitination of Rb via inappropriate activation of an E3 ubiquitin ligase, and as a consequence, inappropriately targets it for degradation by the cellular 26S proteasome [96]. The co-operative actions of E6 and E7 are shown in Figure 1.5. Working in unison, the E7 is able to bring about the degradation of the Rb protein, thus eliminating normal cell cycle control. In conjunction with this action, HPVs are also equipped to circumvent the cellular fail safe mechanism provided by p53. In eliminating p53, HPV can ensure complete unhindered genome replication.

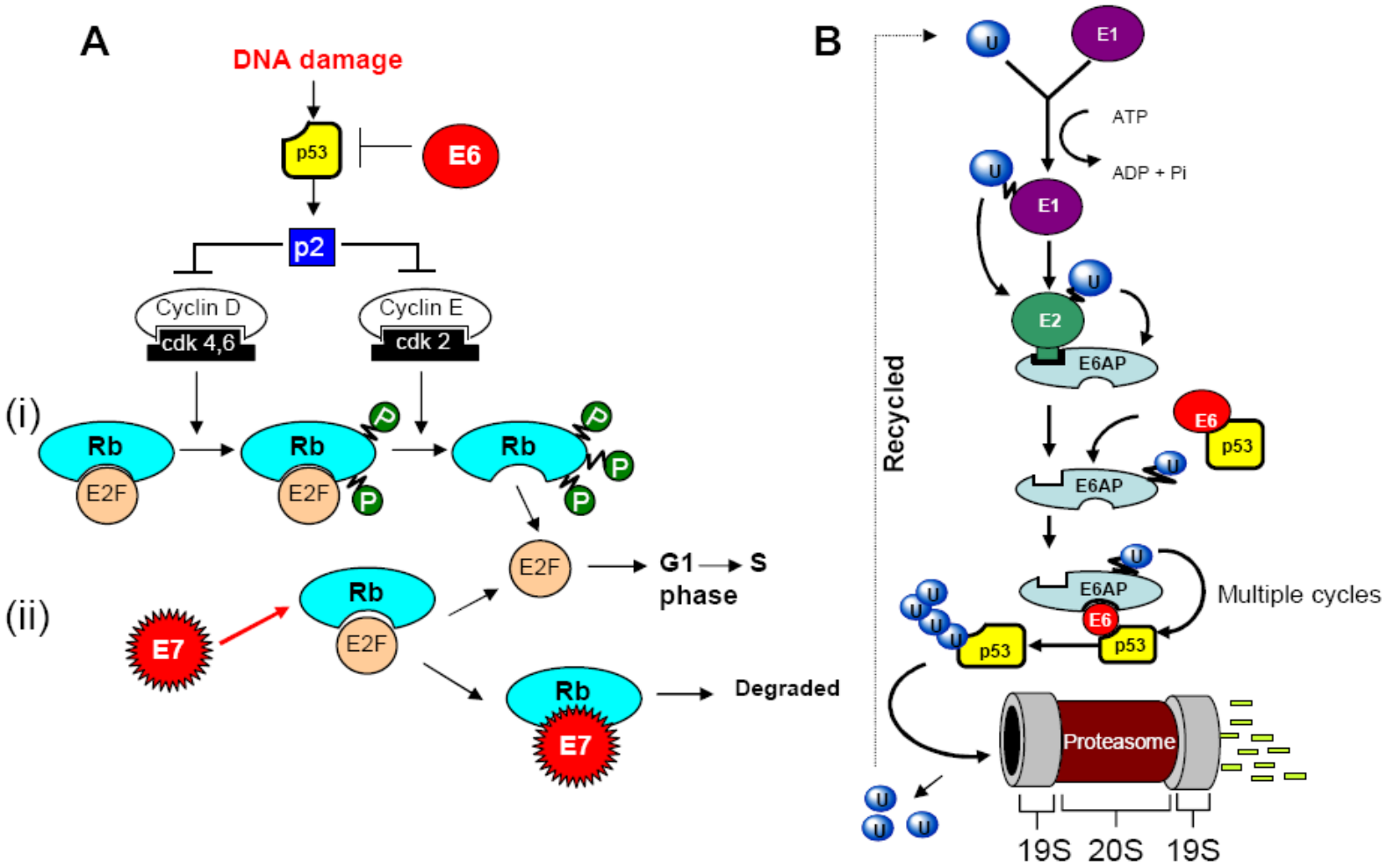
A
DNA damage
p53
E6
p2
Cyclin D
cdk 4,6
Cyclin E
cdk 2
(i)
Rb
E2F
P
(ii)
E7
E2F
G1 → S phase
Degraded
B
U
E1
ATP
ADP + Pi
E2
E6AP
E6
p53
Recycled
Multiple cycles
Proteasome
19S
20S
19S

Figure 1.5 - (previous page) – Synergistic actions of E6 & E7

In the uninfected cell, the Rb-E2F interaction governs cell cycle progression from the G1 through to the S phase. In its hypophosphorylated state, Rb binds E2F, preventing E2F from initiating transcription of genes necessary for cell cycle progression. Phosphorylation of Rb occurs through the actions of Cyclin D and Cyclin E in conjunction with cyclin-dependent kinases 4, 6 and 2 respectively. At the peak of phosphorylation as the cell approaches the G1/ S boundary, Rb releases E2F which is then free to initiate transcription of the necessary cell cycle proteins. In the presence of DNA damage or aberrant cellular proliferation, p53 is activated and inhibits cell cycle progression and also initiates apoptosis. The synergistic actions of E6 and E7 overcome this tight regulation of cell cycle progression. (A) The E7 protein is thought of as the primary transforming protein of HPV. It binds to Rb in its hypophosphorylated state, thus releasing E2F to initiate transcription of proteins necessary for cell cycle progression. (B) In the presence of the atypical cellular proliferation caused by E7/Rb binding, p53 would normally regain cellular control, or initiate the apoptotic cascade. The HPV E6 protein is able to overcome this cellular failsafe mechanism by inappropriately targeting p53 for proteasomal-mediated degradation. The ubiquitin-proteasome system is tightly regulated and involves addition of multiple targeting molecules named ubiquitin to the target protein; in the cascade, ubiquitin is transferred from an E1 ubiquitin activating enzyme to an E2 ubiquitin conjugating molecule, before being transferred to the target protein by means of an E3 ubiquitin-ligase molecule. In the case of E6 mediated degradation, E6AP binds directly to p53 and functions as the E3 ubiquitin-ligase. This leads to poly-ubiquitination of p53 which targets it for proteasomal mediated degradation.

1.2.2.5. Alternative Binding Partners for E6 and E7

The inhibition of the normal functions of p53 and Rb through virally encoded oncoproteins is a key step in the life cycle of many small DNA tumour viruses including HPV, HBV and Simian Virus 40 (SV40) [97]. Whilst overcoming G1/S checkpoint restriction through inhibition of p53 and Rb are key events in HPV pathogenesis, it is also apparent that in order to fully subvert normal cell function the association of E6 and E7 with several other cellular proteins plays an important role. As mentioned, the HPV genome is a fraction of the size of the human target cell and given this vast stoichiometric imbalance, it is clear that viral proteins must be extremely pleiotropic in nature. These p53/Rb-independent interactions can take the form of both inappropriate protein activation, and also a loss of protein function as a consequence of misdirected protein degradation at the proteasome [98]. The known E6 and E7 interacting proteins, and the consequence of the interaction, are detailed in Table 1.1.

Previous work from this laboratory has indicated that the PDZ domain Tax interacting protein 1 (Tip-1), a target of the HTLV-1 Tax protein and RhoA activator, also interacts with the HPV type 16 E6 protein [99]. The data suggested that E6 may increase cell motility by augmenting GTP RhoA mediated activation of RhoA-kinases (ROCK) and that this is dependent on the expression of Tip-1 protein [99]. Furthermore, recent data, also from this laboratory suggests that HPV type 16 E6, Tip-1 and guanine nucleotide exchange factor 16 (ARHGEF16) may co-operate to activate the Rho protein Cdc42 [100]. This is significant as guanidine exchange factor-catalysed activation of Cdc42 is known to play a crucial role in cellular transformation, malignant progression and invasion and suggests a functional link between E6 and Cdc42 activation [100].

Table 1.1 – E6 & E7 binding partners

E6 Binding Partner	Cellular Function of the binding partner	Possible consequence of interaction for the cell/degradation (+/-)
p53	Tumour suppressor protein: Regulation of cell response to mitogenic events	Loss of cell cycle control: antiapoptotic effect (+)
E6AP	Regulation of signal transduction in proliferation	Deregulation of signal transduction in proliferating cells (+)
E6BP (ERC55)	Member of calcium-binding proteins; involved in signalling pathways of cell growth and differentiation	Inhibition of terminal differentiation of epithelial cells. P53-independent inhibition of apoptosis (+)
Paxillin	Focal adhesion protein: has a role in cell adhesion and regulation of the actin cytoskeleton	Change of the cellular morphology and disruption of the actin cytoskeleton (+)
hDLG	Human homologue of the *Drosophila* Dlg tumour suppression protein; plays an important role in epithelial cell growth and in formation and maintenance of tight junctions	Change of cell growth, adhesion and polarity; invasiveness of the transformed cell (+)
MCM7	Minichromosome maintenance protein 7; a component of replication licensing factors	Induction of chromosomal abnormalities; overriding the early G1-phase arrest point (+)
IRF-3	Transactivator of Interferons; induction of IFN-β mRNA	Disruption of the antiviral response (-)
myc	Transcription factor	Induction of hTert expression and modulation of cell proliferation and differentiation (+)
bak	A member of Bcl-2 family; proapoptotic protein	Antiapoptotic effects (+)
E6TP1	GTPase activating protein; negative regulator of Rab	Inhibition of Rab-mediated mitogenic signalling; E6-induced oncogenesis (+)
CBP/p300	p53 co-activator; regulation of signalling modulating events	Down-regulation of p53-dependent transcription (-)
hScrib	Human homologue of the *Drosophila* Scribble tumour suppressor protein; controls formation of cell junctions and inhibition of epithelial cell growth	Loss of epithelial cell adhesion and polarity (+)
PKN	Protein kinase	Affects Rho-mediated signalling (+)
MUPP1	Multi-PDZ scaffold protein; regulation of signal transduction	Disruption of the assembly of signalling complexes at the epithelia cell membrane (+)
MAGI-1/2/3	Tight junction proteins; regulation of PTEN tumour suppressor	p53-independent inhibition of apoptosis (+)
Gps2	G-protein pathway suppressor protein; enhanced p300 activity	Suppression of Gsp2 (+)
XRCC1	DNA repair protein	Interference with DNA repair efficiency (-)
Tip-1	PDZ domain Tax interacting protein 1; RhoA Kinase Activator	E6 may increase cell motility by augmenting GTP RhoA mediated activation of ROCKs and that this is dependent on the expression of the Tip-1 protein (+)

E7 Binding Partner	Cellular Function of the binding partner	Possible consequence of interaction for the cell/degradation (+/-)
pRb	Regulation of cell cycle control via complex formation of E2F transcription factors	Phosphorylation of pRb and subsequent release from E2F, ubiquitination and subsequent degradation
pRb-pocket proteins	Regulation of cell cycle control	Loss of cell cycle control and activation of specific genes for cell cycle progression
Cyclin A,E	Kinase activity	Enhancement of HPV replication by directly altering cyclin-dependent kinase-2 activity
p21(cip)	Cyclin-dependent kinase inhibitor	Growth stimulation via loss of cell cycle control
p27(kip1)	Cyclin-dependent kinase inhibitor	Growth stimulation via loss of cell cycle control
α-glucosidase	Glycolytic control enzyme	Key role in the genesis of cervical carcinoma
M2 pyruvate kinase	Modulation of the activity of glycolytic enzyme 2	Promotion of cell transformation and proliferation
AP-1	Transcription factor	Transactivation abrogation of IRF-1 transcriptional activity
p48	IFN regulatory protein; key messenger protein	Inhibition of IFN signalling pathways via nuclear translocation of p48 of IFN-α signalling
IRF-1	Regulates expression of IFN-β	E7-mediated immune evading mechanism by interfering with IFN signaling
Mpp2	Forkhead transcription factor	Abrogation of IRF-1 transcriptional activation
TBP	TATA-box binding protein; initiator of transcription	Interference with the activation of p53-responsive promoters
TAF110	Initiator of transcription	Modulation of transcription
Mi2	Histon deacetylase	Abrogation of IRF-1 transcriptional activation
S4 subunit	S4 subunit of the 26S proteasome	pRb degradation via targeting to the proteasome
hTid-1	Human homologue of the *Drosophila* tumour suppressor protein Tid56	Activation of E2F-responsive promoters
IGFBP-1	Insulin-like growth factor-binding protein	Antiapoptotic effect
Histon H1 kinase	Kinase Activity	Interference with G2/M transition of cell cycle

(Table from [99, 101]

1.2.3. HPV Viral life cycle

Reviewed in Hebner and Laimins (2006), HPV are highly epitheliotrophic and the life cycle of HPV is entirely dependent on actively differentiating cells that are found only in stratified epithelium. Normal non-infected epithelial cells grow in distinct layers, where the basal layer stem cells are the only layer capable of active division [29]. Following division, one of the daughter cells then begins to migrate through the stratified layers. At this stage, the cell exits the cell cycle and begins the process of terminal differentiation. During this process, the cells begin to produce high molecular weight keratins, which accumulate in the cell. As the cell is no longer undergoing normal cell cycle, the nuclear membrane begins to deteriorate, and cells in the upper most layers exist as keratin filled membranes, which are no longer viable cells. At this point shedding of dead cells occurs with the journey from basal membrane to shedding taking approximately 10-14 days to occur [102] (Figure 1.6).

Figure 1.6 - Normal development and stratification of the epithelium

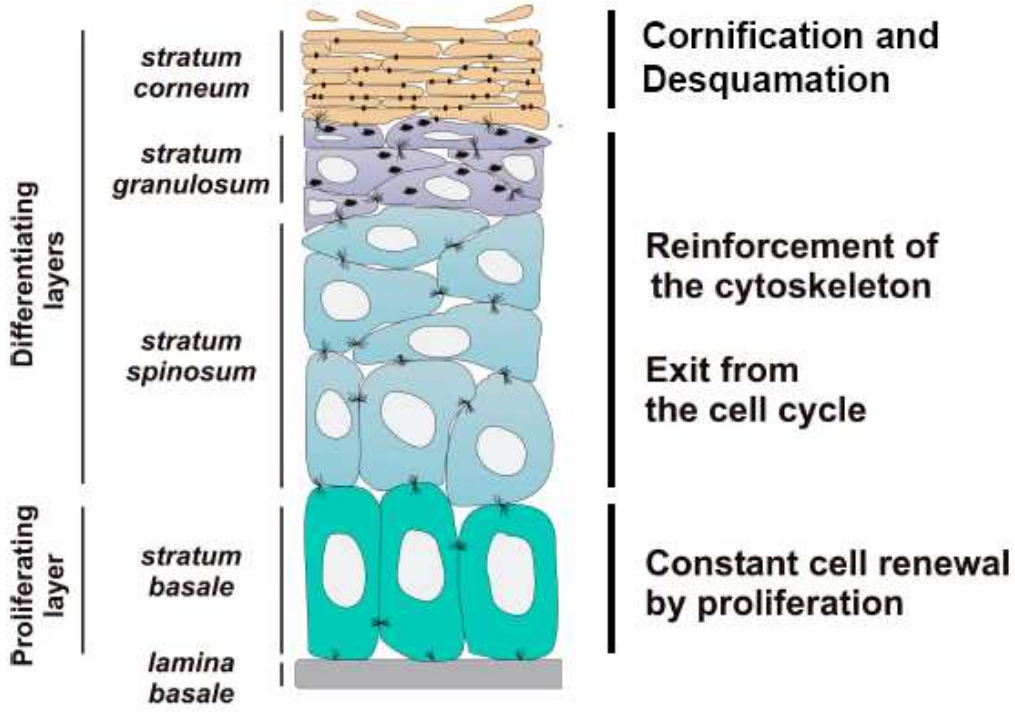

Figure 1.6 – Development and stratification of cells in the uninfected epithelium. Cells in the basal level undergo active division, before undergoing terminal differentiation, cornification and desquamation (adapted from [103]).

In a HPV infected epithelium, the scenario is quite different. Following infection and internalisation, the viral genome is established as an episome and the early viral promoter, p97, is activated which results in low level viral replication, maintaining the viral genome at 50-100 copies per cell [30]. As the cells of the epithelium divide, the viral genome also undergoes replication and division between daughter cells and it is at this point that the paths of uninfected and infected cells start to differ [29]. A differentiating daughter cell containing the replicating HPV episome begins to rise through the epithelial layers; however, it does not exit the cell cycle as occurs in non-infected cells. As the reproduction of the viral episome is totally dependent on the replicative machinery of the infected cell, HPV has developed a means by which it can overcome the terminal differentiation of the host cell. The synergistic actions of the HPV E6 and E7 proteins (Figure 1.5) force the infected cell back into the S-phase of the cell cycle, thus allowing continued viral replication [104]. As infected cells pass into the stratum spinosum (see Figure 1.6), the late promoter is activated, leading to expression of the late proteins and a massive up regulation in viral replication [29]. As the still actively dividing cells reach the highest layer the DNA is packaged into a complete virion and release of infectious virus is aided by the disintegration of the upper most cell layer [41].

1.2.4. HPV, the immune response and interferon.

The mammalian host immune response is composed of two interlinked pathways; the innate and adaptive immune response pathways. The innate immune response provides a fast-acting, generalised, non-pathogen specific response and is associated with a local inflammatory response. Prolonged activation of the innate immune response will eventually culminate in activation of T-helper lymphocytes which regulate the cell mediated immunity of the adaptive immune response. Recruitment of both phagocytic and antigen presenting cells leads to activation of the adaptive immune pathway which provides a longer lasting antibody-dependent and pathogen-specific response [105]. As discussed previously, the life cycle of HPV is exclusively linked to the terminally differentiated stratified cells of the epithelial basement membrane cells. In addition, HPVs are non-lytic viruses as their life cycle is exclusively restricted to the stratified epithelium composed of cells that are fated to undergo programmed cell death. As a consequence, these cells are therefore free from immune surveillance and as a consequence, HPV infection fails to induce any sort of local inflammatory response, and therefore fails to trigger the adaptive immune response accordingly. Furthermore, HPV does not induce viraemia [106].

Interferons (IFN) [107] (Discussed in greater detail in Section 5.1.1) are a group of multifunctional secreted proteins involved with antiviral defence, cell growth regulation and immune activation and can be split into two broad categories, type I and Type II; the type I IFNs, IFN-α and IFN-β, are produced as a direct consequence of viral infection and mediate the host antiviral response. In addition to the well known effects on p53 and Rb, E6 and E7 also possess abilities that allow them to subvert the interferon response. High risk HPV E7 has been shown to inhibit IFN-α signalling through binding with P48/IRF-9 which subsequently prevents nuclear translocation

and activation of the nuclear Interferon specific response element (ISRF) [106]. In addition E7 has also been shown to associate with interferon response factor-1 (IRF-1), thus inhibiting IFN-β dependent transcription. Furthermore, E6 has been shown to bind with TYK2, preventing its binding with the interferon response receptor, thus inhibiting the JAK-STAT signalling cascade associated with the IFN pathways [106].

However, despite this apparent ability of HPV to successfully evade the host immune response, approximately 90% of HPV infections are eventually cleared within two years of the initial infection [108]. A cell-mediated immune response is eventually directed against the HPV early E2 and E6 proteins, characterised by the infiltration of specific helper and cytotoxic T-lymphocytes, macrophages and pro-inflammatory cytokines [105]. Subsequently, low levels of serum neutralizing antibodies directed against the HPV L1 major capsid protein are produced, with low levels of IgG and IgA antibodies found in cervical mucosa [105]. Subsequently, HPV infections may undergo full clearance, or in a subset of infections, viral persistence (See section 1.3, below).

1.3. Viral persistence and Viral integration

1.3.1. Viral Persistence

HPV infection is a necessary but insufficient stage in the development of cervical cancer. As stated, less that 1% of those women infected with HPV will go on to develop malignant changes [11] highlighting the complex nature of the virus-host relationship. For example, HPV is known to evade the host immune system, its replication does not induce cytolysis, necrosis or viraemia and viral proteins are released in high numbers in terminally differentiated cells which are pre-programmed to undergo apoptosis and are therefore free from immune surveillance [24]. HPV has also been demonstrated to elicit a weak immune response as a consequence of inhibition of interferon synthesis [24]. Regardless, the majority of HPV infections (~90%) are successfully cleared or suppressed within 2 years of infection. Those infections that fail to resolve naturally within 2 years are considered persistent infections [28]. The definition of viral persistence is poorly defined yet many studies define it as having two or more HPV-positive colposcopy clinic visits with a medium interval between HPV tests of 6 months (range 2-72) [28]. Whilst both environmental and host factors may contribute to viral persistence, the greatest predictor of the likelihood of persistence remains HPV type and variant. High-risk HPV types (e.g. 16 & 18) are known to persist longer than low-risk types, and more specifically, non-European (Section 1.1.3) HPV 16/18 types have been shown to persistent longer than European types [24]. With increased length of viral persistence the probability of viral clearance reduces and accordingly, the risk of malignant progression increases [28].

1.3.2. Persistence and Viral Genome Integration

The integration of the HPV genome into the host genome is frequently associated with invasive squamous cell carcinoma [28, 109], the frequency of which increases with increasing severity of carcinoma [110].

Figure 1.7 – HPV genome integration

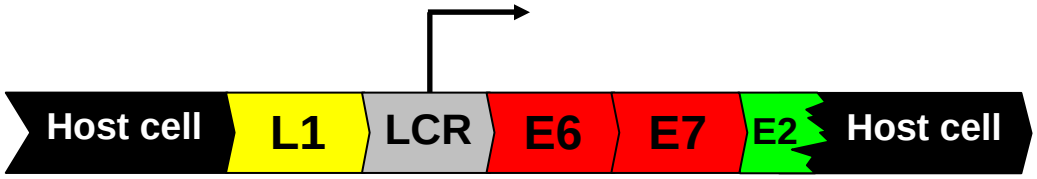

Figure 1.7 - HPV genome integration. In the majority of cervical cancers, the HPV genome is no longer reproduced episomally, and has instead become integrated into the host cell at a common fragile site. Typically, disruption of the viral genome occurs, and integrants have an interrupted E2 ORF, with subsequent loss of E2 mediated transcriptional repression of the E6 and E7 proteins.

The HPV E2 protein regulates HPV gene transcription, with arguably its most important role being transcriptional repression of E6 and E7 mRNA. The HPV genome most commonly integrates into host DNA at the E2 ORF, whereby this is disrupted. Thus, HPV integrants retain both E6 and E7 genes however since the E2 ORF is disrupted the E2-mediated transcriptional repression of E6 and E7 proteins is lost [111]. This loss of transcriptional repression leads to an uncontrolled up regulation of these proteins, with inevitable consequences for cell immortalisation and proliferation [21, 109, 112]. In conjunction with this, E2 has also been shown to regulate human telomerase (hTert) expression in cell culture models and again, loss of transcriptional control would result in up-regulation of hTert and an enhancement of cellular immortalisation [113].

In addition, HPV genome integration has been shown to occur at common fragile sites in host cell chromosomes [114]. Furthermore, integration has a number of consequences. When compared to episomal viral transcripts, E6 and E7 mRNAs from integrated virus display increased stability and half-life, which in turn induces increased genomic instability in the host thereby enhancing the possibility of malignant progression [115] when compared to episomal transcripts and an increase HPV protein expression and integration status as it relates to CIN progression is shown below in Figure 1.8 (Figure adapted from [110]).

Figure 1.8 HPV protein expression and progression to squamous cell carcinoma

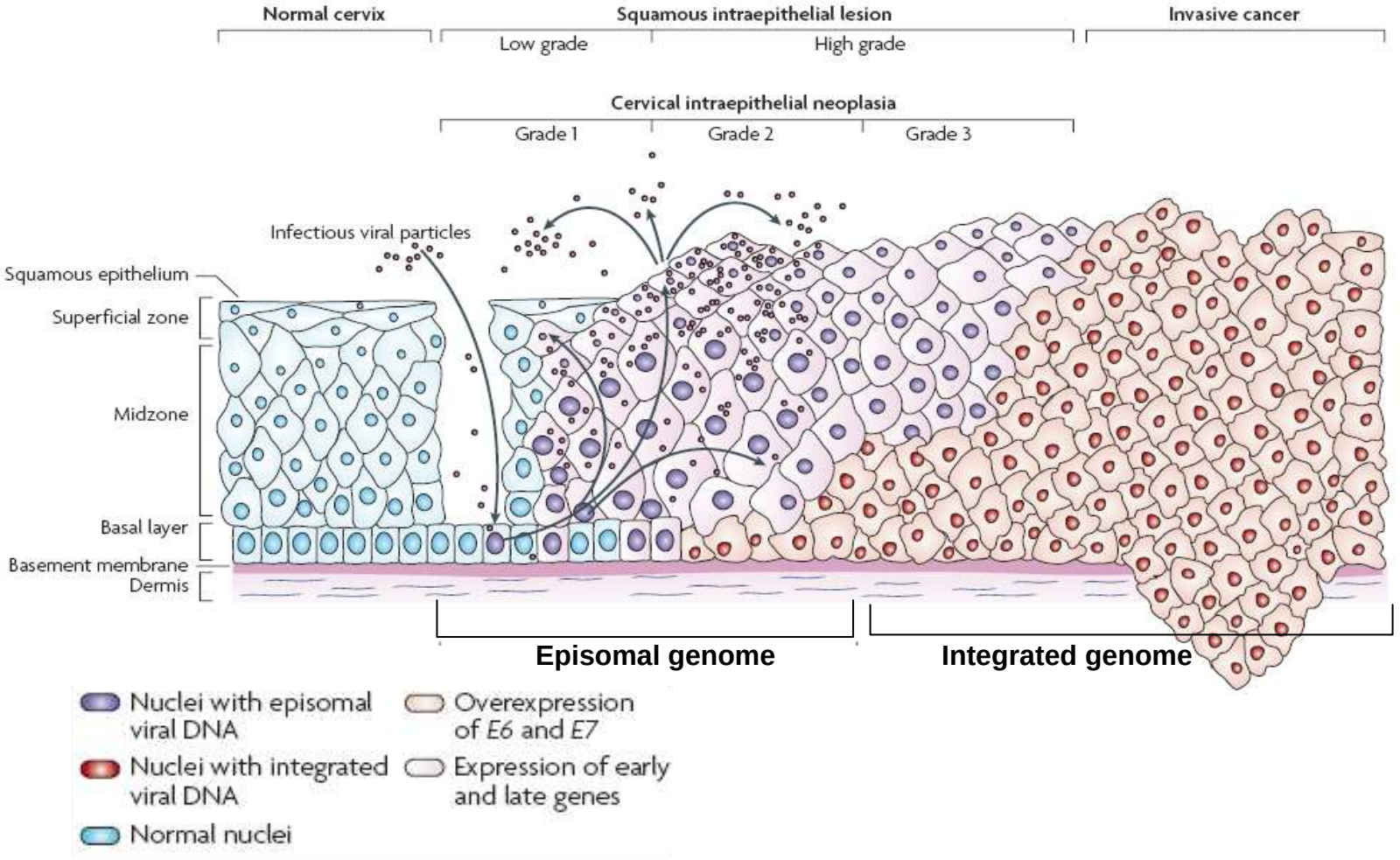

Figure 1.8 (previous page) – Viral genome integration and progression to cervical carcinoma

Infection of the actively dividing basal cell membrane occurs through micro-abrasions in the cervical epithelium. Following infection, the viral genome is maintained as an episome (purple nuclei) and infection manifests itself as a non-cancerous CIN-type lesion. The expression of both early and late viral proteins is carefully regulated by the early and late viral promoters culminating in the release of infectious viral particles. Left untreated, the progression from CIN-1 type lesion through to invasive SCC is associated with viral genome integration (red nuclei). Upon integration, E2 is known to become interrupted resulting in loss of transcriptional repression and over expression of the oncogenic E6 and E7 proteins resulting in the progression to invasive squamous cell carcinoma of the cervix (Diagram from [110]).

1.4. The Burden of HPV infection and Therapeutic Intervention Strategies for HPV-related malignancy

When comparing developed and developing countries, the age-standardised incidence rates (per 100,000 women) for cervical cancer vary dramatically (Figure 1.9); of the estimated 529,409 new cases of cervical cancer in 2008, >80% were shown to occur in developing countries, with Africa, in particular, suffering a disproportionately high incident rate [10].

Figure 1.9 – World Age Standardised Incident Rates for Cervical Cancer

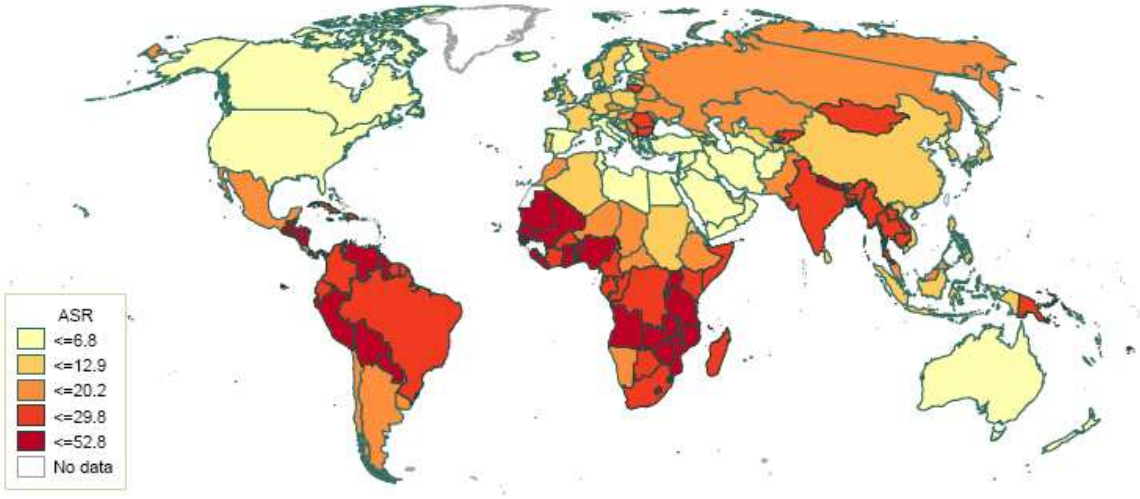

Figure 1.9 – World age standardised incident rates for cervical cancer. Approximately 80% of the estimated 529,409 new cervical cancer cases (2008) occurred in developing nations (ASR, Age standardised incident rate per 100,000 women. Figure from [1])

It is estimated that in Europe, with a population of 321.8 million women at risk of HPV infection, approximately 6.6% of women within the general population are estimated to harbour HPV infections. This results in approximately 59,931 new cases of cervical cancer annually and 29,812 deaths, making cervical cancer the 7th most frequent cancer of women in Europe. In contrast to this, approximately 24.9% of African women in the general population are estimated to harbour HPV infections. With a population of 267.9 million women at risk of cervical cancer, there are an estimated 78,897 new cases and 61,671 deaths each year making cervical cancer the most frequent cancer of women in Africa [10].

This disparity in cervical cancer incident rates between developed and developing nations is partly related to the heavy burden of HIV infection, particularly in Africa, and the lack of effective cervical screening programmes.

1.4.1. HPV and HIV in Developing countries

By the end of 2008, there were an estimated 33.4 million people living with Human Immunodeficiency Virus (HIV). Of these infections, 22.4 million were living in sub-Saharan Africa (Figure 1.10,), representing ~67% of all HIV infections worldwide, 68% of all new HIV infections worldwide and 91% of all new HIV infections among children. These infections accounted for 72% of all World AIDS-related deaths in 2008 [1].

Figure 1.10 – Global Prevalence of HIV infection

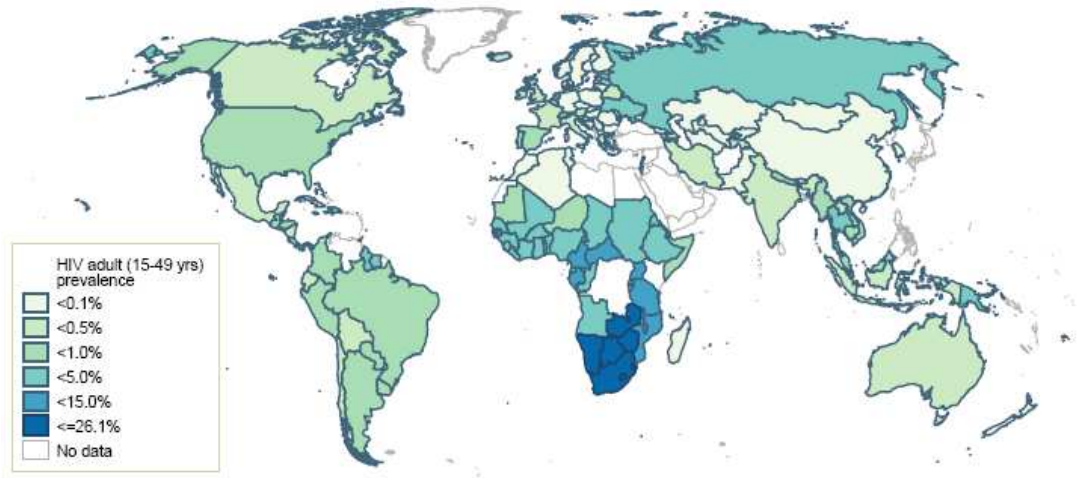

Figure 1.10 – Global prevalence of HIV infection, 2008 (Figure from [1]).

Interestingly, HIV infection amongst women and girls in sub-Saharan Africa is still disproportionately high, with female HIV infections accounting for 60% of the total cases in the region (UNAIDS/ WHO AIDS Epidemic Update, 2009; (Full Report available online ttp://www.unaids.org/en/dataanalysis/epidemiology/2009aidsepidemicupdate/).

As a consequence of HIV-induced immunosuppression, opportunistic infections such as Human Herpesvirus 8 (HHV8) are now common. This in turn leads to the development of Kaposi's Sarcoma (KS) which is now a defining marker of HIV infection [116]. Squamous cell carcinoma was classified as an AIDS-defining illness in 1993 based on evidence of an increased prevalence of cervical cancer in HIV-positive women [117]. Women with HIV demonstrate an overall higher prevalence of HPV infection when compared to HIV negative women [118]. Furthermore, they demonstrate infections with both a broader range of HPV types and also an increased prevalence of co-infection with multiple HPV types when compared to the general population [118, 119]. Interestingly, HPV-16 was less commonly associated high grade CIN lesions when compared to women in the general population [118, 120], a finding which will undoubtedly limit the effectiveness of either of the currently available vaccines, should they be introduced into the region (See Section 1.6).

As stated previously, persistent infection with a high-risk HPV type is associated with an increased risk of disease progression [28]. It has been demonstrated that HIV positive women have a higher risk of persistent infection than HIV negative women, regardless of the high-risk HPV type, and hence, have an increased risk of early CIN-type lesions progressing to cervical cancer [118, 121]. Indeed, women with HIV infection have been shown to have a five-fold increased risk of developing cervical cancer when compared to HIV negative women in the general population [122].

1.4.1.1. Effects of Highly Active Antiretroviral Therapy (HAART) on HIV and HPV

The 'Guidelines for the Use of Antiretroviral Agents in HIV-1-Infected Adults and Adolescents report 2011' has been used for information regarding HAART (available online from http://www.aidsinfo.nih.gov/contentfiles/AdultandAdolescentGL.pdf). In the absence of an effective cure and/or vaccine targeting HIV infection, the specific aims for Highly Active Antiretroviral Therapy (HAART) are to (i) reduce HIV-associated morbidity and prolong the duration/ quality of survival, (ii) restore and preserve immunological function, (iii) maximally and durably suppress plasma HIV viral load and (iv) to prevent HIV transmission. Currently there are 20 approved antiretroviral drugs for HIV management, from 6 mechanistic classes:

- Nucleoside/Nucleotide Reverse Transcriptase inhibitors (NRTIs)
- Non-Nucleoside Reverse Transcriptase inhibitors (NNRTIs)
- Protease Inhibitors (PIs)
- Fusion Inhibitors (FIs)
- CCR5 Antagonists
- Integrase strand transfer inhibitors (INSTIs)

HAART takes the form of combined therapy, utilising drugs from a range of these mechanistic classes with the aim of achieving long lasting suppression of viral load which leads to restoration of host immunity. However, the exact components of the HAART regime can vary dramatically depending on factors such as previous HAART treatments used which may generate drug resistance, pregnancy status, drug-drug interactions with other treatments, HAART-associated adverse effects, patient adherence and convenience.

Lopinavir is a highly potent and specific peptidomimetic inhibitor of the HIV-1 protease, which is an homodimeric aspartic protease involved in the post-translational processing of the HIV *gag-pol* polyprotein [123]. This is an essential step in the maturation process of infectious HIV particles and HIV PIs prevent the cleavage of *gag* and *gag-pol* polyproteins, arresting maturation thereby blocking the infectivity of nascent virions [123]. Therefore, the main antiviral mechanism of HIV PIs is to prevent further infection of susceptible cells. Indeed, these compounds possess no antiviral effects against cells in which HIV proviral DNA has integrated into the host genome [123].

Derived from the PI drug ritonavir, lopinavir (Figure 1.11) overcomes the problems of HIV drug-resistance commonly associated with ritonavir-based therapy [124] although there are limitations to its use; Lopinavir demonstrates poor bioavailability and undergoes extensive and rapid oxidative hepatic metabolism regulated by the Cytochrome P450 3A4 isozyme [125]. This results in a short elimination half life, effectively prohibiting the use of lopinavir as a single agent in HAART regimes [123].

Figure 1.11 – Chemical structure of lopinavir and ritonavir

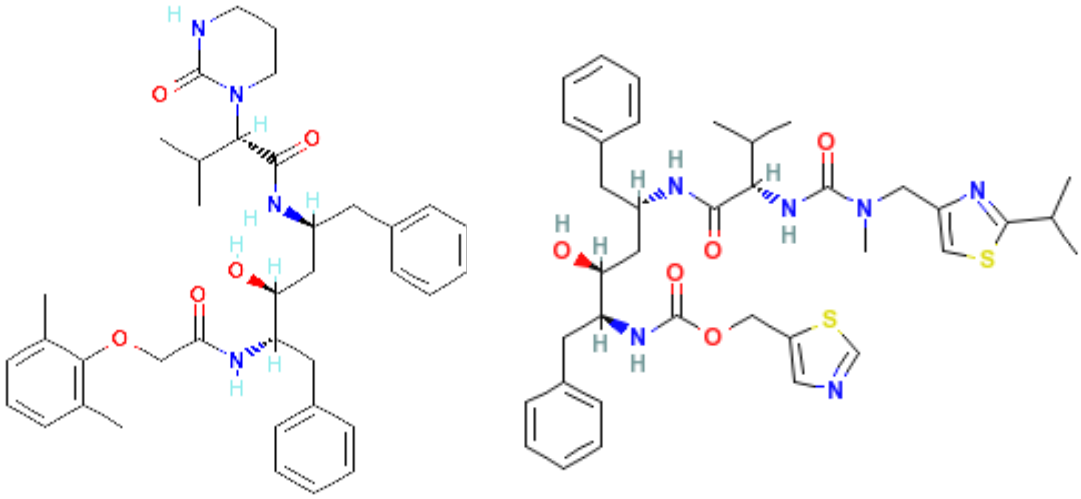

Figure 1.11 - Chemical structures of lopinavir, $C_{37}H_{48}N_4O_5$ (left) and ritonavir, $C_{37}H_{48}N_6O_5S_2$, (right) which are the main components of Kaletra, mixed in a 4:1 ratio. (Images taken from http://pubchem.ncbi.nlm.nih.gov).

To circumvent this problem, lopinavir is now routinely co-administered with a sub-therapeutic dose of ritonavir, a potent inhibitor of the Cytochrome P450 3A4 isozyme, which inhibits the metabolism of lopinavir resulting in an enhancement of its pharmacokinetic properties [126, 127]. This formulation, marketed as Kaletra®, is prepared in a ratio of 4:1 (lopinavir:ritonavir), and is available in tablet and soft gel capsule forms (reviewed in [128]), but also as an oral solution containing 42.4% alcohol (v/v) (Kaletra® data sheet available from http://www.rxabbott.com/pdf/kaletratabpi.pdf).

Whilst initially designed as an HIV-specific antiretroviral, previous work has demonstrated an off-target ability of lopinavir to inhibit the 26S proteasome [129, 130]. More importantly it was demonstrated that selective inhibition of the 26S proteasome in HPV positive cervical carcinoma cells lead to a stabilisation of the p53 protein [131].

Following the introduction of HAART the incidence of HIV-related KS fell dramatically in high-resource countries [132]. It was anticipated that the restoration of the host immune system would also result in improved clearance of HPV infection leading to a reduction in persistent infections which would ultimately result in a reduction in HPV-related cervical cancer [132]. Disappointingly, whilst subsequent studies went on to demonstrate potential regression of HPV-related CIN lesions in HIV positive women receiving HAART [133-135] it was also demonstrated that there were no improvements in cervical carcinoma incidence levels over the same time period [136-139].

Prior to the introduction of HAART, the lack of cervical screening programmes for HIV positive women in developing countries had little impact on life expectancy due to the competing mortality associated with other causes [140]. However, the restoration of the host immune system following the introduction of HAART, has lead to a significant reduction in the morbidity and mortality associated with HIV infection [141]. As a consequence, the average life-expectancy of HIV positive individuals has also increased hence increasing the opportunity for persistent HPV infections to progress to carcinoma over time [142]. Therefore, prevention of carcinoma in HIV positive women receiving HAART through cytology screening is essential [140].

1.4.2. National Health Service Cervical Screening Program (NHSCSP) and lack of screening in developing countries

Globally, the malignant burden attributable to HPV infection is estimated to be 3.7% of all cancers [143] representing a significant proportion of cancers that are, in theory, entirely preventable. The mean age for diagnosis of cervical cancer is 52 years of age, however CIN-I type lesions are generally observed in younger women [144, 145] indicating that the progression from CIN to malignancy may take several years. Clearly, this provides a window of opportunity to intervene in the development of HPV-related malignancies.

The purpose of the National Health Service Cervical Screening Program (NHSCSP) is to reduce cervical cancer incidence and mortality. The Cervical screening program does not aim to detect cervical cancer, instead it aims to reduce the burden of HPV-related malignancy through early detection and eradication of premalignant CIN-type precursor lesions [146]. An automated and systematic cervical screening program was introduced in England in 1988 (reviewed in [146]) wherein all women between the ages of 25-64 are now invited for gynaecological examination - every 3 years between the ages of 25-49 and every 5 years between the ages of 50-64. Exfoliated cell are collected around the neck of the cervix, the cervical transformation zone, and analysed by cytologists for signs of cellular atypia (Figure 1.3). Introduced in 2006, exfoliative Liquid Based Cytology (LBC) has now largely replaced the traditional Papanicolaou (‘pap smear’) method of cell collection. The main improvement being a major reduction in inadequate sample collection, along with an increased rate of sample throughput and an increased rate of detection of histologically

high grade CIN lesions (The Cervical Screening Programme 2009-10 report, http://www.cancerscreening.nhs.uk/cervical/statistics.html) [146, 147].

The NSHCSP has proven itself to be highly effective - since its inception, there has been an increase in screening coverage from 40% to over 80% of women in the target age group (25-64), which has seen a 50% reduction in invasive cervical cancer incidence and mortality in the United Kingdom [146, 148].

Whilst clearly effective in developed countries there are however considerable barriers to setting up efficient cytology-based screening programs in developing countries [149]. Sub-Saharan Africa, in particular, suffers from widespread poverty: only 41% of the total population has access to safe drinking water, and only 26% have access to sanitation [149]. This widespread poverty is reflected in the poor availability of facilities for screening or treatment; for example, as of 2006, Malawi, with a cervical cancer incident rate of 47/10,000 women, had one pathologist, one colposcope and no trained cytologists, a situation representative of many sub-Saharan countries [149]. Where they exist, primary health care facilities, where screening would take place, are often under-resourced, under-staffed and over-burdened and unable to offer effective screening [149].

1.5. Current Surgical Strategies for the management of HPV-related malignancy

Regardless of geographical location, socio-economic status or screening procedure, the treatment approach following detection of pre-cancerous cervical lesions remains the same – excisional or ablative removal of pre-cancerous cells from the cervical transformation zone [150]. While locally destructive/ ablative techniques such as radical diathermy and laser vaporisation are effective, excisional removal of the entire cervical transformation zone is preferred [150]. As approximately 60-70% of histologically abnormal cases will revert to normal over time surgical treatment of CIN-1 type lesions is generally not advocated. Clinical guidelines recommend an observational follow-up approach based on repeat screening visits [150]. For more advanced CIN lesions, there are a number of techniques for the complete removal of the cervical transformation zone [150]:

- Large Loop Excision of Transformation Zone (LLETZ)
- Cold Knife Conisation
- Laser excision
- Needle Excision of Transformation Zone (NETZ)

While surgery remains the treatment of choice for mid/high grade cervical lesions, the surgical techniques employed are evolving and the preservation of obstetric function is now paramount [151, 152].

Women treated for high grade cervical lesions require extensive post-surgical cervical cytology screening, which usually takes place at 6, 12 and 24 months followed by annual cytological screening for a further 5 years [150]. However surgical intervention for HIV-positive women is

known to be less effective and, despite follow up screening, CIN recurrence rates in these women are much higher than in HIV-negative women [153]. Alongside this it has also been demonstrated that surgical intervention for CIN in HIV-positive women can result in an extensive (10,000-fold) increase in HIV titre in vaginal secretions, clearly increasing the risk of HIV transmission [154, 155]. Interestingly, it has recently been demonstrated that HPV infection actually increases the risk of HIV infection [156].

1.6. HPV Vaccination – Developed versus Developing countries

It is known that approximately 70% of cervical cancers are attributed to infection with HPV types 16 & 18 [10], therefore prophylactic vaccination against these specific high-risk HPV types has the potential to significantly reduce HPV-related cervical malignancy.

There has been extensive research into HPV-specific vaccines based on an early observation that the antibody response to papillomavirus infection is in the form of a serum neutralising antibody against the major capsid protein, L1 [157, 158]. The viral life cycle is entirely dependent on differentiating epithelia, and as a result, HPV cannot be grown in bulk in cell culture, precluding the use of inactive/ attenuated virus vaccines [148]. As a result, HPV vaccines are subunit vaccines, composed of L1 protein self-assembled into a virus-like particle (VLP) [148] - essentially an empty capsid that is geometrically and antigenically identical to native virions [158]. The VLPs generate serum neutralising antibodies, yet contain no DNA and are therefore non-infectious [148]. To date, two HPV vaccines have been developed: Gardasil™, developed by Merck Vaccines (Merck and Co Inc, Whitehouse Station, NJ,USA) is a quadrivalant vaccine targeting HPV types 16, 18, 6 & 11, whilst Cervarix™ developed by GlaxoSmithKline Biologicals (Rixensart, Belgium) is a bivalent vaccine targeting HPV types 16 & 18. Both vaccines are almost 100% effective in the prevention of incident and persistent HPV infection (against HPV types covered by the vaccine in use) [159-162], however Cervarix™ was eventually licensed for use as a prophylactic vaccination in the European Union in 2007 (www.ema.europa.eu/humandocs/Humans/EPAR/cervarix/cervarix.htm).

In the U.K, a nationwide school-based vaccination scheme was introduced in 2008. Aiming to vaccinate girls prior to sexual debut, girls aged 12-13 years old were initially invited for vaccination with a follow up program for girls up to 18 years of age [163]. By maintaining 80% coverage, it is predicted that in time there will be a 63% reduction in invasive cancer, a 51% reduction in CIN-3 type lesions, and a 27% reduction in cytological abnormalities in women before the age of 30 [163]. However, while effective, vaccination programmes would need to achieve cervical cancer prevention rates of 85-90% before the pre-existing cervical screening procedures could be discontinued [148] and are therefore not considered a replacement.

Whilst initial results regarding vaccination in developed countries are encouraging, the economic barriers that prevent an effective cervical screening program will again limit the success of any vaccination scheme in developing countries. The current Cervarix™-based vaccination

regime follows a three-dose schedule, with doses at 0, 1 and 6 months, at a current cost of $120/dose [164]. Regardless of the lack of infrastructure required to implement a vaccination scheme, the cost of vaccine alone is clearly prohibitively expensive for developing countries. It is estimated that for developing countries, where extreme poverty is common, that the 'per dose' cost would need to be as low as $1 to $2 to make vaccination a financially viable option [165].

Economic restrictions aside, it is currently unknown whether L1-based vaccines will be efficacious in immunocompromised/HIV positive women. With limited access to antiretrovirals there are concerns over safety, immunogenicity and the ability of the vaccine to induce an effective and meaningful immune memory in these individuals [158].

It is thought that for every five year delay in implementing a vaccination program in developing countries there will be an additional 1,500,000 – 2,000,000 deaths as a result of HPV-related malignancy [165]. For the foreseeable future, HPV vaccination in low-resource nations will not be a financially viable option. In light of this, and in combination with the reduced efficacy of surgical intervention in HIV-positive women, who form a large proportion of the HPV/CIN affected women in developing countries, it is clear that research into alternative therapies for HPV infection is important.

1.7. Future Therapeutic Strategies

1.7.1. Emerging Strategies for Cervical Cancer Management

Despite significant improvements in the understanding of the molecular biology of HPV and its role in cervical malignancy, the mortality rates, particularly in low-resource countries remains high. Whilst HPV vaccination is expected to play a key role in reducing the burden of HPV-related malignancy, the true impact will not be observed for many years [166]. Thus, it is thought that the greatest chances to reduce the HPV burden will centre on primary prevention through improved screening techniques and the restriction of the spread of HPV [166]. The recent/ on-going investigations are detailed in Table 1.2 and extensively reviewed in [166].

Table 1.2 Current research patents relating to HPV therapy

Patent Number	Invention	Mechanism of Action
US20080171051	c-FLIP inhibitor	Enhances cytotoxicity of Chemotherapy
US20080113340	Biomarkers	Target therapy
US20080187513	Angeloyl substituted ingenanes	Induce primary necrosis; activate the immune system
US20080286781	Biomarkers	Target therapy
US20080213220	Viral vectors	Target cancer cells
WO2008104804	Biomarkers	Target therapy
US20080260729	VEGF-B antagonist	Target therapy
US20070269407	Interleukin-19	Activate the immune system
US20070166328	Alphavirus vectors	Activate the immune system
US20060029613	Metabolically active yeast cells	Retard tumor growth; prolong survival
US20060039919	Fusion protein	Activate the immune system
US20046825226	Adamantly derivates	Induce apoptosis of cancer cells
US20030161811	IL-20	Activate the immune system

(Table adapted from [166]).

1.7.2. Repositioning of Existing Drugs for Novel Uses – The Antitumour effects of Antiretroviral therapy

The development of a new drug can be an extremely lengthy and costly procedure. For example, the time from initial research through to launch and post-marketing safety surveillance, can be as long as 15 years and cost ≥ $900 million. As a consequence, the repositioning of an existing drug for novel purposes is an attractive alternative. Indeed, Sir James W. Black, pharmacologist and 1988 Nobel Laureate in medicine, once said *"The most fruitful basis for the discovery of a new drug is to start with an old drug"*. There are clear advantages to the repositioning of an existing drug, namely an implicit understanding of its proposed mode of action, an understanding of its pharmacokinetic, metabolic and toxicity profile along with an understanding of drug-drug interactions [167]. Perhaps the most relevant example of the repositioning of an existing drug for a novel use is that of zidovudine (azidothymidine). Originally designed as an anti-cancer agent, its use as a monotherapy in a clinical setting was limited due to poor anti-cancer activity and unacceptable toxicity levels [167]. Designed in 1964, the ability of zidovudine to limit HIV growth *in vitro,* through inhibition of the viral reverse transcriptase, was not discovered until 1984. In 1987 zidovudine went on to become the first pharmacological agent to be approved for the treatment of HIV infection [167] and is a good example of the potential successes of drug repositioning.

Drugs used in the treatment of HIV target many pathways of the HIV viral life cycle; NRTIs/ NNRTIs target the viral reverse transcriptase, PIs target the viral protease, whilst newer agents (reviewed in [168]) prevent the binding, fusion and integration of HIV within the host cell. Whilst both NRTI and NNRTI compounds have demonstrated limited anti-cancer activities extensive research has involved protease inhibitors and their potential for use as anti-cancer therapeutics (reviewed in [167, 169]).

1.7.2.1. Protease Inhibitors as anti-cancer agents –Kaposi's Sarcoma (KS)

The regression of KS and an increase in KS-free survival has been observed in patients receiving HAART [170, 171]. Whilst initially attributed to the restoration of the host immune system, the regression of KS was, however, shown to precede both a drop in HIV titre and the restoration of the host immune response [167]. Furthermore, when comparing PI-based HAART regimes to NRTI/NNRTI-based regimes, it was noted that whilst both were associated with disease regression, complete disease remission was more commonly associated with PI-based regimes. Furthermore, relapses in KS-related disease were observed in patients switched from PI-based to NRTI/NNRTI-based regimes indicating that the anti-cancer properties were directly related to a previously unknown, non-immune based mechanism(s) of HAART-PIs [167, 169].

KS is an angio-proliferative disease characterised by angiogenesis, endothelial spindle cell growth (KS cells), inflammatory-cell infiltration and edema [172]. Angiogenesis is a complex sequential process, requiring degradation of the basement membrane by the matrix metalloproteinase (MMP) MMP2 (MMPs reviewed in [173]). This leads to endothelial cell migration and proliferation towards the site of invasion [172]. Latent MMP2 is highly expressed in both KS-cells and endothelial cells and proteolytic activation of MMP2 is initiated by membrane type-1 MMP (MT1-MMP). MT1-MMP cleaves latent MMP to produce pre-MMP2 which then undergoes autoproteolytic cleavage mediated by $\alpha_v\beta_3$-integrin to produce functional MMP2. At physiological concentrations, saquinavir and ritonavir inhibit the activation of MMP2 through inhibition of MT1-MMP and/or $\alpha_v\beta_3$-integrin [169]. Furthermore, KS lesions demonstrate increased levels of inflammatory cytokines such as TNF-α, IL-6, and IL-8, and also the cell adhesion molecules VCAM1, ICAM1 and Selectin E, which are all essential in lesion development [169, 172]. Protease inhibitors have been shown to inhibit the activation of monocytes, lymphocytes and endothelial cells, thereby limiting inflammatory cytokine production [174]. Inflammatory cytokines are further associated with the production of pro-angiogenic factors, including Basic Fibroblast Growth Factor (bFGF) and Vascular Endothelial Growth Factor (VEGF) [172]. Saquinavir and ritonavir have been shown to inhibit the formation of angiogenic lesions following the inoculation of pro-angiogenic factors in nude mice [172], as well as bFGF and VEGF-induced angiogenesis in the chicken chorioallantoic membrane (CAM) assay [172]. Whilst *in vitro* test systems demonstrated that PI treatment did not inhibit bFGF-induced cell proliferation, it was however, shown to completely block the angiogenic invasion by both bFGF-induced endothelial and KS-cell types. This was shown to occur at PI concentrations similar to those found in the plasma samples of patients receiving

HAART (0.1-1.0μM) [172]. Thus, the off-target anti-angiogenic effects associated with PI treatment are thought to be mediated by a combination of inhibition of VEGF and bFGF function [172], inhibition of MMP2 activation, and a reduction in inflammatory cytokine synthesis [169, 172, 174].

In addition to these anti-inflammatory, anti-angiogenic actions, perhaps more importantly, protease inhibitors can modulate and indeed block the function of the cellular proteasome [175]. HIV-1 maturation relies on proteasomally-mediated processing of the *gag* polyprotein, and it is now thought that part of the antiviral actions of HAART-PIs in HIV patients relies on inhibition of the 26S proteasome [176]. However, the inhibitory actions on the proteasome require drug concentrations above those present in sera of treated patients (5-100μM) [175]. At these elevated concentrations ritonavir led to a selective inhibition of intracellular protein degradation and a fully reversible arrest of the cell cycle in the G1/S phase [177]. It was demonstrated that these effects were a consequence of selective binding between ritonavir and the MB-1(X) and LMP7 subunits of the 20S active core of the proteasome, known to regulate chymotryptic-like activity [177]. Interestingly, whilst virtually eliminating the chymotryptic-like activity, ritonavir was actually shown to induce a modest increase in the tryptic-like activity of the proteasome [177] demonstrating the importance of the chymotryptic-like activity of the proteasome in regulating the G1/S transition.

The proteasome controls several important pathways through the rapid degradation of damaged, abnormal or incorrectly folded proteins. The system is responsible for the tightly regulated control of a wide range of proteins, including those involved with transcription (reviewed in [49]), cell cycle progression [50, 51], IkB which regulates NFkB mediated transcription [52], antigen presentation [53, 54], cell surface receptors and apoptosis [54]. Thus, the PI-mediated inhibition of these activities can inhibit tumour cell survival, tumour cell proliferation in association with limiting tumour-associated inflammation and endothelial cell activation [169]. Significantly, PI treatment can also sensitise tumour cells to ionising radiation and promote apoptosis [98, 178, 179].

1.7.2.2. The proteasome as a drug target

The proteasome is clearly a potential target for cancer therapy. For example, in non- virally induced cancer, NFkB plays a key role in cancer development. NFkB is responsible for the transcription of several genes involved with growth, apoptosis and cell adhesion. Its activity is regulated by an endogenous inhibitor, IkB, which is a substrate for the cellular proteasome and studies have shown that NFkB promotes oncogenesis and is over expressed in malignant cells [130]. Inhibition of the degradation of IkB by the 26S proteasome would therefore allow for the binding and repression of the transcriptional activities of NFkB with subsequent restrictions on abnormal cellular proliferation [130]. In virally induced cancers, such as those linked with HPV, it is predicted that inhibition of the proteasome could lead to an accumulation of cell cycle regulatory proteins, such as p53 [98] and Rb that would, otherwise be misdirected for inappropriate proteasomal-mediated degradation by the action of viral proteins. Following the identification of the tubular, multi unit structure of the 26S proteasome, selective and specific proteasome inhibitors

were able to be synthesised. The tripeptide aldehyde MG-132 (Carbobenzoxy-L-leucyl-L-leucyl-L-leucinal) is able to reversibly inhibit the actions of β2 and β5 through the formation of aducts with the active sites on the β subunits [74]. However, due to their poor specificity, and association with widespread toxicity, they have limited use *in vivo* [180]. Following from this research, more selective and potent proteasome inhibitors were synthesised, best characterised by the boronic acid dipeptide Bortezomib, which brings about proteasome inhibition through a stable but reversible intermediary compound that binds to amino-threonine residues of the catalytic core region [74]. When compared to the relatively non-specific inhibitor MG-132, Bortezomib displays 1000 fold greater potency, with selectivity for the chymotrypsin-like activity of the core [74].

Bortezomib (Velcade ® - data sheet available from http://www.velcade.com/Files/PDFs/VELCADE_PRESCRIBING_INFORMATION.pdf) has since been licensed as the first therapeutic inhibitor of the proteasome, and is now in use for the treatment of chronic myelagenous leukaemia, relapsed mantle cell lymphoma and a subset of B-acute lymphoblastic leukaemias [181, 182].

1.7.3. Proof of Concept

The development of Bortezomib has provided a 'proof of concept' regarding the use of proteasome inhibition as a means of targeted cancer therapy. However Bortezomib-induced p53 activation has been shown to be reduced in E6-expressing LNCaP-Pro5 cells, potentially limiting the use of Bortezomib in targeting HPV-immortalised cells [183].

Despite being originally developed for the specific inhibition of the HIV-1 viral protease, HAART-PIs have since demonstrated anti-proliferative, anti-angiogenic and anti-inflammatory properties, whilst promoting apoptosis and radiosensitisation mediated through inhibition of the 26S proteasome and MMP2. Clearly, this suggests that their use may be of benefit in non HIV-associated tumours. Accordingly it was proposed that HAART-PIs, either as a monotherapy or in combination with other cytotoxic agents would be of use against tumours known to be sensitive to anti-angiogenic therapy, including colon and renal cancer, and also multiple myeloma, or to prevent the invasion of pre-malignant diseases such as *in situ* carcinomas of the cervix and oral cavity [169].

1.8. Project Rationale and Aims

In light of these observations it is clear that a non-surgical, preferably self-applied, treatment for HPV related cervical dysplasia would be extremely useful particularly in low-resource countries where high levels of HIV infection exacerbate the situation.

Previous work from this laboratory investigated the ability of HIV protease inhibitors to combat HPV infection and demonstrated that the antiretroviral drug lopinavir could stabilise the p53 protein and induce apoptosis of HPV positive cervical carcinoma cells *in-vitro* albeit at higher doses than those achieved by oral administration [98]. These data indicated that lopinavir could potentially be used as an anti HPV therapeutic. Prior to a clinical trial to test this new indication work was carried out in order to further characterise how lopinavir works against HPV. In this regard we have used Fourier Transformation Infra Red spectroscopy to analyse the metabolic changes occurring in lopinavir treated cervical carcinoma cells [184] and direct Raman spectroscopic imaging to identify the site of action of the drug in cells [185]. Evidence is provided here to further support these initial observations and present data on the specific molecular mechanisms by which lopinavir works against HPV with two specific aims:

- To identify cellular proteins, in addition to p53, degraded by HPV that are stabilised in the presence of lopinavir

- To identify potential new effectors of lopinavir that account for its anti-HPV activity and to fully characterise the potential mechanism(s)

1.9. Conferences and Presentations

This work has been presented as a poster at the 2008 National Cancer Research Institute conference, Birmingham, and also as a poster at the 2009 International Papillomavirus conference in Malmö, Sweden.

This work has also been presented as an oral presentation at the 2008 Central Manchester and Manchester children's university hospitals Research and Innovation meeting, and also as an oral presentation at the 2009 Gynaecological Visiting Society meeting, Manchester.

2. Chapter 2 - Does Lopinavir Inhibit the Proteasome in HPV positive cells?

2.1. Introduction

Mincheva *et al* (1987) used in-situ hybridisation analysis of metaphase chromosomes to demonstrate that SiHa cervical cancer cells contain 1-2 integrated copies of HPV 16 DNA. Their work showed that the HPV genome persists in an integrated state, in the host chromosome 13, at region q21-q31 [186] making the SiHa cell particularly useful for lab based investigations into HPV.

In order to further assess proteasomal inhibition, SiHa cells stably expressing a commercially available proteasome sensor vector, pZsProSensor-1 (Appendix 1, Clontech) were generated. The pZsProSensor-1 plasmid is a eukaryotic expression vector which expresses a naturally occurring green fluorescence protein (GFP) from the button polyp coral (*zoanthus sp.*) as a fusion complex coupled to a mouse ornithine decarboxylase (MODC) degradation domain at its C-terminus region. Ornithine decarboxylase is a key enzyme in the synthesis of polyamines involved in cell proliferation and has an extremely high turnover rate [187]. The MODC domain contains several PEST sequences, defined as a region rich in proline (P), glutamic acid (E), serine (S) and threonine (T) which are involved with the rapid degradation and turnover of many regulatory proteins [188, 189]. MODC is degraded by the proteasome, although in contrast to other proteins, the process is not linked to polyubiquitination of the target protein; instead, MODC degradation is mediated by a polyamine induced enzyme inhibitor, antizyme, that destabilises the complex and leads to its degradation at the proteasome [190]. In cells containing a fully functioning proteasome, the GFP/MODC fusion protein is rapidly targeted for proteasomal degradation. In contrast, following proteasomal inhibition, the GFP accumulates within the cell to levels that can be detected by fluorescent microscopy or flow cytometry (Figure 2.1).

Figure 2.1 – Function of the pZsProSensor-1 vector in SiHa cells

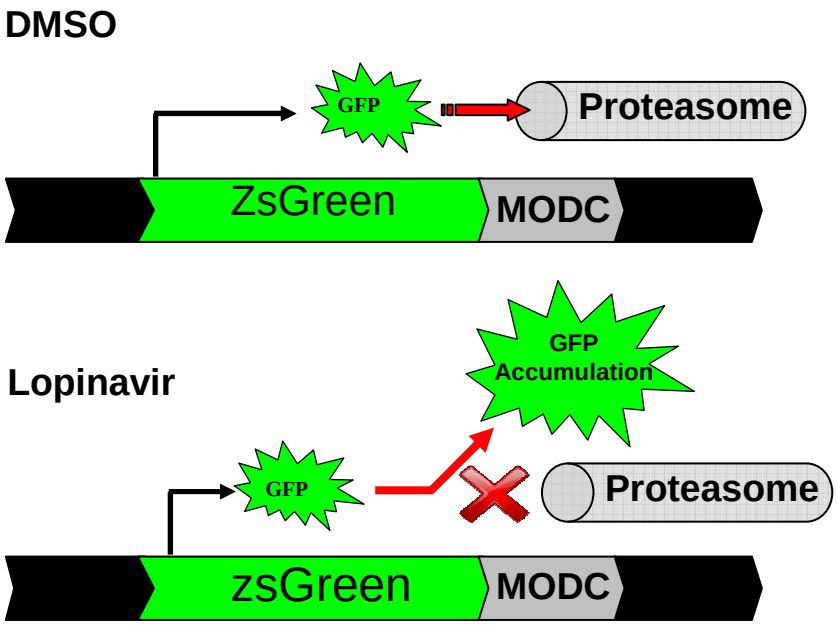

Figure 2.1 – SiHa cells were engineered to stably express the pZsProSensor-1 proteasome sensor vector. The eukaryotic vector expresses the coral reef green fluorescent protein (GFP) coupled to a mouse ornithine decarboxylase degradation domain (MODC). The MODC domain targets the GFP for rapid proteasomal degradation. In the control DMSO treated cells (upper panel), the GFP is rapidly degraded at the proteasome. In contrast, the addition of lopinavir leads to inhibition of proteasomal function, therefore leading to an accumulation of GFP, detectable by fluorescent microscopy with a FITC filter.

2.2. Aims

2.2.1. Transiently transfect C33A parent and C33AE6 cells with the pZsProSensor-1 proteasome sensor vector in order to confirm its function and to allow optimisation of GFP detection techniques. Proteasome inhibition by lopinavir and MG-132 will be assessed by flow cytometric measurement of GFP levels

2.2.2. Generate stable pZsProSensor-1 transfected SiHa cells in order to assess the ability of lopinavir to inhibit the proteasome in an HPV positive cell line. Analysis of proteasome inhibition will be assessed by flow cytometry and fluorescence microscopy to determine GFP level

2.3. Methods

Details of all solutions used throughout this thesis are detailed in Appendix 2. All reagents, unless otherwise stated were purchased from Sigma-Aldrich (Dorset, UK) or Invitrogen (Paisley, UK). All PCR primers were purchased from Eurofins Genetic Services Ltd. (Ebersberg, Germany).

2.3.1. General Cell Culture

All cell culture was carried out using a class II biological safety cabinet (Envair, Lancashire, UK) and unless otherwise stated, all cells were cultured using RPMI-1640 growth medium (Invitrogen, Paisley, UK) supplemented with 10% foetal bovine serum (Sigma-Aldrich, Dorset, UK) and 2 mM L-Glutamine (Sigma-Aldrich, Dorset, UK) at 37℃ in a humidified atmosphere containing 5% CO_2 (incubator from Forma Scientific, Loughborough, UK). Stocks of C33A parent, C33AE6 [191], C33A Vector [191], SiHa cells were provided by Dr Lynne Hampson and the ATCC. C33A and C33AE6 have been extensively used as a model test system through which to study the effects of E6 in the context of HPV infection. SiHa cells were also included as previous work, on which this current thesis is based, investigated the effects of lopinavir in HPV positive SiHa cells, as they contain a fully integrated HPV genome. SiHa cells are therefore more representative of the intended target cell.

2.3.2. Thawing Cells

Cells were removed from liquid nitrogen and rapidly thawed in a 37℃ water bath. A disposable Pasteur pipette was used to transfer cells to a culture flask containing complete RPMI-1640 growth medium and these returned to the incubator. Twenty-four hours later the RPMI-1640 growth medium was aspirated and replaced with fresh complete medium and cells maintained at 37℃/ 5% CO_2.

2.3.3. Sub Culture of Cells

Cells were routinely passaged on reaching 80% confluency. The growth medium was aspirated, and cells were washed with PBS. Following this, pre-warmed trypsin/ EDTA (0.25%) (Invitrogen, Paisley, UK) (230 µl for T-25 culture flasks or 800µl for T-75 culture flasks) was added, and the flasks returned to the 37℃ incubator for 3 – 4 minutes or until all cells had rounded up and detached. The trypsin was neutralised by addition of 10 ml complete medium before being transferred to a 50 ml falcon tube, and cells counted using a haemocytometer. Cells were reseeded at 5 x 10^5 cells per T-25 in a total volume of 10 ml medium, and 1 x 10^6 cells per T-75 in a total volume of 20 ml medium.

2.3.4. Freezing Cells

At 80% confluency, cells were harvested and counted as detailed in section 2.3.3. These were then pelleted by centrifugation at 528 x g for 5 min using a Sigma Aldrich 1-14 bench top microfuge (Sigma Aldrich, Dorset, UK). Following centrifugation, the growth medium was aspirated and the cell pellet was thoroughly resuspended in freezing medium (10% DMSO in FBS) at a concentration of 1 x 10^6/ml in labelled cryovials (Nunc, Roskilde, Denmark). Cryovials were transferred to an isopropanol gradient freezing pot (Nalgene, Roskilde, Denmark), and placed at -80℃ overnight before being transferred to liquid n itrogen for long term storage.

2.3.5. Drug Preparations

Lopinavir was provided as a kind gift by Abbott Laboratories (Park Road, Abbott Park, IL 60064-6187, USA). A 20 mM working stock solution of lopinavir was prepared in DMSO (Sigma-Aldrich, Dorset, UK). MG-132 (Carbobenzoxy-L-leucyl-L-leucyl-L-leucinal) was purchased from (Calbiochem, Nottingham, UK) and a 10 mM working stock solution was prepared in DMSO.

2.3.6. Preparation of Competent XL-1 Blue *E.coli*

An LB agar plate was streaked with 10 µl of the XL-1 Blue strain of *Escherichia coli* (Stratagene, CA, USA) before being incubated overnight at 37℃. A single colony was picked and used to inoculate a 5 ml volume of Luria-Bertani (LB) medium without antibiotics, and left overnight at 37℃ with gentle shaking. The 5 ml starter cultu re was then added to 250 ml LB containing 20 mM $MgSO_4$ and grown at 37℃ to an optical density of between OD_{600} 0.4 - 0.6. At this point, the culture was put on ice for 10 min, with all solutions, pipette tips, eppendorf tubes and falcons also placed on ice. The culture was split into 5 x 50 ml falcon tubes and the cells were pelleted by centrifugation at 1646 x g for 5 min at 4℃. The su pernatant was discarded and the cells in each falcon were resuspended in 2 ml of TFB-1 buffer using a Pasteur pipette. Once resuspended, the resulting solutions were pooled into a single 50 ml falcon, and placed on ice for 30 min. This was then made up to a volume of 50 ml with TFB-1. All falcon tubes were left on ice for 10 min before centrifugation for 5 min at 1646 x g at 4℃. The su pernatant was discarded and the cells were gently resuspended in 5 ml TFB-2 buffer and left on ice for 30 mins. Subsequently, 50 µl of this was aliquoted into chilled eppendorf tubes and immediately frozen at -80℃. Control transformations with 100 ng of a control plasmid were carried out to confirm competency.

2.3.7. Transformation of XL-1 Blue *E. coli* cells

Competent cells were thawed on ice and incubated with 50-100 ng of plasmid DNA on ice for 30mins. The cells were heat shocked at 42℃ for 45 sec and then returned to ice for 2 min.

Following this, 1 ml of pre warmed LB media was then added and the mixture incubated at 37℃ for 30 minutes with shaking (150 rpm). During this incubation, LB agar plates were prepared, with a negative control plate containing 100 µg/ml of carbenicillin antibiotic. Following the incubation period, 100 µl of the transformation mix was then plated onto one LB agar plate containing 100 µg/ml of carbenicillin antibiotic. The remaining mix was then pelleted, and the supernatant aspirated and the cells resuspended in 100 µl fresh LB media which was then plated onto a separate LB agar plate containing 100 µg/ml of carbenicillin. Positive control plates contained plasmid but no antibiotic and negative control plates contained antibiotic but no plasmid. All plates were incubated at 37℃ overnight.

2.3.8. Maxi Prep of pZsProSensor-1 Vector plasmid

The large scale plasmid purification protocol of Sambrook *et al.,* (1989) was used for plasmid purification [192]. A single colony from the plates grown in section 2.3.6 was picked and used to inoculate 5 ml of carbenicillin-containing LB media (100 µg/ml). This was then incubated at 37℃ for 6 hr with shaking at 150 rpm and then made up to a total volume of 250 ml with fresh LB media containing carbenicillin (100 µg/ml), and incubated at 37℃ overnight with shaking at 150 rpm before being split equally between 50 ml falcon tubes and centrifuged at 1646 x g for 15 min at 4℃. Subsequently, the supernatant was discarded and 9 ml of solution-1 used to resuspend and pool all cell pellets. A small amount of lysozyme was added to the falcon, and the tube gently shaken and incubated for 10 mins at room temperature. Following this, 20 ml of solution-2 was added, and the tube gently shaken until the contents became a clear viscous and homogenous solution after which, 15 ml of solution-3 was added to the falcon, and the tube gently inverted for several minutes before placing on ice for 10 min. The mixture was then pelleted by centrifugation at 1646 x g for 15 min at 4℃ and the supernatant filtered through several layers of gauze into a fresh falcon tube and 0.6 x volume isopropanol added and incubated on ice for 10 min. The falcon was centrifuged at 1646 x g for 15 min at room temperature and the supernatant aspirated carefully. The pellet and walls of the falcon were rinsed in 70% ethanol, which was discarded and the pellet allowed to air dry. The pellet was subsequently dissolved in 3 ml of 1 x tris-Ethylenediamenetetraacetic acid (TE) buffer (pH 8) and 3 ml of ice cold lithium chloride added and the tube mixed by inversion. This was then centrifuged at 2150 x g for 10 min at 4℃, and the supernatant decanted into a fresh falcon tube. An equal volume of isopropanol was added and centrifuged at 2150 x g for 10 mins at room temperature. The isopropanol was aspirated and the pellet washed in 70% ethanol and allowed to air dry at room temperature. The pellet was dissolved in 500 µl 1 x TE buffer containing 1 µl RNAase (10 µg/ml) and transferred to an eppendorf and stored at room temperature for 30 min. Following this, 500 µl of polyethylene glycol (PEG)/NaCl was added, mixed well by inversion, and the eppendorf centrifuged at 10,625 x g for 5 mins. The supernatant was aspirated, and the pellet of plasmid DNA dissolved in 400 µl 1 x TE and an equal volume of phenol-chloroform and mixed well. The tube was centrifuged at 10,625 x g for 3 min, and

the aqueous phase aspirated into a fresh eppendorf. To this eppendorf, 1/10th x volume of sodium acetate was added and mixed well and 2 x total volume of 100% ethanol added, and the tube stored at -20℃ for 5 min. Following this, the tube was centrifuged at 7,378 x g for 10 min after which, the supernatant was aspirated and 200 µl of 70% ethanol (at 4℃) added. Following a brief vortex, the tube was centrifuged at 10,625 x g for 2 min, after which, the supernatant was removed and the tube allowed to air dry at room temperature. Finally, the pellet was dissolved in 500µl 1xTE and stored at -20℃.

The plasmid yield was determined by measuring the optical density (OD) at a wavelength of 260nm using a UV1101 photometer (WPA, Cambridge, UK) since an optical density of 1.0 equates to 50 µg dsDNA/ml at this wavelength.

2.3.9. Transient transfection with Lipofectamine-2000

C33A vector cells and C33AE6 cells were grown as described (section 2.2.1) to 80% confluency whereupon cells were transfected using the lipofectamine-2000 method (Invitrogen, Paisley UK) according to the manufacturer's instructions. Initially, a lacZ reporter plasmid, pcDNA 3.1 V5/his was used to check transfection efficiency. In brief, for one T-25 a 7.5 µl aliquot of lipofectamine-2000 was mixed with 116.7 µl OptiMem (reduced serum medium, Invitrogen, Paisley UK), and in a separate vial, 2.5 µg pcDNA 3.1 V5/his LacZ was mixed with 116.7 µl OptiMem and both vials were incubated for 5 min at room temperature. The contents of both tubes were combined, incubated at room temperature for a further 20 min and added drop wise to the cell culture flasks, containing fresh medium. This was then incubated over night at 37^{o}C/5%$CO_{2.}$

2.3.10. ß-Galactosidase staining

Twenty-four hours post-transfection, the medium was aspirated, the cells were washed once in PBS and fixed with 1 ml 2% paraformaldehyde for 10 min at room temperature. ß-Galactosidase staining solution was prepared (for 1ml of stain: 10 µl 200 mM magnesium chloride, 10µl 400 mM potassium ferricyanide, 10 µl 400 mM potassium ferrocyanide, 50 µl 20 mg/ml X-Gal in 920 µl PBS. Cells were gently washed twice in PBS and 2 ml/T25 of staining solution was added and these incubated at 37℃ for 0.5-2 h until colou r began to develop. Once staining was complete the staining solution was aspirated and the reaction quenched using PBS.

2.3.11. Calculating transfection efficiency

To calculate transfection efficiency, one hundred cells were counted in a vertical line, within 5 random fields of view, using a Nikon Eclipse TS100 microscope. The number of blue transfected cells was expressed as a percentage of the total number of cells counted.

2.3.12. Analysis of transient transfected pZsProsensor-1 vector activity by flow cytometry

Transient transfection of 80% confluent C33A vector and C33AE6 cells with pZsProSensor-1 was carried out as detailed in section 2.3.8 with Lipofectamine-2000 only treated cells used as a negative control. Twenty-four hours post-transfection the medium was aspirated and replaced with fresh medium supplemented with 10 µM MG-132 (Calbiochem, Nottingham, UK) or an equal volume of DMSO (Sigma Aldrich, Dorset, UK). All flasks were incubated at 37℃/5% CO_2 for 4 hrs, after which cells were trypsinised and counted as detailed in section 2.3.3. 1 x 10^6 cells were aliquoted, pelleted by centrifugation at 528 x g for 5 min in a Beckman-GP bench top centrifuge (Beckman Coulter UK Ltd, High Wycombe, UK) and fixed by incubation with 2% paraformaldehyde (PFA) in PBS for 10 min at room temperature. Following this the cells were washed with PBS as above and finally resuspended in fresh PBS prior to analysis by flow cytometry using a Dako Cyan flow cytometry machine (Beckman Coulter UK Ltd, High Wycombe, UK) according to the manufacturers' instructions for the detection of GFP.

2.3.13. pZsProSensor-1 Vector digestion

The pZsProsensor-1 vector was linearised by digestion with Apa-L1 prior to its use for stable transfection since this cuts within the pUC origin of the vector which is not essential for its function in eukaryotic cells (for the supplied vector map see Appendix 1). Ten microlitres of digestion buffer was added to 20 µg vector, along with 1 µl 3% BSA and 2 µl of Apa-L1 which was made up to 99 µl total volume using sterile distilled water. The resulting mix was then placed in a water bath at 37℃ for 75 min, after which a further 1 µl Apa-L1 added and the digestion again incubated for 75 min at 37℃. Agarose gel electrophoresis was carried out to confirm a successful digestion.

2.3.14. Agarose Gel Electrophoresis

Agarose gel electrophoresis was carried out using a thermo Minicell Primo EC320 system according to manufacturers' instructions. Agarose gels were prepared in 1 x tris-acetate-EDTA (1 x TAE) buffer with 2 µl ethidium bromide added per 40 ml agarose gel solution. Sample loading buffer was added to the samples prior to loading into the wells. Appropriate 100 bp and 1 kb DNA ladders (New England Biolabs, Hertfordshire, UK) were separated alongside the samples which were separated by electrophoresis at 80 V for 30 mins. DNA bands were visualised using a UVP GDS 7500 Gel documentation system (Ultra violet Products Ltd., Cambridge, UK)

2.3.15. Post-digestion processing of plasmid

An equal volume of a 50:50 solution of phenol chloroform was added to the digested plasmid and the eppendorf was spun at 14,462 x g for 2 min. The upper phase of the solution was then removed carefully to a fresh eppendorf and 1/10th of the volume recovered of 3M sodium acetate (pH 5.2) was added. The eppendorf was mixed by inversion. Twice the total eppendorf volume of ethanol was then added, and the contents mixed and stored overnight at -20℃ after which the eppendorf was spun for 10 min at full speed. Two hundred microlitres of 80% ethanol was then added, and incubated for 5 min. The eppendorf was again spun at full speed for 5 min, before aspirating the ethanol. Washing with ethanol was repeated once more. Following the final spin, the ethanol was aspirated, and the eppendorf inverted and allowed to air dry. Finally, the pellet was dissolved in 1 x TE buffer providing a stock solution at 1 µg/µl, which was and stored at -20℃ until future use.

2.3.16. G-418 Kill Curve

Prior to using G-418-sulphate / Genetecin® (Invitrogen Paisley UK) for selection of resistant cells it was necessary to identify a suitable concentration of this antibiotic that results in total cell death in 7-10 days. Untransfected SiHa cells were seeded at 1 x 10^6 cells in 5 x T-25 cell culture flasks in complete RPMI-1640 growth medium. Twenty-four hours later, the growth medium was aspirated and replaced with growth medium supplemented with G-418 at a range of concentrations from 200 to 1000 µg/ml. Cells were maintained at 37^{o}C/5%CO_2 and daily visual inspections carried out to assess cell growth and death over a period of 10 days. Following this, cells were washed, resuspended in medium minus G418 and returned to the incubator for a further period to monitor for signs of rebound growth of surviving cells. A G-418 concentration that resulted in 100% cell death in approximately 7-10 days was chosen for selection of stable transfectants.

2.3.17. Stable transfection and single cell colony selection

Stable transfection was carried out on SiHa parent cells as detailed in section 2.3.8, using the pZsProSensor-1 vector linearised in section 2.3.13. Twenty-four hours post-transfection the transfected cells were washed, trypsinised, resuspended in 10 ml medium, as detailed in section 2.3.3, and counted. In order to facilitate single colony isolation, transfected cells were seeded in 9 cm dishes at range of concentrations from 0.25 -10 x 10^5 in a total volume of 15 ml fresh medium. These were incubated overnight then the growth medium was replaced with 15 ml fresh medium supplemented with 500 µg/ml G-418 solution. The cells were monitored over a period of several weeks with a G-418 selection medium change every 2-3 days. Over dense plates were discarded as single colonies could not be discriminated.

Once single celled colonies had expanded to contain approximately 20-30 cells, they were transferred to a 96-well plate. In order to do this, the growth medium was aspirated and the cells were washed in PBS. For colony picking, sterile loops were prepared by cutting the lower rim of a yellow tip and autoclaving. The lower rim of a sterile hoop was coated in sterile Vaseline and gently placed over the colony, a process which was repeated for each colony to be picked. Subsequently, 30 µl of trypsin was added into the sterile hoop and the dish incubated at 37℃ for 2 min, or until complete cell rounding had occurred. Once cells had fully detached they were resuspended in 50 µl RPMI-1640, transferred to a 96-well plate, and made up to a total volume of 200 µl. This was repeated for each colony to be picked, with each colony transferred to a separate well of the 96-well plate. Twenty-four hours later, the growth medium was aspirated from the 96-well plate and replaced with 200 µl medium supplemented with G-418. Cells were expanded before being trypsinised and transferred from 96-well plate to 24-well plates and eventually to 6-well plates with changes of selection medium every 2-3 days.

Cells were eventually transferred to T-25 culture flasks and grown to 80% confluency whereupon stocks of cells were frozen as detailed in section 2.3.4. In total, 4 colonies were successfully picked and expanded to T-25 culture flasks. These colonies were labelled A4, A5, A7 and C5.

2.3.18. Assessment of lopinavir and proteasome inhibition of stable transfected pZsProsensor-1 cells

2.3.18.1. Fluorescent Microscopy

Stable pZsProsensor-1 transfected SiHa cells (SiHa-PSV) were seeded in duplicate wells of an 8-well slide flask (BD Biosciences, Bedford, UK) at a concentration of 2 x 10^4 cells/well in a total volume of 500 µl of growth medium and maintained overnight at 37^{o}C/5%CO_2. Following this the medium was replaced with 500 µl G418 selection medium and the cells allowed to attain 80% confluency. The medium was then replaced with fresh medium supplemented with either 10 µM MG-132 (Merck (Calbiochem), Nottingham, UK) or 25 µM lopinavir and incubated at 37^{o}C/5%CO_2 for 4 and 6 hours respectively. Duplicate wells were treated with an equivalent volume of DMSO as a control. Cells were washed in PBS, treated with 2% paraformaldehyde (PFA) for 10 min, re-washed with PBS and stained with 40 µl 0.5 µg/ml Hoechst 3345 (Sigma-Aldrich, Dorset, UK) for 10mins at room temperature. The cells were rinsed with PBS, the cover slip mounted and the GFP fluorescence visualised using an FITC filter on an Olympus Heinrich widefield microscope (Olympus, Essex, UK) using the Metavue software package.

2.3.18.2. Reverse Transcriptase Polymerase Chain reaction

All RT-PCR work was carried out using an Applied Biosystems - GeneAmp PCR System 2700 (Applied Biosystems, California, USA). Stable pZsProSensor-1transfected SiHa cells were thawed as detailed in section 2.3.2 and grown to a confluency of 80%, at which point they were harvested and counted as detailed in section 2.3.3, and 1 x 10^5 cells transferred to sterile eppendorf and spun at 528 x g for 5 min. Following this, the supernatant was aspirated and PBS used to wash the cells. Cells were pelleted with one final centrifugation at 528 x g, and the PBS aspirated, allowing the pellet to air dry

A master mix of resuspension buffer (Invitrogen, Paisley, UK) and lysis enhancer solution (Invitrogen, Paisley, UK) was prepared at a ratio of 1:9 and 50 µl was used to thoroughly resuspend the cell pellet. This was then transferred to a PCR tube which was heated to 75℃ for 20 min, followed by 5 min at 85℃. A DNAse treatment m aster mix was also prepared containing 7 µl 1 x DNAse (Ambion, Warrington, UK) combined with 2 µl 10 x DNAse buffer (Ambion, Warrington, UK). Subsequently, 9 µl of the DNAse treatment master mix was combined with 11 µl of the RNA sample and this incubated at 37℃ for 90 min follow ed by 5 min at 75℃. The remaining RNA sample was stored at -80℃ for future use. Reverse transcription (RT) master mix (A) was prepared which contained 6 µl dNTP mix (Roche, West Sussex, UK) and 9 µl random decamer mix. A 5 µl volume of this was added to the DNAse-treated RNA sample which was heated to 70℃ for 3 min and then placed on ice for 3 mins. Prior to the RT step, 5 µl of this sample was removed and mixed with 5 µl sdH_2O to act as an RT negative control. For the RT step, master mix (B) was prepared which contained 7 µl 5 x RT buffer, 7 µl sdH_20, 0.5 µl of RTase and 0.5 µl RTase inhibitor and 15 µl of this was then added to the sample tube. The RT step was carried out by heating to 42℃ for 60 min followed by 10 min at 70℃. The final cDNA samp le volume of 35 µl was then stored at -20℃ for future use. All RT reagents were purchased from Bioline, London, UK.

The PCR step was carried out using a master mix containing 10µl Biomix red (Bioline, London, UK), and 0.5 µl of pZsProSensor-1 specific forward and reverse primer (from 20pmol stock solutions), detailed in (Appendix 3), and 1 µl cDNA sample in a total reaction volume of 20µl. Thermal cycle parameters are detailed in Appendix 3. Agarose gel electrophoresis was used to visualise PCR products, as described in section 2.3.14.

2.4. Results

2.4.1. Transient transfection of C33A vector and C33AE6 cells with pZsProSensor-1 vector

The results of the ß-Galactosidase staining (section 2.3.10) of pcDNA 3.1V5/His LacZ transfected C33A vector and E6 cells is shown in Figure 2.2. It demonstrates equivalent levels of transfection between cell types (Representative Figures are shown). Figure 2.3 shows the results from the flow cytometry analysis of pZsProSensor-1 transfected C33A vector and E6 cells following MG-132 treatment. Each data set was repeated in triplicate. Mean values, standard deviations and p values were calculated in Microsoft Excel, and a p value below 0.05 was considered significant.

Figure 2.2 - Transient transfection of C33A vector and C33AE6 cells with pZsProSensor-1 vector – B-Galactosidase staining

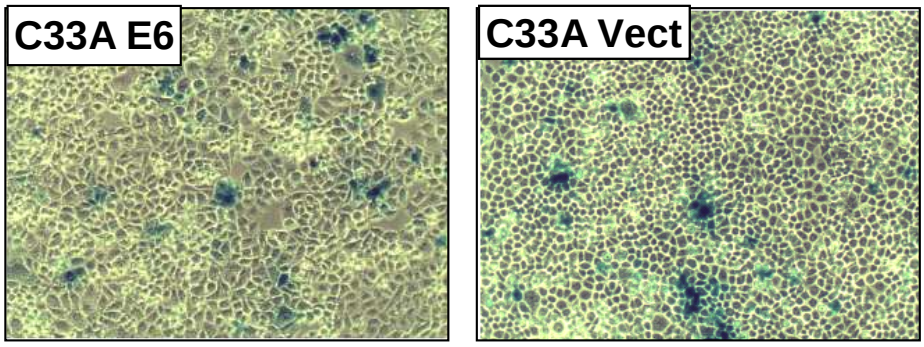

Figure 2.2 - In order to confirm transfection efficiency C33A vector and C33AE6 cells were transiently transfected using a lacZ expressing plasmid (pcDNA 3.1 V5/his LacZ). Twenty-four hours following transfection, cells were fixed and stained for ß-Galactosidase activity. ß-Galactosidase staining was similar in vector and E6 cells. Representative images from several fields of view.

Mean values for each cell type are shown below in Figure 2.3. Untransfected cells, as expected, produced only minimal background interference. Both C33A vector and C33AE6 pZsProSensor-1 transfected cells demonstrated an increase in GFP signal, however as these cells contain an active proteasome, the newly synthesised GFP was rapidly targeted for proteasomally mediated degradation. In contrast, the levels of GFP in pZsProSensor-1 transfected C33A vector and C33AE6 cells were significantly elevated following MG-132 treatment, when compared to corresponding pZsProSensor-1 transfected untreated cells ($p<0.01$ for both C33A vector and C33AE6 cells).

Figure 2.3 Flow cytometry analysis of pZsProSensor-1 transiently transfected C33A vector and E6 cells

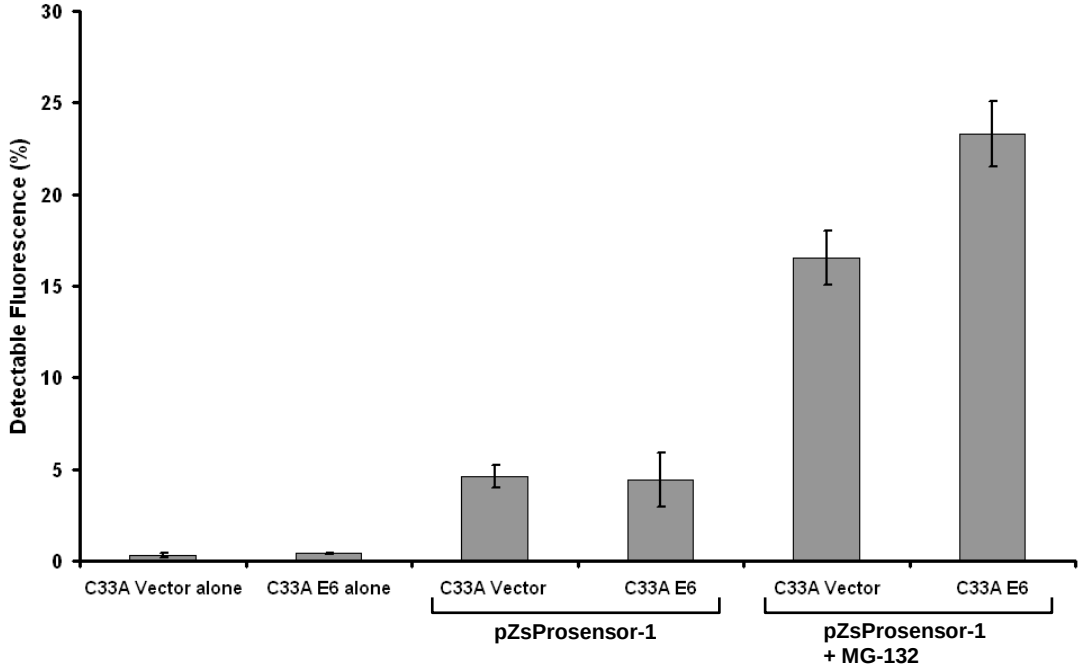

Figure 2.3 - C33A vector and C33AE6 cells were transiently transfected with pZsProSensor-1. Duplicate samples of C33A vector and E6 cells were treated with MG-132 for 4hrs at 10µM after which, cells were harvested and counted. 1 x 10^6 cells were fixed and processed for flow cytometry analysis. Green fluorescence protein levels were measured and expressed as a percentage for each cell type, both with and without MG-132 treatment. Values shown are mean values from a triplicate data set from a single experiment. Standard deviations were calculated in Microsoft Excel 2003.

Interestingly, the data also demonstrated that following MG-132 treatment of pZsProSensor-1 transfected C33A E6 cells resulted in a significantly higher GFP expression ($p<0.05$) than the corresponding C33A vector cells.

2.4.2. Production of a pZsProSensor-1 stable transfected cell line

2.4.2.1. Stable Transfection

SiHa cells were stably transfected pZsProSensor-1 vector after this was linearised by digestion with Apa-L1 which cuts within the pUC origin of the vector. Successful digestion of the vector was confirmed by agarose gel electrophoresis, on a 1% agarose gel (section 2.3.14) as shown in Figure 2.4.

Figure 2.4 Confirmation of Restriction Digest of pZsProSensor-1 vector using Apa-L1 restriction enzyme

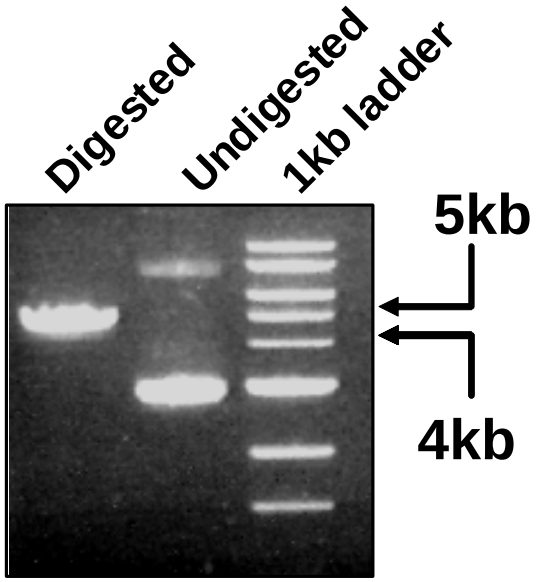

Figure 2.4 – Successful digestion of pZsProSensor-1 was confirmed by agarose gel electrophoresis. Undigested vector was included for control purposes. The digested plasmid presented a band of the expected size, approximately 4.8kb.

Following linearisation and stable transfection, 4 colonies (termed A4, A5, and A7 and C5) were successfully picked and expanded from 9 cm dishes, to T-25 culture flasks. Aliquots of each expanded stable cell colony were frozen for long term storage in liquid nitrogen (section 2.3.4).

2.4.2.2. Confirmation of pZsProSensor-1 expression by fluorescent microscopy

The results following fluorescent microscopy assessment of GFP levels are shown below in Figure 2.5. Of the 4 cell lines tested, both ‘C5’ and ‘A4’ cells produced detectable levels of GFP following proteasomal inhibition with 10 µM MG-132 treatment, indicating a functional proteasome sensor vector. Surprisingly, GFP was not detected in any of the remaining cell lines.

Figure 2.5 – Fluorescent microscopy on pZsProSensor-1 stable transfected SiHa cells following proteasomal inhibition with MG-132

C5 pZsProSensor-1 Transfected cell
No Proteasome inhibition

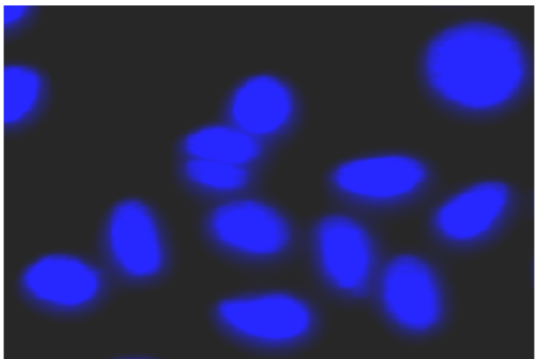

C5 pZsProSensor-1 Transfected cell
10 µM/ 4hr incubation with MG-132

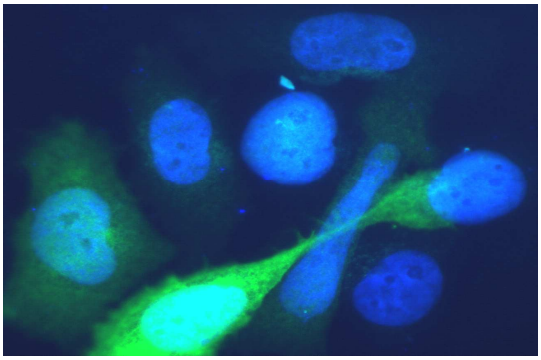

Figure 2.5 –stable transfected cells were cultured to 80% confluency then treated with MG-132 at a final concentration of 10µM for 4hrs, before being fixed and counterstained with Hoechst 3345 nuclear counter stain. GFP was visualised using a FITC filter on an Olympus Heinrich widefield microscope at the Michael Smith Building, University of Manchester. Images acquired using the Metavue software package. A GFP signal was observed in pZsProSensor-1 transfected SiHa treated with MG132 whereas the same cells without MG132 showed no signal.

2.4.2.3. Confirmation of pZsProSensor-1 expression by RT-PCR

Having used fluorescent microscopy to confirm the pZsProSensor-1 was functioning correctly in stable transfected SiHa cells reverse transcriptase polymerase chain reaction (RT-PCR) analysis of stable pZsProSensor-1 transfected SiHa cells was carried out to confirm the integration and stable expression within the cell line (as described in section 2.3.18.2). RT-PCR data are shown below in Figure 2.6.

Figure 2.6 –RT-PCR analysis of pZsProSensor-1 stable transfected SiHa cells

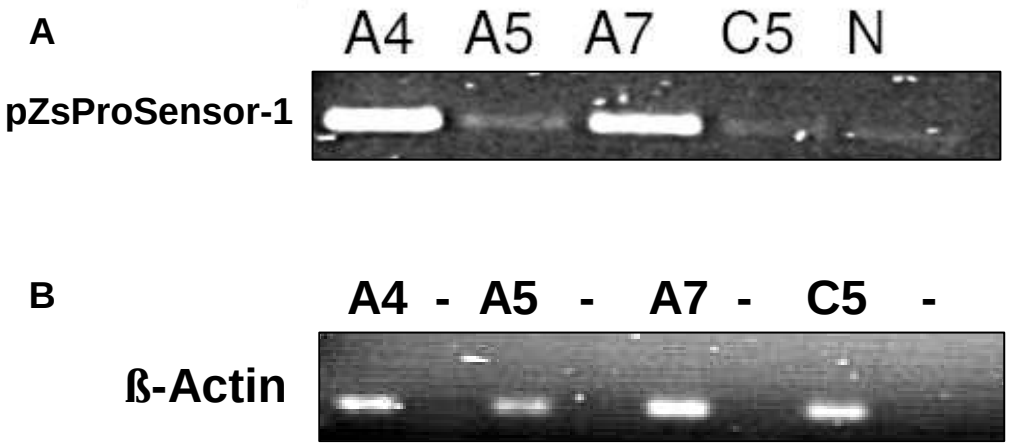

Figure 2.6 - Stable transfected cells were cultured. At 80% confluency cells were harvested and counted and cell pellets of 1 x 10^5 cells used to generate cDNA for each cell line. PCR products visualised with agarose gel electrophoresis and ethidium bromide staining. (A) PCR was carried out using pZsProSensor-1 specific primers (A4,A5,A7,C5, stable transfected cell colonies; N, PCR negative control) (B) PCR was also carried out using ß-actin specific primers to confirm equal loading. RT negative control samples (-) were also included to rule out genomic contamination of cDNA samples.

RT-PCR confirmed the presence of pZsProSensor-1 vector within the cell lines. PCR using ß-Actin specific primers demonstrated the four cDNA samples were well balanced and free from genomic contamination (Figure 2.6(B)). PCR carried out using the pZsProSensor-1 primers demonstrated the presence of pZsProSenso-1 sequences within the cell line although the signal strength varied significantly between samples (Figure 2.6(A)). Colonies ‘A4’ and ‘A7’ produced markedly stronger signals than both the ‘C5’ and ‘A5’ colonies, however the C5 colony was the only cell line to produce easily detectable levels of GFP.

2.4.3. pZsProSensor-1 activity, following lopinavir treatment, assessed by fluorescent microscopy

Previous data demonstrated that the ‘C5’ colony stable transfected cell line produced high levels of detectable GFP following proteasome inhibition mediated by MG-132 treatment (Figure 2.5). RT-PCR also demonstrated the presence of pZsProSenor-1 within this cell line (Figure 2.6).

The ability of lopinavir to inhibit the proteasome in these stably transfected HPV positive cell line was assessed using ‘C5’ cells. Figure 2.7 demonstrates that lopinavir leads to a substantial

increase in visible GFP in pZsProSensor-1 stable transfected cell lines, when compared to both DMSO treated stable transfected control and MG-132 treated cells.

Figure 2.7 - Fluorescent microscopy analyses of stable transfected pZsProSensor-1 SiHa cells following lopinavir treatment

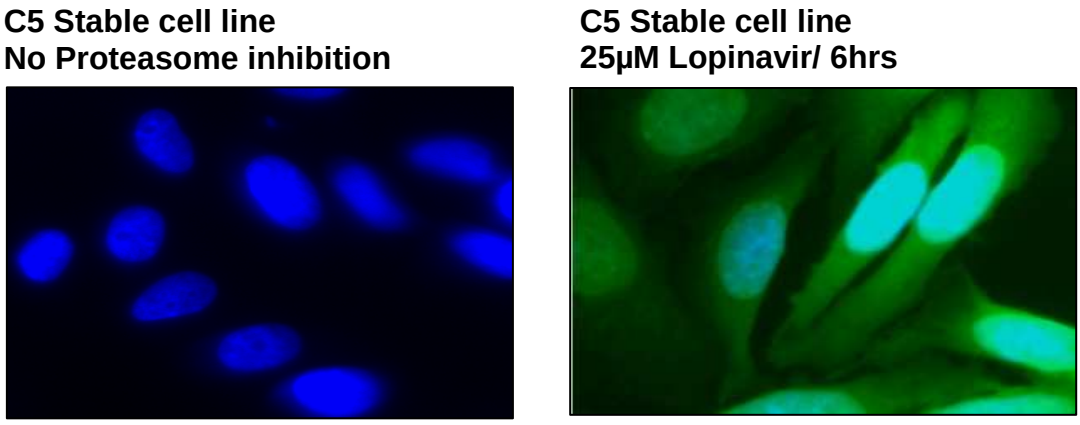

Figure 2.7 – Fluorescent microscopy analysis of stable transfected SiHa cells expressing the proteasome sensor vector pZsProSensor-1. Cells were cultured in slide flasks to a confluency of 80%, at which point one well was treated for 6hrs with lopinavir at a final concentration of 25µM. The control cells were treated with an equal volume of DMSO. Cells were fixed and stained with a nuclear counterstain. GFP was visualised using a FITC filter on an Olympus Heinrich widefield microscope. Lopinavir treated cells demonstrated extremely high levels of GFP when compared to untreated transfected control cells.

2.5. Chapter Summary and Discussion

MG-132 is a potent (Ki = 4 nM) reversible, and cell-permeable proteasome inhibitor. However, although potent, MG-132 lacks specificity and it is known that wide spread non-specific proteasome inhibition is toxic in both *in vitro* [98] and *in vitro* settings [193] clearly limiting the potential clinical use of MG-132 outside laboratory test systems. In contrast, previous work has demonstrated the ability of lopinavir to selectively inhibit the human cellular proteasome [129, 130]. More importantly, previous work carried out in this laboratory has demonstrated that lopinavir treatment of SiHa cells specifically inhibited the chymotrypsin-like activity of the proteasome, producing a 7% reduction in activity [98]. This could potentially eliminate the toxicity associated with non-specific proteasomal inhibitors.

The pZsProSensor-1 proteasome sensor vector was used to further assess the ability of lopinavir to inhibit the proteasome in several cell lines, namely HPV negative C33A and HPV positive SiHa cell lines. Transient transfection of C33A vector and C33AE6 cells with the pZsProSensor-1 using the lipofectamine-2000 method was carried out in order to confirm the vector was functioning correctly. Flow cytometry analysis of transiently transfected C33A Vector and E6 cells demonstrated a significant increase in detectable GFP levels in both C33A vector ($p<0.01$) and C33AE6 ($p<0.01$) following MG-132 treatment (Figure 2.3). Surprisingly, the data also demonstrated that HPV E6 expressing cells produced a significant increase in detectable GFP following MG-132 treatment when compared to pZsProSensor-1 transfected vector cells. As preliminary experiments with the pZsProSensor-1 vector, this data confirmed the vector was functioning as expected within the cell line.

Stable transfection using linearised vector was carried out in order to generate SiHa cells stably expressing the pZsProSensor-1 vector. Following RT-PCR analysis to confirm pZsProSensor-1 expression within cells, fluorescent microscopy on stable transfected cells following treatment both with MG-132 (Figure 2.5) and lopinavir (Figure 2.7) demonstrated marked accumulation of GFP within the cells. However, whilst fluorescence microscopy clearly demonstrated detectable GFP within both MG-132 and lopinavir treated cells, RT-PCR data generated interesting results, as can be seen in Figure 2.6. The C5 clone of pZsProSensor-1 vector cells demonstrated a low RT-PCR signal, in contrast to both the A4 and A7 clones which both demonstrated high expression of pZsProSensor-1 vector, yet undetectable levels of GFP. This may relate to random integration-generated errors within in the pZsProSensor-1 vector or difficulties associated with mRNA transcript processing. Fluorescence-coding transcripts are being synthesised by the C5 colony cells, as evidently without these, we would not detect any GFP through microscopy. It may simply be that the low expression level seen for C5 colony cells in Figure 2.6 represents basal transcript levels. Highly efficient ribosomal processing of GFP mRNA transcripts would result in their limited detection. In contrast random integration events may have resulted in an altered mRNA transcript sequence from the remaining stable cell lines. An inability of a transcript to be successfully processed in the ribosome would ultimately result in failure to

synthesise GFP protein, as was observed with the current findings. In addition, this may also result in an accumulation of transcripts, as was seen in Figure 2.6.

The consequences of targeted proteasome inhibition on the cellular protein expression profile of lopinavir treated HPV positive cells will be assessed in subsequent chapters.

2.6. Further work

The data presented in this chapter has demonstrated that the proteasome in SiHa cells, C33A vector and C33AE6 is inhibited following incubation with lopinavir/MG-132 at a fixed concentration, as has previously been demonstrated [129-131]. This does not, however, demonstrate the dose or time dependent nature of the inhibition process; is the lopinavir induced inhibition of the proteasome a simple on/off switch? Does the proteasome function gradually degrade with an increasing concentration of lopinavir, or following an extended increase in incubation time? Time and dose dependent assays of proteasome function could be carried out, with the proteasome function assessed by means of flow cytometry initially. Facilities permitting, live fluorescent imaging of cells could also be carried out using cells treated with both an escalating lopinavir dose and also an increasing lopinavir incubation period, which would provide a more precise understanding of the exact time scale of proteasomal inhibition in SiHa cells exposed to lopinavir.

3. Toxicity studies – long and short term effects of lopinavir

3.1. Introduction

Prior to studying the ability of lopinavir to influence the protein expression profile in HPV positive cells, its toxicity was assessed by two means; The effects of continuous short term exposure were evaluated by a colourimetric growth assay whereas the long term effects of a brief exposure were determined by clonogenic assay.

The colourimetric CellTiter 96® AQ_{ueous} One Solution reagent (Promega, Southampton, UK) contains a tetrazolium compound (3-(4,5-dimethylthiazol-2-yl)-5-(3-carboxymethoxyphenyl)-2-(4-sulfophenyl)-2H-tetrazolium, inner salt; MTS) and an electron coupling reagent (phenazine ethosulfate, PES). The MTS tetrazolium compound interacts with PES and is bio-reduced by living cells to produce a coloured product, formazan. The development of the formazan product is therefore directly proportional to the number of proliferating viable cells, and its absorbance can be measured at 490 nm. This assay is therefore a quick, efficient alternative to other isotope based cell proliferation assays, such as those utilising [^{3}H]-Thymidine incorporation.

The second assay, the clonogenic assay, is best defined by Nicolaas Franken *et al.,(2006)* as "*an in vitro cell survival assay based on the ability of a single cell to grow into a colony. The colony is defined to consist of at least 50 cells. The assay essentially tests every cell in the population for its ability to undergo 'unlimited division*." [194]. Consequently, the clonogenic assay is therefore an extremely useful tool by which to assess the ability of cells to form viable progeny following a short exposure to drug or treatment agent that may limit replicative potential [195]. The first use of the clonogenic assay was described by Puck and Marcus, in which they investigated the effects of ionizing radiation on the colony forming abilities of HeLa cervical cancer cells [196].

Interestingly, this type of assay was recently used to investigate the long term effects of treatment with low dose cidofovir, a viral DNA polymerase inhibitor licensed for the treatment of cytomegalovirus infections. This drug is currently being used off-license to treat HPV related recurrent respiratory papillomatosis (RRP). Infection with HPV types 6 and 11 has been implicated in respiratory tract head and neck squamous cell carcinomas (HNSCC), specifically the development of squamous papillomas of the larynx, a condition known as recurrent respiratory papillomatosis (RRP) [197-202]. Reviewed in Stamataki *et al.* (2006), RRP has a bimodal age distribution with cases observed in adults in later life, but the more problematic cases are those that occur in juvenile patients (≤ 5 years of age) [203]. The current treatment of choice is surgical excision which aims to maintain an open airway preventing asphyxiation and also to improve speech, however recurrence is quite common. Repeated surgical procedures can severely affect quality of life in the patient as well as imposing a financial burden [203]. Surprisingly, and rather worryingly it was recently shown that cidofovir actually improved the survival and cell growth of cells expressing either low or high risk HPV E6 proteins [204]. This data clearly demonstrates the importance of correctly controlling dosage, treatment time and treatment interval in the management of RRP, and in the implementation of any prospective new drug indication.

3.2. Aims

3.2.1. Assessment of the short term toxicity of lopinavir in a range of HPV positive and HPV negative cell lines using colourimetric cell proliferation assays

3.2.2. Assessment of the effects of lopinavir on long-term cellular replication competency by clonogenic cell survival assays

3.3. Methods

3.3.1. Cell culture of Tert cells

3.3.1.1. Thawing Tert Cells

Aliquots of Tert cell line were removed from liquid nitrogen and rapidly but gently thawed in a water bath at 37℃. Tert cells are a karyotypically normal telomerase-immortalised human keratinocyte cell line that demonstrates a down regulation in the expression levels of $p16^{INK4a}$, a cyclin D/cdk inhibitor [205]. E6 Expressing Tert cells, generated previously [206], were also used. Whilst C33A and C33AE6 cells provide a model test system for assessing E6-mediated effects of lopinavir in cell culture, they are however, a fully transformed cell line. In contrast, parental Tert cells are a karyotypically normal non-transformed cell line, and are potentially more representative of the intended target cell; non-transformed precancerous cervical lesions. In addition, stable E6-expressing Tert cells allow for assessment of E6-dependent effects.

Once thawed, the cells were transferred to a 50 ml falcon tube using a Pasteur pipette. Ten millilitres of warmed keratinocyte serum free medium (Invitrogen, Paisley, UK) supplemented with 100 ng epidermal growth factor (EGF) (Invitrogen, Paisley, UK), 25 µg/ml bovine pituitary extract (Invitrogen, Paisley, UK) and 0.3 M calcium chloride, was then added to the cell suspension drop wise, whilst gently mixing the cells after which these were pelleted by centrifugation at 528 x g for 5 min. Following centrifugation the supernatant was aspirated and the pellet thoroughly resuspended in 10 ml complete serum free medium before being split equally between two T-75 flasks. Culture flasks were made up to a total volume of 20 ml with complete medium and cells were then incubated at 37℃ in a humidified atmosphere containing 5% CO_2.

3.3.1.2. Sub culture of Tert Cells

During routine passage, Tert cells were not allowed to exceed 30% confluency as they become difficult to detach from the culture flask surface if this occurs. At 30% confluency, the growth medium was aspirated and the cells washed once in PBS. Cells were trypsinised with 500 µl trypsin, and returned to the incubator for 3-4 min to ensure complete cell detachment. Trypsin was neutralised and the cells were resuspended in 10 ml neutralising medium, composed of Ham F-12 nutrient mix (Invitrogen, Paisley, UK) supplemented with 10% bovine serum, before being centrifuged at 528 x g for 5 min. The supernatant was aspirated and the cell pellet resuspended in 10 ml keratinocyte serum free medium. Cells were counted and new flasks seeded at 0.5 x 10^6 cells/T-75 flask in a total volume of 20 ml.

3.3.1.3. Freezing Tert cells

Tert cells were frozen in freezing medium consisting of a 50/50 mix of keratinocyte serum free medium and Ham F-12 nutrient mixture, supplemented with 10% DMSO and 10% bovine serum. Cells were harvested and counted as detailed above in section 3.2.1.2 before being pelleted by centrifugation 528 x g for 5 min and the supernatant aspirated. The cells were resuspended in an appropriate volume of freezing medium to provide a cell suspension at 0.5 x 10^6 cells/ml, and 1ml aliquots frozen overnight at -80°C in an isopropanol freezer gradient pot, before being transferred to liquid nitrogen for long term storage.

3.3.2. AQ-96 cell proliferation assay to assess short term toxicity of lopinavir

Prior to studying the long term effects of lopinavir on cell proliferation, the short term effects were assessed using a range of untransfected and stable transfected cells. Samples of SiHa, Tert parent, Tert vector and Tert Type 16 E6 were harvested and counted (as detailed in sections 2.3.3 and 3.3.1.2). Cell proliferation was assessed using the AQ-96 reagent assay (Promega, Southampton, UK).

Cells were seeded at 2 x 10^3 cells/ well in a total volume of 200 µl, in each well of a 96 well plate with one full 96 well plate seeded per cell type. Twenty four hours post-seeding, 20 µl of the AQ 96 reagent was added to the first three wells of each row in order to provide a time zero (T0) data point, and the plates returned to the incubator. Two hours post-incubation, absorbance at 490 nm was measured for each triplicate using a Dynex MRX plate reader (Dynex Technologies, West Sussex, UK).

Following this, the growth medium from the remaining wells was aspirated and replaced with 200 µl RPMI-1640 supplemented with lopinavir at concentrations ranging from 5 µM to 30 µM, with DMSO volumes adjusted to remain constant. One full row was used for each drug concentration. Untreated and DMSO-only treated cells were included as controls and the plates were then returned to the incubator. Assessment of cell proliferation using AQ-96 reagent was repeated at 24, 48 and 72 hrs following the addition of lopinavir.

3.3.3. Effects of lopinavir on the long term survival of cells

A novel 96-well based clonogenic cell survival assay [207] was used to assess the long term survival of cells following short term exposure to lopinavir. Parental Tert and stable HPV 16 E6 expressing (Tert HPV T16 E6) cells were used to assess the effects of lopinavir treatment on their long term survival. Prior to this assay a colourimetric AQ-96 dose response growth assay (as described in section 3.3.2) was carried out to determine the susceptibility of all Tert cells to lopinavir.

Triplicate cell culture flasks of parental Tert, Tert HPV T16 E6 cells and Tert cells stably transfected with empty vector were cultured for 2 or 4 days in growth medium supplemented with

either DMSO control or lopinavir at a concentration of 7 µM (high dose) or 5 µM (low dose) in a total volume of 20 ml complete serum free medium. DMSO levels were adjusted to remain constant. Treatment time periods were staggered so that all flasks were trypsinised harvested and counted simultaneously (as described in section 2.3.3). The cell suspension was diluted using complete serum free medium to a concentration of 15 x 10^3 cells/ml.

Using a 96 well plate for each cell type, 200 µl cell suspension of untreated, low dose treated and high dose treated cells were each added to three wells in row A of the 96 well plate. Two hundred microlitres of complete serum free medium without lopinavir was added to the remaining wells in rows B to H. Into row B, 100 µl of cell suspension was added and thoroughly mixed. From row B, a 1/3 serial dilution was carried out to providing cells from concentrations of 3000 cells/well down to 1 cell/well in row H. Cells were returned to the incubator and allowed to proliferate at 37℃/ 5% CO_2 for a further 7 days, with one change of growth medium at 72 hrs. After 7 days, viable cells were measured by the addition of 20 µl AQ-96 reagent to all wells and optical densities (measured at 490nm) were measured using a Dynex MRX plate reader (Dynex Technologies, West Sussex, UK) 2 hrs post-incubation.

A visual appreciation of cell growth was obtained by toluidine blue staining (Sigma Aldrich, Dorset, UK). The growth medium was aspirated from all wells, and the cells gently washed once in PBS and stained by 10 min incubation with 200 µl toluidine blue, before being gently washed twice in PBS and the plates inverted and allowed to air dry.

3.3.4. AQ-96 Cell proliferation assay of lopinavir treated E6/E7 immortalised and control PHFKs

Stable E6/E7 immortalised primary human foreskin keratinocytes (PHFKs) were treated with lopinavir at concentrations between 5 µM and 40 µM and cell growth assessed at 72 hours by means of the CellTiter 96® AQ_{ueous} One Solution Cell Proliferation Assay (AQ-96 assay) (Promega, Southampton, UK). This work was carried out in the laboratories of Professor Ingeborg Zehbe (Lakehead University, Thunder Bay, Ontario, Canada), and the data is provided with kind permission of this group (See Batman et al., 2011, accompanying Antiviral Therapy manuscript).

3.4. Results

3.4.1. AQ-96 cell proliferation assay to assess short term toxicity of lopinavir

The effects of an escalating dose of lopinavir on the growth of SiHa cells were assessed initially. Figure 3.1 depicts the 72hr AQ-96 data expressed as percentage growth change (mean values from triplicate data points) for SiHa. Lopinavir had no noticeable effects on SiHa cell growth at the lower concentrations used with concentrations below 15 µM having little effect on cell growth. Lopinavir produced a clear dose-dependent inhibition of growth in SiHa cells at concentrations of 15µM and above (Figure 3.1).

Figure 3.1 – 72 hr AQ-96 Cell Proliferation assay in SiHa cells exposed to an escalating dose of lopinavir

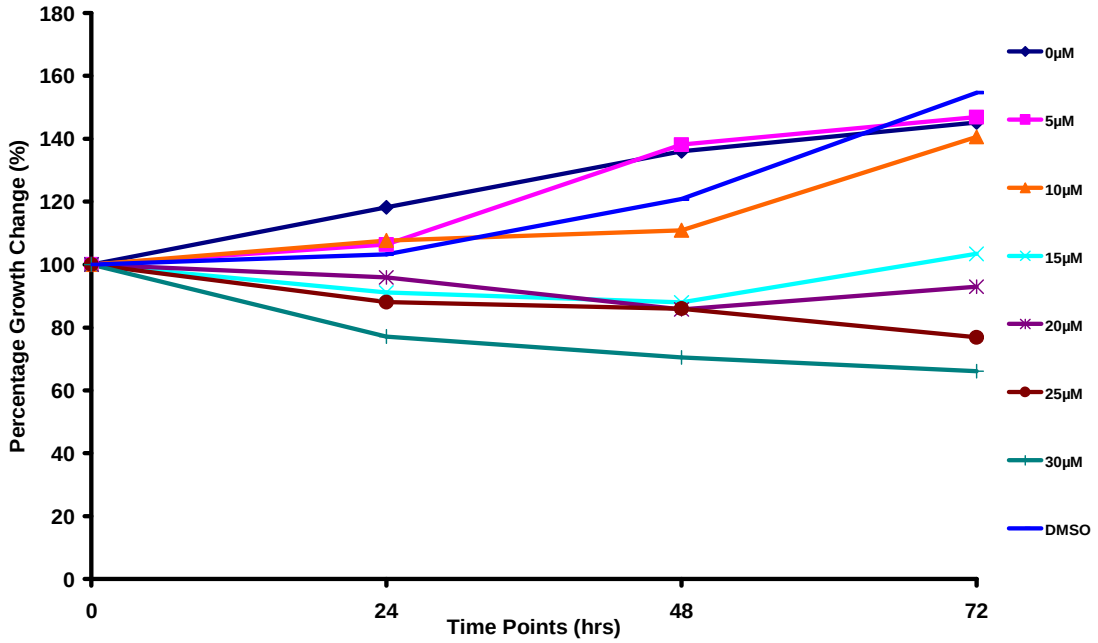

Figure 3.1 – A 72hr cell proliferation assay was carried out using SiHa with an escalating dose of lopinavir. Viable cell numbers were measured at the time points indicated using AQ-96 reagent. Data is presented as percentage growth change based on triplicate data for each time point, based on a single experiment. Lopinavir produced dose-dependent growth inhibition. The growth of SiHa cells was unaffected at concentrations below 10µM. Data is presented in terms of percentage change in growth and is based on triplicate data from a single experiment.

The effects of lopinavir on parental Tert cells, vector cells and Tert cells stably expressing the HPV T16 E6 protein (Tert-HPV 16 E6) were then assessed. The data from this set of cell proliferation represents triplicate data points from one assay, and is shown below in Figure 3.2.

Figure 3.2 – 72hr AQ-96 cell proliferation assay using Tert parent, Tert Vector and Tert T16E6 cells and an escalating dose of lopinavir

A – 72hr growth curve, lopinavir treated Tert Parent cells

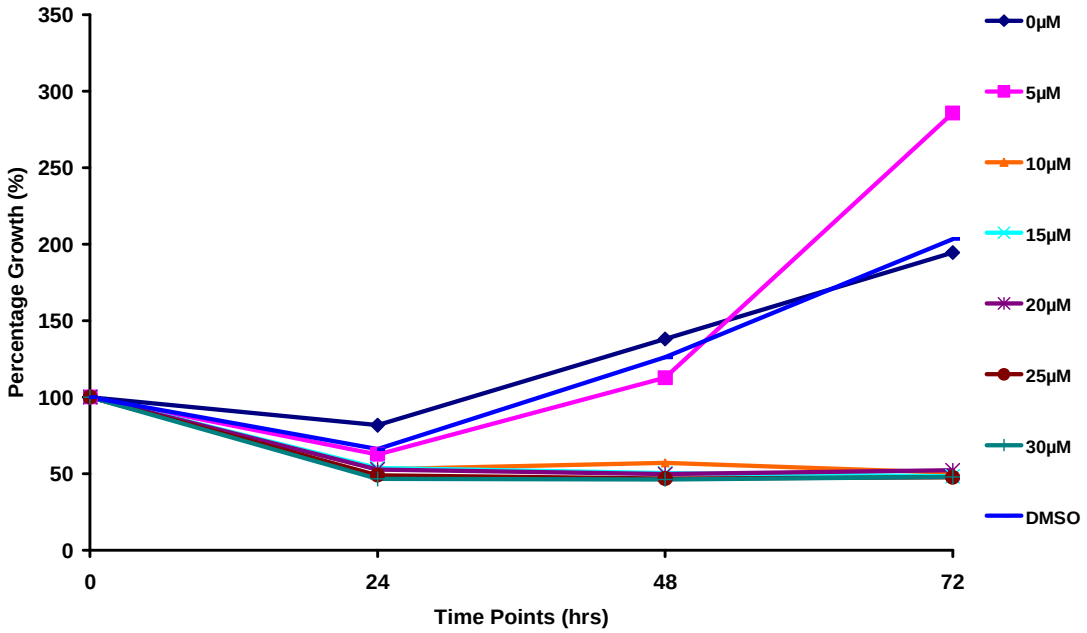

B – 72hr growth curve, lopinavir treated Tert HPV vector control cells

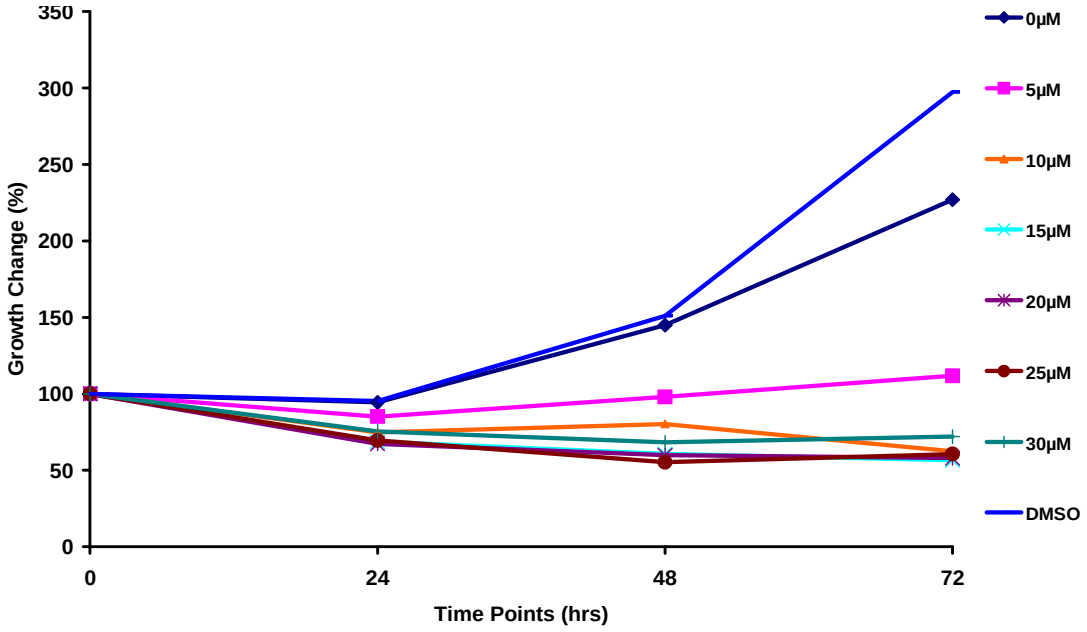

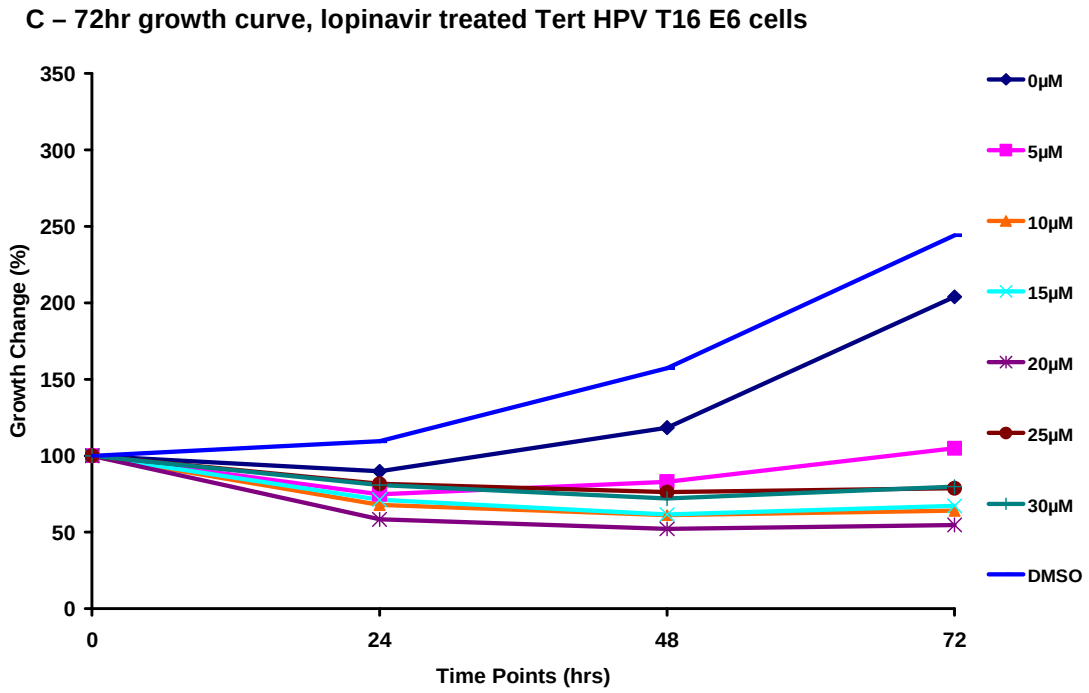

Figure 3.2 - A 72hr Cell proliferation assay was carried out using parental Tert cells (panel A) Tert vector cells (panel B) and Tert HPV T16 E6 cells (panel C) treated with an escalating dose of lopinavir. Viable cell numbers were measured at the time points indicated using AQ-96 reagent. Data is presented as percentage growth change based on triplicate data for each time point. In comparison to SiHa cells (Figure 3.1) Tert parent cells (panel A) were shown to be much more susceptible to lopinavir treatment, with lopinavir concentrations over 5μM inhibiting cell growth. Compared to Tert parent (panel A) cells, Tert vector (panel B) and Tert T16E6 (panel C) cells were more susceptible to lopinavir. In these cells 5μM lopinavir was shown to also inhibit cell proliferation over 72 hrs. Data is representative of triplicate data points from a single experiment.

In comparison to SiHa cells (Figure 3.1) the full range of Tert cells (Figure 3.2 A, B & C) were shown to be much more susceptible to lopinavir treatment. Lopinavir concentrations as low as 10 μM was shown to inhibit cell growth in Tert parent cells over 72 hrs. Curiously parental Tert cells grown in the presence of 5 μM lopinavir were shown to actually outgrow both DMSO treated control and untreated control cells over the 72 hr time period. Whilst this enhancement in growth was not shown to be significant based on triplicate data points, it was however indicative of an effect which should be further investigated with clonogenic assays.

In comparison to Tert parent cells, Tert vector cells (panel B) and Tert T16E6 cells (panel C) were again, more susceptible to lopinavir with concentrations as low as 5 μM lopinavir also noticeably inhibiting cell proliferation over 72 hrs.

3.4.2. Long term survivability of Tert cells exposed to lopinavir

The long term survival of cells following a brief exposure to lopinavir was assessed using a novel clonogenic assay as described by Donne *et al.,* (2009) [207]. After a visual appraisal of toluidine blue staining, DMSO treated cells were shown to have similar growth levels at both 2 day and 4 day time points in matched cell lines and at matched cell numbers. Both low and high dose lopinavir treatment led to a relatively equal increase in the growth of Tert parent cells following exposure for 2 days and 4 days. Tert T16 E6 cells were shown to grow noticeably more than Tert parent cells at all time and lopinavir dose points. When looking at Tert T16 E6 cells (wells seeded with 333 cells), high dose exposure appeared to induce a greater level of cell growth than low dose exposure, at both treatment time points. When compared to the 2 day treatment time point, the 4 day treatment with low dose lopinavir appeared to inhibit cell growth of Tert T16 E6 cells, when compared to DMSO treated control T16 E6 cells.

Statistical analysis based on data generated by the AQ-96 assay was carried out in section 3.3.3.

Figure 3.3 Toluidine blue staining of Tert parents and Tert T16 E6 cells exposed to short term doses of lopinavir and grown for a subsequent 7 days

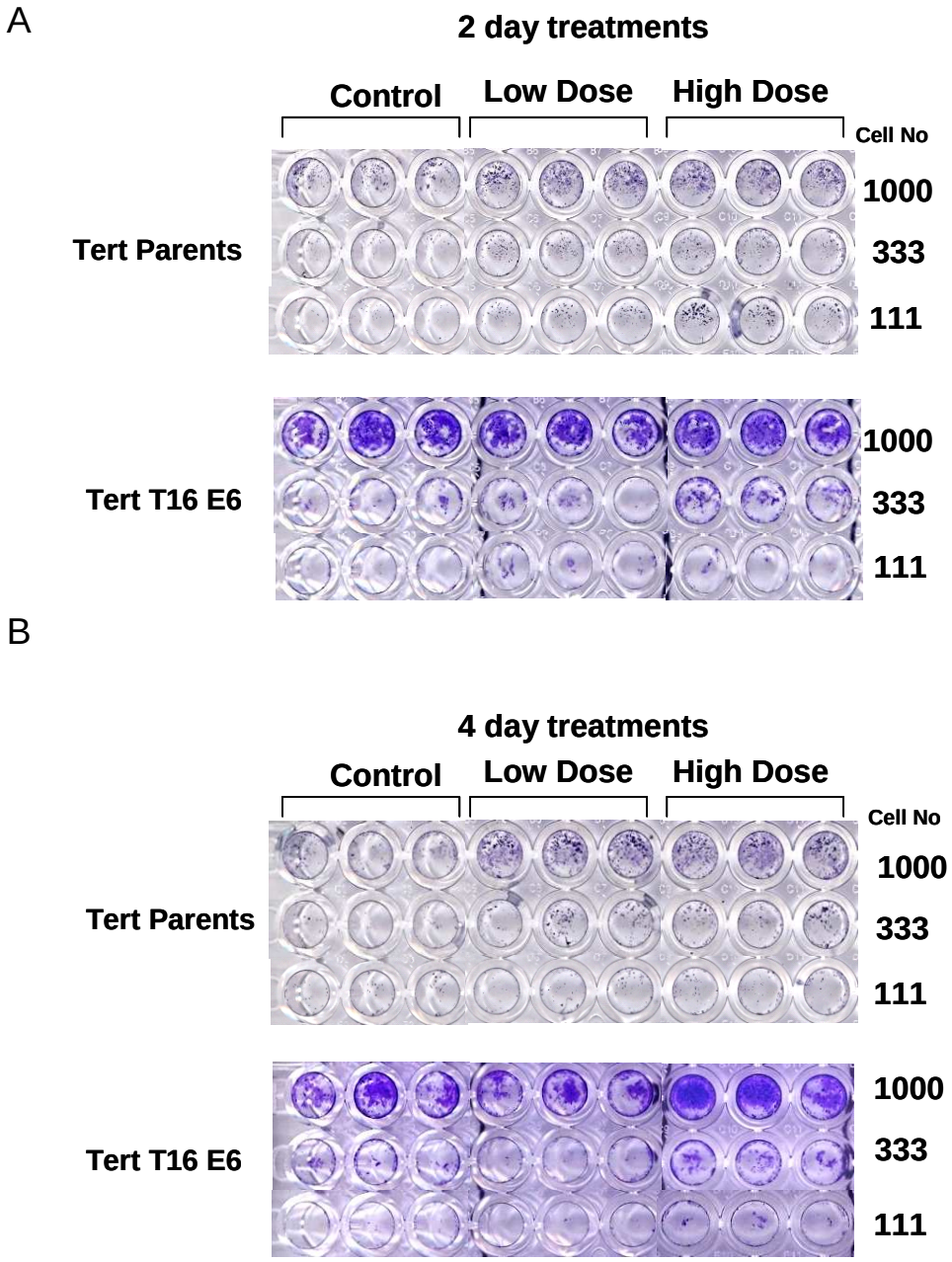

Figure 3.3 – Tert parent and Tert T16 E6 cells were grown for either 2 (Figure 3.3 (A)) or 4 days (Figure 3.3 (B)) in the presence of low and high doses of lopinavir. DMSO treated cells were included for control purposes. Cells were harvested and re-seeded at a range of cell numbers and allowed to grow for a further 7 days, before being stained with toluidine blue. Images are shown for wells seeded with 1000, 333 and 111 cells. DMSO treated cells were shown to have similar growth levels at both 2day and 4day time points in both cell lines and at both cell numbers. Both low and high dose lopinavir treatment were shown to increase growth of Tert parent cells relatively equally following exposure for 2 days and 4 days. Tert T16 E6 cells were shown to grow noticeably more than Tert parent cells at all time and lopinavir dose points. When looking at Tert T16 E6 cells (333 cells seeded), high dose exposure appeared to produce a greater level of cell growth than low dose exposure, at both time points. In the 4 day treatment data set, low dose treatment appeared to inhibit cell growth in Tert T16 E6 cells.

3.4.3. Colourimetric Clonogenic Assay – AQ-96 data

The AQ-96 data is shown in Figure 3.4. Control DMSO Tert T16 E6 cells were shown to out grow Tert parents at all levels. In order to account for this variation in starting cell number of untreated control cells from each group, a one-way ANOVA was performed to find a point at which starting cell numbers provided similar starting densities. The vertical arrows represent the starting cell numbers that were optimal for analysis across both cell times and both drug treatment time points.

For each triplicate, consisting of control, low dose and high dose treated cells, a one-way ANOVA was performed followed by Dunnett's post hoc test to find where, if any, significant differences occurred. Dunnett's post hoc test allows comparison of each experimental test sample (low dose and high dose), within each group, to a nominated control group (DMSO treated control). P values below 0.05 were considered significant.

Statistical analysis of the data indicates that 2 days exposure to high dose lopinavir leads to a significant improvement in cell survival in both Tert Parent cells ($p = 0.005$) and Tert type 16 E6 cells ($p = 0.016$) when compared to their corresponding DMSO control cells. Low dose exposure failed to produce a significant increase in cell survival in either cell type regardless of treatment time. No statistically significant increase in cell survival was observed in either cell type following 4 day treatment.

Figure 3.4 – AQ-96 assay data

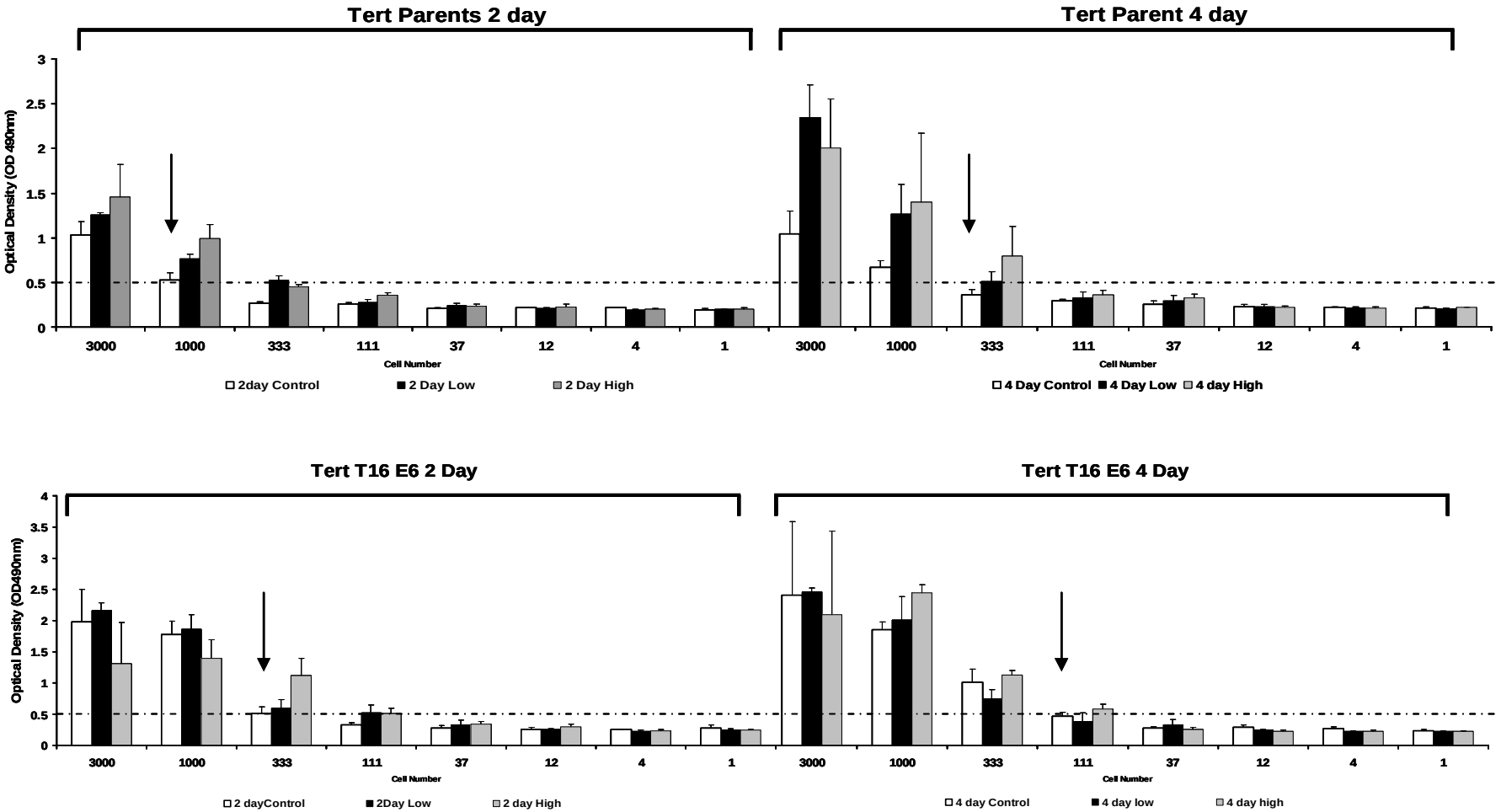

Figure 3.4 – AQ-96 Data generated from parental Tert cells and Tert T16 E6 cells exposed to lopinavir for either 2days or 4days, at either a high or low dose. Cells were then reseeded and allowed to grow for 7 days in lopinavir-free medium. Cell growth at 7 days was assed by means of an AQ-96 Assay. Data represents mean values based on triplicate data points. Mean values and standard deviations were calculated using Microsoft Excel. Based on statistical analysis by one-way ANOVA, vertical arrows show starting cell numbers that were optimal for comparison across all cell types and time points.

3.4.4. Analysis of growth in lopinavir treated E6/E7 immortalised and control PHFKs

The data provided by the Zehbe group (Figure 3.5) demonstrated that lopinavir toxicity was highly selective, preferentially targeting cells immortalised by stable expression of high risk HPV E6/E7. At concentrations up to 25 µM E6/E7 expressing PHFKs and SiHa cells were noticeably more susceptible to lopinavir treatment than normal, non-transduced PHFKs, growth of which progressed uninhibited in contrast to E6/E7 PHFKs and SiHa cells which demonstrated clear dose-dependent growth inhibition. Beyond 25 µM the selective toxicity of lopinavir was lost, with normal PHFKs now demonstrating dose dependent growth inhibition comparable to both SiHa and E6/E7 expressing PHFK cell types.

Figure 3.5 – selective toxicity of lopinavir against E6/E7 expressing immortalised primary human foreskin keratinocytes

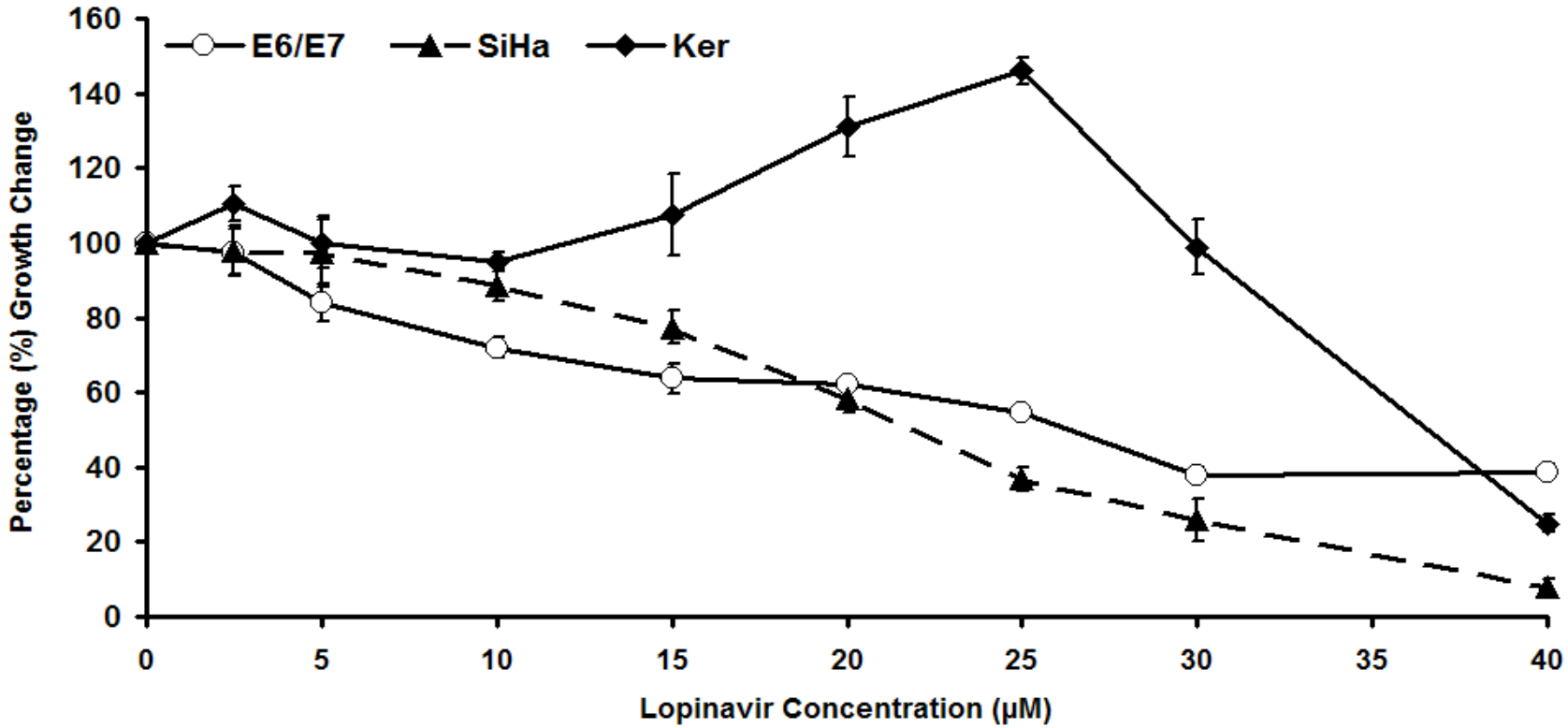

Figure 3.5 - E6/E7 immortalised PHFKs, normal PHFKs and SiHa cells were treated for 72 hours with lopinavir over a dose range of 5-40µM. Cell growth was assessed and expressed in terms of percentage growth change when compared to untreated control cells (KER, control primary human foreskin keratinocytes).

3.5. Chapter Summary and Discussion

Prior to assessing the consequences of short term exposure to lopinavir on the long term survival of cells, the short term toxicity was assessed in SiHa, Tert parent, Tert vector and Tert T16 E6 cells. Using lopinavir over a concentration range of 5-30 µM, cell growth over a period of 72 hrs was assessed using the cell proliferation assays. Cell growth of parental SiHa cells (Figure 3.1) was unaffected at the lopinavir concentrations ≤10 µM. However at concentrations ≥15 µM lopinavir produced clear dose-dependent inhibition of growth over 72 hrs. Non-transformed, telomerase immortalised cells were noticeably more susceptible to lopinavir over 72hrs (Figure 3.2) with all lopinavir concentrations producing marked growth inhibition, with the one exception being Tert Parent cells, in which 5 µM lopinavir appeared to improve growth when compared to DMSO treated control cells.

Whilst the SiHa cell line has been widely used for laboratory based studies of HPV and cervical carcinoma, it is a fully transformed cell line. If lopinavir is to be used to treat the pre-cancerous immortalised cells associated with HPV-dependent cervical neoplasia, it is necessary to assess its effects in a cell type more representative of the intended target cell. This was carried out by using a combination of E6/E7 immortalised primary human foreskin keratinocyte (PHFK) cells and control PHFKs exposed to an escalating dose of lopinavir (5-40 µM) over a 72 hr period (Figure 3.5). Lopinavir showed much greater toxicity towards E6/E7 expressing cells when compared to control PHFKs. Whilst the growth of control PHFKs progressed uninhibited up to concentrations of 25 µM the growth of both E6/E7 expressing PHFKs and SiHa cells showed clear dose dependent inhibition. Interestingly, beyond 25 µM lopinavir the selective toxicity of lopinavir was lost, with control PHFKs exhibiting growth inhibition comparable to E6/E7 expressing cells. These data suggest that lopinavir has a relatively good therapeutic index for E6/E7 expressing immortalised cells when compared to mortal PHFK control cells.

Having assessed the short term toxicity of lopinavir, the ability of cells to produce progeny following a short term exposure to lopinavir was assessed using the clonogenic assay detailed in section 3.3.2. The data showed that in both Tert parent and Tert T16 E6 cells, exposure to a high dose of lopinavir for a 48 hr period lead to a significant improvement in cell growth over the following 7 days when compared to DMSO treated control cells. Forty-eight hour low dose treatment had no significant effect in cell growth in either cell type. Four day treatment with high dose lopinavir also produced no significant change in cell growth. It is hypothesised that the improvement in the growth of high dose treated cells may relate to a phenomenon of lopinavir induced cellular quiescence which is defined as a reversible state in which cellular proliferation is temporarily halted [208]. The clonogenic assay assesses the ability of cells to form progeny following exposure to compounds that can cause persistent long-term damage so as to limit their replication potential [194, 196]. The clonogenic assays on lopinavir treated Tert cells demonstrated a significant improvement of growth only in those cells exposed to a high dose of lopinavir for a period of 48 hrs. One possible explanation for this may be that lopinavir has forced the cell into a quiescent state of growth arrest, which may reduce the chances of drug induced damage to cellular

machinery. Thus, in the subsequent chase period, growth then resumes unaffected. Following the drug treatment period, these cells out grew both control DMSO treated and low dose treated cells, both of which may have, in theory, accumulated damage following treatment with lopinavir at a concentration which failed to produce the state of quiescence observed in high dose treated cells.

Initially it was thought that the combination of parental Tert, vector control, and HPV T16 E6 expressing cells would constitute a model test system with which to study the interaction between the HPV T16 E6 protein and lopinavir. However, based on our findings, it was decided that these cells were not ideal. The data in Figure 3.2 initially suggested that E6 expressing Tert cells demonstrated an increased susceptibility to lopinavir, thus potentially suggesting an underlying E6-mediated effect that would require further study; however, the demonstration that Tert vector cells also demonstrated an increased susceptibility to the drug requires explanation. This is discussed further in Chapter 7.

3.6. Further work

Further work to investigate the rationale behind the improvement in cell survival and re-growth following lopinavir treatment could be carried out. The protein p130 has been shown to form a complex with the E2F transcription factor, a complex which is only found in quiescent G_0 cells. This interaction is known to decay as cells proceed through cell cycle [209]. As there has been no published data linking HIV protease inhibitor treatment with cellular quiescence or p130, assays to measure the extent of the E2F-p130 interaction could be performed to assess the ability of high dose lopinavir to induce cellular quiescence.

4. Effect of lopinavir on Cellular Protein Levels

4.1. Introduction

4.1.1. Proteomics

'The proteome' is a phrase coined by Wilkins *et al* (1996) to define the full complement of proteins expressed within a given cell [210]. This gave rise to the new study of proteomics, which is the study of the protein expression pattern within a cell. More specifically, cancer proteomics is the study of the alterations in protein expression, or 'protein signatures' that are associated with cellular transformation and malignant progression. From a clinical point of view, proteomic analysis may provide clues as to the 'protein signature' or biomarkers associated with a given disease, which can therefore be translated into improved and more specific diagnostic tests [211, 212].

4.1.2. Techniques for Proteomic analysis

4.1.2.1. 2D-Gel electrophoresis

The first approach that allowed the cell proteome to be explored was that of comparative 2D gel electrophoresis. Using this method, proteins are first separated based on their isoelectric properties by use of a tube gel [213], termed isoelectric focussing (IEF). Following separation, proteins are then separated at 90° by molecular mass using a gel containing sodium dodecyl sulphate (SDS) and proteins are visualised either by silver staining or coomassie blue staining. As proteins very rarely have the same isoelectric point and molecular mass the number of proteins that can be separated by 2D gel electrophoresis is in theory only limited by the size of the gel [213]. 2D gel electrophoresis is however quite cumbersome and provides no information as to the identity of the protein in question. 2D also have a relatively poor dynamic range, and are biased towards extremely large proteins [213].

4.1.2.2. Mass Spectrometry

Another approach to proteomic analysis is that of mass spectrometry (MS), which can be coupled with liquid chromatography, LC-MS. Along with basic MS, the development of time-of-flight MS (TOF) and matrix assisted laser desorption ionization (MALDI-TOF) [213], greatly improved proteomic analysis capabilities. These techniques still rely on an initial comparative separation of proteins by 2D gel electrophoresis, followed by isolation and protease digestion of unique signals with a protease such as trypsin. From this point MS can be performed directly, or for MALDI-TOF analysis, proteins are immobilised within an acidic matrix which absorbs energy in the UV range and rapidly emits this in the thermal range. This rapid change in energy vaporises the proteins into the gaseous phase where they acquire a charge. The presence of an electrical charge between the

MALDI apparatus and the MS equipment rapidly separates proteins based on their mass to charge ratio.

Whilst representing an improvement compared to either lone 2D gel or MS analysis, the data provided is still relatively limited in terms of protein identification. In order to identify proteins, the indicated mass of the analytes must then be compared to predicted product sizes based on previous empirical data. Another weakness of such an approach is set up costs, since MS equipment can be extremely expensive.

4.1.2.3. DNA Arrays

For several decades, DNA arrays (such as the Affymetrix genechip) have been used successfully to measure gene expression at the mRNA level [212]. Whilst providing a relatively quick, high-throughput technique, DNA arrays do have their limitations; The human genome contains 20-25,000 genes, which due to alternative splicing and post-translational modification, can give rise to 500,000 proteins [214]. As such, analysis at the mRNA level provides limited insight, providing only a suggested rather than defined mode of action for any given protein. Furthermore, it gives no clues as to sub cellular location or the presence of any interacting proteins [215] and there is not always a direct correlation between mRNA and protein expression levels, [216].

4.1.2.4. Antibody Microarrays

Antibody microarrays are a relatively recent technology which overcome some of the limitations of the preceding approaches. They are a cost effective method which allow rapid comparative analysis of the expression of a wide range of proteins whilst in their native state [217]. They permit direct effects of pharmacological treatments on the levels of a given protein to be compared to control untreated cells.

Previous work has shown that lopinavir causes proteasomal inhibition and can selectively kill E6-dependent cervical cancer cells *in vitro* [98]. This work demonstrated that lopinavir induced inhibition of the proteasome was associated with a stabilisation of the p53 protein which is inappropriately targeted by HPV E6 for degradation by the proteasome. Thus, it was hypothesised that lopinavir treatment may also alter expression levels of a number of other cellular proteins that could be involved in the anti-HPV toxicity of lopinavir.

The Panorama Xpress profiler725 antibody microarray (Sigma Aldrich, Dorset, UK) was used to assess the changes in the proteome between lopinavir treated and untreated SiHa cells (section 2.1). The array contains 725 different antibodies immobilised in duplicate addresses on a nitrocellulose-coated glass slide. The antibodies are against proteins involved in a wide range of diverse biological pathways. Non-denaturing protein extracts are from the test system; in this case, lopinavir or DMSO treated SiHa cells. These are fluorescently labelled by use of Cy3 or Cy5 fluorophore [218], and then incubated with the antibody array as shown in Figure 4.1. The

fluorescent signal associated with binding to a particular address is captured by means of a fluorescent scanner, and is directly proportional to the quantity of bound protein in the sample (Figure 4.1).

In contrast to the Affymetrix gene chip full expression profile microarrays which require multiple-comparison statistical analysis, the Panorama XPRESS Profiler-725 antibody microarray compares protein expression levels using duplicate antibody spots, combined with a variety of antibodies against house keeping protein for signal normalisation. The accompanying Perkin Elmer ProScanArray fluorescent scanner software converts scan intensities into numerical values and treated versus control cell values are plotted for each protein. This analysis produces a ratio rendering the data semi-quantitative. More traditional protein quantitation techniques, such as western blotting can then be used to validate antibody array results.

Figure 4.1 – Antibody microarray schematic

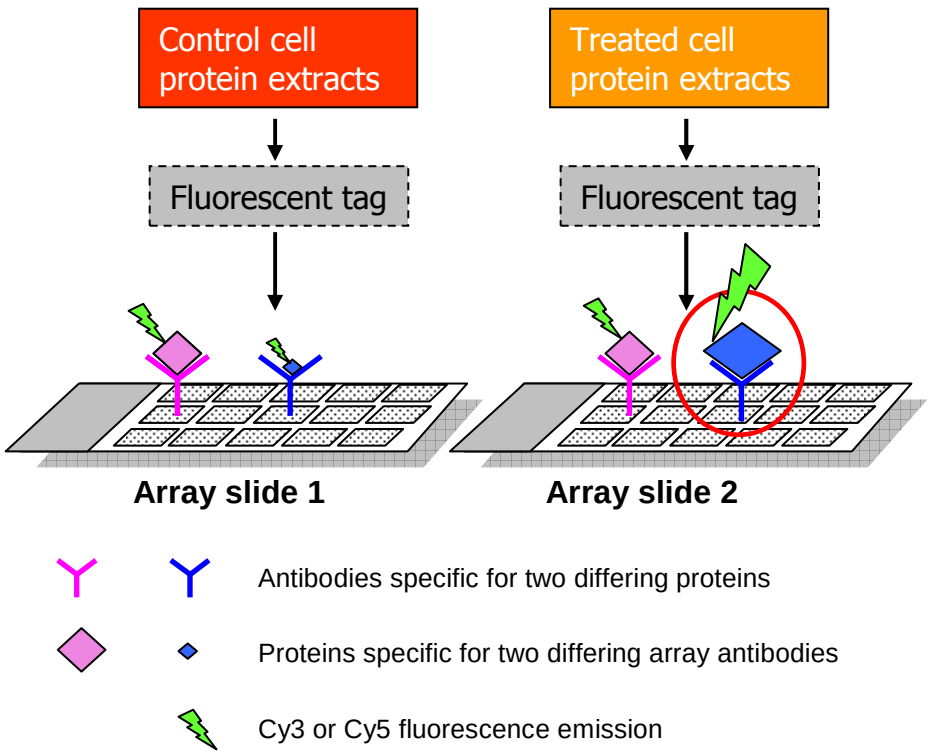

Figure 4.1 – The Panorama Xpress 725profiler antibody microarray contains 725 antibodies immobilised on a nitrocellulose coated glass slide. Antibodies are spotted in duplicate, and for ease of analysis are arranged into 32 sub-arrays, each including a positive and negative control. Protein lysate samples from control DMSO treated and lopinavir treated SiHa cells were labelled with either a Cy3 or Cy5 fluorophore before being used to immunoprobe the array slide. Fluorescently labelled proteins bind to their specific antibodies. The fluorophore emissions are measured by means of a fluorescence scanner, and are directly proportional to the amount of bound protein. The pink protein/antibody interaction remains constant following lopinavir treatment, and is therefore unaffected by lopinavir treatment. In contrast, lopinavir has caused a marked increase in the expression of the blue protein in this diagram. This suggests this protein may be of importance in explaining HPV specific toxicity of lopinavir and therefore requires further investigation.

The Panorama Xpress profiler725 antibody array does however, also have limitations. Clearly, with coverage of only 725 proteins, it does not equate to the coverage offered by Affymetrix gene chip arrays. Furthermore, the efficiency of the antibody microarrays is wholly dependent on the specificity of the antibodies immobilised on the array surface, and on the quality of the array in use. Another problem is that fluorophore labelling efficiencies may vary between the Cy3 and Cy5 fluorophores used to label the proteins. In order to circumvent the latter of these potential problems, antibody arrays are generally performed under dye swap conditions, in which samples of treated lysates are labelled with both Cy3 and Cy5 dyes separately and used to immunoprobe duplicate array slides (Dye swap schematic shown in Figure 4.2).

Figure 4.2 – Normalising antibody microarray data by dye swap analysis

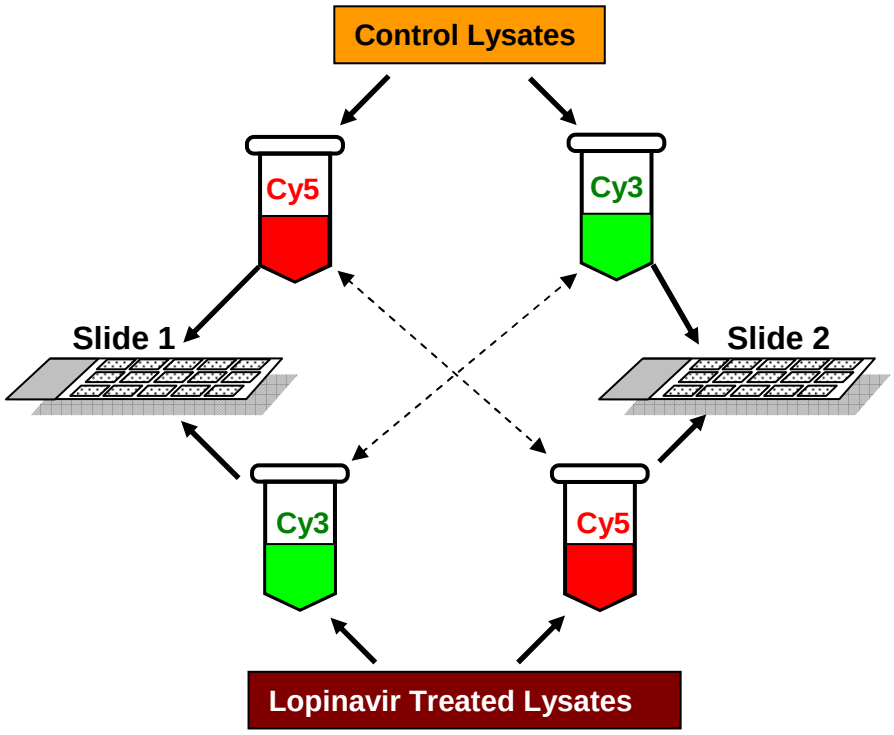

Figure 4.2 – lopinavir treated lysates were labelled with both a Cy3 and Cy5 fluorophore. The same strategy is used to label the control protein lysate samples, and two array slides were incubated with opposing dye mixes. Normalising data this way prevents variations in protein/ fluorophore binding efficiency between Cy3 and Cy5 from adversely affecting results. The dotted arrowed lines represent the points of internal control: Slide 1 contains control lysates labelled with Cy5 and treated lysates labelled with Cy3, whilst slide 2 contains control lysates with Cy3 probe, and treated lysates with Cy5 fluorophore. An alteration in protein levels observed on slide 1, should also be observed on slide 2, if it is a true result rather than a variation due to fluorophore binding.

The same labelling strategy is employed with the control protein lysates. By using this arrangement of sample labelling, duplicate array slides can be probed simultaneously, thus allowing for internal normalisation of data. This strategy is depicted in Figure 4.2. Slide 1 contains control lysates labelled with Cy5 and lopinavir treated lysates labelled with Cy3, whilst slide 2 contains control lysates with Cy3 probe, and lopinavir treated lysates with Cy5. Thus, a genuine signal difference should be observed on both slide 1 and slide 2, whereas this will not be the case if it is due to a variation in fluorophore binding efficiency.

As discussed, the main limitation of the antibody array related to the antibodies represented on the array. The antibodies immobilised on the Panorama Xpress profiler725 antibody array represent only a small fraction of the proteins expressed within a eukaryotic cell. The proteins represented by the array are involved with a range of pathways involved with cell regulation, proliferation and apoptosis, proteins that could conceivably be involved with lopinavir induced toxicity. However, with current technology it is not possible to analyse the full proteome on such a platform. As such the use of this type of array should be regarded as an initial investigation into the proteomic effects of lopinavir. Any observed alterations in protein expression will be subsequently confirmed by the use of more established techniques, such as western blot analysis.

Should lopinavir be shown to alter the expression of any proteins, bioinformatics and literature searches will be carried out in order to provide a clue as to which may be proteins of interest and may be worthy of further investigations.

4.2. Aims

4.2.1. The Sigma Aldrich panorama Xpress profiler-725 protein-antibody microarray will be used to assess alterations in protein levels that occur in lopinavir treated cells

4.3. Methods

4.3.1. Preparation for Panorama XPress Profiler 725 antibody microarray

The panorama Xpress profiler-725 antibody array (Sigma-Aldrich, Dorset, UK) was used according to the manufacturers' instructions. In brief, protease inhibitor cocktail was reconstituted with sdH_2O and stored at room temperature. PBS/Tween-20 (pH 7.4), also supplied with the kit, was reconstituted using sdH_2O filter sterilised using a 0.45 µm filter and stored at 4℃ until use. A working stock of 20 mM lopinavir was made up in DMSO. Benzonase working solution was made up by adding 2 µl benzonase ultrapure solution to 18 µl of extraction/ labelling buffer and stored on ice until use. Buffer A was made up; 10 µl of the reconstituted protease inhibitor, 100 µl of the phosphatase inhibitor cocktail II and 1.2 µl of the benzonase working solution was added to 10 ml extraction/ labelling buffer.

Whilst both the C33A/C33AE6 and Tert/TertE6 cell systems have been used in previous chapters, the main advantage being the ability to assess E6-dependent effects, the decision was made to assess the proteomic effects of lopinavir in SiHa cells. As discussed, SiHa cells, whilst a fully transformed cell line, contain a fully integrated HPV genome. It was thought that the anti-HPV effects of lopinavir may involve more of the HPV arsenal than simply E6, so to fully ascertain the effects of toxic effects of lopinavir against HPV-infected cells, a fully integrated genome is essential. SiHa cells were seeded into T-75 culture flasks and cultured as described in section 2.3.1 to a confluency of 80% whereupon the growth medium was aspirated from all culture flasks and replaced with fresh complete medium supplemented with lopinavir at a final concentration of 25 µM or an equal volume of DMSO. All flasks were returned to the incubator for 6 hrs. In order to obtain a sufficient amount of protein for the antibody array, all cells from two lopinavir or two DMSO treated flasks were pooled and processed. Remaining flasks were lysed with 2 x Laemmle sample buffer and used for western blotting, as described in section 5.3.2.4.

4.3.2. Protein extraction from cells

Six hours post-incubation with lopinavir, the growth medium was aspirated and the cells were washed twice in PBS/Tween-20 (pH 7.4) and 1.25 ml of ice cold buffer A (prepared in section 4.3.1) was then added to one T-75 flask from each pair, and this incubated on ice for 5 min. Following this, cells were detached from the flask surface using a sterile cell scraper, and the cell lysate transferred to a second lopinavir treated T-75 flask as above. This was again incubated for 5 min on ice and the cells detached. The total cell lysate solution, now containing the pooled contents of 2 x T-75 lopinavir treated cells was transferred to a sterile 1.5 ml eppendorf. This extraction process was also repeated with two DMSO treated control T-75 flasks.

The lysates were centrifuged at 10,000 x g for 10 seconds, and the pellet dislodged before being centrifuged once more at 10,000 x g for 10 seconds. The supernatant was then transferred to

a fresh labelled eppendorf tube. Before proceeding, the protein concentration was determined using the Bradford Assay (section 4.3.4).

4.3.3. Preparation of protein lysates for western blot

Cells grown in T-75 flasks were harvested and counted as detailed in section 2.2.3. The cells were then pelleted by centrifugation for 5 min at 528 x g and the supernatant aspirated. The cell pellet was then resuspended in 500 µl PBS and transferred to a 1.5 ml eppendorf, before being centrifuged at 10,000 x g for 5 min. Cells were then resuspended in a volume of PBS calculated to give a final concentration of 1.0 x 10^6 cells in 20 µl and an equal volume of 2x Laemmle sample buffer [219] added to this (Final concentration of 0.5 x 10^6 cell/20 µl volume). Samples were then subjected to three cycles of heating to 95℃ for 5 min, before being snap frozen in liquid nitrogen. Finally, the samples were stored at -20℃ until use .

4.3.4. Estimation of protein content by Bradford Assay

Protein content was estimated using the Bradford assay kit (Thermo Fisher Scientific, Northumberland, UK) carried out according to the manufacturer's instructions. Plates were incubated in the dark for 15 min, after which, the absorbance was read at 490 nm using a Dynex MRX plate reader (Dynex technologies Ltd., West Sussex, UK).

4.3.5. Protein Labelling

For protein labelling, Cy3 and Cy5 fluorophores were used (GE Healthcare (Amersham), Buckinghamshire, UK). Vials of Cy3 and Cy5 protein labelling dye were each resuspended in 20 µl fresh DMSO and 10 µl of Cy3 protein labelling dye placed into 2 labelled eppendorfs. Five hundred microlitres of lopinavir treated and DMSO control lysates (prepared in section 4.3.2) were each added separately to the Cy3 and Cy5 labelling dyes. These were then thoroughly mixed and incubated, in the dark at room temperature, for 30 min, with inversion mixing every 10 min.

Free Cy3/ Cy5 dye was removed from the protein sample using Sigma Aldrich spin columns (Sigma Aldrich, Dorset, UK) according to manufacturers' instructions. The spin columns were centrifuged at 750 x g for 2 min, and the eluate from each tube discarded. The spin columns were then placed into fresh eppendorf tubes, and 150 µl of the lysates/ dye mixes pipetted directly onto the centre of the membrane of a separate spin column. The remaining cell lysates were stored at -80℃. Columns were then centrifuged again at 750 x g for 2 min and the eluate retained. The protein concentration of each fluorophore labelled sample was then determined using the Bradford assay as described in section 4.3.4.

4.3.6. Determination of Dye/ Protein molar ratio

The Cy3 and Cy5 absorbencies were read at 552nm and 650nm respectively, using a Nandrop-8000 machine (Thermo Scientific, Nanodrop products, Delaware, USA). In brief, the machine was initialised by placing 2 µl ultra pure sdH_20 on each absorbance reading head in use. Following this, 2 µl buffer A (prepared in section 4.3.1) was placed on each of the absorbance reading heads to zero the machine. Following this the absorbance of each sample was read and recorded. The dye/ protein ratio (D/P) was calculated based on the following formulae:

µM coefficient ($\varepsilon^{\mu M}$) calculations:

- Cy3 $\varepsilon^{\mu M}(552nm) = 0.15\mu M^{-1}\ cm^{-1}$
- Cy5 $\varepsilon^{\mu M}(650nm) = 0.25\mu M^{-1}\ cm^{-1}$

Therefore the Cy3/ Cy5 concentrations were calculated as follows:

- Cy3 concentration (µM) = $A_{552}/0.15$
- Cy5 concentration (µM) = $A_{650}/0.25$

Protein (µM) concentration:

- $[Y(mg/ml)/60,000] \times 10^6$

(Where Y represents protein concentration estimated with the Bradford assay)

Finally the D/P ration was calculated:

$$D/P = \frac{\text{Cy3 or Cy5 concentration}}{\text{Protein concentration of sample}}$$

4.3.7. Sample incubation on the array

One hundred nanograms (100 ng) of each labelled protein lysate sample was used to label duplicate array slides. To allow for a dye swap controlled experiment, slide A was probed with Cy5 labelled untreated (UT) lysates and Cy3 labelled treated (T) lysates. Slide B was probed with the reverse. Two separate 5ml aliquots of the array incubation buffer were made up containing 100 ng Cy5 untreated and 100 ng Cy3 treated or 100 ng Cy3 untreated and 100 ng Cy5 treated. These were mixed gently without vortexing, placed in separate wells of the slide incubation trays, and the

two slides immersed fully into two separate protein lysates mix. The trays were then covered in foil and incubated at room temperature for 30 min on a rotary shaker with gentle shaking. Following this, the slides were removed from the labelled protein mixture and washed with three 5 minute washes in the wash buffer provided. Slides were then air dried completely at room temperature, in the dark, before being scanned using a Perkin-Elmer Pro ScanArray fluorescent scanner (Perkin-Elmer, Massachusetts, USA) according to the manufacturers' instructions.

4.3.8. Data analysis of antibody microarray results

Each protein is represented in duplicate on the array arranged in 32 sub arrays including positive and negative controls. Protein differences could be determined between treated and untreated samples based on the visual scan results. However, to calculate numerical differences in protein levels, mean intensities were calculated for each spot pair, with the mean spot background level subtracted. Protein intensities were then plotted graphically with average intensities and standard deviations calculated using Microsoft Excel 2003.

Antibody arrays are specific for a qualitative measurement of protein expression for tissue or cell extracts. By determining relative changes in protein expression, it is possible to compare control DMSO treated samples to its matched lopinavir treated sample. This analysis produces a ratio rendering the data semi-quantitative. The use of an antibody microarray is a rather speculative approach by which to identify those proteins altered following exposure to lopinavir. As the array represents 725 different proteins, it was decided to utilise a two-stage approach in order to identify potentially interesting proteins requiring future studies:

A. Proteins in which upper/lower extremities of error bars did not overlap were considered 'proteins of interest'. Extremely low expression proteins and array spots suffering from slide manufacturing inaccuracies were disregarded.

B. Bioinformatic searches to identify function(s) of highlighted 'proteins of interest' were subsequently carried out. Prior to obtaining array data, it was anticipated that the most likely protein of interest, with regards to lopinavir toxicity, would be a protein which was elevated/stabilised in the presence of lopinavir. In addition, the protein of interest would also ideally possess functions relating to cell growth, apoptosis or the antiviral response of the cell. Proteins possessing these attributes would be prioritised for future investigations

4.4. Results

4.4.1. Fluorescent scan data

Equal amounts of Cy3 and Cy5 labelled protein samples were used to immunoprobe the Sigma-Aldrich panorama XPress725 antibody microarray (section 4.3). In order to rule out the possibility of misinterpreting the antibody microarray due to differences in Cy3/ Cy5 fluorophore labelling efficiencies, it was initially planned on processing the antibody array under dye swap conditions. This was done by labelling duplicate samples of DMSO control and lopinavir treated protein lysates with both Cy3 and Cy5 fluorophores and immunoprobing duplicate antibody arrays. Protein levels are colour coded from blue, representing a low protein level, through to white representing high level protein expression. Figure 4.3 below shows the results from the first fluorescent scan showing the full array slide, and demonstrates a problem encountered with the Cy5 fluorophore, preventing a full dye swap analysis.

Figure 4.3 - Failure of Cy5 fluorophore to scan effectively

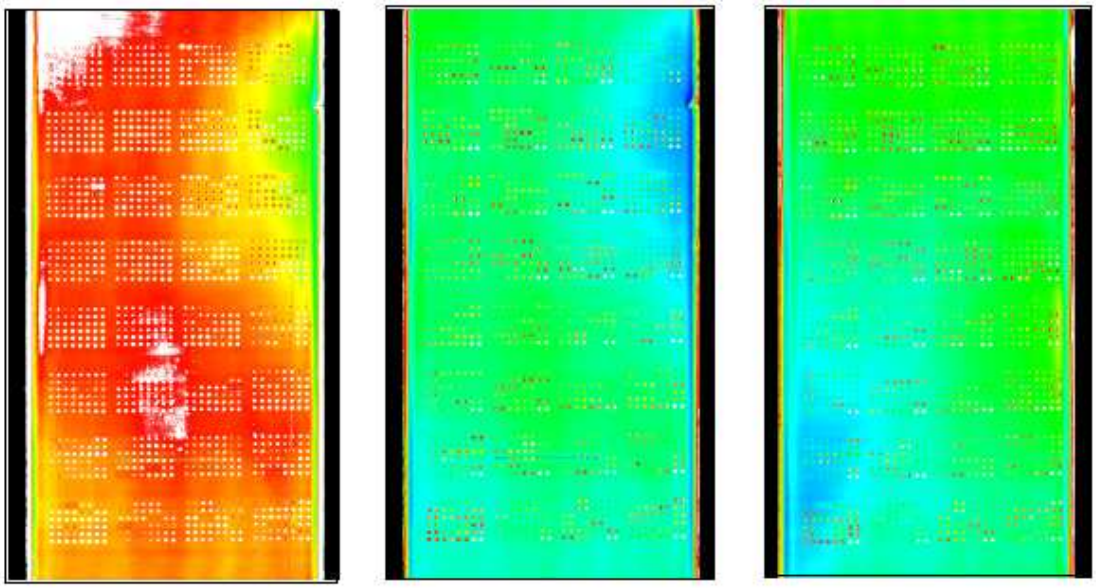

Figure 4.3 – Cy3 and Cy5 fluorophore labelled cell proteins were used to immunoprobe the Panorama Xpress-725 profiler antibody microarray. The Cy5 fluorophore was scanned using the Perkin-Elmer ProScanArray fluorescent scanner according to the manufacturers' instructions. The scan was carried out using several scan settings, the results of which are shown above in 3 separate panels, each representing one full array image taken under a range of laser setting. Regardless of the scanning parameters used, it was not possible to get a scan image that was suitable for further analysis.

Based on these findings, it was decided that a full dye swap analysis was not possible, and subsequent analysis would be based on the Cy3 fluorophore signal. The scan image results shown below in Figure 4.4 demonstrate the clear difference in image quality between the Cy3 and Cy5 fluorophores.

Figure 4.4 – Fluorescent scan images obtained from Cy3 fluorophores

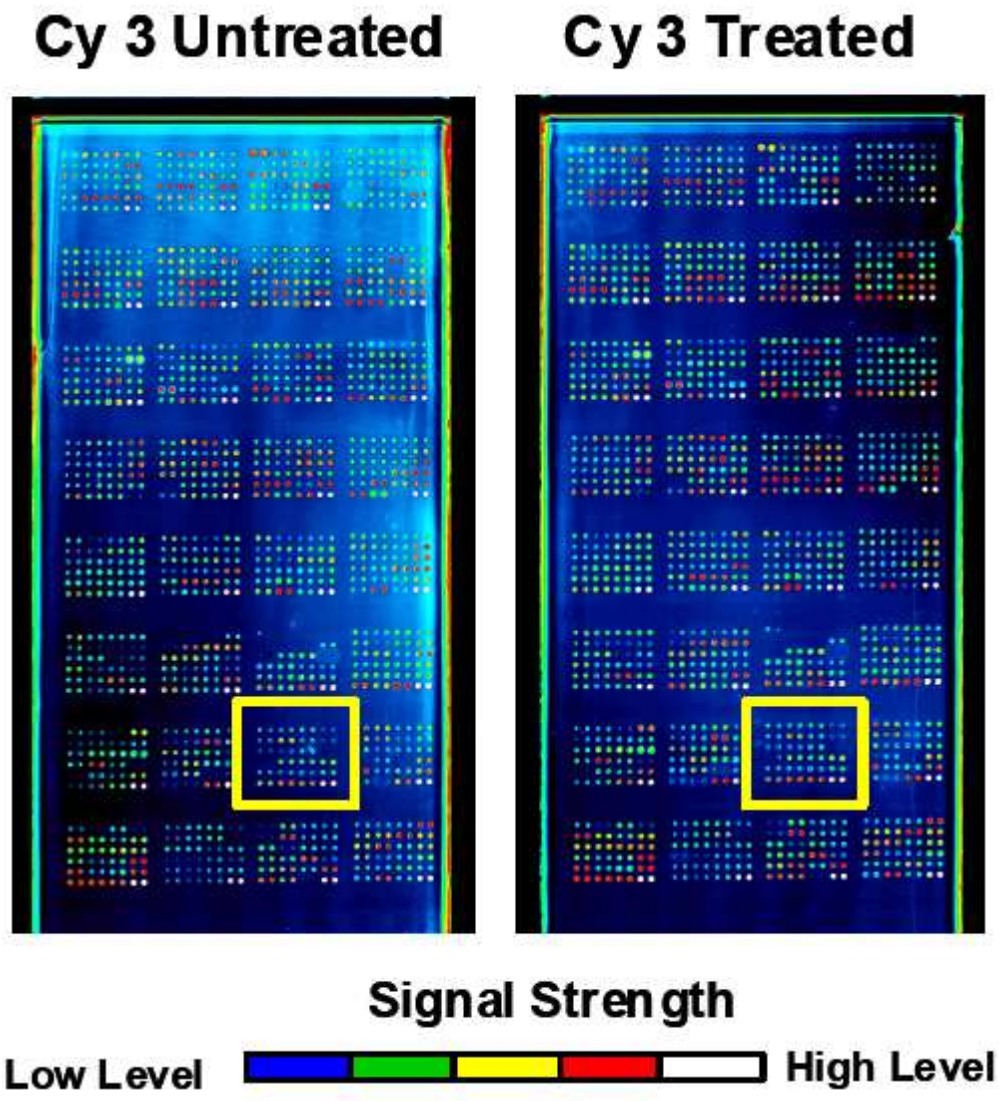

Figure 4.4 – Lopinavir treated (6hrs, 25 µM) and DMSO control treated SiHa cells were harvested and labelled with a Cy3 fluorophore. Cy3 dye-labelled protein samples were used to immunoprobe two Panorama XPRESS profiler725 antibody microarray slides. Fluorescent scans were carried out using a Perkin-Elmer ProScanArray fluorescent scanner. Yellow box represents one sub array containing 24 proteins spotted in duplicate including positive and negative control spots.

Figure 4.4 shows the Cy3 fluorescence scan data for the panorama antibody microarray. The 725 antibodies are arranged into 32 sub-arrays, each including 22 separate proteins in duplicate addresses, along with positive and negative controls. The yellow boxed area represents a single sub array, a close-up of which is shown below in Figure 4.5.

Figure 4.5 – Close up an a single sub array - Cy3 fluorescent scan data

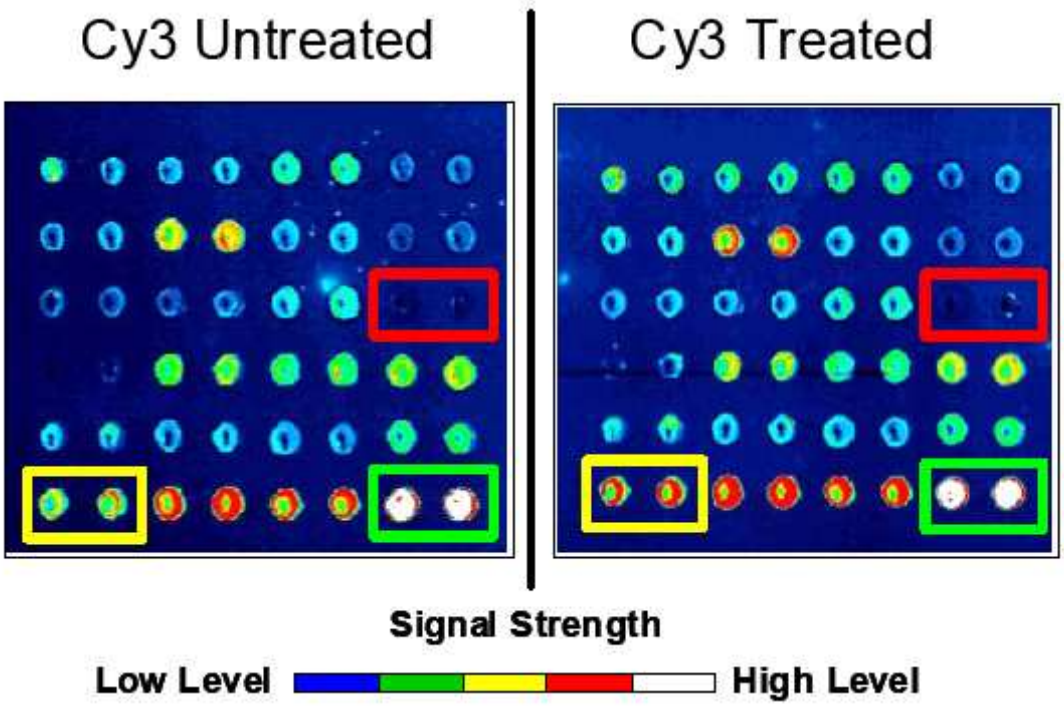

Figure 4.5 – Close up on a single sub-array for the Cy3 fluorophore. The left panel represents the untreated protein lysates and the right panel represents the lopinavir treated protein lysates. The red boxed pair, on each panel, represents an internal negative control in duplicate, whilst the green boxes represent the Cy3/Cy5 positive control. The yellow boxed pairs represent a single protein in duplicate, namely Ribonuclease L, levels of which have increased following lopinavir treatment.

The background signal was subtracted from each spot and mean intensities were plotted for each duplicate signal. Of the 725 proteins covered by the antibody microarray 51 proteins were shown to have altered expression levels in the lopinavir treated protein lysates. The raw data signal strengths for these 51 proteins are shown below in Figures 4.6 and 4.7, with the colour coded signal intensities shown above converted to numerical values using the software package accompanying the Perkin Elmer Scanner. Of these 51 proteins, 5 proteins, namely Aurora B, bcl-10, connexin-43 (two variants), GFAP and mTOR had decreased levels following lopinavir

treatment. The remaining 46 proteins all exhibited varying increases in expression following lopinavir treatment (For details function and fold-changes of each protein, please refer to table 7.1).

Figure 4.8 shows the data from Figures 4.6 and 4.7 represented in terms of log fold change compared to matched DMSO treated control values.

The numerical values for each of the 725 proteins represented on the Panorama Xpress Profiler-725 antibody microarray can be viewed as an excel file on the accompanying data CD, with file name ‘Full Antibody Microarray data set.xlsx’

Figure 4.6 – Proteins exhibiting alterations in expression levels following lopinavir treatment

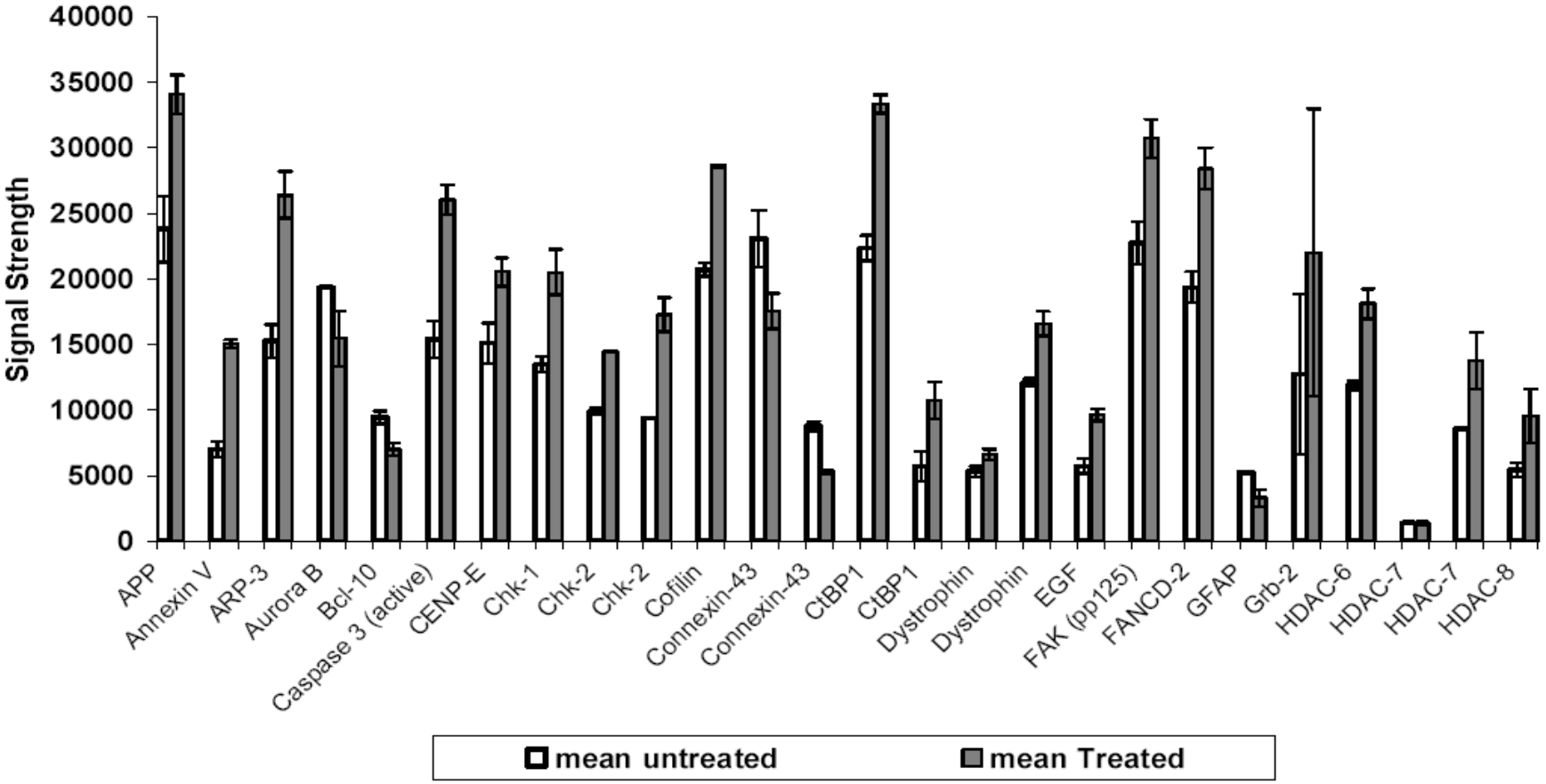

Figure 4.6 – Protein expression levels are shown for DMSO treated control proteins and lopinavir treated proteins. Mean values were calculated using Microsoft Excel.

Figure 4.7 – Protein expression levels following lopinavir treatment (continued)

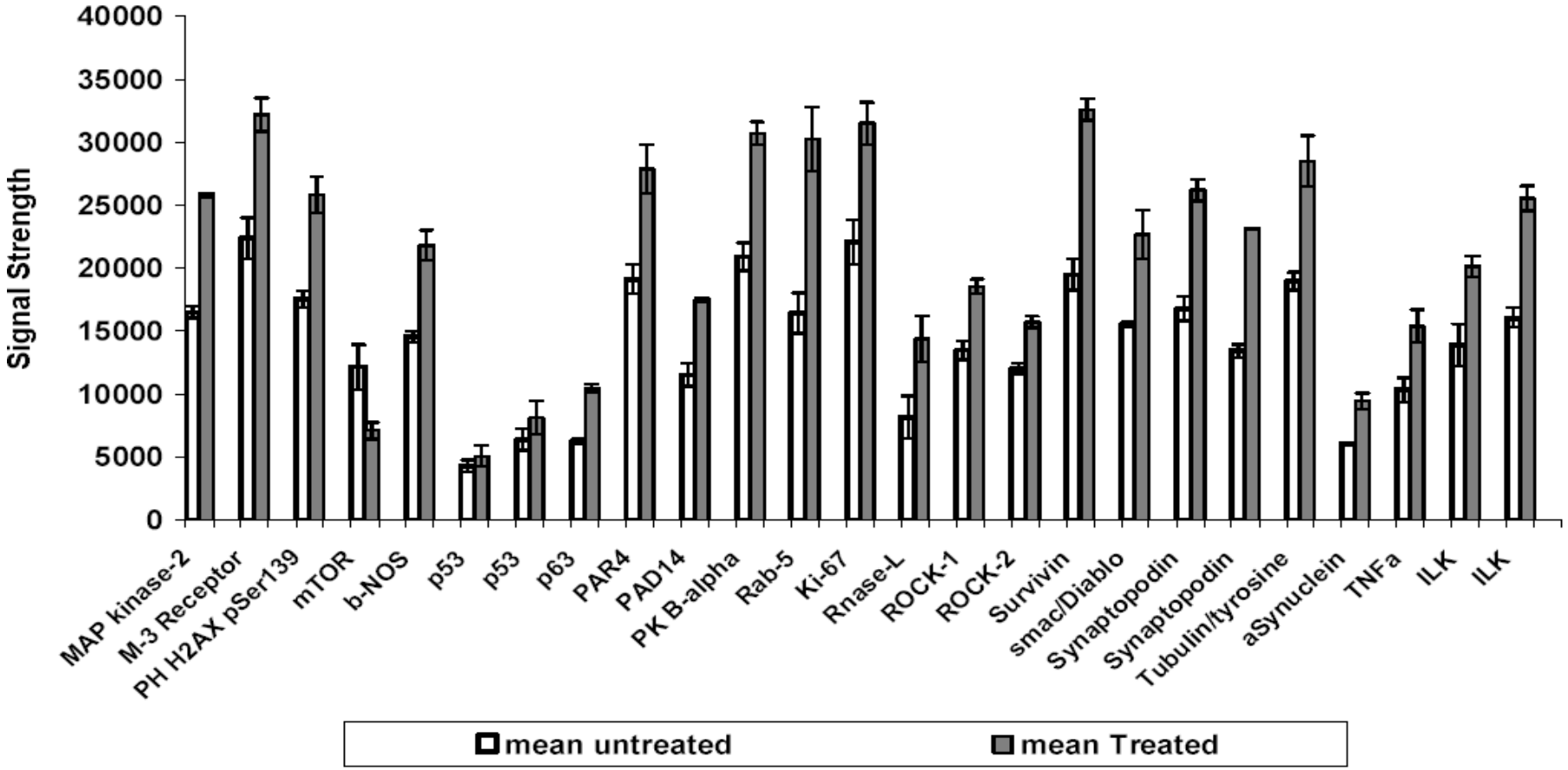

Figure 4.7 – Protein expression levels are shown for DMSO treated control proteins and lopinavir treated proteins. Mean values were calculated using Microsoft Excel.

Figure 4.8 – Protein expression levels following lopinavir treatment – Log fold change

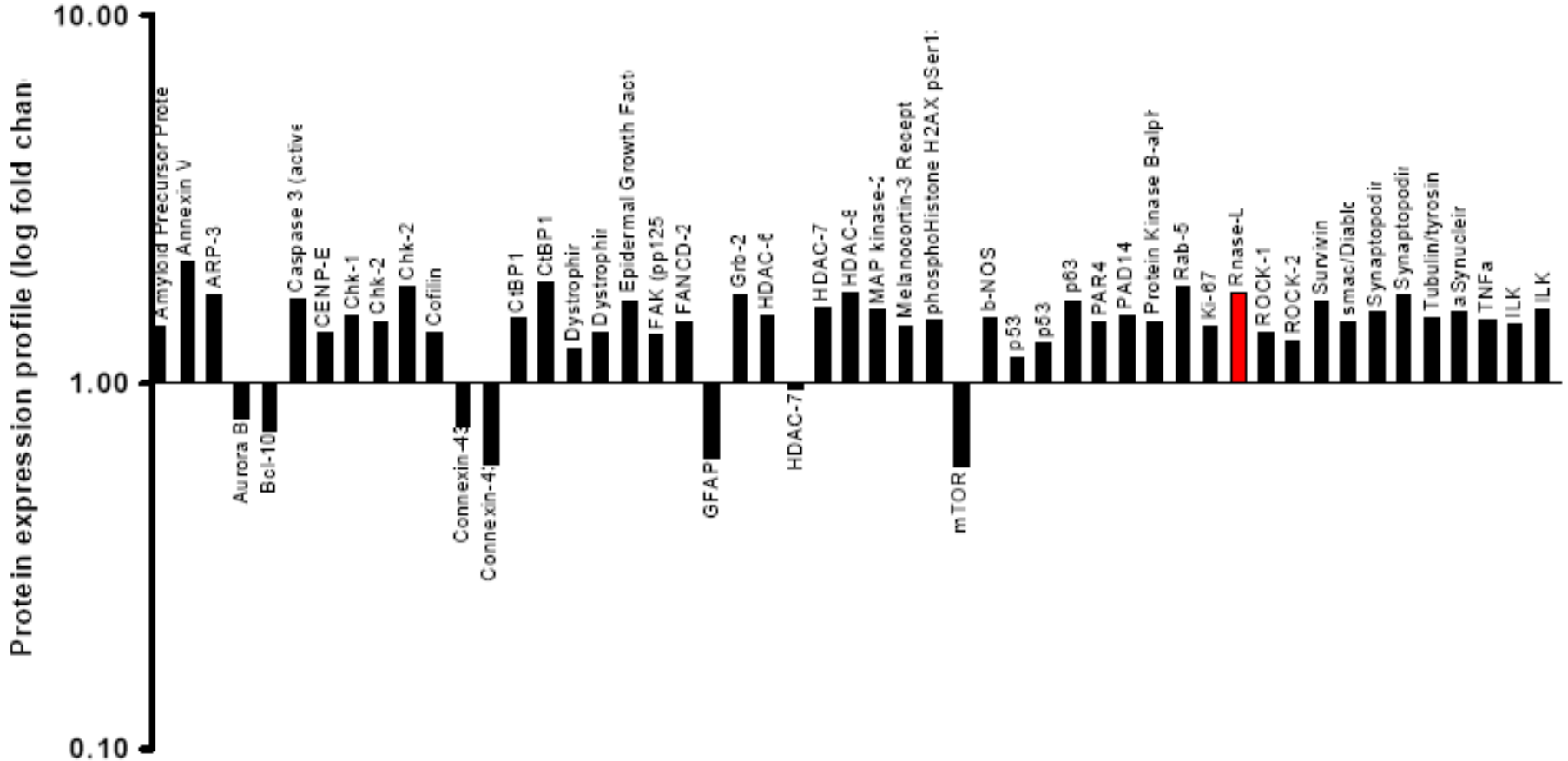

Figure 4.8 - Lopinavir treated protein expression profile represented in terms of log fold change compared to DMSO control. The red bar represents RNase L protein, levels of which were shown to be elevated following lopinavir treatment. As a known antiviral protein, the role of RNase L in lopinavir toxicity was assessed in subsequent chapters.

4.5. Chapter Summary and Discussion

It is known that lopinavir is able to induce selective inhibition of the 26S proteasome [130, 131]. It was hypothesised that inhibition of proteasomal degradation would lead to changes in cell protein levels in lopinavir treated cells, which were not apparent in untreated control cells. Further to this, it was thought that one or more of the proteins exhibiting altered expression following lopinavir treatment could potentially account for the anti-HPV activity of lopinavir. The protein expression profiles of lopinavir treated and DMSO control treated HPV positive SiHa cells were compared using the Panorama Xpress725 profiler antibody microarray (Sigma Aldrich, Dorset, UK). In total, lopinavir was shown to alter the levels of 51 proteins, shown in Figures 4.6 and 4.7 and table 7.1. Of these 51 proteins, lopinavir caused an increase in protein expression in 46 proteins, and a decrease in 5 proteins.

Literature searches were carried out in order to gain an understanding of all the proteins shown to be affected by lopinavir treatment. Not surprisingly, lopinavir treatment was shown to up-regulate several known apoptosis-markers such as Annexin-5 (ANXA5), the active form of Caspase-3 (CASP3), Tumour necrosis factor (TNF) and p63, and as previously demonstrated, p53 [131]. Interestingly the majority of those proteins were shown to be known targets for proteasomal degradation, as highlighted in table 5.1. Since p53 is a known target of the HPV type 16 E6 protein the. Virus Molecular INTeraction database was searched in order to identify any other potential known E6 and/or E7 interacting proteins affected by lopinavir treatment (http://mint.bio.uniroma2.it/virusmint/, reviewed in [220]). However, at this stage, only p53 has previously been shown to interact with E6.

As demonstrated, lopinavir treatment also down-regulated some proteins in SiHa cells, although of particular interest was the down regulation of the Mammalian Target of Rapamycin (mTOR). Interestingly, mTOR has recently been shown to be constitutively over expressed in cervical carcinomas [221], and most importantly, it has been shown that the HPV type 16 E6 protein activates mTOR signalling resulting in increased protein synthesis [222] (see Chapter 7 for a full discussion of mTOR). In addition, it was also significant that lopinavir-induced down regulation of Glial Fibrillary Acidic Protein (GFAP), a protein known to be capable of inhibiting the proteasome [223].

However, of most interest was the observation that lopinavir caused a 1.7-fold increase in levels of a protein known as Ribonuclease L (referred to as RNase L for the remainder of this thesis, whilst the gene name is referred to as RNASEL) since this is a well known interferon-inducible antiviral protein (Figure 4.7). This increase was later confirmed by western blotting (see chapter 5, Figure 5.7). It is true that the anti-HPV effects of lopinavir may be potentially related to the synergistic actions of more than one of the differentially regulated proteins identified by the antibody array. However, taking into account the well established antiviral function of RNase L [224, 225] it was decided to focus further investigations on the effects of lopinavir on this protein in particular.

4.6. Further work

We have access to a range of other HIV protease inhibitors. Thus, based on the previously discussed observations it is suggested that additional western blot and/or microarray analysis of PI treated SiHa cells could be carried out. This would establish whether these agents produced similar effects to those identified for lopinavir and determine whether these were lopinavir-specific or whether they are a general consequence of protease inhibitor treatment.

5. RNase L and further lopinavir Studies

5.1. Introduction

One aim of this research project was to assess the link between lopinavir and HPV-specific toxicity, with a particular aim being to identify potential proteins that could account for this toxicity. Previous results from the Panorama Xpress profiler725 antibody array (Chapter 4) demonstrated that in SiHa cells, lopinavir caused alterations in the expression of a number of proteins with a wide range of functions.

Many viruses are known to inhibit the function of, or inappropriately degrade, host cell proteins detrimental to viral persistence [226-230], some by directly 'hijacking' the ubiquitin-proteasome system (as reviewed in [231]). Inappropriate proteasomally-mediated degradation of the tumour suppressor protein p53, facilitated by the E6 protein of high risk HPV types, is a classic example of this adaptive viral response. In removing p53, HPV replication can proceed unhindered. Taking this into account, it was thought that the most likely candidate protein(s) of interest would be ones which were elevated following lopinavir treatment, as this potentially implies that the protein has been suppressed in the untreated HPV-positive cell. When compared to DMSO treated control cells, the data showed that, amongst other proteins, lopinavir induced an increase in the levels of a protein known as RNase L. RNase L is a known antiviral protein, and is the main effector protein of an interferon-induced antiviral pathway, and its role will be investigated in greater detail.

5.1.1. RNase L, Interferon and the 2',5',-oligoadenylate (2-5A) antiviral Pathway

Interferons (IFN) [107] are a group of multifunctional secreted proteins involved with antiviral defence, cell growth regulation and immune activation and can be split into two broad categories; the type I IFNs, IFN-α and IFN-β, which are produced as a direct consequence of viral infection, and IFN-γ, a type II IFN which is produced following recognition of an infection by activated T lymphocytes and natural killer cells [232]. Stimulation of IFN results in an 'antiviral state' wherein cells become refractory to further infection. Four IFN-regulated antiviral pathways that contribute to the antiviral state have previously been described: the Mx GTPase pathway, the double stranded RNA dependent protein kinase pathway (PKR), the ISG15 ubiquitin-like pathway and the 2',5'-oligoadenylate (2-5A) pathway (all extensively reviewed in [233]).

The 2', 5'-oligoadenylate pathway (Figure 5.1) comprises two main enzymes, oligoadenylate synthetases (OAS) and a latent ribonuclease, RNase L. The pleiotropic effects of IFN are regulated through binding of IFN to the IFN-α 1 receptor (IFNR1) which initiates a JAK-STAT signalling cascade resulting in the transcription of more than 300 IFN-stimulated genes (ISG) [234]. The majority of ISGs encode protein products which function as pattern recognition receptors, indirectly modulating the antiviral response through detection of viral molecules [234]. Yet IFN also stimulates a subset of ISGs which are capable of direct modulation of the antiviral

response, namely the OAS genes and their OAS protein products. There are 4 human OAS genes, which are located on chromosome 12, OAS1, OAS2, OAS3, which through splice variation, give rise to 5 functional OAS, and finally OAS-L which encodes a similar protein with two C-terminal ubiquitin-like domains, although it does not synthesise 2-5A (Figure 5.1(B)) [235].

Figure 5.1 – IFN stimulated 2-5A RNase L antiviral pathway

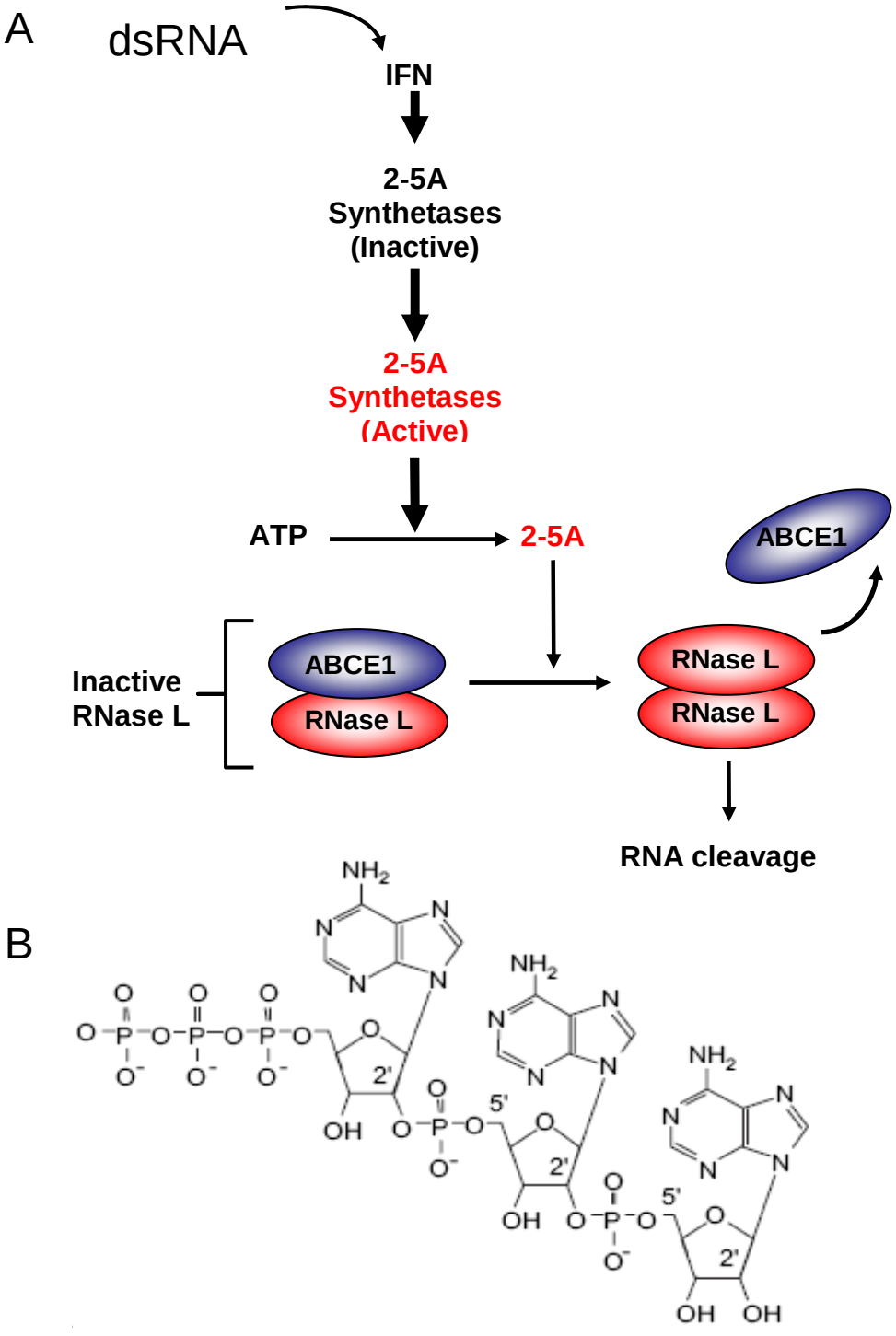

Figure 5.1 – (A) 2-5A/ RNase L antiviral pathway. (B) 2-5A structure (Diagram from [224]).

Double stranded RNA (dsRNA) molecules as small as 15 bp in length are produced by many viruses as replicative intermediates, and these stimulate activation of the OAS system [236]. This involves polymerisation, with OAS3 products producing active dimeric 2',5'-oligomers, whilst OAS1 and OAS2 produce active trimeric and tetrameric 2',5'-oligomers respectively [234]. Following activation, ATP is converted into a series of short 5'-phosphorylated, 2', 5'-linked oligoadenylates jointly referred to as 2-5A (Figure 5.1 B). RNase L is constitutively expressed as an inactive monomer. Binding of 2-5A within the regulatory region binding pocket of RNase L, which requires a 1:1 molar ratio between RNase L and 2-5A, induces a conformational change in the ankyrin repeat region (Figure 5.3), which unmasks the nuclease domain of RNase L. As a consequence of this 'unmasking' homodimerisation of RNase L monomers occurs, resulting in activated RNase L dimers [237]. Following this, RNase L cleaves within single stranded regions of both cellular and viral RNA, preferentially at the 3' side of U_pA_p and U_pU_p dinucleotides [237]. In the absence of 2-5A, the regulatory domain suppresses this ribonuclease activity. The antiviral effects of RNA degradation by RNase L are summarised in Figure 5.2.

Figure 5.2 Antiviral effects of RNase L mediated degradation of RNA

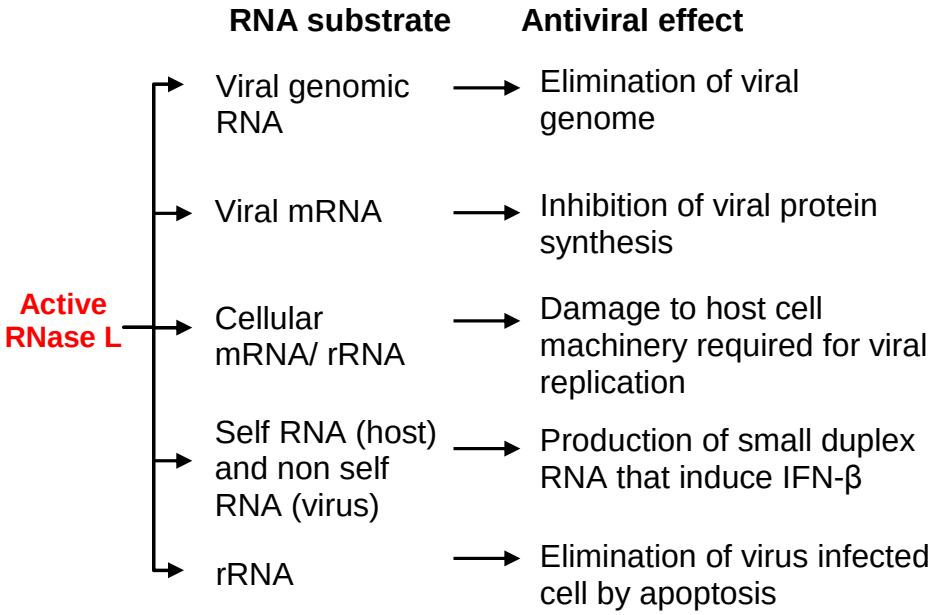

Figure 5.2 – Antiviral effects of RNase L-mediated degradation of cellular and viral RNA substrates (diagram adapted from [238]).

5.1.2. RNase L Structure

RNase L is a 741-amino acid protein with a molecular mass of approximately 83 kDa composed of three domains (Figure 5.3) (as reviewed in [224, 239]): The N-terminal regulatory domain, the kinase-like domain and the nuclease domain.

Figure 5.3 – Domain locations of RNase L

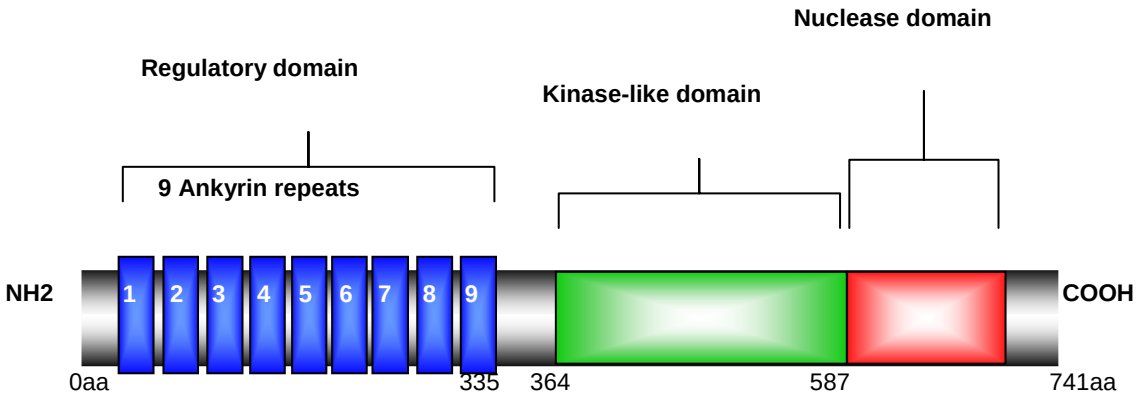

Figure 5.3 – The RNase L protein is 741 amino acids in length and is composed of three domains: the N-terminal regulatory domain contains 9 ankyrin repeat motifs and is associated with 2-5A binding, a protein kinase-like domain, and a C-terminal domain that contains the active ribonuclease region.

5.1.2.1. N-terminal regulatory domain

The N-terminal regulatory domain of RNase L is composed of 8 complete and 1 partial ankyrin repeat motifs (R1-R9). These each consist of 30-34 amino acid residues and mediate protein-protein interactions [240, 241]. Both ankyrin repeats 7 & 8 contain a GXXXXGKT sequence (where X can be any amino acid). This is commonly referred to as a Walker A motif, which mediates nucleotide binding in ATP-dependent enzymes [224, 242]. Work on the crystal structure of RNase L demonstrated that ankyrin repeats 2 – 4 constitute a 2-5A binding pocket and that ankyrin repeats 7 and 9 are involved with protein structural integrity rather than 2-5A binding [243]. Upon binding, 2-5A induces a conformational change in the ankyrin repeat domain of RNase L which unmasks the C-terminal nuclease domain allowing homodimerisation to occur leading to the generation of active RNase L homodimers [237].

5.1.2.2. Kinase-like domain & Nuclease domain

The kinase-like and nuclease domain of RNase L are structurally homologous to IRE1p [224]. This is a kinase/ribonuclease that functions in the unfolded protein response in *Saccharomyces cerevisiae* [244], which is a process essential for chromosome maintenance [245]. Unlike IRE1p, the kinase-like domain of RNase L is less well researched and has been shown to lack several residues that are highly conserved amongst other protein kinases [246, 247]. Whilst there has been no demonstrable kinase-like functions of RNase L, studies have shown that mutations at nucleotide position 392 lead to an extensive (>100-fold) reduction in ribonuclease activity, relating to an inability of RNase L to fully dimerise [247].

5.1.3. Endogenous regulation of RNase L

RNase L activity is regulated in a number of ways. For example, 2-5A molecules are relatively unstable, short lived proteins, which are rapidly degraded by a combination of 2'-phosphodiesterases and 5'-phosphatases [225]. Following the successful cloning of RNase L [239], Bisbal et al (1995) described the cloning and characterisation of an endogenous polypeptide inhibitor of the 2-5A-dependent RNase L antiviral pathway [248], labelling it RLI or RNase L inhibitor. RLI, later termed ABCE1 (*A*TP-*B*inding *C*assette, subgroup *E*), is a 599 amino acid protein with a molecular weight of approximately 68 kDa. Inhibition of RNase L activity does not occur through ABCE1-mediated degradation of 2-5A or irreversible inactivation of RNase L [224]. Instead, ABCE1 reversibly binds to the ankyrin repeat region of RNase L antagonising the binding of endogenous 2-5A and thus preventing the activation of RNase L [248].

5.1.4. The RNase L pathway and viral evasion strategies

As a consequence of co-evolution, host-virus interactions are highly dynamic and complex with both organisms constantly adapting and developing strategies against the other. Clearly there are highly sophisticated innate and adaptive host immune responses which provide both fast acting 'first-line' and longer lasting pathogen-specific defences. However, it is not surprising that there are a plethora of equally sophisticated and efficient strategies employed by viruses to circumvent cellular defences to allow viral replication and dissemination. As mentioned previously, a classic example of virally-mediated host defence evasion is that of high risk HPV E6 & E7-mediated degradation of p53 and Rb respectively. However, the RNase L/ 2', 5'-oligoadenylate pathway is also an important antiviral pathway and as such, is targeted by a number of DNA and RNA viruses using a range of strategies (summarised in Figure 5.4).

Figure 5.4 – Viral intervention strategies targeting the RNase L pathway

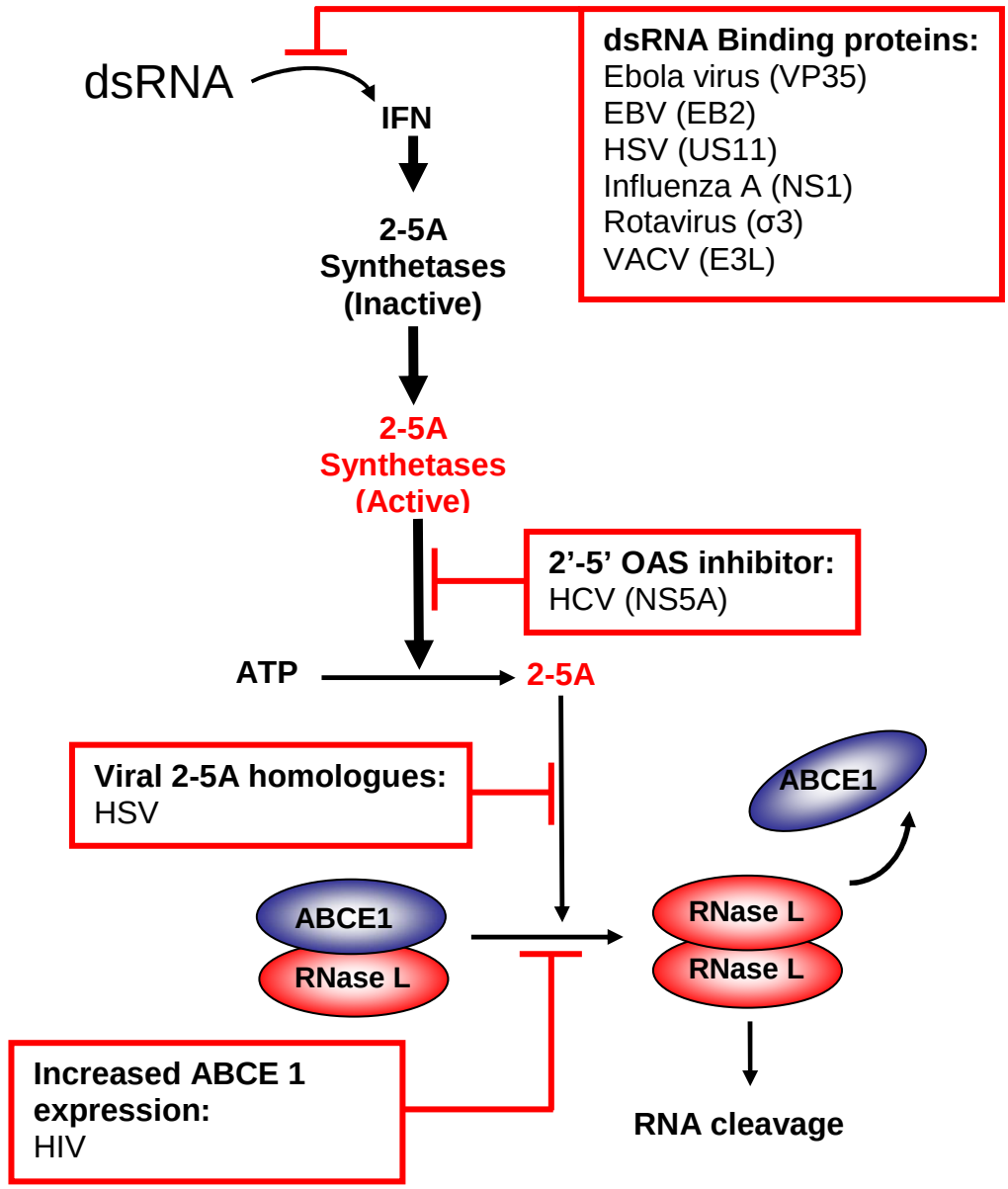

Figure 5.4 – The 2-5A Oligoadenylate/ RNase L system is a key antiviral defence pathway. However, many viruses have strategies by which they can circumvent the antiviral effects of the pathway allowing complete viral replication to proceed unhindered (target points are shown in red). (Diagram adapted from [224, 249].

5.1.4.1. Viral 2-5A homologues

The Herpes Simplex viruses I/II (HSV I/II) employ a multi-faceted approach to disabling the RNase L pathway utilising virally encoded proteins. Initially, early in its productive phase of replication, HSV is capable of inhibiting the accumulation of interferon stimulated gene (ISG) transcripts through the actions of virally encoded proteins. For example, ICP0, an immediate-early protein inhibits IRF3-mediated transcriptional activation of ISGs, and virion host shutoff protein (*vhs*), an endonuclease that associates with the translation initiation factor eIF4F, resulting in cellular degradation of cellular mRNA and shut-off of host cell protein synthesis (reviewed in [250] and [251]). However, these activities do not explain the ability of HSV to replicate *in vitro* in cells previously primed with IFN treatment, which indicates alternative mechanisms [250]. It was noticed that much higher doses of α or β IFNs (100-1000 reference units/ml) were required to inhibit the growth of HSV I/II infected Chang cells than the same cells infected with encephalomyocarditis virus (ECMV) (10-100 reference units/ml) [252]. It was also demonstrated that the levels of 2-5A dependent rRNA cleavage products in HSV I/II infected Chang cells were noticeably lower than those found in ECMV-infected cells, signifying a drop in RNase L/ 2', 5'-oligoadenylate activity. Interestingly, these authors went on to demonstrate the presence of virally synthesised 2-5A homologues in HSV infected cells which, unlike endogenous 2-5A, possessed only weak RNase L-activating capabilities, providing an explanation as to the higher IFN dosage required to successfully treat HSV I/II infections [252].

5.1.4.2. dsRNA binding proteins

Double stranded RNA-binding proteins (DRBPs) (reviewed in [253]) are a family of prokaryotic, eukaryotic and virally encoded proteins containing an evolutionarily conserved dsRNA binding domain (DRBD) of approximately 65-68 amino acids [253]. DRBPs carry out many essential physiological roles, helping to regulate signalling pathways and gene expression [253]. For example, DICER, an RNase-III endonuclease is involved with RNA interference-mediated gene silencing (reviewed in [254]) whilst the NFARs (Nuclear Factors Associated with RNA) NF-90, MMP4 and DRB76 are associated with mRNA post-transcriptional regulation, mRNA stability, export and translation [253, 255].

DRBPs also play a role in host defence pathways, as exemplified by the IFN-dependent double-stranded RNA-dependent protein kinase R (PKR) (reviewed in [234]) which along with its C-terminal catalytic domain, contains two DRBDs in its N-terminal domain. PKR is constitutively expressed at low level however, its expression is up-regulated in the presence of IFN [234]. The antiviral effects of PKR are mediated through phosphorylation of eIF2α, which arrests eIF2α in the translation pre-initiation complex, preventing future rounds of translation from occurring [249].

The use of virally encoded dsRNA-binding proteins to interfere with IFN-dependent host defence mechanisms is a technique employed by several viruses. For example Vaccinia virus

(DRBP - E3L protein), HSV (Us11) Epstein-Barr virus (EB2), Influenza A (NS1), Reovirus (σ3) and Ebola virus (VP35) (as reviewed in [249]) subvert the IFN-dependent PKR/ RNase L pathways through a combination of sequestering dsRNA preventing IFN activation or by directly binding to the DRBD regions of PKR preventing its activation .

5.1.4.3. Inhibition of 2-5A oligoadenylate synthetase and selection of resistant strains

Hepatitis C virus (HCV) is the leading cause of both chronic liver disease and hepatocellular carcinoma (HCC) in western countries, and combination therapy consisting of Interferon and ribavarin is the most effective treatment strategy (reviewed in [256]). HCV, like HSV, has also developed a multi-faceted approach to subvert the host antiviral response utilising two distinct strategies: selection of IFN-resistant strains and inhibition of 2',5'-oligoadenylate synthetase mediated by the viral protein 'non-structural protein 5A' (NS5A). Reviewed in [257] the NS5A protein is localised to the cytoplasmic perinuclear region and is considered an extremely pleiotropic protein with key roles in viral RNA replication and modulation of the host cell physiology. Early work by Enomoto et al (1995) in patients chronically infected with HCV-1b identified mutations within a discreet central region of the HCV NS5A protein that correlated with response to IFN treatment. This was labelled the 'interferon sensitivity-determining region (ISDR)' [258, 259]. Identification of the ISDR suggested that NS5A plays a role in HCV resistance to IFN, which was later confirmed by Gale et al (1997). These authors demonstrated that PKR repression and IFN resistance were mediated through direct binding between NS5A and the PKR ISDR, therefore preventing the dimerisation and resultant activation of PKR [260, 261].

Subsequent work demonstrated that NS5A could also inhibit the effects of IFN in an ISDR and PKA-independent manner, indicating the existence of previously unknown mechanisms of immune evasion by HCV [262]. The work of Taguchi et al (2004) concluded that the exact nature of these mechanisms were due to inhibition of 2',5'-oligoadenylate synthetase, with subsequent inactivation of RNase L. NS5A was shown to physically interact with 2',5'-oligoadenylate synthetase, with the interaction requiring an N-terminal region (aa 1-148) of NS5A, which does not contain the ISDR, and two regions of 2',5'-oligoadenylate synthetase (aa 52-104 and 184-275) [257]. Interestingly the NS5A binding points within 2',5'-oligoadenylate synthetase are known to contain several regions important for enzymatic activity, suggesting inhibition of 2',5'-oligoadenylate synthetase function is mediated through binding within the active site [257].

Chronic HCV infections are a significant cause of worldwide morbidity and mortality and Interferon-α2b treatment, in conjunction with the pro-drug ribavarin, eliminates HCV from patients infected with HCV genotypes 2 and 3 (HCV 2a, 2b, 3a & 3b) much more efficiently than those infected with a HCV genotype 1 virus (HCV 1a & 1b) [263]. Han and Barton (2002) demonstrated that in HCV-1 genotypes, the RNase L sensitive UU/UA sequences occurred much less frequently

than in the more interferon-sensitive genotypes [263]. This data suggests that during the course of IFN treatment mutations could possibly accumulate in HCV-1 mRNA's that result in the escape of HCV from the antiviral effects of RNase L with subsequent positive selection of resistant strains [224].

5.1.4.4. Increased ABCE expression

HIV-1 virion formation requires the assembly of ~5,000 Gag polypeptides into an immature spherical capsid structure. This process occurs in an ATP-dependent, multistep process and requires a host protein of 68 kDa, identified as ABCE1, the endogenous inhibitor of RNase L [264, 265]. RNase L has been shown to degrade HIV-1 transcripts during the early stages of HIV infection and HIV-1 transcript accumulation coincides with a reduction in RNase L activity [266]. Based on these observations, Martinand *et al* (1999), used an *in vitro* system based on human T-cell H9 cells infected with HIV-1, to demonstrate that a decrease in RNase L activity coincided with an increase in the HIV-induced expression of the ABCE1 endogenous inhibitor of RNase L [266].

5.1.5. RNase L and human disease

Whilst the antiviral properties of RNase L are now well documented, it has become apparent that defects within the 2',5'-oligoadenylate (2-5A) pathway are now implicated in a range of human pathologies such as prostate cancer and chronic fatigue syndrome (CFS).

5.1.5.1. Familial Prostate cancer

The prostate is a walnut-sized gland which is a component of the male reproductive system. It is located below the bladder, in front of the rectum, and produces and stores seminal fluid [267]. Prostate cancer is the most common cancer of men in the UK, accounting for almost a quarter of new cancer diagnoses. The risk of developing prostate cancer increases with age and more than half of cases arise in men over the age of 70. Worldwide, approximately 913,000 men were diagnosed with prostate cancer in 2008, leading to approximately 258,000 deaths (data from http://www.cancerhelp.org.uk/type/prostate-cancer/). Whilst age, environmental and hormonal factors are known to play key roles in prostate cancer pathogenesis more recently, host genetics has been shown to play a role in a subset of prostate cancers termed hereditary prostate cancer (HPC). As demonstrated in a case-controlled study by Steinberg et al (1990), men with a father or brother affected with prostate cancer were twice as likely to develop prostate cancer when compared to men with no affected relatives. Interestingly, the risk was shown to increase with

increasing number of first-degree family members affected (a 5 and 11-fold increased risk for two and three first degree relatives affected respectively) [268].

Early linkage analysis studies of families affected by HPC identified several loci that could potentially be harbouring prostate cancer susceptibility gene(s) namely *HPC1* (1q24-25) [269] and subsequently *HPCX* (Xq27-q28), *PCAP* (1q42), *CAPB* (1p36), *HPC20* (20q13) and *HPC2/ELAC* (17p) (reviewed in [270, 271]). The proposed HPC gene(s) were predicted to account for ~43% of early-onset prostate cancer cases (≤55 years of age) and ~9% of all cases [267] whilst further work demonstrated *HPC1* linkage was most common amongst those families in which prostate cancers cases were considered more severe [272]. The proposed link between prostate cancer and RNase L was firmly established with the discovery of germline mutations in *RNASEL* that segregated within prostate cancer families showing linkage to *HPC1* [273] and mutations in *RNASEL* are now unequivocally linked with prostate cancer [274-278]. Several key mutations (reviewed in [279]) have since been identified, the three most extensively studied being:

- **E265X** – A 795G→T transition resulting in conversion of a glutamic acid residue with in the 2-5A binding domain to a stop codon.
- **M1L** – A 3G→A transition resulting in a methionine to isoleucine transition in the translational start codon producing a missense mutation.
- **R462Q** – A missense mutation located within the kinase-like domain. A G→A transition at nucleotide position 1385 results in an amino acid change of arginine to glutamine at position 462.

Both the E265X and M1L variants produce an RNase L with an activity level 50% below that of the wild type protein. The R462Q transition, located within the kinase like domain (Figure 5.1) produces a three-fold reduction in catalytic activity. This was shown to be due to an impaired ability of RNase L to fully dimerise, with a subsequent failure of the protein to induce RNA degradation and apoptosis [224]. Males heterozygous for this variant carry a 1.5-fold increased risk, whilst homozygous males carry a 2-fold increased risk of developing prostate cancer, in fact, R462Q variant is now implicated in up to 13% of prostate cancer cases [280].

5.1.5.2. Chronic fatigue Syndrome (CFS)

CFS (reviewed in [281]) is a debilitating syndrome, predominantly affecting women, thought to affect 240,000 people in the UK. It is characterised by unexplained and extreme fatigue lasting for a period of at least 6 months. Additional symptoms include memory loss/ poor concentration, sore throat, lymphadenopathy, muscle pain and extreme exhaustion after physical exertion, non of which are resolved with bed rest [281]. Both neuroendocrinological and immunological causes have been put forward to explain CFS, although there is also thought to be a link between infection and the disorder. Epstein Bar virus (EBV), *Candida Albicans, Borellia*

Burgdorferi, Enterovirus, Cytomegalovirus, Coxsackie B virus and Hepatitis C virus have all been linked to CFS; however no conclusive link between any of these infectious agents and CFS has been demonstrated [282]. Studies have shown chronic immune activation [281] and dysregulation of the 2',5'-oligoadenylate (2-5A) synthetase/RNase L antiviral pathway occurs in CFS patients [283, 284] potentially indicating a viral aetiology for both CFS and prostate cancer. This prompted research, from several independent groups, into the possibility of viral involvement and led to the identification of a potentially novel gammaretrovirus pathogen.

5.1.5.3. Xenotropic Murine leukaemia virus-Related Virus

5.1.5.3.1. Discovery and potential association with disease

As discussed, RNase L is a key protein in the antiviral response. Thus, rather than reduced apoptosis of aberrant cells being responsible for the development of prostate cancer, it was hypothesised that a mutation-related reduction in the RNase L-dependent antiviral response could enhance cellular susceptibility to infection with an as yet unknown tumour virus (in genetically susceptible individuals). Urisman et al (2006), used a viral detection DNA microarray composed of highly conserved viral sequences, to detect novel gammaretroviral sequences in 7/11 (63%) cDNA samples derived from R462Q-homozygous prostate cancer cases in comparison to 1/8 (12.5%) homozygous (RR)/ heterozygous (RQ) prostate cancer cases [285]. Following on from these initial findings, specific RT-PCR analysis of 86 prostate tumours demonstrated the same gammaretroviral sequences in 8/20 (40%) cases, in comparison to 1/66 (1.5%) RR/RQ cases [285]. The novel virus demonstrated a high degree of sequence homology to known murine leukaemia viruses carried by most mouse strains as endogenous integrated viral genomes yet was shown to be a distinct virus and was named Xenotropic Murine leukaemia virus-Related Virus or XMRV [286]. Having produced a replication-competent viral clone, Dong et al (2007) demonstrated successful XMRV replication in the prostate cancer cell lines DU145 and LNCaP, along with an ovarian cancer cell type (Hey1b) and a cervical carcinoma cell line (HeLa) [287]. Interestingly, XMRV replication in DU145 cells was inhibited by IFN-β treatment [287]. Conversely, LNCaP cells, previously shown to be deficient in JAK1 [288], an integral protein required for IFN signalling, and partially deficient in RNase L [289], were resistant to IFN-mediated inhibition of XMRV replication [287]. This illustrates the importance of a fully functioning RNase L pathway against XMRV. XMRV was also shown to have no sequence homology with known *h*uman *e*ndogenous *r*etro*v*iruses (HERVs) potentially making XMRV the third extant retrovirus known to infect humans, the other two being HIV and the HTLV-family, which belong to the lenti- and δ-retrovirus genera respectively. Sequencing data on full-length XMRV virus cloned from three separate RNase L QQ variant tumours indicated infection had occurred with the same type of virus, however, sequence variation within *gag* and *pol* regions were also suggestive of independent acquisition of the virus in each case [285]. These findings

suggest XMRV is transmitted by an exogenous route [290], and recent work suggests sexual transmission as a possible route of infection [291].

Whilst the original study [285] demonstrated that the presence of XMRV was restricted to prostate stromal fibroblasts, subsequent work have since detected XMRV in epithelial cells of prostate cancer cases [292] and in the prostate epithelial cell line 22Rv1 [293]. However, regardless of tropism, the requirement of the Xenotropic and polytropic retrovirus receptor 1 (XPR1) for viral entry, a cellular receptor thought to be ubiquitously expressed in human cells is a common link [287].

The potential link between XMRV and CFS (5.1.1.5.2) was originally suggested by Lombardi et al (2009) who demonstrated the presence of XMRV DNA in peripheral blood mononuclear cells (PBMCs) from 67% (68 out of 101) CFS patients in comparison to 3.6% (5 out of 218) healthy controls [294]. More recent data from the same research group, using the same sample set, has since demonstrated XMRV DNA in 85% of the original 101 CFS patient samples tested [295] demonstrating the problems faced by researchers due to the lack of standardised assays for XMRV detection.

5.1.5.3.2. Potential mechanism of XMRV oncogenesis

Although work has demonstrated that XMRV possesses no direct transforming abilities in cell culture models, it is capable of causing rare transformations, possibly indicative of indirect activation of endogenous oncogenes [296]. Also, XMRV possesses no oncogenes however the *Env* protein of other retroviruses has previously been shown to cause transformation in susceptible cells [297-301] and it is thought that XMRV may induce oncogenesis through low level insertional activation of oncogene(s) [302].

5.1.5.3.3. XMRV: A new gammaretrovirus or laboratory contamination?

Despite early studies implicating XMRV in human disease, many recent studies have failed to reproduce the findings. In particular, the presence of XMRV in CFS patients [294] has been contested by a number of independent research groups, each failing to identify XMRV specific sequences [303-306]. Indeed, many recent studies have since gone on to suggest that XMRV is merely a result of laboratory contamination with known murine leukaemia viruses (MLVs) [307-310]. Whilst the findings are inconclusive at this stage XMRV research is still on-going.

5.2. Aims

5.2.1. RNase L was identified as a protein of interest based on results from the Panorama Xpress profiler-725 array. The lopinavir induced increase in protein expression will be confirmed initially by western blot using protein lysates isolated from lopinavir treated cells as described in Chapter 4

5.2.2. The relationship between lopinavir concentration/ length of incubation time and RNase L expression in SiHa cells will be assessed by western blot analysis

5.2.3. The expression of the endogenous inhibitor of RNase L (ABCE1) following lopinavir treatment in SiHa cells will be assessed by western blot analysis

5.3. Methods

5.3.1. Analysis of RNase L mRNA expression in lopinavir treated cells

SiHa, CaSKi, C33A parent, C33A E6 (section 2.3.1) and all Tert cell types (section 3.3.1.1) were thawed and cultured, as described in sections 2.3.2 & 2.3.3, at 37℃/ 5% CO_2 to a confluency of 80%. Having identified lopinavir-mediated alterations in the proteome of SiHa cells, highlighting an increase in RNase L, it was important to confirm this finding using more longstanding and robust methods. However as a matter of interest, prior to subsequent work, the endogenous expression levels the endogenous expression of RNase L in a range of cell types was also assessed. Furthermore, to highlight, if any, the association(s) between E6 and RNase L the C33A test system will be utilised as it provides a suitable non-E6 expressing control cell type, a factor lacking when solely using SiHa cells. Should E6 subsequently be found to modulate the activities of RNase L and/or the antiviral properties of lopinavir, CaSKi cells will be a useful cell line with which to confirm these findings; Like SiHa cells, CaSKi cells contain fully integrated HPV. However, in contrast to SiHa cells which contain 1-2 copies per cell [186], CaSKi cells are known to contain 400 – 600 HPV16 copies per cell [311], so in theory, any E6-dependent effects will be much more pronounced in the CaSKi cell system.

Upon reaching 80% confluency, cells were treated with lopinavir or an equal volume of DMSO. All cells were treated with lopinavir at a final concentration of 25 µM with the exception of Tert cells, which, due to their increased sensitivity to lopinavir (demonstrated in chapter 3), were treated at 5 µM final concentration. Cells were returned to the incubator at 37℃/ 5% CO_2 and at 6 hrs, cells were harvested and 1 x 10^5 cells counted and washed twice in PBS. RT-PCR analysis was carried out as described in section 2.3.18.2 using RNase L and PLA specific primer pairs (detailed in Appendix 3).

5.3.2. Western blot analysis of RNase L and ABCE1 protein levels in SiHa cells

5.3.2.1. Dose response sample preparation

SiHa cells were cultured (as described in section 2.3.3) to a confluency of 80% whereupon they were treated with DMSO or an increasing dose of lopinavir over a range of 5 - 30 µM, in 5 µM increments with DMSO levels adjusted to remain constant throughout. Cells were incubated at 37℃/ 5% CO_2 and harvested 6 hrs post-incubation with lopinavir by trypsinisation and counted (as described in section 2.3.3) prior to centrifugation at 528 x g for 5 min, after which, the supernatant was aspirated and discarded. Cells were resuspended in 500 µl PBS and transferred to a sterile eppendorf, and centrifuged at 295 x g for 5 min after which, the PBS was aspirated and the cells resuspended in a sufficient volume of a 1:1 mix of PBS and 2 x Laemmle buffer (see Appendix 2) to ensure a lysate with 0.5 x 10^6 cells/ 20 µl. All samples were then subjected to three flash

freeze/thaw cycles with heating to 95℃ before being stored at -20℃. Proteins were separated using a 12% SDS-PAGE gel as described in section 5.3.2.4, and then transferred onto an Hybond-C nitrocellulose membrane and a western blot carried out, including a GAPDH loading control as described in section 5.3.2.5.

5.3.2.2. Time course sample preparation

SiHa cells were cultured to a confluency of 80% whereupon the growth medium was aspirated and replaced with complete RPMI supplemented with lopinavir at a final concentration of 25 µM or an equal volume of DMSO. Cells were then harvested at 2, 4, 6, 8, 12 and 24 hrs post-incubation and prepared for SDS-PAGE analysis as described in section 5.3.2.1.

5.3.2.3. Effects of 25 µM lopinavir on E6/E7 Immortalised PHFKs

In collaboration with Professor Ingeborg Zehbe (Lakehead University, Thunder Bay, Canada) the effects of lopinavir on E6/E7 immortalised human keratinocytes were evaluated. Karyoptically normal human primary foreskin keratinocytes and immortalised human keratinocytes stably expressing HPV E6 and HPV E7 were treated for 72 hrs with lopinavir over a concentration range of 5 - 40 µM. Cell pellets from E6/E7 expressing PHFKs treated with 25 µM lopinavir over 72 hrs were provided which were thoroughly resuspended in 50 µl CelLytic-M^{TM} cell lysis buffer (Sigma-Aldrich, Dorset, UK). Protein concentrations were estimated using the Bradford assay (described in section 4.3.4) and normalised using CelLytic-M^{TM} cell lysis buffer, to ensure equal loading of proteins. Proteins were separated on a 12% SDS-PAGE gel as described in section 5.3.2.4 and proteins transferred to Hybond-C nitrocellulose membrane. This was immuno-probed with primary rabbit anti-RNase L antibody, followed by primary mouse anti-GAPDH to confirm equal loading (section 5.3.2.5).

5.3.2.4. Sodium dodecyl sulphate Polyacrylamide Gel Electrophoresis

A Whatman minigel twin system (Whatman Biometra, Goettingen, Germany) was used for the separation of proteins by sodium dodecyl sulphate polyacrylamide gel electrophoresis (SDS-PAGE). In brief, gel casting moulds were assembled according to the manufacturers' instructions. A 12% separating gel was prepared (5 ml sdH_20, 6 ml 30% acrylamide solution, 3.8 ml 1.5M Tris-HCL (pH 8.8), 150 µl 10% SDS solution, 150 µl 10% ammonium persulphate (APS) solution (Sigma Aldrich, Dorset, UK) and 6 µl N, N, N', N'-tetramethylethylenediame (TEMED) (Sigma Aldrich, Dorset, UK)), poured and overlaid with sdH_20 to prevent drying out and to ensure a smooth interface between gels. After complete polymerisation, a stacking gel was prepared and poured (2.7 ml sdH_20, 670 µl 30% acrylamide solution, 500 µl 1M Tris-HCL (pH 6.8), 40 µl 10% SDS, 40 µl 10% APS and 4 µl TEMED) allowing a depth of 1 cm between the bottom of the sample well and the separating gel. An appropriate sample well comb was put in place and the stacking gel allowed

to fully polymerise. Proteins from 0.5 x 10^6 cells (20 µl) were loaded along side 10 µl Novex sharp prestained protein standards (Invitrogen, Paisley, UK) and were separated in 1 x Laemmle running buffer at 20 mA.

5.3.2.5. Western blot

Protein transfer and western blotting was carried out using the method originally described by Towbin et al (1979) [312]. Proteins were transferred onto Hybond-C nitrocellulose membrane (Amersham Biosciences, Bucks, UK) soaked in 1 x transfer buffer containing methanol using a Whatman Biometra semidry blotter (Whatman Biometra, Goettingen, Germany) for 40 min at 10 V. The membrane was air dried prior to blocking in PBS containing 5% non-fat milk powder and 0.1% Tween-20 (Sigma Aldrich, Dorset, UK) for 2 hrs at room temperature with gentle shaking. After three PBS washes, membranes were incubated overnight at 4 ℃ with primary rabbit anti-RNase L antibody (ab32307, Abcam, Cambridge, UK) at a concentration of 1/500 in PBS with gentle shaking. Following three 5 min PBS washes membranes were incubated for 2 hrs at room temperature with swine anti-rabbit horse radish peroxidise (HRP) conjugated secondary antibody (Dako, Cambridge, UK) at a concentration of 1/2000 in PBS containing 5% non fat milk powder with gentle shaking. Following three further 5 min PBS washes, proteins were visualised using ECL (Amersham Biosciences, Bucks, UK) and exposure to hyperfilm (Amersham Biosciences, Bucks, UK) according to the manufacturer's recommendations.

Membranes were re-probed with glyceraldehyde-3-phosphate dehydrogenase (GAPDH) housekeeping protein antibody to confirm equal protein loading. Following a brief PBS wash, the membrane was incubated for 1 hr at room temperature in 5% non-fat milk powder in PBS with gentle shaking. Membranes were incubated for 2 hrs at room temperature with primary mouse anti-GAPDH (ab9484, Abcam, Cambridge, UK) at a concentration of 1/1500 with gentle shaking. These were given three 5 min PBS washes then incubated for 2 hrs at room temperature with rabbit anti-mouse HRP conjugated secondary antibody (Dako, Cambridge, UK) at a concentration of 1/2000 in PBS containing 5% non-fat milk powder. Proteins were visualised using ECL and exposure to hyperfilm (Amersham Biosciences, Bucks, UK) according to the manufacturers' instructions.

5.3.3. Analysis of the endogenous inhibitor of RNase L (ABCE1) protein levels in SiHa cells in response to increasing lopinavir concentration and increasing incubation time

Using the protein lysates samples produced in section 5.3.2.1, proteins were again separated using a 12% SDS-PAGE gel and transferred to Hybond-C nitrocellulose membrane as

described in sections 5.3.2.4 and 5.3.2.5 respectively. Primary rabbit anti-ABCE1 antibody (Abcam, Cambridge, UK, ab32270) was used at a concentration of 1/200 in PBS containing 0.1% BSA, and the membranes incubated for 2 hrs at room temperature with shaking. Membranes where then rinsed with three 5 min incubations in PBS and incubated with swine anti-rabbit HRP conjugated secondary antibody (Dako, Cambridge, UK) as described in section 5.3.2.4, before being visualised with ECL and Hyperfilm. A GAPDH loading control western blot was carried out as described above.

5.3.4. Analysis of RNase L expression in lopinavir treated E6/E7 immortalised PHFKs

Having previously demonstrated the increased susceptibility of E6/E7 immortalised PHFK cells to lopinavir when compared to non-transduced PHFK cells (Chapter 3, Figure 3.5) the expression of RNase L protein in E6/E7 immortalised PHFK cells exposed to 25 µM lopinavir for 72 hrs was assessed by western blotting, using the techniques described in sections 5.3.2.4 and 5.3.2.5.

5.4. Results

5.4.1. Analysis of mRNA expression levels following lopinavir treatment

The Sigma Panorama XPRESS-profiler 725 antibody microarray demonstrated that lopinavir treatment caused an up-regulation in RNase L in HPV positive SiHa cells. However, this accumulation of RNase L protein levels could have arisen through several possible mechanisms; lopinavir could be stimulating an up regulation in RNase L mRNA transcription, increasing the rate of protein translation or inhibiting protein breakdown. RT-PCR analysis (section 5.3.1) was used for semi-quantitative comparison of RNase L mRNA levels between lopinavir and DMSO control treated in a range of HPV positive and negative cell lines (Figure 5.5). This confirmed the presence of RNase L mRNA PCR product at the expected size of 194 bp in Caski, SiHa and the full range of Tert cells. These data also demonstrated the absence of RNase L transcripts in C33A vector and E6 cells, which is the subject of further investigated in Chapter 6. Significantly, lopinavir produced no significant changes in the mRNA levels of RNase L when compared to DMSO treated control cells.

Figure 5.5 RNase L mRNA expression levels following lopinavir treatment

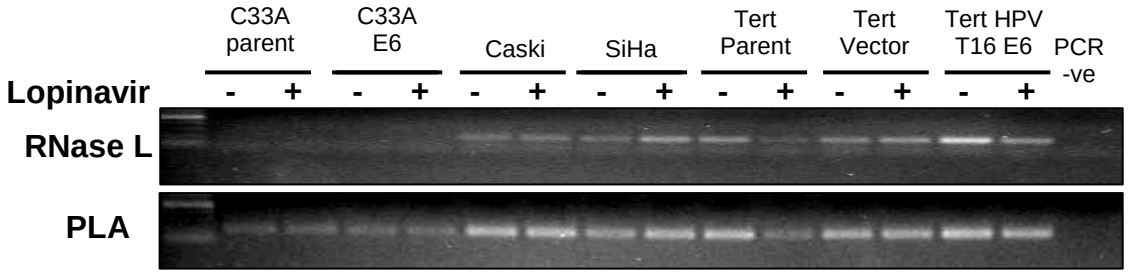

Figure 5.5 – RNase L mRNA expression levels were assessed in a range of HPV positive and HPV negative cell lines. Cells were treated with 25 µM lopinavir (+) or DMSO (-) untreated control. Cells were harvested at 6 hrs and RT-PCR carried out using RNase L specific and PLA control primers. Tert cells were treated at a final concentration of 5 µM. Samples were separated along side a 100bp PCR ladder. No noticeable alteration in mRNA expression was observed.

In order to confirm that lopinavir treatment did not alter RNase L mRNA expression in SiHa cells, the RT-PCR analysis was carried out in triplicate cultures of SiHa cells following 6 hr incubation with 25 µM lopinavir or an equal volume of DMSO (Figure 5.6). Subsequent densitometric analysis was carried out using Image J analysis program (http://rsbweb.nih.gov/ij/), with mean values and standard deviations calculated using Microsoft Excel (2003). Lopinavir treatment was shown to have no effect on RNase L mRNA levels when compared to DMSO treated control cDNA ($p = 0.244$, with values less than 0.05 considered significant).

Figure 5.6 Lopinavir does not significantly alter RNase L mRNA levels

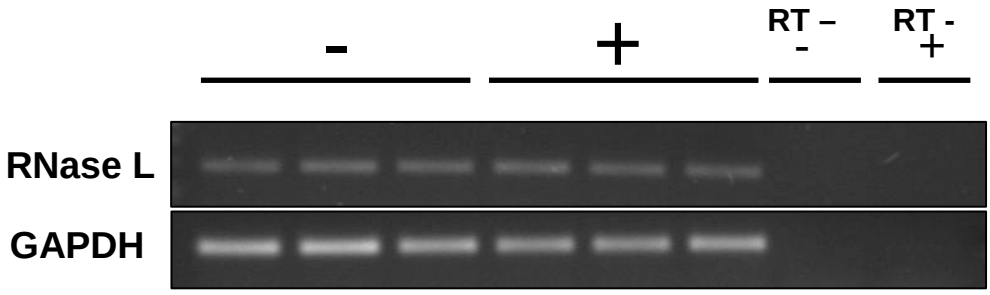

Figure 5.6 – SiHa cells were grown to 80% confluency at which point they were treated with 25 M lopinavir (+) or DMSO control (-) for 6 hrs. Cells were harvested and RT-PCR was repeated in triplicate using RNase L and GAPDH control primers. RT-negative control samples (RT-) were included for both treated and untreated cells to demonstrate the absence of genomic DNA contamination.

5.4.2. Lopinavir produces a dose dependent increase in RNase L protein levels in SiHa cells.

The lopinavir induced increase in RNase L protein levels (Chapter 4) was confirmed with western blot analysis of protein lysates prepared as in section 4.3.2 (Figure 5.7(A)). This demonstrated an increase in RNase L protein levels following 6 hr incubation with 25 µM lopinavir when compared to a DMSO treated control cell protein lysate. Following on from this, the relationship between lopinavir dose and RNase L expression was also assessed by western blotting. Lopinavir was shown to produce a clear dose dependent increase in RNase L over the concentration range studied (Figure 5.7(B)). RNase L signal strengths are displayed as relative intensity compared to matched GAPDH controls, and demonstrate a clear dose-dependent increase in RNase L expression Figure 5.7(C).

Figure 5.7 - Lopinavir produces a dose-dependent increase in RNase L

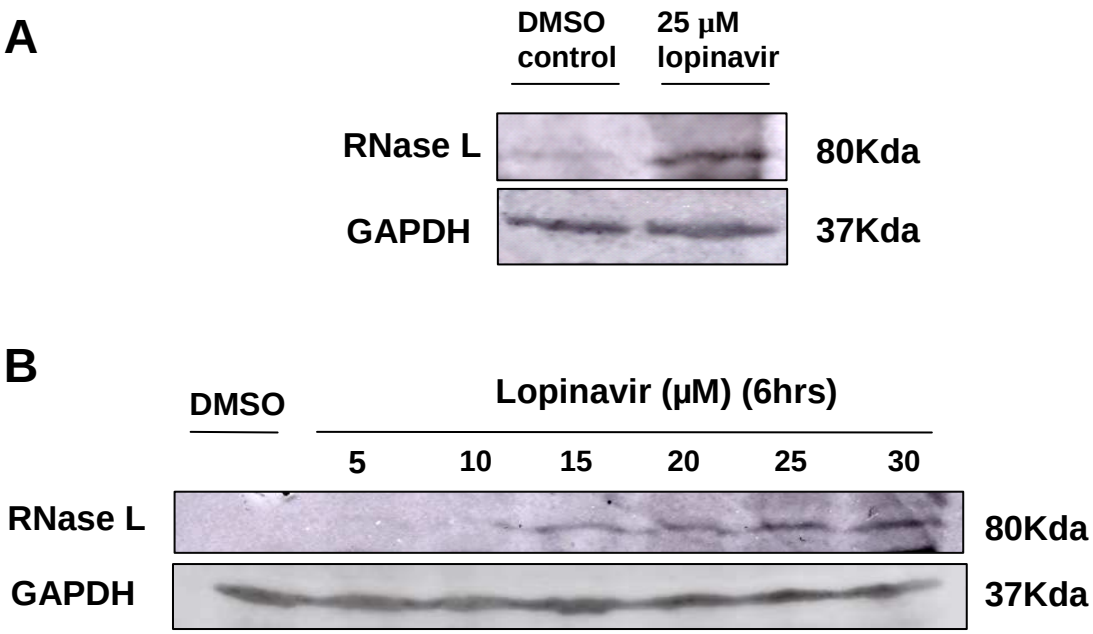

C – Image J density analysis, lopinavir dose response in SiHa cells

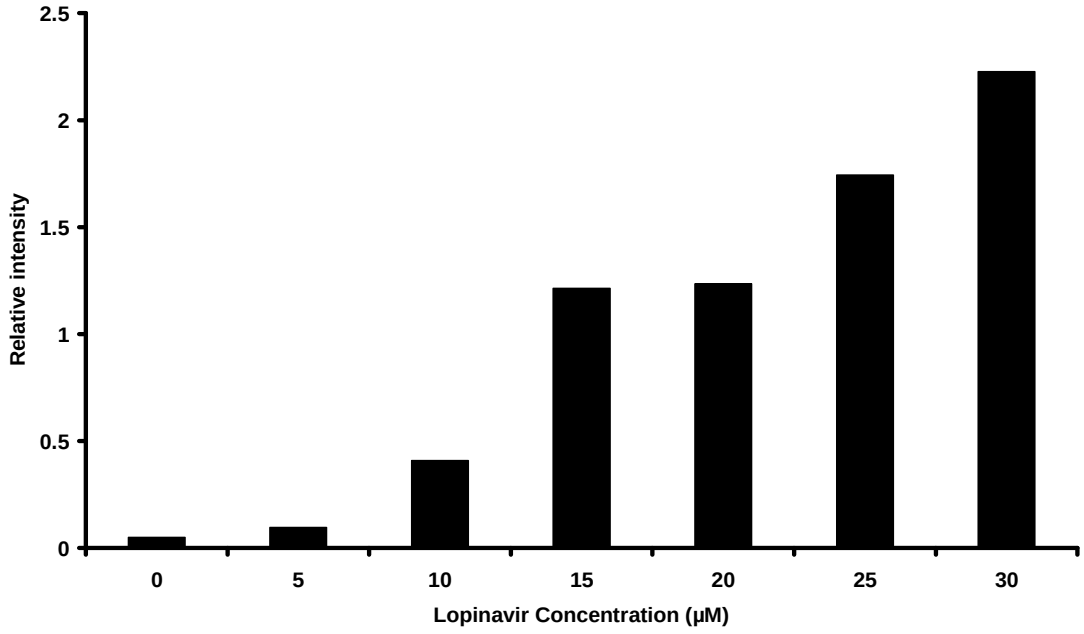

D – Lopinavir Dose Response, RNase L signal Full Blot

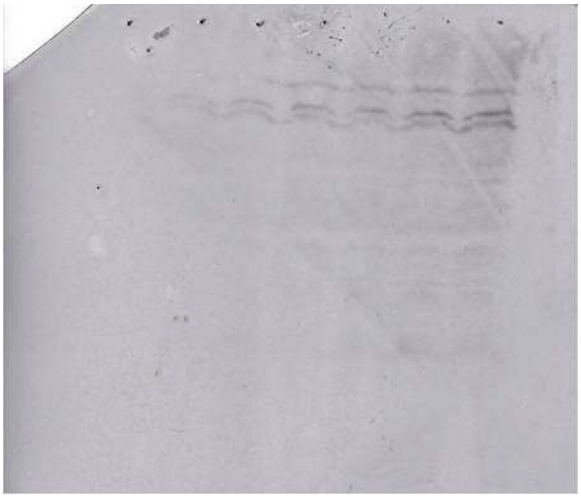

Figure 5.7 – (A) Western blot analysis on 6hr 25 µM lopinavir treated SiHa cells prepared during the antibody microarray analysis. Proteins separated on a 12% SDS-PAGE. A western blot was carried out using primary rabbit anti-RNase L and mouse anti-GAPDH antibodies. Confirms the induction of RNase L protein in lopinavir treated SiHa cells. (B) Western blot analysis on SiHa cells treated with an escalating dose of lopinavir for 6 hrs (C) Image J (available from http://rsbweb.nih.gov/ij/) density analysis of protein signals from western blot, shown as a relative intensity compared to matched GAPDH signals shows a clear dose dependent increase in RNase L protein levels. Analysis based on a single experiment. (D) Full image western blot, RNase L/ lopinavir dose response.

5.4.3. Lopinavir produces time dependent changes in RNase L protein levels in SiHa cells

Having demonstrated the ability of lopinavir to produce a dose dependent increase in RNase L protein levels in SiHa cells, the relationship between changes in incubation times at a fixed lopinavir concentration of 25 µM was assessed. Western blot analysis demonstrated a clear time-dependent increase in RNase L protein level (Figure 5.8(A)). Again, densitometric analysis was used to express RNase L signal as a relative intensity based on matched GAPDH control and demonstrated an almost linear increase in RNase L over the time points studied (Figure 5.8(B)). The peak signal strength occurred 8-12 hrs post-incubation, followed by a reduction in signal strength at 24 hrs.

Figure 5.8 - Lopinavir produces a time dependent increase in RNase L

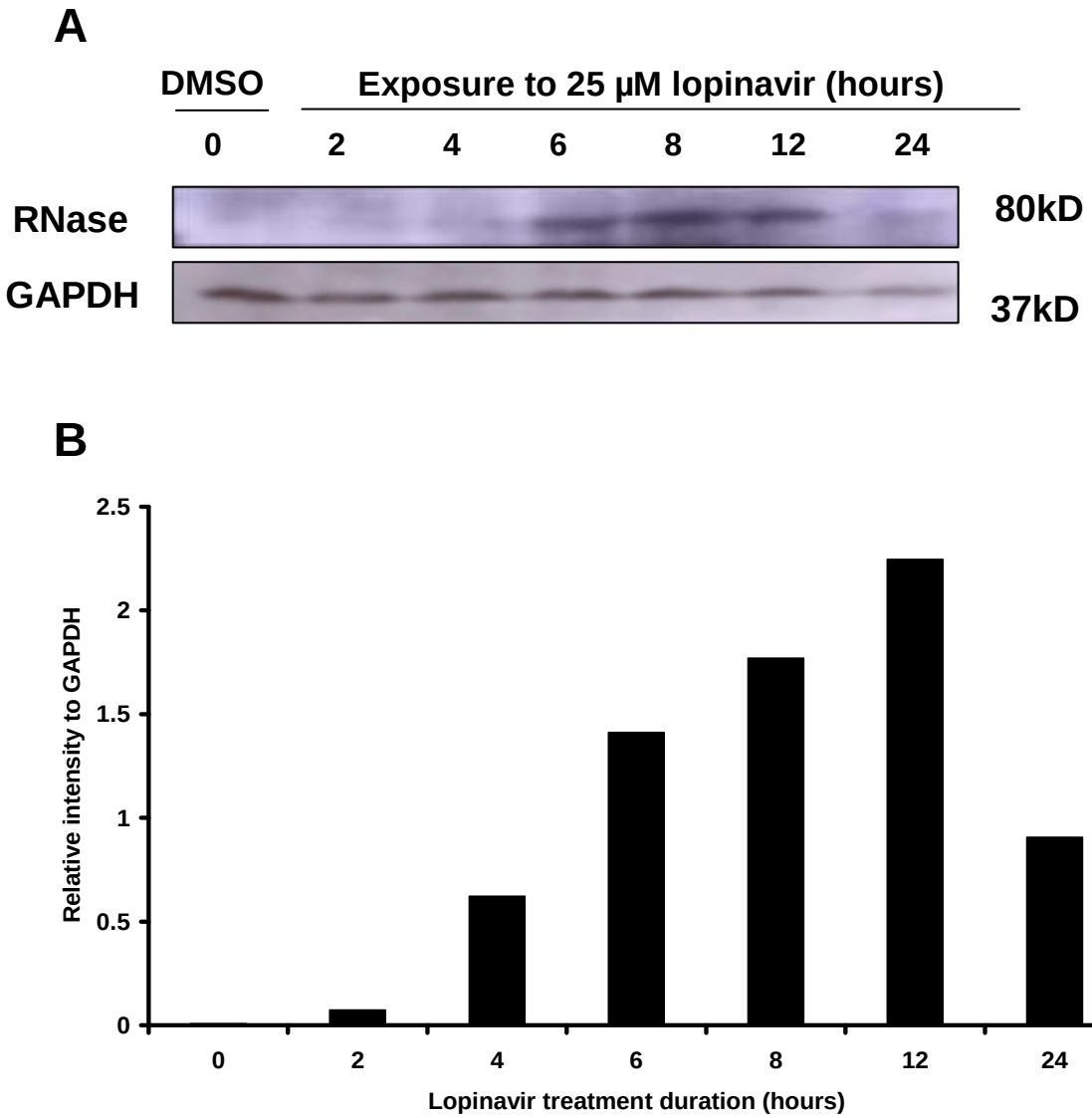

Figure 5.8 – SiHa cells were treated with lopinavir at 25 µM for 2, 4, 6, 8, 12 and 24 hrs before being harvested. (A) Proteins were separated on a 12% SDS-PAGE and transferred to Hybond-C nitrocellulose membrane and a western blot carried out using primary rabbit anti-RNase L and mouse anti-GAPDH antibodies. (B) Image J (http://rsbweb.nih.gov/ij/) density analysis of protein signals from western blot, shown as a relative intensity compared to matched GAPDH signals, based on a single experiment. This demonstrates a clear time dependent increase in RNase L protein levels, with a peak at 12 hrs, followed by a reduction in levels at 24 hrs.

5.4.4. Lopinavir induces a significant increase in RNase L expression

Based on the triplicate RNase L western blot data from Figures 5.7(A) and (B) and Figure 5.8(A), mean RNase L and GAPDH signal strengths were evaluated for all the 6 hr, 25 µM lopinavir data points shown. Using densitometric analysis (Image J) software, mean intensities, mean

relative intensities and standard deviations were calculated using Microsoft Excel, and are shown below (Figure 5.9). A 'p' value below 0.05 was considered significant and a student t-test was performed using Microsoft excel (2003) to compare lopinavir and DMSO treated protein lysates. Cells exposed to 25 µM lopinavir for 6 hrs showed a very significant 9.5-fold increase in RNase L protein ($p = 0.005$) when comparing DMSO control cells (Figure 5.9).

Figure 5.9 – Lopinavir produces a significant increase in RNase L protein levels

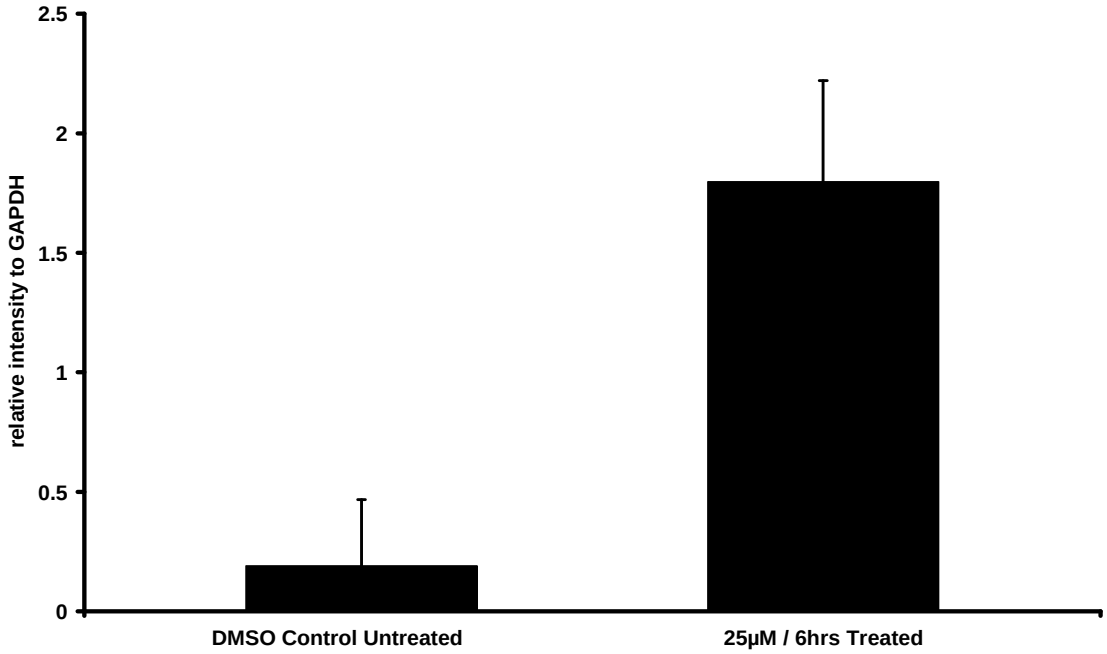

Figure 5.9 – Using the Image J density analysis program, mean relative intensities were calculated based on triplicate data sets of the untreated DMSO control and six hour lopinavir (25 µM) treated RNase L signals. Lopinavir treatment was shown to induce a significant 9.5-fold increase in RNase L protein levels in SiHa cells, when compared to matched DMSO treated control cells.

5.4.5. Lopinavir does not effect ABCE-1 protein levels in SiHa cells

Having confirmed a lopinavir induced time and dose dependent increase in RNase L protein expression in SiHa cells following lopinavir treatment, the effects of lopinavir on the endogenous inhibitor or RNase L (ABCE1) were assessed. Although RNase L protein was increased following lopinavir treatment, it was not known what effect this treatment had on ABCE1 protein levels. Thus, using the dose and time response lysates prepared in section 5.3.2.1 and 5.3.2.2 respectively, proteins were separated using a 12% SDS-PAGE gel (Section 5.3.2.4) and a

western blot was immunoprobed using a primary rabbit anti-ABCE1 antibody (section 5.3.3) with GAPDH as a loading control (section 5.3.2.4).

Figures 5.6 and 5.7 illustrate the western blot data of ABCE1 protein levels in SiHa cells treated with an escalating dose of lopinavir or for increasing time period at a fixed concentration of lopinavir. In contrast to RNase L protein levels, ABCE1 protein levels remain unchanged regardless of lopinavir concentration or incubation time period. This demonstrates that the observed increases in RNase L protein were not accompanied by any alteration in the levels of its endogenous inhibitor, ABCE1.

Figure 5.10 – Lopinavir concentration does not alter ABCE1 protein levels

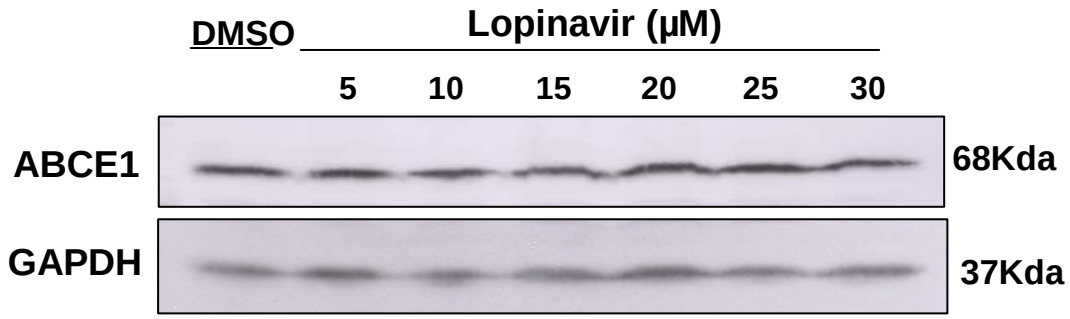

Figure 5.10 - SiHa cells were treated with escalating concentrations of lopinavir. At 6 hrs, cells were harvested and proteins separated on a 12% SDS-PAGE. Proteins were transferred on to Hybond-C nitrocellulose membrane and a western blot carried out using primary rabbit anti-ABCE1 and mouse anti-GAPDH antibodies. No dose dependent changes in ABCE1 protein levels were observed in HPV positive SiHa cells.

Figure 5.11 Lopinavir incubation time does not alter ABCE1 protein levels

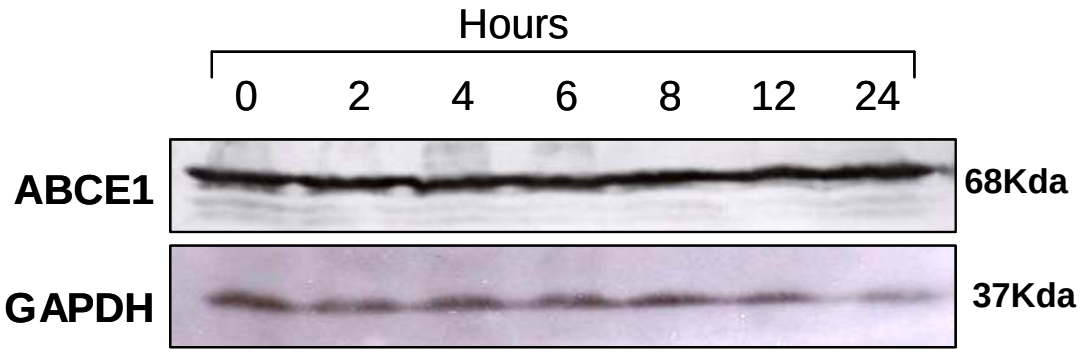

Figure 5.11 - SiHa cells were treated with a fixed dose of 25 µM lopinavir for the incubation periods shown. Cells were harvested at these time points and proteins separated on a 12% SDS-PAGE. Proteins were transferred on to Hybond-C nitrocellulose membrane and a western blot carried out using primary rabbit anti-ABCE1 and mouse anti-GAPDH antibodies. No time dependent changes in ABCE1 protein levels were observed in HPV positive SiHa cells.

5.4.6. Lopinavir up-regulates RNase L in E6/E7 immortalised PHFK

RNase L protein levels in E6/E7 transduced PHFKs exposed to lopinavir were assessed by western blotting. As previously demonstrated for SiHa cells, lopinavir induced an increase in RNase L albeit at a slower rate than was observed in SiHa cells (Figure 5.8(A)). While 25 µM lopinavir caused a peak RNase L signal in SiHa cells after 8 h with a subsequent drop after 24 hr (Figure 5.8), E6/E7 expressing PHFKs peaked at 48 hr followed by a subsequent drop after 72 hr (Figure 5.12).

Figure 5.12 - Lopinavir up-regulates RNase L in E6/E7 expressing PHFK

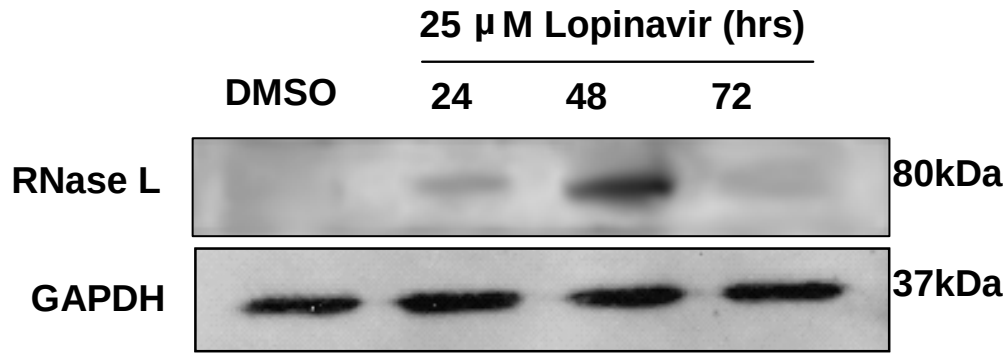

Figure 5.12 - E6/E7 immortalised PHFK were exposed to lopinavir (25 µM) over a 72 hr time period and harvested at the time points indicated. Proteins were separated on a 12% SDS-PAGE and transferred to Hybond-C nitrocellulose membrane and a western blot carried out using primary rabbit anti-RNase L and mouse anti-GAPDH antibodies.

5.5. Chapter Summary and Discussion

As previously demonstrated, lopinavir treatment of SiHa cells was shown to alter protein expression of a number of proteins with a variety of biological functions. Of most interest, was the observed increase in the levels of the antiviral protein RNase L following lopinavir treatment (Chapter 4).

These data are the first to demonstrate this effect in HPV positive cervical carcinoma SiHa cells and in stable HPV16 E6/E7 transfected human keratinocytes (PHFK).

In order to further investigate the relationship between lopinavir and RNase L, RT-PCR and western blotting was carried out in order to determine both dose and time dependent variations in RNase L expression. Lopinavir associated variations in the level of ABCE1 were also investigated since it was not known if this would increase in parallel with RNase L, which would effectively limit its effectiveness.

Interestingly, the RT-PCR data (Figure 5.5) demonstrated an absence of RNase L in C33A vector and E6 cells implying that the function of RNase L protein may be deleterious to the growth of these cells. Thus, as a consequence RNase L expression is down-regulated in these cells. This is an interesting finding, and one that is further utilised in Chapter 6.

RT-PCR also demonstrated no apparent changes in the RNase L mRNA levels in a range of HPV positive and negative cell lines following lopinavir treatment (Figure 5.5). Triplicate RT-PCR analysis of lopinavir treated SiHa cells demonstrated no significant difference in RNase L mRNA levels (Figure 5.2 (B), $p = 0.24$) indicating that the increase in RNase L protein levels is not related to an increase in gene **transcription** (Figure 5.6). This does not, however, rule out a lopinavir-induced increase in protein **translation**. However, by measuring the rate of incorporation of ^{35}S-Methionine into newly formed proteins as a surrogate marker for protein translation, Pyrko *et al.,* demonstrated that the HIV protease inhibitors atazanavir (Reyataz®) and nelfinavir (Viracept®) were not associated with an increase in protein translation [313]. Taking these findings into account, it is suggested that the observed increase in RNase L protein is related to an accumulation of protein as a consequence of lopinavir-induced inhibition of proteolysis. This is due to its ability to cause selective inhibition of the chymotryptic-like function of the proteasome [131]. The relationship between lopinavir and RNase L in SiHa cells was further investigated by assessment of the time and dose dependent response to this drug. Lopinavir was shown to produce a clear dose-dependent increase in RNase L levels over a concentration range of 5 - 30 µM (Figure 5.7 (B) & (C)) at a fixed incubation time of 6 hrs. It was noticed that lopinavir precipitated at concentrations above 30 µM (data not shown), so this was chosen as a maximum treatment dose.

Figure 5.8 demonstrates the clear time dependent increase in RNase L protein levels following lopinavir treatment. Time dependent increase in levels of the proteasomally-targeted protein p53 following lopinavir treatment of SiHa cells has been previously demonstrated [131]. The peak of RNase L expression at 8-12 hrs post-incubation with lopinavir is consistent with this earlier data. The drop in RNase L protein levels at 24 hrs lopinavir treatment was associated with a drop in

GAPDH loading control protein levels. The explanation for this is most likely due to the previously reported apoptotic/ toxic effects of the drug at this time point [131].

Based on our data, statistical analysis established that in SiHa cells, 6 hr treatment with lopinavir at a final concentration of 25 μM produced a significant 9.5-fold increase in RNase L levels ($p = 0.0053$), when assessed by western blot and triplicate densitometric analysis (Figure 5.9). Interestingly, whilst still exhibiting a lopinavir-dependent increase in RNase L expression, E6/E7 immortalised PHFKs demonstrated a much slower accumulation of RNase L (Figure 5.12). Whilst SiHa cells demonstrated a peak in signal strength at approximately 8 hrs, the PHFK data demonstrated a peak after approximately 48 hrs followed by a reduction at the 72 hr time point, which may related to differences in cell growth rates, or perhaps differences in the kinetics associated with proteasomal inhibition between these cell types.

RNase L protein is regulated by an endogenous inhibitor, ABCE1, and previous studies have shown that ABCE1 expression can be induced during HIV-1 infection, with subsequent down regulation of the RNase L antiviral pathway [266]; In a similar fashion to HIV, it was hypothesised that HPV may also be facilitating an increase in ABCE1 levels in SiHa cells and it was therefore suggested that the increase in RNase L protein level could conceivably be related to a fall in ABCE1 protein levels as a result of lopinavir treatment. Alternatively, lopinavir may induce an increase in ABCE1 levels, which would therefore reduce the pro-apoptotic functions of RNase L. A fall in ABCE1 levels would in turn increase availability of functional RNase L monomers that are capable of activation. Our data demonstrated no alterations in ABCE1 protein levels, regardless of lopinavir concentration or incubation time (Figures 5.10 and 5.11 respectively). Therefore, these studies support the concept that lopinavir-induced inhibition of proteasomal degradation is responsible for the observed increase in RNase L protein in SiHa cells. The importance of RNase L in HPV-specific lopinavir toxicity will be further assessed in Chapter 6.

6. RNase L and Lopinavir Toxicity

6.1. Introduction

The results discussed previously demonstrated a dose dependent increase in RNase L protein levels over a concentration range of 5-30 µM with a peak occurring 12 hours post treatment in SiHa cells. It was also shown that this lopinavir-induced increase in RNase L was not accompanied by altered expression of the endogenous inhibitor of RNase L (ABCE1) regardless of concentration or incubation time. The following section describes gene silencing, forced expression and co-immunoprecipitation experiments to assess the contribution of RNase L and its inhibitor ABCE1 to toxicity of lopinavir against HPV positive cells.

6.1.1. Gene silencing

The RNA interference (RNAi) system is an essential pathway through which the expression of specific target genes is inhibited (Figure 6.1), with a subsequent reduction in protein levels. It is initiated by double stranded RNA (dsRNA) and is involved with natural protein degradation and turnover in animals and plants [314, 315]. Most notably, this mechanism can be artificially used to silence specific genes of interest, which greatly facilitates ascribing function to their corresponding protein. There are two main laboratory-based techniques to bring about targeted gene silencing: short hairpin RNA (shRNA) and small interfering RNA (siRNA)

Figure 6.1 – Mechanism of siRNA mediated inhibition of protein synthesis

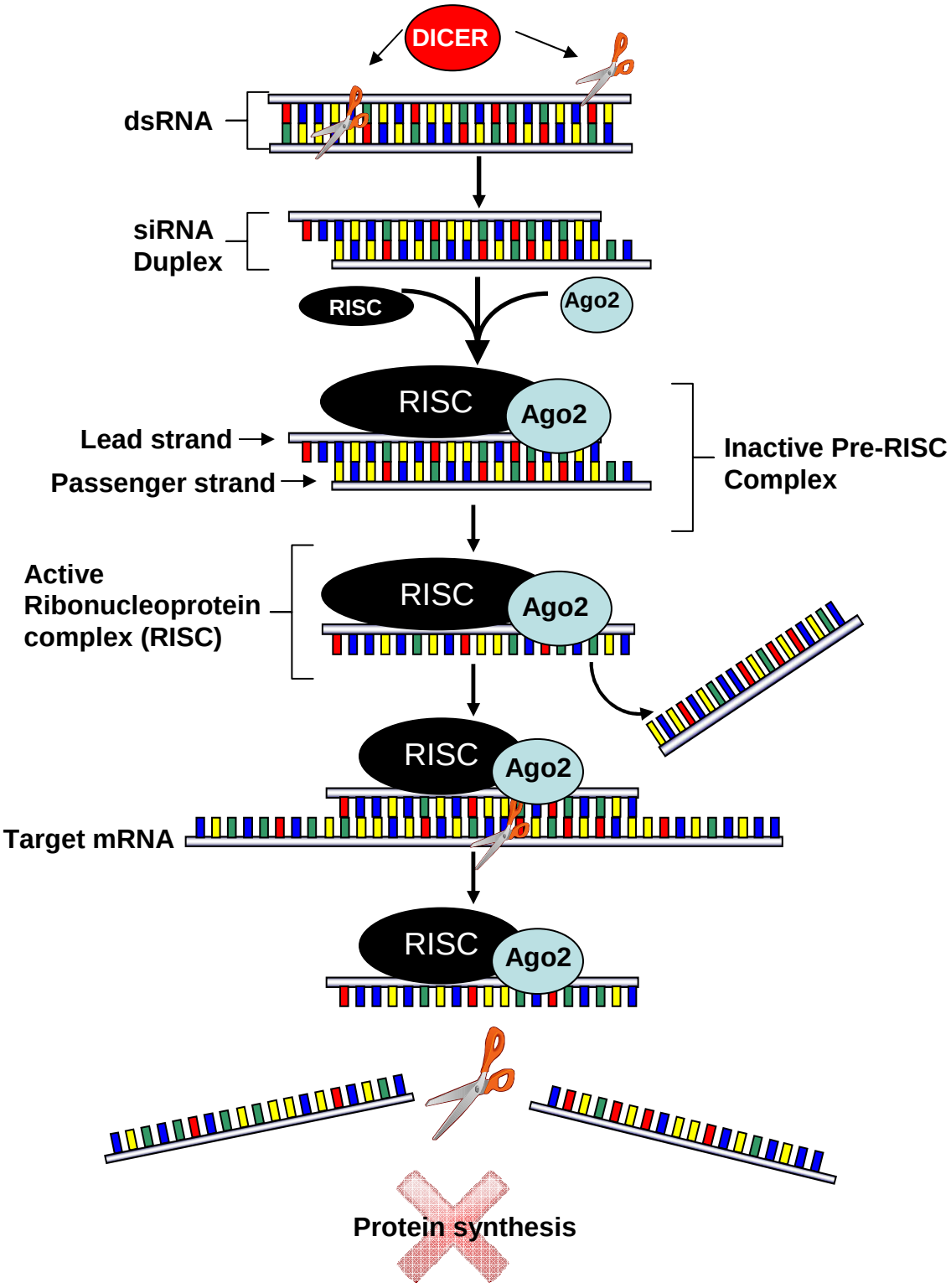

Figure 6.1 – Mechanism of siRNA-mediated inhibition of protein synthesis. dsRNA is degraded by DICER to produce siRNA complexes with 2nt over hangs at the 3' ends of each strand. The lead siRNA strand binds to target mRNA sequences in a sequence specific manner through interaction with the RNA Induced Silencing Complex (RISC) which has the Argonaute-2 (Ago2) protein at its core. mRNA degradation prevents protein synthesis of the target protein.

6.1.1.1. Advantages and disadvantages of siRNA and shRNA

In order to assess the role of RNase L, small interfering RNA (siRNA) mediated gene silencing is one possible option to knock down production of the protein. During siRNA-mediated RNA interference (RNAi), mRNA for a given protein is degraded by introduction of corresponding double stranded RNA (dsRNA) as reviewed in [254, 316, 317]. An alternative method is that of short hairpin RNA interference (shRNA) with the main difference between siRNA and shRNA's relating to the means of delivery and generation of the dsRNA silencing duplexes [318]. Direct liposome-mediated siRNA oligonucleotide interference has the advantage of being rapid, but is only transient. When using this approach siRNA oligonucleotides are observed within the cell within as little as 4hrs of lipofection, producing a peak of activity at 24 hrs. However, as little as 1% of the initially introduced siRNA duplex remains by 48hrs, highlighting the 'hit and run' nature of siRNA-based protein knockdown [319]. Short hairpin, shRNA sequences are delivered as DNA encoded within an integrated mammalian expression vector which allows constitutive expression of siRNA silencing duplexes. Although this approach is considerably more efficient [318], it can introduce clonal selection artefacts. Therefore, given the short timescale of the planned growth assays, it was decided to use transient siRNA oligonucleotide lipofection to silence RNase L expression.

6.1.2. Constitutive expression of RNase L

In a similar fashion to the previously described methods of gene silencing, proteins can also be artificially expressed as stable or transient transfectants. However, in order to achieve stable expression of a toxic protein it is usually necessary to use an inducible system. Alternatively, if the intended assay permits, transient expression of the target protein is a quick alternative for the study of toxic proteins; Because a cell death assay provides an ideal means to assess the impact of re-introducing RNase L into cells, it was decided that transient expression would be appropriate.

6.1.3. Protein-Protein interactions by Co-immunoprecipitation

Protein-protein interaction studies will be performed in order to confirm the role of the RNase L/ ABCE1 interaction in the observed toxicity of lopinavir. Co-immunoprecipitation will be used to identity or confirm protein-protein interactions and is summarised in Figure 6.2. Briefly a target protein (X) specific antibody is firstly incubated with a homogenised cell protein lysate. This is then mixed with protein G sepharose beads which bind to the constant region of immunogloblins from many species. The antibody plus protein X binds to the protein G beads and unbound proteins are removed by washing. Any proteins (Y) which interact either directly or indirectly with protein X should remain associated with the beads and will thus be eluted along with protein X. Western blots can then be used to analyse protein X immunoprecipitated material for the presence of both

protein X and Y. The main advantage of a Co-IP reaction is that it is a quick means to demonstrate the association of two or more proteins in a cell lysate, although it does not confirm a **direct** physical association as the interaction may occur as part of a larger multi-protein complex [320]. Other considerations are the quality of the available primary target antibodies and the strength of the interaction between the two ligands (X & Y) – If this is a weak interaction, it is unlikely that the Co-IP will be successful.

Figure 6.2 – Simplified Co-immunoprecipitation schematic

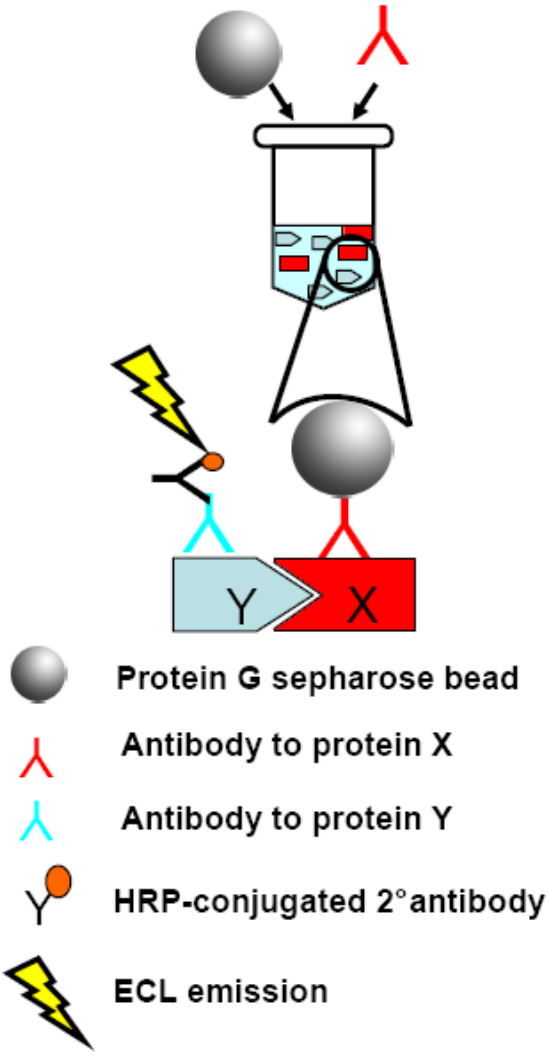

Figure 6.2 – Co-immunoprecipitation (Co-ip) allows protein-protein interactions to be studied. The antibody to protein X is immobilised on a solid support such as protein G sepharose beads, before binding to protein Y. Should Protein X and protein Y interact *in vivo*, the interaction can be confirmed by western blot analysis using a primary antibody targeting protein Y. This demonstrates that Protein X and protein Y are interacting in their native cellular states.

6.2. Aims

6.2.1. Assess the effects of siRNA mediated degradation of RNase L on cell growth in untreated cells and also in lopinavir treated cells

6.2.2. Assess the effects of over expression of RNase L in RNase L-deficient C33A cells by transient transfection

6.3. Methods

6.3.1. siRNA mediated degradation of RNase L mRNA

6.3.1.1. Pilot study to test siRNA effectiveness

siRNA mediated degradation of RNase L was carried out using Qiagen's flexitube system specific for RNase L (Qiagen, West Sussex, UK) which provided four RNase L specific siRNA (1, 2, 3 and 4), and were designed to exhibit no off-target effects. ALLSTAR negative and MAP kinase positive controls were also used (All siRNA target sequences used are shown in Appendix 4) All siRNAs were reconstituted in 100 µl sterile RNase-free water providing a 10 µM stock solution.

Previous work (Chapters 4 & 5) highlighted a lopinavir-induced alteration in a range of protein expression levels. Of most interest was the observed increase in the antiviral protein RNase L in SiHa cells exposed to lopinavir. However, whilst an interesting protein, the anti-HPV effects of lopinavir may be as a result of synergism between a range of proteins, rather than simply being restricted to RNase L-mediated effect. It is therefore essential that the true importance of RNase L in mediated HPV-specific toxicity be assessed. Furthermore, the E6 protein of high risk HPV types is known to be an extremely pleiotropic protein, mediated a wide range of responses. Based on this observation, it is feasible that E6 may in some way interact with RNase L and/or lopinavir. It is again essential, that the true significance of E6 be assessed, and again C33A/ C33AE6 cells provide a perfect cell culture system by which to assess this.

Briefly, SiHa cells were seeded at 5 x 10^4 cells/ well in 6-well plates in a total volume of 2 ml complete RPMI-1640 growth medium and allowed to reach 80% confluency at 37℃/ 5% CO_2. Cells were transfected using the lipofectamine-2000 reagent according to the manufacturers' recommendations (Invitrogen, Paisley UK). In a round-bottomed cryovial a 6 µl aliquot of siRNA was combined with a 250 µl aliquot of OptiMem (serum free medium, (Invitrogen, Paisley UK)). In a separate round bottomed cryovial, a 25 µl aliquot of lipofectamine-2000 (Invitrogen, Paisley, UK) was combined with 250 µl of OptiMem. Both tubes were then incubated at room temperature for 5 min. The contents of both tubes were then combined, incubated for a further 20 min at room temperature and 106.2 µl of transfection mix was added drop wise to each well as detailed in Figure 6.3.

Figure 6.3 – 6-well plate layout for pilot siRNA study

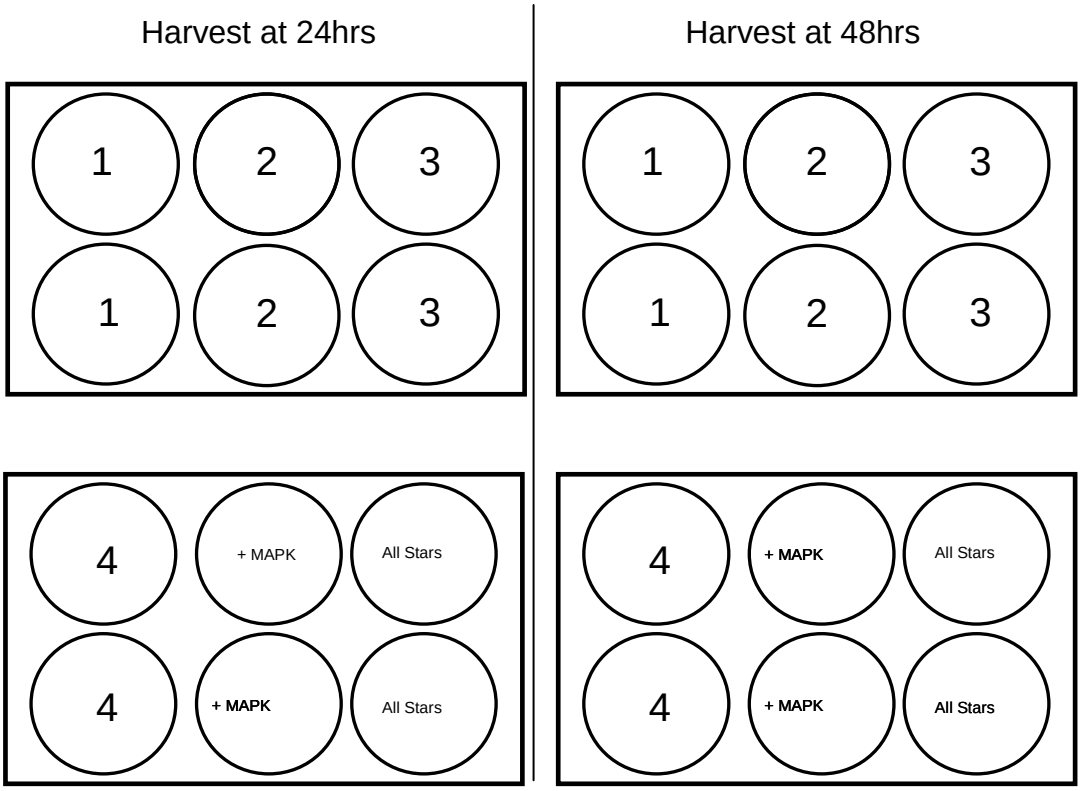

Figure 6.3 - 6 well plate layouts for siRNA transfection. In order to provide sufficient cell numbers for analysis, cells were seeded into all wells of four plates, allowing duplicate wells for each siRNA/ control samples to be harvested at both 24 hrs and 48 hrs to identify time dependent differences in protein knockdown. Four wells were transfected for each of the four siRNAs and two control siRNAs (1, 2, 3, 4 – Test siRNA; MAPK, Map Kinase negative control; All Stars, Negative control).

Six hours prior to harvesting, cells were exposed to 25 µM lopinavir as a means to artificially elevate low levels of endogenous RNase L. Twenty-four hours post-transfection, the growth medium was aspirated and each well washed with 2 ml PBS. 100 µl of trypsin was added and the plates returned to the incubator for 2-3 min, or until complete cell detachment had occurred. Addition of 1ml complete RPMI-1640 was then used to neutralise the trypsin and resuspend the cells and appropriate duplicates pooled. Cell numbers were determined using a haemocytometer (as detailed in section 2.3.3) and protein lysates prepared for SDS-PAGE/ western blot analysis (as detailed in section 5.3.2.1) which were stored at -20℃ until use. These were separated on a 12% SDS-PAGE gel as detailed in section 5.3.2.4 and a western blot carried out as described in section 5.3.2.5 immuno-probing the membrane with primary rabbit anti-RNase L antibody and GAPDH as a loading control.

6.3.1.2. AQ-96 Cell Proliferation assay in siRNA transfected SiHa +/- Lopinavir

Two thousand cells were seeded per well in a 96-well plate in a total volume of 200 µl complete RPMI-1640. Twenty-four hours later the cells were transfected with RNase L (siRNA-1), MAPK or ALLSTAR control siRNA using the same transfection mixture detailed above in section 6.3.1.1 with volumes adjusted for the different well size. Twenty-four hours later the growth medium was aspirated from all wells and replaced with 200 µl complete RPMI-1640 growth medium supplemented with lopinavir at final concentrations of 20, 25 and 30 µM. A 72hr AQ-96 cell proliferation assay was then carried out as described in section 3.3.2.

6.3.2. Lopinavir does not up-regulate RNase L in lopinavir resistant CaSKi cells

CaSKi cells were cultured (as described in section 2.3.3) to a confluency of 80% whereupon they were treated with DMSO or an increasing dose of lopinavir over a range of 5 - 30 µM, in 5 µM increments with DMSO levels adjusted to remain constant throughout. Six hours post incubation with lopinavir cells were harvested and prepared and separated by SDS-PAGE as described in sections 5.3.2.1 and 5.3.2.4 and a western blot immunoprobed with RNase L and GAPDH loading control as described in section 5.3.2.5.

6.3.3. Over expression of RNase L in C33A parent and C33AE6 cells

6.3.3.1. Maxi prep of RNase L vector

An RNase L mammalian expression vector (EX-U1047-M02 Vector GeneCopoeia, MD, USA – See Appendix 1 for vector map) was used for studies involving the over expression of RNase L and was reconstituted using 50 µl 1 x Tris-EDTA (TE) buffer, and incubated at room temperature for 60 min. A 6.5 µl aliquot was then used to transform a 50 µl aliquot of chemically competent XL-1 Blue *E.*coli cells, and plated onto LB agar plates as detailed in section 2.3.8. Laboratory stocks of the RNase L expression vector were prepared using the Qiagen Maxi plasmid purification kit according to the manufacturer's instructions (Qiagen, West Sussex, UK) and the sample adjusted to 1 µg/µl using 1 x TE buffer and stored at -20℃ until further use.

6.3.3.2. Transient transfection of C33A parent and C33AE6 cells with RNase L

The RNase L vector prepared in section 6.3.3.1 was used to transiently transfect C33A parent and C33AE6 cells. Cells were grown in T-25 culture flasks to a confluency of 80%,

whereupon they were each transiently transfected with the RNase L vector DNA as follows. Plasmid DNA (3.33 µl from 1 µg/µl stock solution) was combined with 116.7 µl OptiMem serum free medium whilst 15 µl of lipofectamine-2000 was combined with 116.7 µl of OptiMem aliquoted into a separate tube and incubated at room temperature for 5 min. Both solutions were then combined and incubated at room temperature for a further 20 min prior to drop wise addition to the culture flask. A lipofectamine-2000 only control transfection mix was also set up as above. Transfection efficiency was assessed by co-transfection of RNase L expression vector with the β-galactosidase expression vector pCDNA 3.1 V5-HIS lacZ at a ratio of 4:1. Shortly prior to the transfection, growth medium containing free floating viable cells was removed from each of the T-25 culture flasks and placed in a labelled 50 ml falcon tube and the cells pelleted by centrifugation, at 528 x g for 5 min. The supernatant was aspirated and the cell pellets resuspended in 10 ml complete RPMI-1640 and returned to the correct T-25 culture flask. All flasks were incubated at 37℃/ 5% CO_2.

6.3.3.3. Twenty-four hour Live/Dead cell count

Twenty four hours post-transfection, the growth medium containing free floating cells was removed from the culture flasks and transferred to a 50 ml falcon tube. Cell monolayers were washed with PBS and 230 µl of pre-warmed trypsin added and the flasks returned to the incubator for 3 min until complete cell detachment had occurred. The trypsin was then neutralised by addition of the complete growth medium previously removed from each specific flask, thoroughly resuspending the cells. A haemocytometer live/dead cell count was then performed using trypan blue exclusion (Sigma Aldrich, Dorset, UK) and number of blue cells expressed as a percentage of the total number of cells counted. Duplicate cell counts were performed for each culture flask.

Subsequently, the lacZ expressing cells were fixed and stained for ß-Galactosidase activity as described in section 2.3.10 and the transfection efficiencies for both C33A parent and C33AE6 cells calculated as detailed in section 2.3.11. Transient transfection and 24 hr live/dead counts were repeated in triplicate.

6.3.4. The effect of the HPV type 16 E6 protein on RNase L and its endogenous inhibitor of RNase L (ABCE1)

6.3.4.1. Transient Transfection and cell harvesting

C33A parent and C33AE6 cells were transiently transfected with RNase L as previously described and protein extracts harvested at 4, 8, 12 and 24 hrs post transfection (described in section 6.3.3.2). Protein lysate was also prepared from lipofectamine-only untransfected control cells. All samples were subjected to three cycles of freeze/thaw, with heating to 95℃.

6.3.4.2. SDS-PAGE and Western Blot

Protein samples were then separated using a 12% SDS-PAGE gel as described in section 5.3.2.4 and a western blot carried out as detailed in section 5.3.2.5. The membrane was probed using primary rabbit anti-RNase L antibody and also rabbit anti-ABCE1 antibody, as described in sections 5.3.2.5 and 5.3.3 respectively. GAPDH was used as a loading control as described previously.

6.3.5. Effect of HPV E6 protein and/or lopinavir on the Nuclear/ Cytoplasmic shift of RNase L

6.3.5.1. Immunohistochemistry staining of RNase L

SiHa cells were seeded at 2 x 10^4 cells per well in two 8-well slide flasks (BD Falcon Biosciences, Oxford, UK) in a total volume of 500 µl complete RPMI-1640 and incubated at 37℃ 5% CO_2. Upon reaching 80% confluency the growth medium was aspirated and replaced with 500 µl fresh complete RPMI-1640 supplemented with either 25 µM lopinavir or an equal volume of DMSO. The flasks were returned to the incubator for 6 hrs after which the growth medium was aspirated and all cells rinsed twice in 500 µl PBS before being fixed for 10 min with 500 µl 2% paraformaldehyde. Cells were washed twice in 500µl PBS and permeabilised with 200µl PBS/0.1% Triton solution (Sigma-Aldrich, Dorset, UK) for 5 min at room temperature followed by treatment with 200 µl peroxidase inhibitor for 15 min at room temperature. These were then incubated with 200 µl blocking solution (3% BSA in 1 x PBS) at room temperature for 45 min. The cells were washed with PBS and a 200 µl aliquot of each antibody dilution in PBS/ 0.015% triton added per well (Sigma-Aldrich mouse anti-RNase L (antibody R3529), 1:100 & 1:500, Abcam rabbit anti-RNase L (antibody 32307), 1:50 & 1:250, and mouse anti-β-Actin loading control, 1:500 (Sigma Aldrich A1978)). DAB and all secondary-only antibody controls were treated with an equal volume of PBS/0.0.15% Triton and the slides were placed in a humidified chamber and incubated overnight at +4℃.

Following washing with PBS, a 200 µl aliquot of a 1:500 dilution of the appropriate biotin conjugated secondary antibody was added in PBS/3% BSA. At this stage, PBS/3% BSA was added to the DAB only control wells and the slides were then incubated at room temperature for 45 min. Following washing with PBS, cells were incubated with 200 µl Streptavidin-HRP conjugate (made up at a dilution of 3 µl/ml in PBS) for 30 min at room temperature then washed with PBS. All the wells were then incubated with 200 µl DAB solution for 10 min (DAB reagent diluted 1:10 with DAB kit buffer). The reaction was quenched with PBS and the cells dehydrated through an ethanol gradient prior to two 5 min xlyene incubations and mounting.

6.3.5.2. Nuclear/ cytoplasmic Fractionation

C33A and C33AE6 cells were transiently transfected with RNase L as described in section 6.3.3.2. Eight hours post-transfection, the growth medium was aspirated and replaced with 10 ml complete RPMI-1640 supplemented with 25 µM lopinavir or an equal volume of DMSO and all flasks returned to the incubator at 37℃/ 5% CO_2 for 6 hrs. The growth medium was then removed from the culture flasks and the cells detached with 230 µl trypsin which was subsequently neutralised by the addition of the complete medium previously removed from the flask. An aliquot containing 5 x 10^6 cells was then pelleted by centrifugation at 528 x g for 5 min after which the supernatant was then aspirated and discarded. The resulting cell pellet was washed with PBS and re-pelleted by centrifugation.

Cell fractionation was carried out using the nuclear/ cytoplasmic fractionation kit from Thermo-Fisher Scientific (Fisher Scientific UK Ltd., Leicestershire, UK) according to the manufacturer's directions. In brief, cytoplasmic extraction reagent-1 (CER1) and nuclear extraction reagent-1 (NER1) buffers were prepared with protease inhibitor cocktail (20 µl inhibitor cocktail/ml buffer) and 500 µl of ice cold CER1 buffer was added to each cell pellet, which was then vortexed for 15 sec. The sample was then incubated on ice for 10 min after which, 27.5 µl of ice cold cytoplasmic extraction reagent-2 (CER2) buffer was added, the sample vortexed for a further 5 sec and incubated on ice for 1 min. This was then centrifuged for 5 min at 16,000 x g after which the supernatant containing the cytoplasmic fraction was immediately transferred to a chilled eppendorf and stored at -80℃. The remaining cell pellet was re-suspended in 250 µl of ice cold NER1 buffer and vortexed for 15 sec placed on ice and vortexed for 15 sec every 10 min for a total of 40 min. The sample was subsequently centrifuged at 16,000 x g for 10 min and the supernatant containing the nuclear fraction transferred to a chilled eppendorf, before being stored at -80℃.

In order to ensure equal loading of proteins, a Bradford assay was carried out as described in section 4.3.4. Cytoplasmic and nuclear samples were each normalised in CERI or NERI buffer respectively and the cell samples prepared for western blot analysis as described in section 5.3.2.1 using 4 x Laemmle lysis buffer. A 15% SDS-PAGE gel (3.5ml sdH_20, 7,5ml 30% acrylamide mix, 3.8ml 1.5M Tris (pH 8.8), 150µl 10% SDS, 150 µl 10% APS and 6 µl TEMED) was prepared and overlaid with a stacking gel as detailed in section 5.3.2.4. Prior to loading, 1 µl ß-mercaptoethanol was added to each sample and proteins then separated as described in 5.3.2.4 and a western blot carried out as described in section 5.3.2.5 immuno-probing the membrane using primary rabbit anti-RNase L antibody as described in section 5.3.2.5. Efficient sub fractionation of nuclear and cytoplasmic proteins was confirmed by immunoprobing the extracts with mouse anti-GAPDH (section 5.3.2.5) and rabbit anti-HDAC1 (New England Biolabs, Herts., UK) used at a concentration of 1/800 in PBS. Subsequent washes and detection were carried out as described in section 5.3.2.5.

6.3.6. Co-Immunoprecipitation of RNase L and ABCE1 from RNase L transiently transfected C33A parent and E6 cells

C33A and C33A6 cells were transiently transfected with RNase L as described in section 6.3.3.2. Eight hours post-transient transfection, the growth medium was aspirated from all culture flasks and replaced with 20 ml fresh complete RPMI-1640 supplemented with 25 µM lopinavir or an equal volume of DMSO. Six hours following the addition of lopinavir or DMSO control the growth medium was aspirated, cells washed with PBS and 500 µl ice cold CelLytic-M^{TM} cell lysis buffer was added (Sigma Aldrich, Dorset, UK). The flasks were then incubated on ice for 5 min after which cells were detached using a sterile cell scraper, transferred to chilled eppendorf tubes and incubated at 4℃ for 15 min with gentle vertical rotation. Extracts were subsequently centrifuged at 10,000 x g for 15 min at 4℃ after which the supernatant was transferred to a chilled eppendorf and a Bradford protein assay carried out to determine protein levels as described in section 4.3.4. Equivalent protein concentrations were achieved by adding Cellytic-M^{TM} cell lysis buffer.

A uniform suspension of protein-G sepharose beads (Sigma Aldrich, Dorset, UK) was transferred to an eppendorf, and pelleted by centrifugation at 5,000 x g for 1 min, washed twice with 500 µl PBS, pelleted by centrifugation as above before finally being resuspended in 500 µl ice cold CelLytic-M^{TM} cell lysis buffer (Sigma Aldrich, Dorset, UK). In order to minimise non-specific binding due to IgG contamination the samples were then incubated with 30 µl of the protein-G sepharose bead suspension for 2 hrs at 4℃ on a vertical rotator followed by centrifugation at 10,000 x g for 1 min, and the supernatant transferred to a chilled eppendorf.

Extracts were incubated overnight at 4℃ with 1.5 µg anti-ABCE-1 antibody and 75 µl of the protein-G sepharose suspension with gentle vertical rotation. The beads were pelleted by centrifugation at 10,000 x g for 2 min at room temperature, the supernatant containing unbound protein discarded and the protein-G sepharose beads washed once with 200 µl ice cold CelLytic-M^{TM} buffer. The beads were then pelleted by centrifugation at 5,000 x g for 1 min, the CelLytic-M^{TM} cell lysis buffer aspirated and the samples resuspended in 80 µl 2 x Laemmle sample buffer prior to heating to 95℃ for 5 min. These extracts were then separated using a 12% SDS-PAGE gel as described in section 5.3.2.4 and a western blot carried immunoprobed with primary rabbit anti-RNase L as described in section 5.3.2.5.

In order to further assess the association between lopinavir and the ABCE1/RNase L complex, the co-immunoprecipitation reaction was repeated to include duplicate flasks grown with complete RPMI medium supplemented with 25 µM lopinavir or an equal volume of DMSO, and extracts harvested at 6, 12 and 24 hrs and processed as detailed above.

6.4. Results

6.4.1. siRNA mediated protein knock down of RNase L

6.4.1.1. mRNA degradation efficiencies of available siRNA

Figures 6.4(A) & (B) show the western blots of siRNA transiently transfected SiHa cells harvested at 24 hrs and 48 hrs respectively. In comparison to two separate controls, a MAP Kinase specific siRNA and an ALLSTAR negative siRNA, the RNase L specific siRNA's have significantly reduced the RNase L protein signal at 24 hrs. A MAP kinase-specific siRNA transfection was carried out in order to demonstrate that RNase L knockdown was a specific consequence of the RNase L specific siRNA, as opposed to a general consequence of siRNA transfection of SiHa cells in culture. In comparison to the 24 hr transfection results, 48 hrs post transfection RNase L levels appeared elevated, appearing as a small double band.

Figure 6.4 - RNase L protein knock down assessed 24 & 48 hrs post siRNA transfection

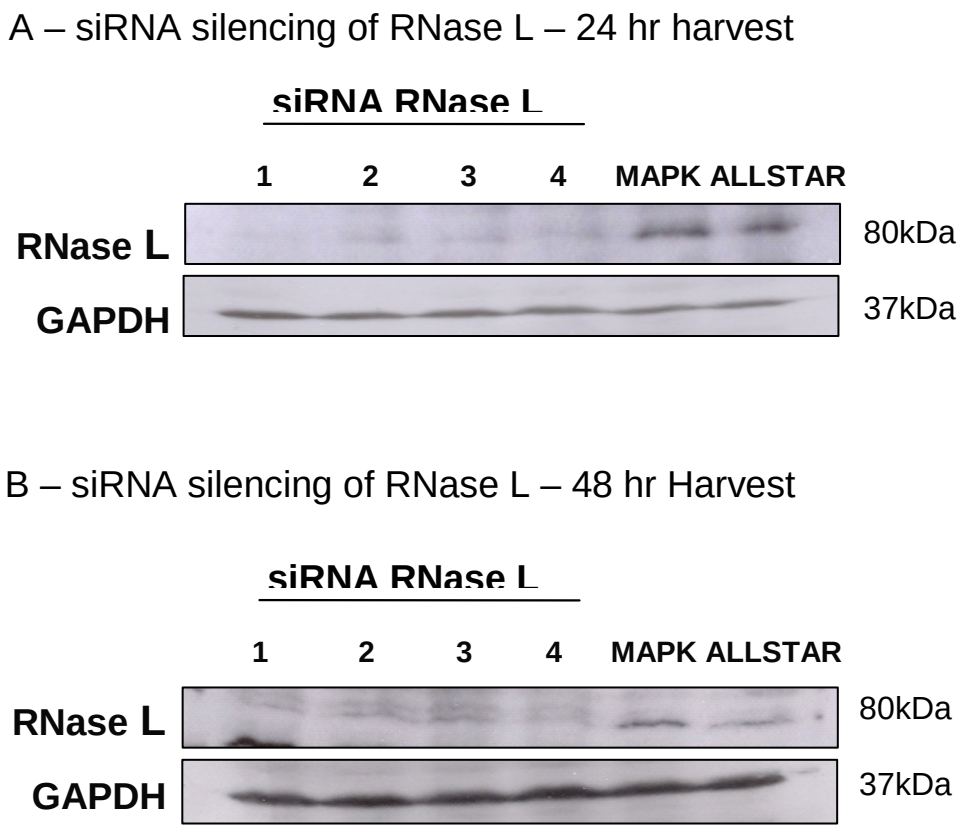

Figure 6.4 – SiHa cells were grown to 80% confluency before being transfected, using lipofectamine-2000, with either siRNA targeting RNase L (1-4) or one of two controls siRNA. Duplicate cell samples were harvested at 24 hrs (panel A) and 48 hrs (panel B) following transfection and proteins separated using a 12% SDS-PAGE gel. A western blot was carried out probing with primary rabbit anti-RNase L antibody and a GAPDH loading control. Proteins were visualised with ECL and exposure to hyperfilm. 24hr transfection with siRNA appears to produce the most efficient degradation of RNase L. In comparison to 24 hr transfection results, at 48 hrs post transfection, RNase L levels appear slightly elevated, appearing as a small double band.

In order to quantify the degree of RNase L protein knockdown at 24 hrs densitometric analysis of western blot signals was carried out using the Image J analysis program (http://rsbweb.nih.gov/ij/). Figure 6.5(A) shows relative intensities for each sample compared to matched GAPDH loading controls. All siRNAs were shown to produce high levels of RNase L protein knockdown, when compared to ALLSTAR or MAPK siRNA transfected control cells. Figure 6.5(B) shows the data from Figure 6.5(A) presented as a percentage down-regulation when compared to the ALLSTAR transfected controls, assuming the ALLSTAR signal represents 100% protein expression. Whilst all were very effective, siRNA-1 proved to be the most efficient, reducing the detectable levels of RNase L by 98.1% when compared to the ALLSTAR transfected cells.

Figure 6.5 - Densitometric analysis of RNase L protein level 24hrs post-siRNA transfection

A – Image J density analysis of siRNA targeting RNase L

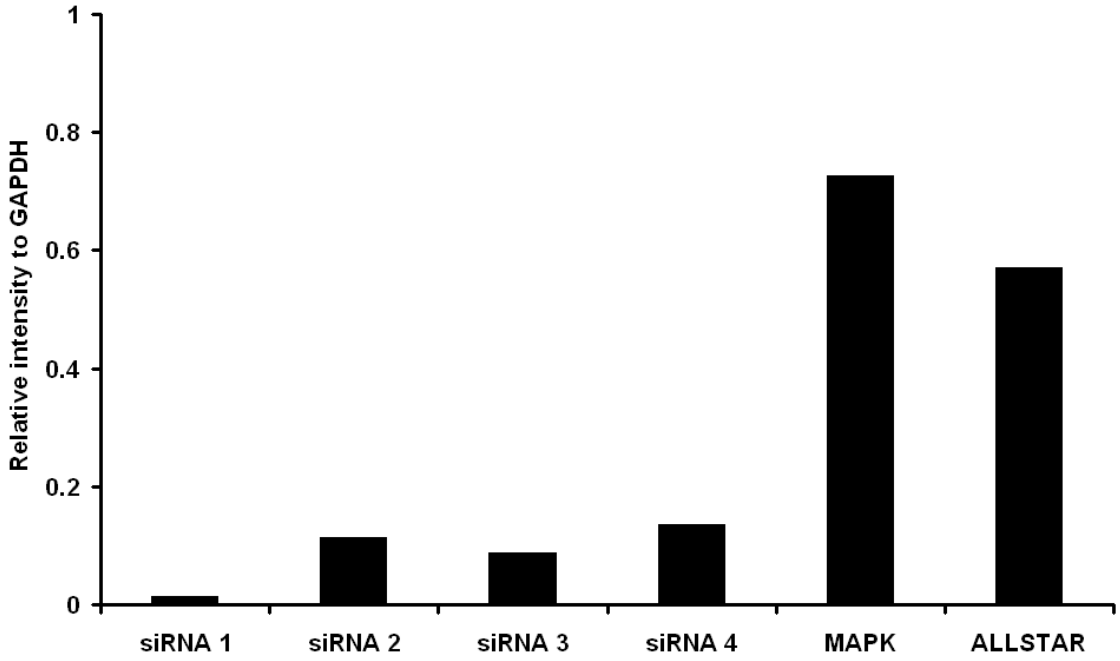

B – Percentage protein knock-down of RNase L following siRNA silencing

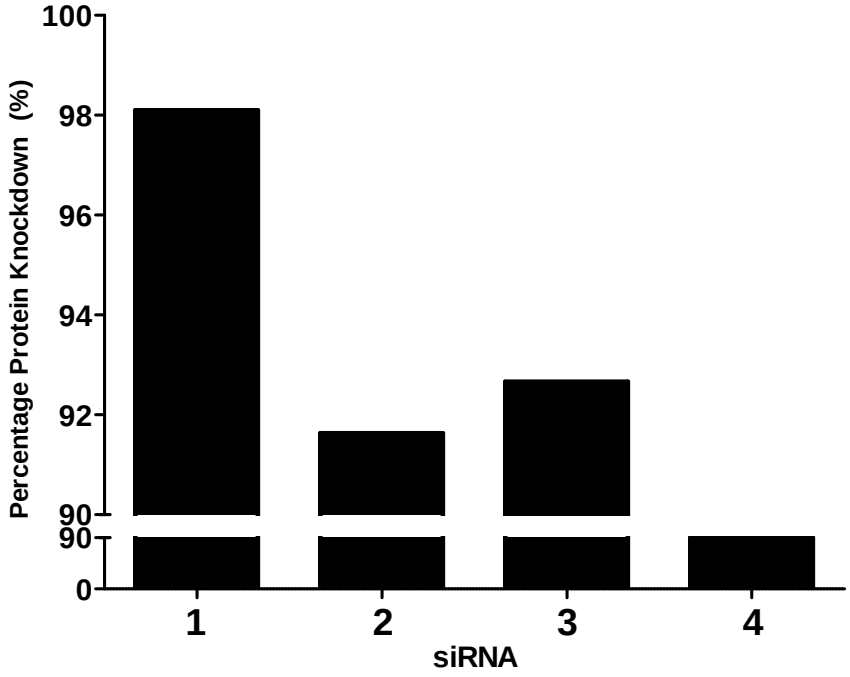

Figure 6.5 – (A) Image J density analysis software was used to plot signal intensities for each siRNA treated cell sample harvested at 24hrs. Signals are expressed as relative intensity compared to the matched GAPDH signal, and are based on a single experiment. Clearly demonstrate a high level of protein knockdown in RNase L siRNA treated cells. (B) For each siRNA protein levels are expressed as a percentage knockdown compared to ALLSTAR siRNA. All four siRNA demonstrated high level of protein knockdown, with siRNA-1 being the most efficient, producing 98.1% protein knockdown.

Curiously, a double RNase L band was observed in the 48 hr post siRNA transfection proteins (Figure 6.4B) which complicated the Image J quantification analysis. However, it was clear that the RNase L signal intensity was slightly higher for each siRNA at 48 hrs than at 24hrs indicating a restoration of RNase L protein synthesis.

6.4.1.2. Effect of siRNA mediated inhibition of RNase L on cell growth in SiHa cells

All the siRNA sequences tested were capable of inducing transient reduction in the expression of the RNase L protein, although siRNA 1 was clearly the most efficient. Thus, 72 hr colorimetric cell proliferation assays were carried out (section 6.3.1.2) in cells transfected with either siRNA 1 or the ALLSTARS negative control, both with and without lopinavir.

Figure 6.6 shows cell proliferation assay for siRNA1, ALLSTAR and lipofectamine-only control transfected cells in the absence of lopinavir. The data are presented as percentage change from the starting density at T = 0. Statistical analysis was carried out using Microsoft excel, with student T-tests carried out comparing siRNA-1 cells to ALLSTAR control cells based on triplicate data sets - p-values below 0.05 were considered significant. When comparing siRNA-1 transfected cells to ALLSTAR transfected cells the growth rate in siRNA-1 transfected cells was significantly higher at all data time points (24hrs $p = 0.005$, 48hrs, $p = 0.0004$, and 72hrs $p = 0.003$).

The growth of cells exposed to lipofectamine-2000 only did not significantly differ from ALLSTAR control transfected cells.

Figure 6.6 – 72hrs AQ-96 growth proliferation assay following siRNA mediated inhibition of RNase L

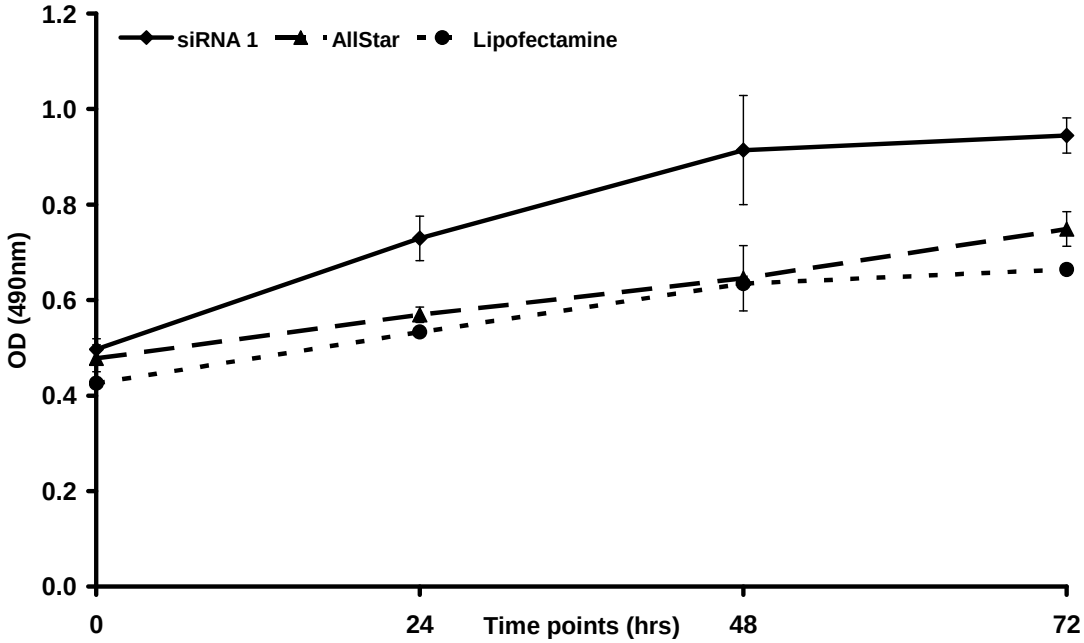

Figure 6.6 – 72hr AQ-96 cell proliferation growth curve. Data represented as percentage growth change. SiHa cells were transfected with siRNA targeting RNase L or an ALLSTAR control siRNA. Lipofectamine only transfected control cells were also included. Based on OD_{490} data, when compared to ALLSTAR controls RNase L degradation with siRNA-1 produced a significant ($p<0.05$) improvement in cell growth at each data point over 72hrs. Data based on triplicate data points from a single experiment

6.4.1.3. Effect of siRNA mediated inhibition of RNase L following lopinavir treatment

The results shown in Figure 6.7 are the cell proliferation assays carried out on siRNA 1 and ALLSTAR control transfected cells treated with an escalating dose range of lopinavir (20, 25 and 30 µM). The data are presented as percentage growth change based on triplicate data points (Figure 6.7A-D).

Figure 6.7 (subsequent pages) – 72hr growth assays following siRNA transfection and lopinavir treatment

SiHa cells were transiently transfected with either siRNA-1 or ALLSTAR negative control before being subsequently grown in RPMI-1640 supplemented with either DMSO or lopinavir at the concentrations shown. Growth was monitored over 72hrs and shown percentage growth change (panels A-D). Findings based on triplicate data points from a single experiment.

A – DMSO Control

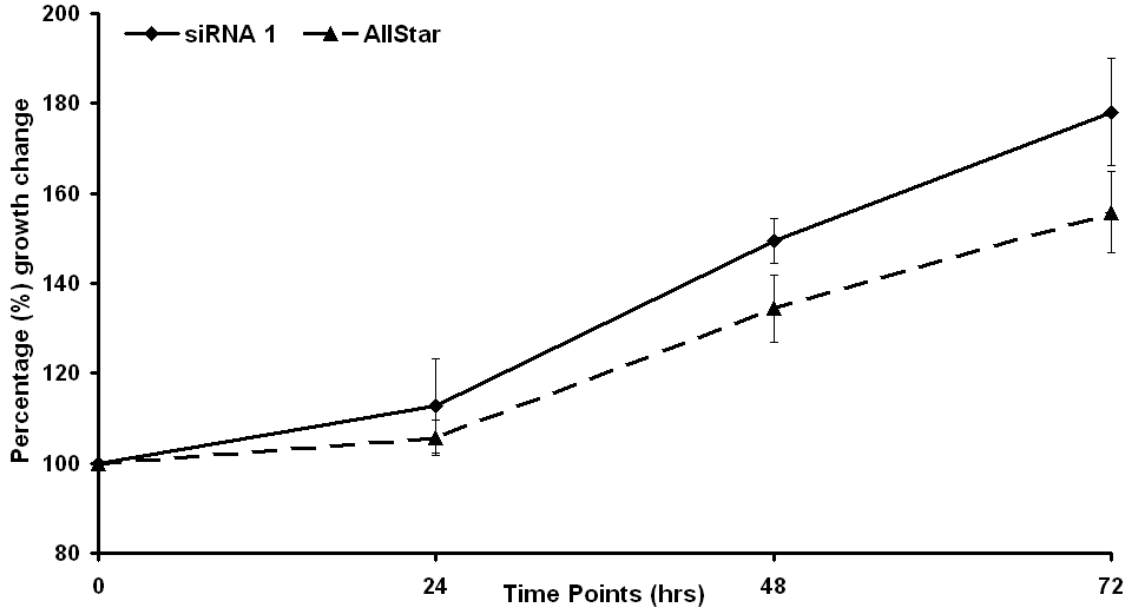

B – 20 µM lopinavir treated

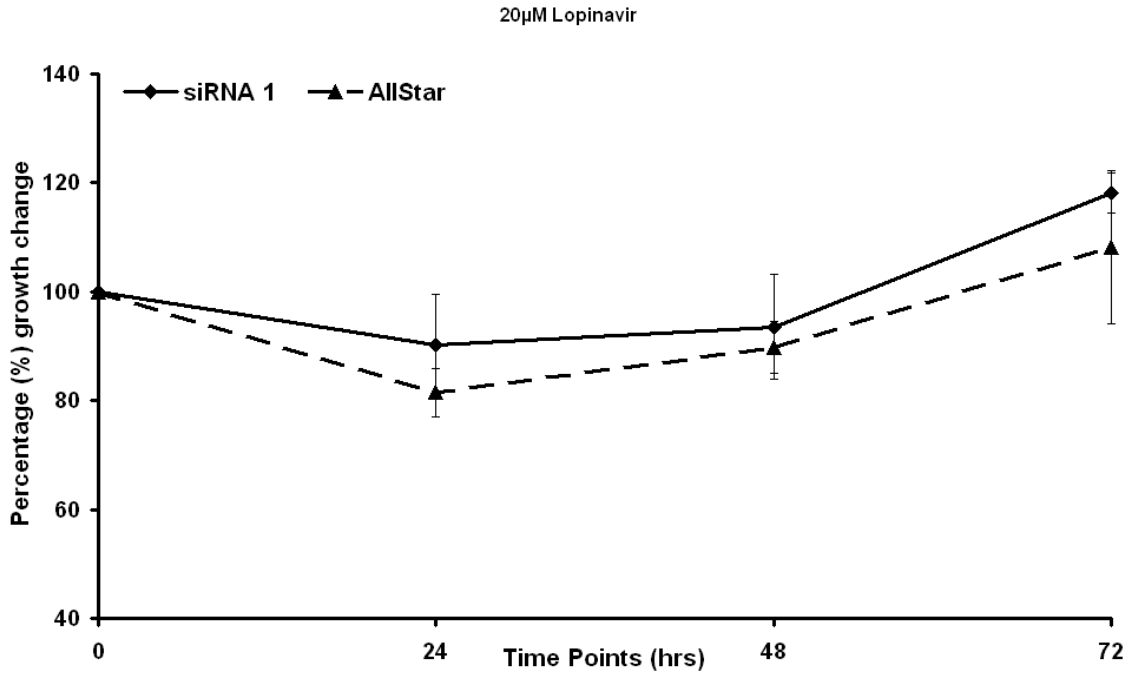

C – 25 µM lopinavir treated

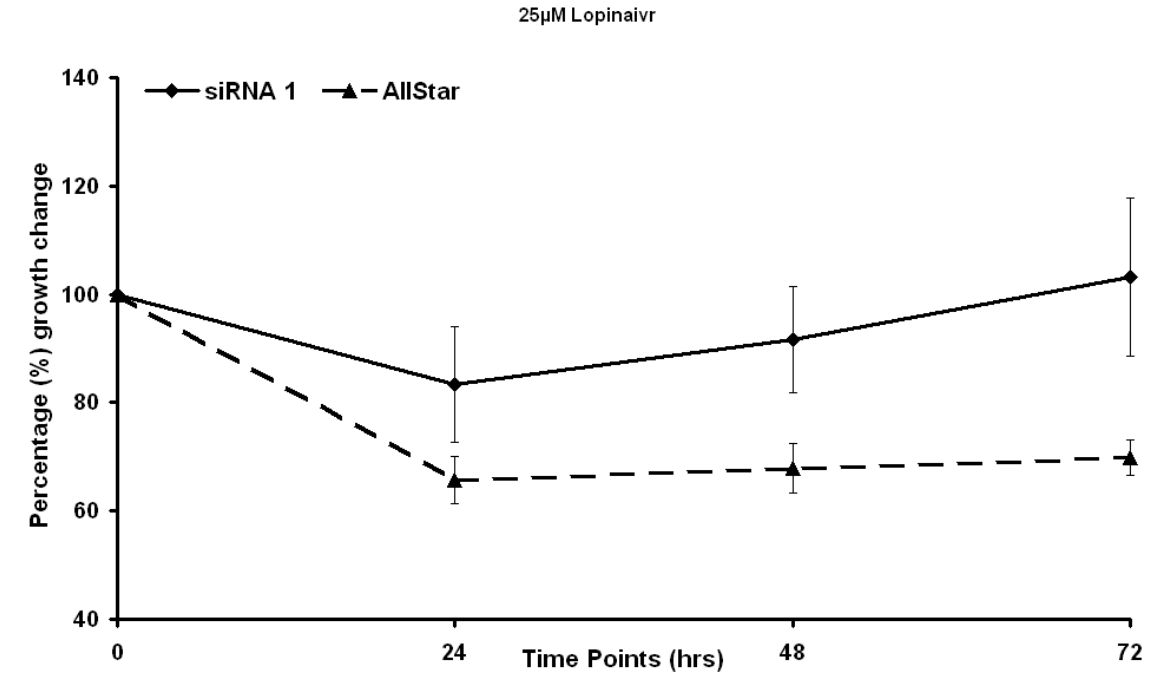

D – 30 µM lopinavir treated

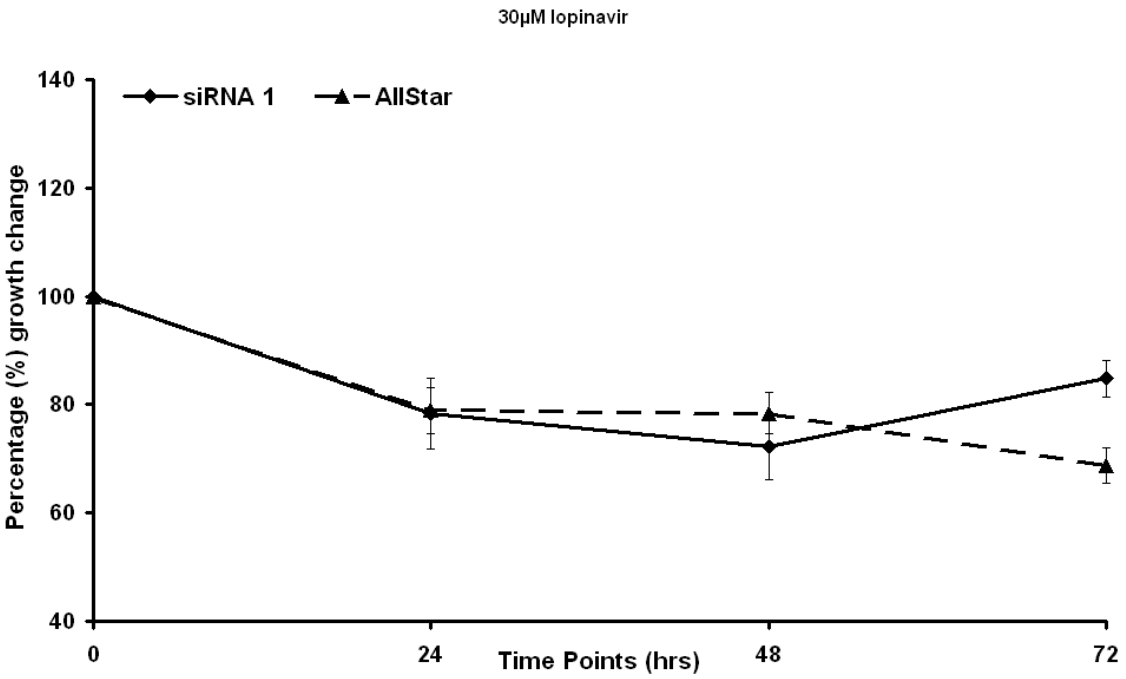

Consistent with the results obtained in untreated transfected cells (Figure 6.6) DMSO-only treated siRNA transfected cells (panel A) showed steady growth over the 72 hr period. It was also noticed that siRNA 1 transfected cells had a modest growth advantage over ALLSTAR control cells. Significantly, a divergence in the growth characteristics of these cells occurred when they were grown in the presence of lopinavir over a relatively small dose range of 20 - 30 µM. In the presence of 20 µM, cell growth was inhibited when compared to DMSO treated cells, yet after an initial drop in cell number, both siRNA-1 and control cells demonstrated growth recovery at the 48 hr and 72 hr time points. At this concentration of lopinavir, no statistically significant variation in growth was observed between siRNA 1 and control transfected cells. With 25 µM lopinavir (panel C) both siRNA-1 and ALLSTAR transfected cells again demonstrated an initial drop in cell number after the first 24 hrs, although this was much more pronounced in the ALLSTAR cells. After 48 hrs the siRNA-1 transfected cells showed a marked recovery in growth, in contrast to the ALLSTAR cells, in which growth appeared to plateau producing a statistically significant difference in growth at 72 hrs ($p<0.05$). At 30 µM lopinavir this selective toxicity was lost with all cells showing pronounced growth arrest irrespective of the transfection procedure (Figure 6.7, panel D). It is significant that the difference in selective toxicity observed between 25 and 30 µM lopinavir is entirely consistent with the previously shown growth assays carried out on E6/E7 immortalised keratinocytes (Figure 3.5). E6/E7 expressing keratinocytes demonstrated a time dependent increase in RNase L protein expression in cells treated with 25 µM lopinavir, and were markedly growth inhibited when compared to control treated keratinocytes. However, most significantly, this growth selectivity was lost at concentrations of lopinavir greater than 25 µM.

6.4.2. Lopinavir does not up regulate RNase L in lopinavir-resistant CaSKi cells

Figure 6.8 demonstrates western blot analysis of RNase L protein in CaSKi cells exposed to an escalating dose of lopinavir. In contrast to SiHa cells, no lopinavir-dependent increase in RNase L protein expression was observed. CaSKi cells were used as they have previously shown to be resistant to lopinavir treatment [131]. The CaSKi cell line is a fully transformed HPV positive cervical carcinoma cell line. However, in contrast to SiHa which contains 1-2 integrated copies of HPV type 16 [186] it is known that CaSKi cells contain several hundred copies of HPV type 16 (Figure 6.8(B)).

Figure 6.8 – Lopinavir does not up-regulate RNase L in resistant CaSKi cells

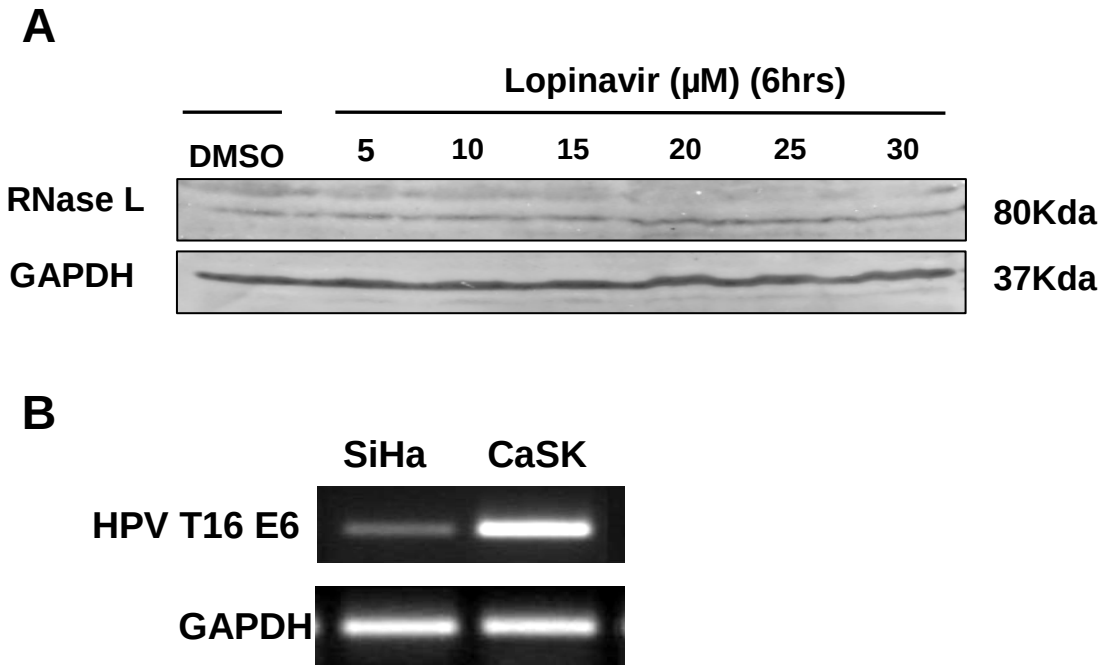

Figure 6.8 – (A) CaSKi cells were exposed to an escalating dose of lopinavir. Cells were harvested 6 hrs post incubation and separated by SDS-PAGE. A western blot was immunoprobed with RNase L and GAPDH loading control. No increase in RNase L was observed based on a single experiment. (B) RT-PCR data reproduced with permission from Dr Xiaotong He. RT-PCR demonstrates the increased levels of E6 protein in CaSKi cells when compared to SiHa cells.

6.4.3. Over expression of RNase L in an RNase L-deficient cell line

6.4.3.1. Effect of reintroducing RNase L into C33A parent and C33AE6

Figure 6.9(A) shows the results from the live/dead cell counts taken 24 hrs post-transfection with an RNase L expression vector in C33A parent and C33AE6 cells. Statistical analysis showed no significant difference in percentage background cell death when comparing control untransfected C33A parent and C33AE6 cells ($p = 0.50$) (Figure 6.9(A)). Test values with background death removed are shown in Figure 6.9(B).

Figure 6.9 – Assessment of cell death 24 hr post-transfection of RNase L into C33A parents and C33AE6 cells

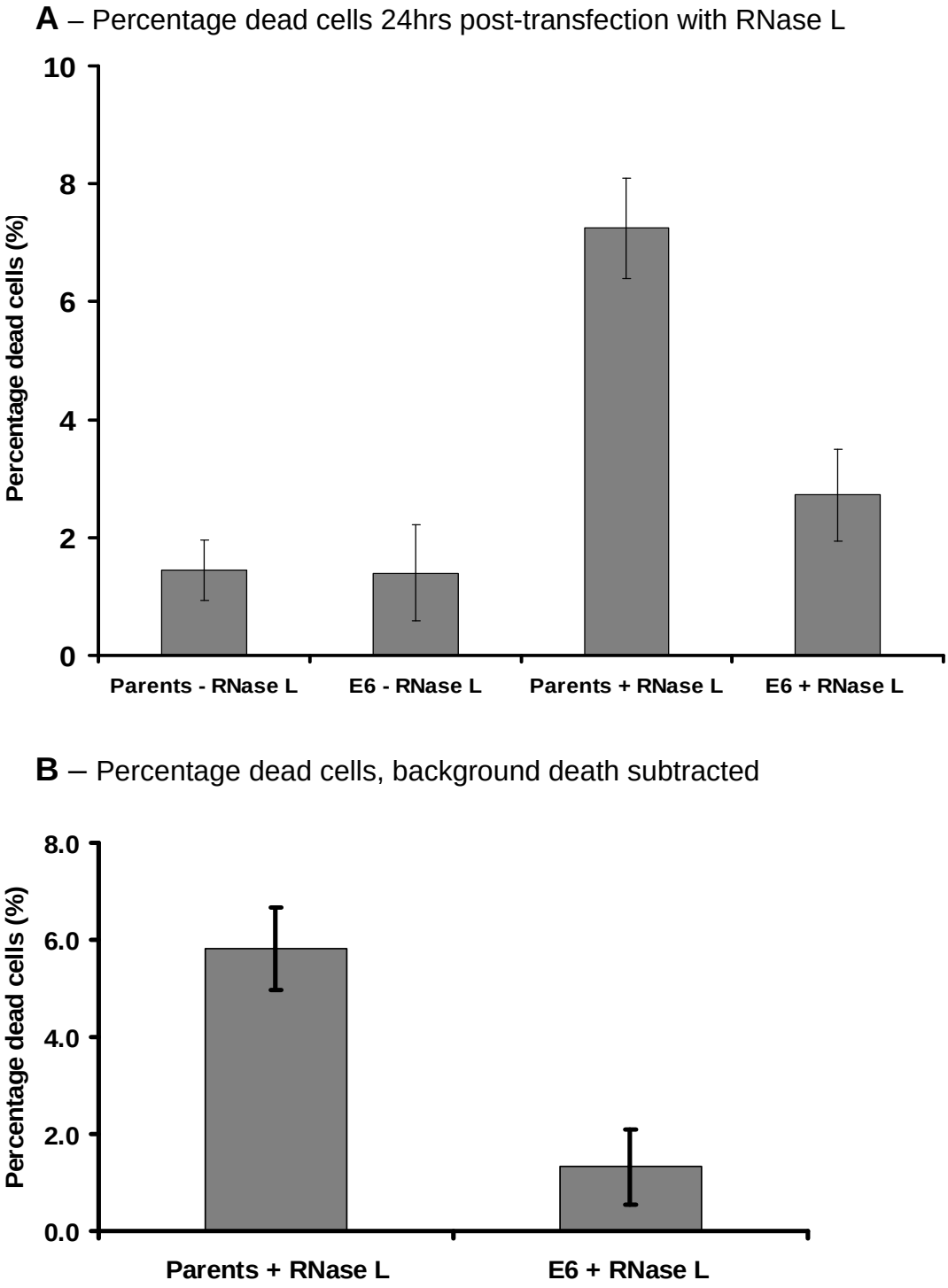

Figure 6.9 – (A) C33A Parent and C33AE6 cells were transfected with an RNase L expression vector using Lipofectamine-2000. The number of dead cells was assessed at 24 hrs using trypan blue exclusion and control Lipofectamine-2000 treated control cells were also included. (B) The percentage of dead cells observed at 24 hrs minus the background cell death. Data presented based on triplicate data points from a single experiment.

In order to account for potentially differing transfection efficiencies between C33AE6 and C33A parent cells, triplicate flasks were stained for ß-Galactosidase activity, demonstrating transfection efficiencies of 8.4 % ± 0.53 and 9.07 % ± 0.46 for C33A parent and C33AE6 respectively. In order to fully account for this slight variation in transfection efficiency, the observed dead cells were expressed as a percentage of the transfected cells based on the ß-Galactosidase staining data, as shown in Figure 6.10. Based on this analysis, the data suggests that transient transfection of the RNase L expression vector produced a significant ($p<0.01$) 4.7 fold increase in cell death in the C33A parent cells when compared to C33AE6 cells.

Figure 6.10 – Percentage dead cells observed at 24hrs post transfection with RNase L, expressed as a percentage of successfully transfected cells

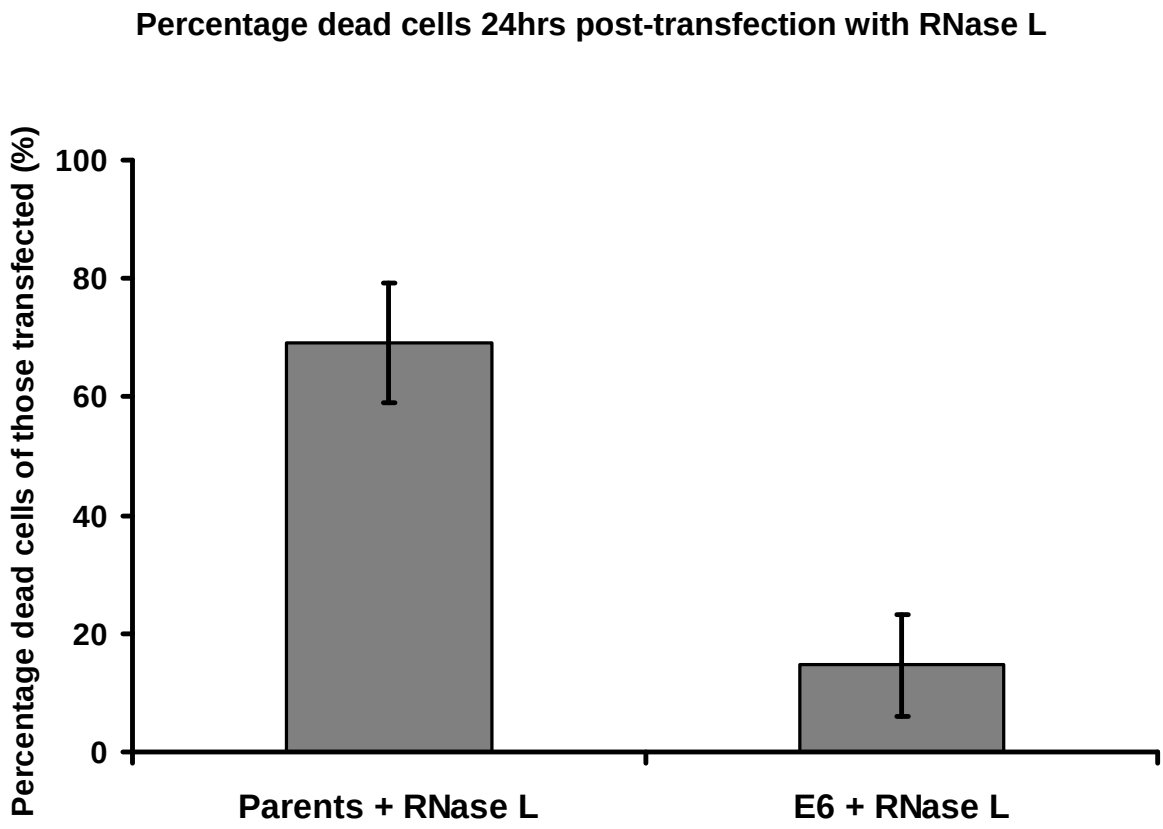

Figure 6.10 – Percentage of dead cells observed 24hrs following transfection of RNase L into C33A Parent and C33AE6 cells expressed as a percentage of those cells successfully transfected based on ß-Galactosidase staining. Transient transfection of the RNase L expression vector produced a highly significant 4.7 fold increase ($p < 0.01$) in cell death in C33A parent cells when compared to C33AE6. Data based on Triplicate data points.

6.4.3.2. Effect of HPV E6 protein on RNase L and ABCE1

The preceding results indicate that the presence of the HPV Type 16 E6 protein appeared to confer a survival advantage on C33A cells transiently transfected with RNase L. Based on these findings, it was initially hypothesised that E6 may be facilitating the degradation of RNase L in vitro. In order to address this issue, flasks of C33A parent and C33AE6 cells were again transiently transfected with RNase L (section 6.3.3.2). Protein lysates were prepared from cells harvested at 4, 8, 12 and 24 hrs post-transfection, and separated by SDS-PAGE, and RNase L and ABCE1 expression was assessed by western blot analysis (section 6.3.4.2) shown in Figures 6.11 (A) & (B) respectively. Figure 6.11(A) demonstrates the lack of endogenous RNase L expression in untransfected C33A parent and C33AE6 cells and also demonstrates that following transient transfection, an incubation period of approximately 8 hrs is required before RNase L protein detected. It is also clear that the E6 protein has no effect on RNase L protein levels, regardless of harvest time point, up to and including 24 hrs. Figures 6.11 (A) & (B) also confirm the presence of equivalent levels of endogenous ABCE1 protein in both C33A parent and E6 cells. It is also apparent that the presence of the HPV type 16 E6 protein does not exert any effect on ABCE1 levels, regardless of harvest time (Figure 6.11B).

Figure 6.11 – Effect of the HPV E6 protein on RNase L and ABCE1 protein levels in C33A parent and C33AE6 cells

A – RNase L protein levels in RNase L transfected C33A parent/ E6 cells

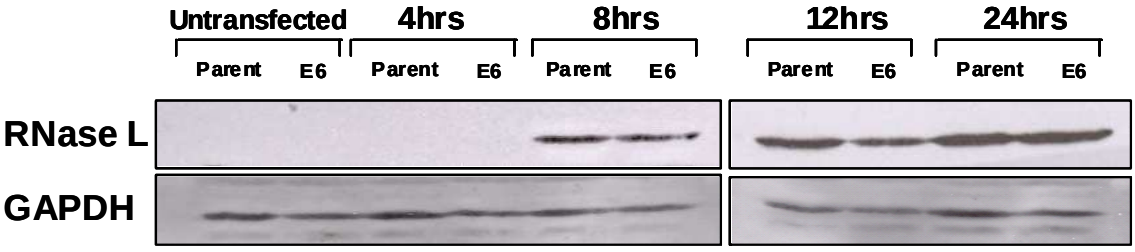

B – ABCE1 protein levels in RNase L transfected C33A parent/ E6 cells.

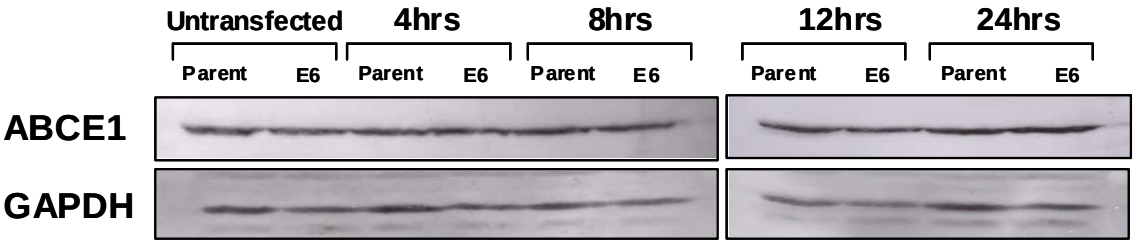

Figure 6.11 – C33A Parent and C33AE6 were transfected with equal amounts of RNase L expression vector using the Lipofectamine-2000 reagent. Cell lysates were prepared at the time points indicated and proteins were separated on a 12% SDS-PAGE gel. A western blot was carried out with membranes probed for RNase L (panel A) levels along with ABCE1 levels (panel B). GAPDH control blots were also carried out. The HPV type 16 E6 protein appears to have little effect on the levels of RNase L protein or ABCE1, regardless of transfection time, with levels remaining constant. Panel A also demonstrates a transfection time of approximately 8 hrs is required for RNase L expression.

6.4.3.3. Effect of the HPV E6 protein on the nuclear/cytoplasmic localisation of RNase L

6.4.3.3.1. Immunohistochemistry staining

Having demonstrated that the HPV type 16 E6 protein does not facilitate the degradation of RNase L, it was decided to evaluate E6 mediated alterations in nuclear/cytoplasmic localisation by immunohistochemistry. Immunostaining with anti-Actin was included as a positive control, with the results shown in Figure 6.12.

Figure 6.12 – Immunohistochemistry staining – β-Actin controls

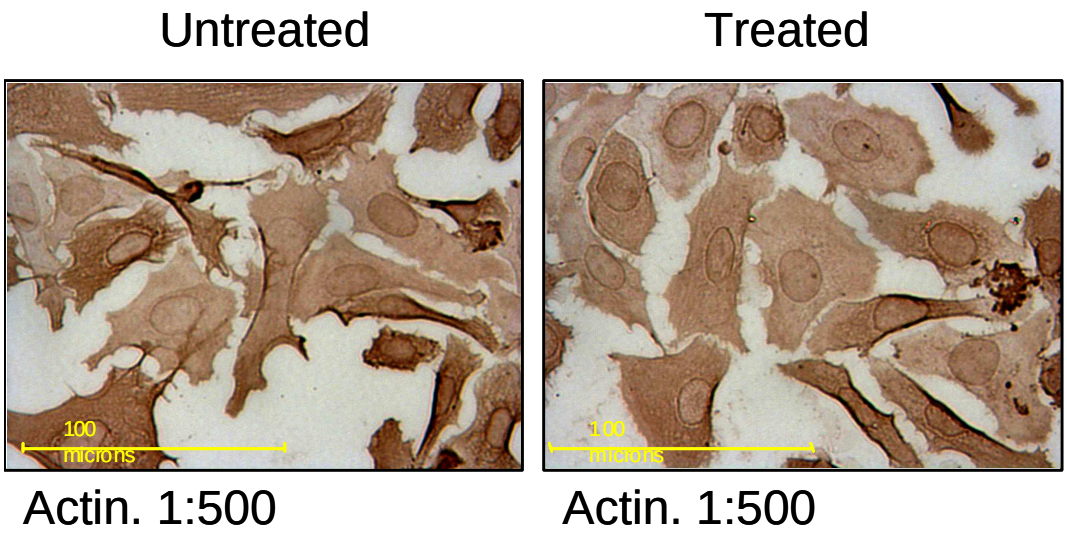

Figure 6.12 – SiHa cells were grown using slide flasks. At a confluency of 80% cells were treated with lopinavir at a final concentration of 25µM. Control untreated cells were treated with an equal volume of DMSO. Following 6 hrs incubation with lopinavir, cells were fixed and stained using a positive control anti-Actin antibody at a concentration of 1:500 and an appropriate biotinylated secondary antibody. Cells were visualised using DAB staining, and staining is based on a single experiment.

Figure 6.13 demonstrates the staining obtained using a Sigma Aldrich mouse primary anti-RNase L antibody (Sigma-Aldrich antibody R3529), at concentrations of 1:100 and 1:500. RNase L expression was predominantly cytoplasmic, and lopinavir did not alter RNase L localisation, regardless of the primary antibody concentration used to assess protein levels.

Figure 6.13 – Immunohistochemistry staining of RNase L in lopinavir treated SiHa cells

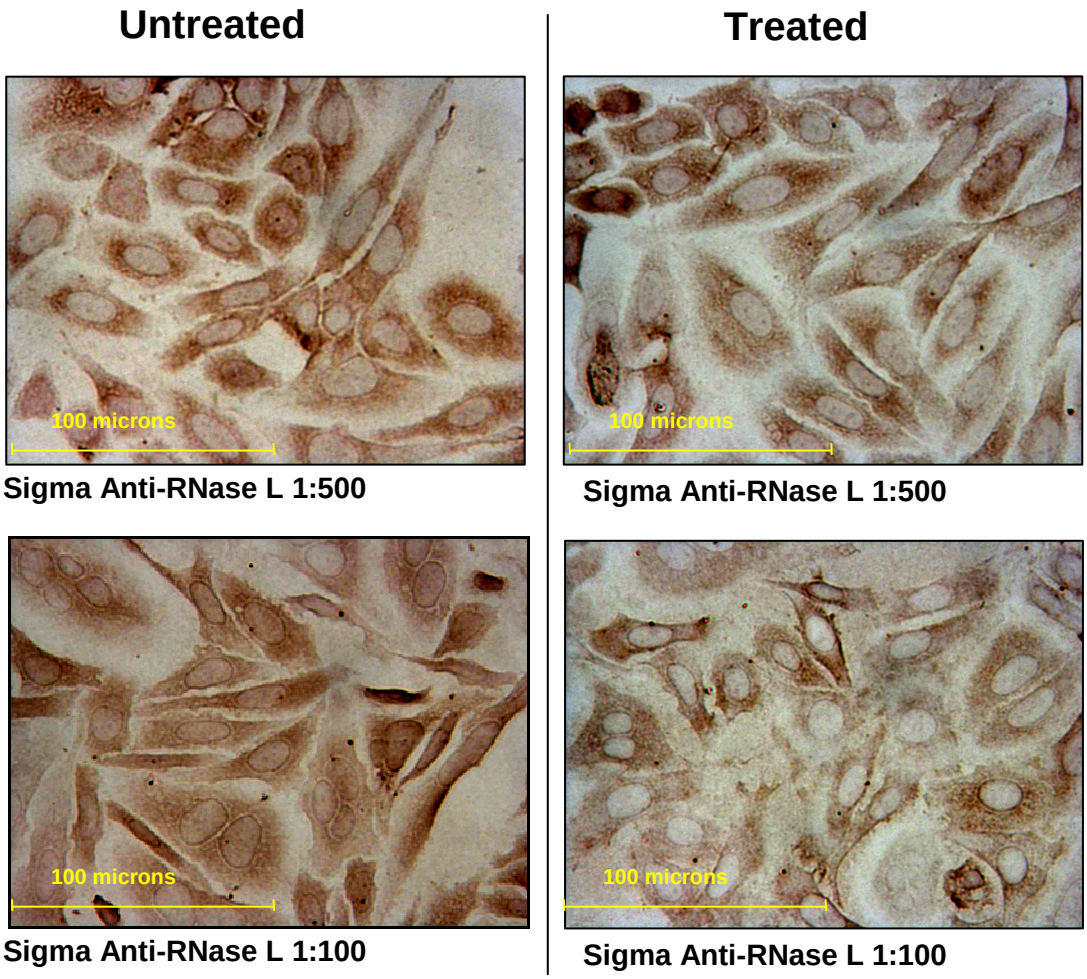

Figure 6.13 – Immunohistochemistry staining. SiHa cells were grown using slide flasks to a confluency of 80% whereupon cells were treated with lopinavir at a final concentration of 25µM or an equal volume of DMSO. Following 6hrs incubation with lopinavir, cells were fixed and stained using a Sigma Aldrich mouse anti-RNase L antibody at a concentration of 1:500 and 1:100, and an appropriate biotinylated secondary antibody. Cells were visualised using DAB staining. RNase L expression was predominantly cytoplasmic, and the localisation or RNase L intensity did not alter following treatment with lopinavir, based on a single experiment with over a range of primary antibody dilutions.

Figure 6.14 demonstrates the RNase L staining obtained using the Abcam rabbit anti-RNase L antibody (Abcam antibody 32307) at concentrations of 1:50 and 1:250. Looking first at cells stained at a primary antibody concentration of 1:50, the RNase L expression pattern appears similar to the results obtained using the Sigma Aldrich antibody (Figure 6.13). RNase L appears predominantly restricted to the cytoplasm, and lopinavir does not produce any widespread changes in RNase L localisation. Treatment did however appear to have increased nuclear expression of RNase L in a small number of cells (arrowed), which presumably is a consequence of the extremely pleomorphic morphology of SiHa cells. In contrast to this, in cells stained using primary anti-RNase L at a concentration of 1:250, RNase L expression has demonstrated a dramatic

nuclear to cytoplasmic shift in localisation. In the DMSO treated cells, RNase L expression is predominantly nuclear, with very little cytoplasmic staining observed, however, following lopinavir treatment, the expression of RNase L in the cytoplasm is much more intense, with an apparent drop in nuclear staining levels.

Figure 6.14 – Immunohistochemistry staining of RNase L in lopinavir treated SiHa cells

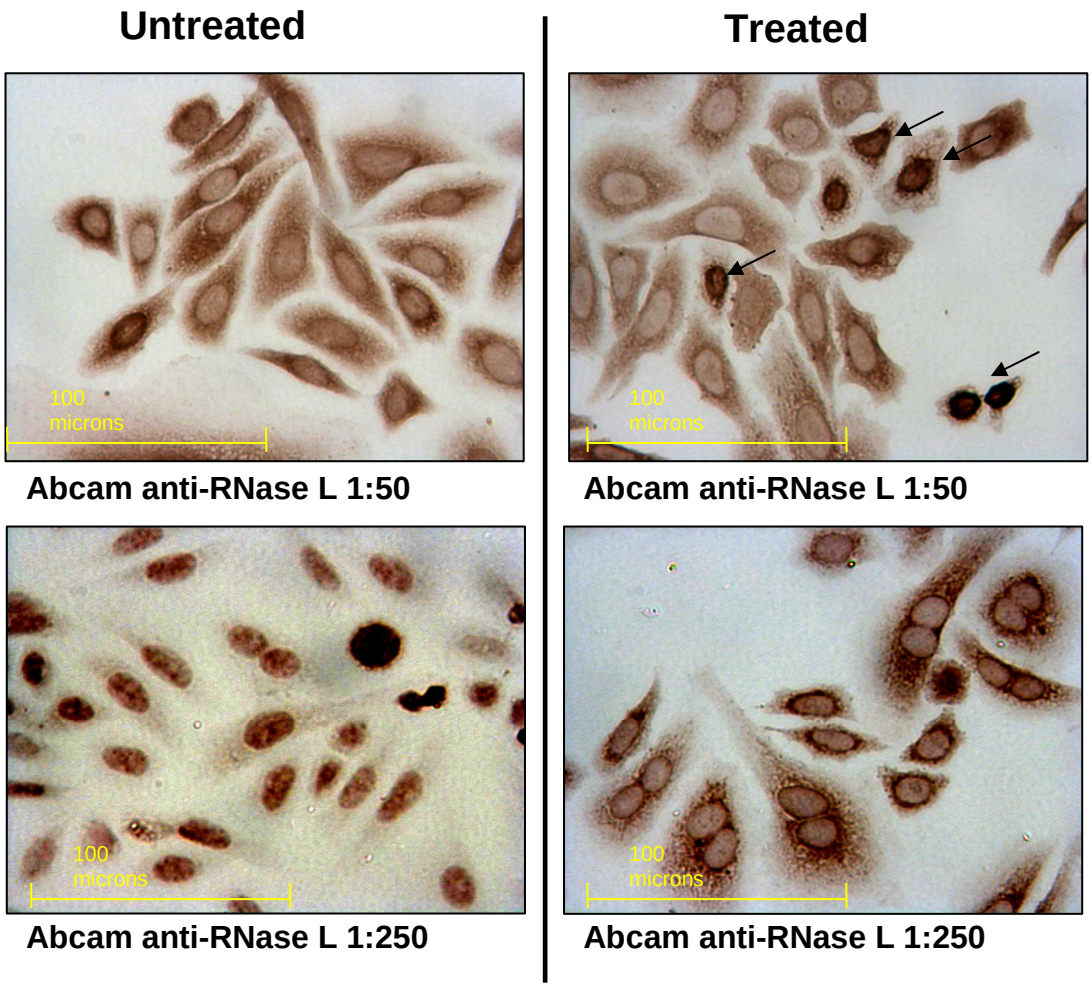

Figure 6.14 – Immunohistochemistry staining of RNase L in control DMSO treated and lopinavir treated SiHa cells. SiHa cells were grown using slide flasks. At a confluency of 80% cells were treated with lopinavir at a final concentration of 25 µM. Control untreated cells were treated with an equal volume of DMSO. Following 6 hrs incubation with lopinavir, cells were fixed and stained using an Abcam rabbit anti-RNase L antibody at a concentration of 1:50 and 1:1250, and an appropriate biotinylated secondary antibody. Cells were visualised using DAB staining. At a 1:50 concentration, RNase L appears predominantly restricted to the cytoplasm, and lopinavir does not produce any widespread changes in RNase L localisation. However, lopinavir treatment does appear to have increased nuclear expression of RNase L in a small number of cells (arrowed). In comparison, in cells stained with primary antibody at a concentration of 1:250, RNase L was shown to exist predominantly in the nucleus. In these cells, lopinavir appeared to produce a nuclear to cytoplasmic shift in RNase L expression based on a single experiment.

6.4.3.3.2. Nuclear/ Cytoplasmic Fractionation

The preceding Immunohistochemistry results (section 6.4.3.3.1), do not convincingly demonstrate lopinavir-induced alterations in RNase L localisation. Since it was concluded this could be due to the pleomorphic nature of SiHa cells, it was decided to use an alternative cell system. Nuclear/cytoplasmic fractionation of transiently RNase L transfected C33A and C33AE6 cells treated with lopinavir was used to further assess the ability of the drug to effect nuclear/ cytoplasmic localisation in the presence and absence of E6.

Figure 6.15 shows the western blot result from the RNase L transfected cells. The GAPDH and HDAC1 signals demonstrate that a successful fractionation has taken place. Cytoplasmic fractions from each pair tended to contain higher levels of RNase L than nuclear fractions, in both parent and E6 cells.

Neither the presence of the E6 protein or treatment with lopinavir altered the detectable levels of RNase L in either cellular compartment.

Figure 6.15 – Effect of the HPV E6 protein and lopinavir on the nuclear/ cytoplasmic localisation of RNase L

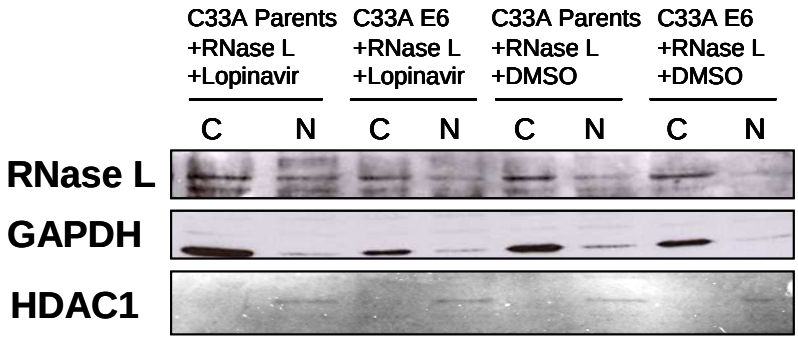

Figure 6.15 – C33A parent and C33AE6 cells were transfected with RNase L. Duplicate samples were also treated with 25 µM lopinavir for 6 hrs. Cell samples were separated into nuclear and cytoplasmic fractions, and proteins separated on a 12% SDS-PAGE gel. A western blot was carried out and probed with primary rabbit anti-RNase L and GAPDH loading control (C, cytoplasmic. N, nuclear). Based on a single experiment.

6.4.4. Co-immunoprecipitation of RNase L and ABCE1

Since no convincing difference in lopinavir-induced sub-cellular localisation of RNase L was observed, it was decided to use co-immunoprecipitation to investigate whether the drug could alter the physical association between RNase L and its endogenous inhibitor ABCE1. Anti-ABCE1 immunoprecipitates were prepared from transiently RNase L transfected C33A and C33AE6 cells treated with lopinavir or DMSO control. These were western blotted and sequentially immunoprobed with anti-ABCE1 and anti-RNase L antibodies (Figure 6.16(A)). These data confirmed that lysates from RNase L transfected C33A and C33AE6 showed a signal at the predicted molecular weight. This confirms the interaction between the transfected RNase L proteins and its endogenous inhibitor ABCE1 in C33A parent and C33AE6 cells.

Image J density analysis of RNase L signals was carried out and the results shown in Figure 6.16(B) are represented as a relative intensity compared to matched-ABCE1 protein levels. Based on these observations, C33AE6 cells had 1.9-fold more RNase L associated with ABCE1 than equivalent C33A control cells. Significantly, lopinavir was shown to produce a modest drop in RNase L protein levels in RNase L transfected C33AE6 cells.

Figure 6.16 - Co-immunoprecipitation of RNase L and ABCE1 in RNase L transfected C33A parent and C33AE6 cells

A – Initial Co-Immunoprecipitation followed by Western blot of RNase L transfected C33A cells

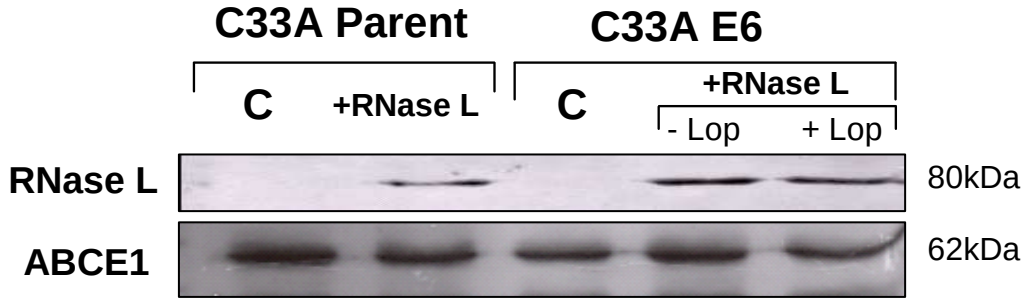

B – Image J density analysis of Co-IP lysates

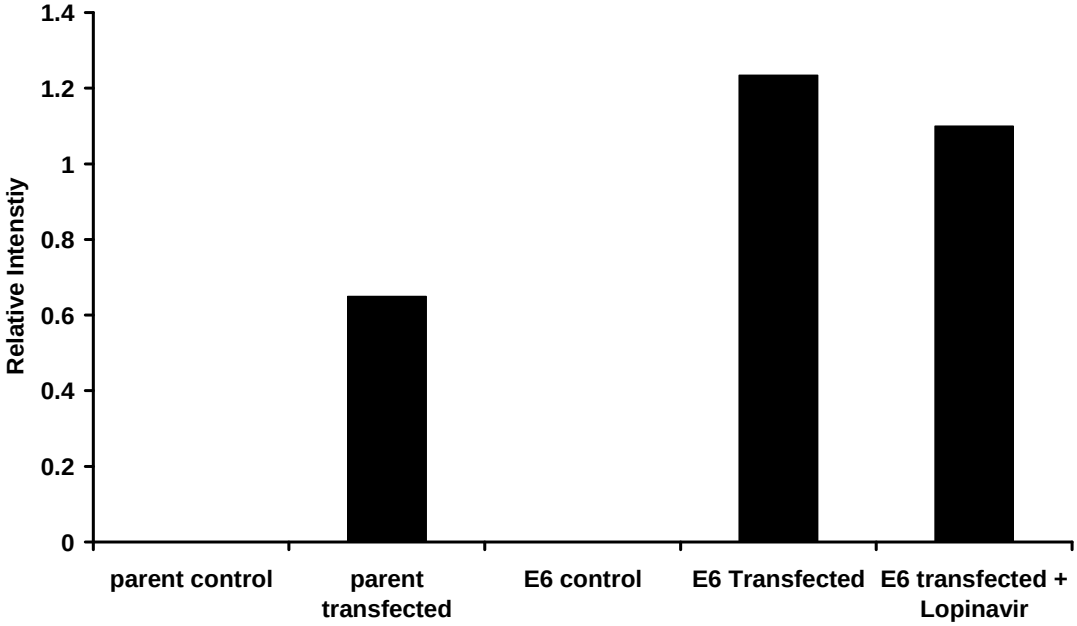

Figure 6.16 - (A) western blot analysis following co-immunoprecipitation of RNase L with ABCE1 in RNase L transfected C33A parent and C33AE6 cells. Duplicate untransfected controls (C) were included along with 25µM 6hr lopinavir (+/- lop) treated RNase L transfected C33AE6 cells. Data confirms the physical interaction of ABCE1, and also that the interaction appears stronger in E6 expressing cells. (B) Image J density analysis of signal strength following western blot based on a single representative western blot. Signals are represented as a relative intensity compared to ABCE1 signal strengths. When compared to C33A Parent cells, C33AE6 transfected cells exhibited a 1.9-fold increase in RNase L/ ABCE1 binding, which was slightly reduced following lopinavir treatment.

To further assess the effects of lopinavir on the RNase L/ ABCE1 interaction, the previous co-immunoprecipitation reaction was repeated including samples treated with lopinavir for 6, 12 and 24 hrs. The results of this western blot are shown in Figure 6.17(A) with relative intensities calculated using image J shown in Figure 6.17(B). As expected, neither control untransfected cell types demonstrated a signal. The interaction between RNase L and ABCE1 was again confirmed as being stronger in C33AE6 cells than in parent C33A cells (a 1.4-fold increase). Further to this, treatment for 6, 12 and 24 hrs subsequently produced a linear decrease in signal intensity with 24 hrs lopinavir treatment producing a signal a third of the intensity of the DMSO treated RNase L transfected cells.

Figure 6.17 – Repeat Co-immunoprecipitation of RNase L and ABCE1 in RNase L transfected C33A parent and C33AE6 cells followed by a lopinavir time course

A – Co-Immunoprecipitation following lopinavir time course

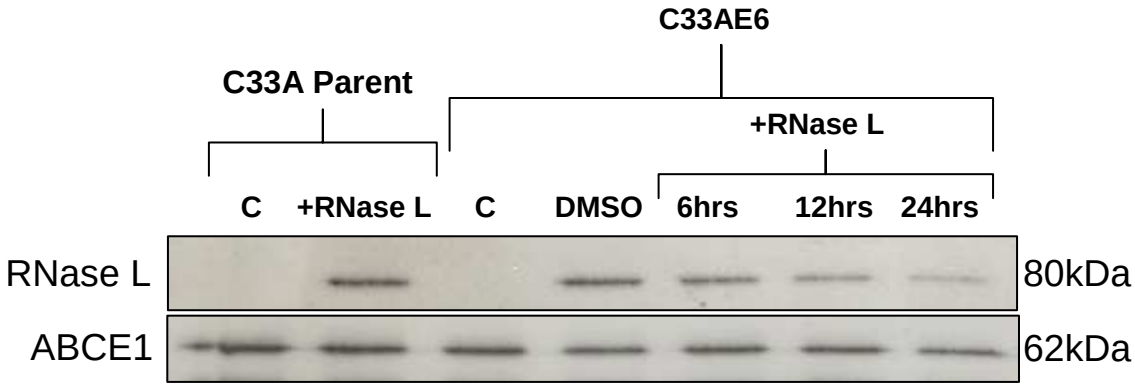

B – Image J density analysis

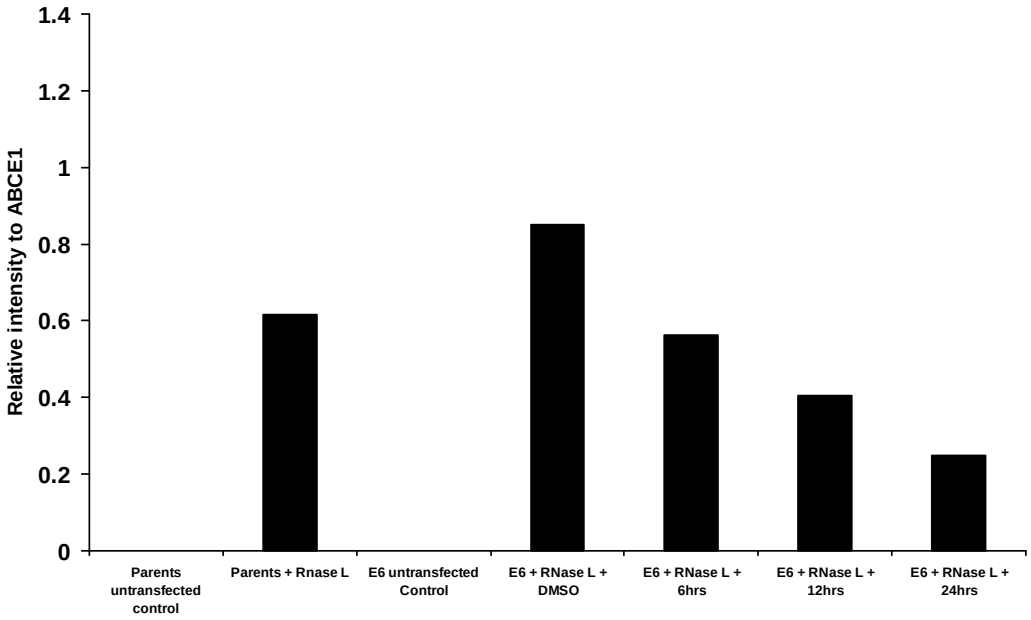

Figure 6.17 - (A) western blot analysis following co-immunoprecipitation of RNase L with ABCE1 in RNase L transfected C33A parent and C33AE6 cells. Duplicate untransfected controls (C) were included along with 25µM lopinavir treated RNase L transfected C33AE6 cells, treated for the time indicated. Data confirms the physical interaction between RNase L and ABCE1, and also that the interaction appears stronger in E6 expressing cells. (B) Image J density analysis of signal strength following western blot based on a single representative western blot image. Signals are represented as a relative intensity compared to ABCE1 signal strengths. When compared to C33A Parent cells, C33AE6 transfected cells exhibited a 1.4-fold increase in RNase L/ ABCE1 complex signal. In contrast to Figure 6.18, lopinavir produced a marked decrease in RNase L/ABCE1signal at 6hrs, and over the remaining time points produced a linear decrease in RNase L/ ABCE1 signal strength.

6.5. Chapter Summary and Discussion

As previously discussed it has been demonstrated that lopinavir produces a dose dependent growth inhibition of growth in SiHa cells (Figure 3.1(A)) with a dose dependent increase in the levels of the RNase L protein. This effect was observed over a dose range of 5 - 30 µM, with a peak intensity occurring at 12 hrs. In order to assess the role of RNase L in the toxicity of lopinavir against cells expressing HPV oncoproteins, siRNA mediated degradation of RNase L was used.

The work carried out in collaboration with Professor Zehbe demonstrated that lopinavir induced an increase in RNase L in E6/E7 immortalised PHFKs (Figure 5.12). These data clearly support our observation of a lopinavir induced increase in RNase L expression in SiHa cells. Furthermore, cell proliferation assays demonstrated pronounced differences in the growth rates of E6/E7 expressing PHFKs when compared to control PHFKs exposed to lopinavir. The E6/E7 expressing cell lines were shown to be much more susceptible to lopinavir growth inhibition than the corresponding control cells (Figure 3.5). These studies also demonstrated the importance the dose range of lopinavir – when used at concentrations approaching 25 µM, normal PHFKs showed steady growth, whereas the growth of E6/E7 immortalised PHFKs was dramatically reduced. At concentrations >25 µM the selective toxicity was lost and cell proliferation was inhibited equally in both cell types.

It was of interest that siRNA 1 mediated silencing of RNase L in untreated SiHa cells induced a significant improvement in cell growth over 72 hrs, when compared to control ALLSTAR siRNA transfected cells (Figure 6.7). What is the potential explanation of this result? Although endogenous RNase L is known to exert anti-proliferative effects in virally infected cells, it is also considered to a potential tumour suppressor [267]. Since untreated SiHa cells express RNase L, albeit at low levels (see Figures 5.7 & 5.8), it is possible that siRNA silencing of the expression of this product may lead to an improvement in the growth of these cells. As stated previously, siRNA achieves peak silencing within 24 hrs of transfection which is subsequently followed by a rapid decline in effectiveness and concomitant restoration of protein synthesis by 48 hrs. This 'hit and run' nature of siRNA-mediated silencing provides an effective, yet very small window of opportunity to study the true effects of RNase L silencing on cell proliferation. This is in contrast to shRNA which would provide constitutive stable knockdown of RNase L. Whilst the AQ-96 cell proliferation assay indicates metabolic activity, cell proliferation can be assessed with a number of techniques; Assays for **p**roliferating **c**ell **n**uclear **a**ntigen (PCNA) (reviewed in [321]) and DNA synthesis by 5'-2'-bromodeoxyuridine incorporation in conjunction with flow cytometric analysis of apoptotic markers would provide a multifaceted approach to assessing the implications of endogenous RNase L knockdown on cell proliferation.

In order to determine whether RNase L plays a role in lopinavir-induced toxicity, a 72hr cell proliferation assay was carried out following siRNA silencing of RNase L in lopinavir treated SiHa cells. The data shown in Figure 6.7 demonstrated that in those cells with reduced RNase L expression, lopinavir had less of an impact on cell growth, implying a reduction in lopinavir toxicity.

This effect was found to be optimal at 25 µM lopinavir, and was lost at concentrations higher than this. It is significant that these data are consistent with the growth differential observed between E6/E7 immortalised PHFKs and control PHFKs which was also seen to be maximal at 25 µM lopinavir (Figure 3.5).

Taking all these observations together, our results support a functional link between RNase L and lopinavir toxicity in HPV infected cells. It is of note that the 25 µM optimum drug concentration for these effects is much higher (>15 fold) than that which is achieved in the cervico/vaginal fluid in HIV patients taking oral Kaletra [322], a factor which has been previously discussed [131].

The data shown in Figure 6.8(A) demonstrates the absence of RNase L induction in CaSKi cells exposed to lopinavir. This data is potentially indicative of a functional interaction between RNase L and E6. We have demonstrated the importance of RNase L in lopinavir toxicity in SiHa cells, suggesting that the increased expression of E6 protein in CaSKi cells (shown in Figure 6.8(B)) may be limiting the effects of RNase L by promoting the association with ABCE1, which would in turn account for the increased resistance of CaSKi cells to lopinavir treatment.

These data raise the question of how does HPV compromise the function of RNase L? It is known that the high risk HPV E6 protein inappropriately activates the cellular E3 ubiquitin ligase, E6AP, which leads to the uquitination and degradation of the p53 tumour suppressor protein by the proteasome [56]. Thus, we hypothesised that the HPV E6 protein could also facilitate the inappropriate degradation of RNase L in order to suppress its antiviral/ anti-proliferative functions in the HPV infected cell. In order to further investigate this hypothesis, HPV negative C33A cells and stable HPV type 16 E6 transfected cells were used since it was found that these cells lack endogenous RNase L expression (Figure 5.5), therefore overcoming the limitation of a lack of a suitable control cell when using SiHa model systems. Transient transfection of both of these cells with an RNase L expression vector demonstrated that C33A parent cells exhibited a highly significant 4.7-fold increase in dead cells compared to C33AE6 cells when observed 24 hrs post-transfection (Figure 6.10). These data provided a first indication that that the HPV E6 protein was potentially capable protecting these cells from RNase L induced cell killing. However, this was not found to be due to E6 inducing the degradation of RNase L, since equivalent levels of the RNase L protein were observed in transiently transfected C33A and C33AE6. Another possible explanation was that E6 could be up-regulating the levels of the endogenous RNase L inhibitor, ABCE1, yet this was shown to be unchanged in both cell types, regardless of harvest time point (Figure 6.11(B)). Although these data provide an initial insight into the association between E6 and RNase L they can only be thought of as preliminary data. This particular live/dead assay suffers from several flaws which prevent a definitive conclusion from being made. Initially, the cell numbers involved in the analysis of this particular assay are extremely low, and are therefore potentially open to interpretation when considering relative +/- standard deviation values for both control and E6 expressing cells. In addition, before a definitive conclusion could be made, it would be necessary to repeat the assay utilising a range of cell types that endogenously express both

RNase L and E6, to rule out an RNase L-induced cell death phenomenon that is strictly restricted to the C33A cell line.

What other factors could explain this difference in sensitivity to RNase L? Having ruled out E6-mediated degradation of RNase L, the ability of E6 to alter cellular localisation was assessed, which provided conflicting results. Based on immunohistochemical staining (Figure 6.14), the RNase L expression pattern following lopinavir treatment of SiHa cells was shown to vary depending on the primary antibody, and the concentration at which it was used. To clarify these findings, western blot analysis of fractionated RNase L transfected cells was carried out (Figure 6.15). These data from western blot analysis demonstrated that RNase L expression was elevated in the cytoplasmic fractions when compared to nuclear fractions however lopinavir did not significantly alter its cellular localisation, in either C33A parents of C33AE6 cells, when compared to DMSO control cells.

Having demonstrated that the E6 protein does not facilitate the degradation of RNase L or cause an increase in ABCE1 levels, or affect its cellular localisation, the interaction between RNase L and its endogenous inhibitor was evaluated (Figure 6.16 & 6.17). Co-immunoprecipitation of ABCE1 and RNase L was carried out in C33A parent and C33AE6 cells exposed to lopinavir following transient transfection with an RNase L expression vector. These data demonstrated an increase in the levels of RNase L associated with ABCE1 in C33AE6 cells, when compared to equivalent C33A control cells, of between 1.4 - 1.9-fold. This implies that the E6 protein is in some way enhancing or promoting the interaction between ABCE1 and RNase L, thus inhibiting the interaction between RNase L and its endogenous activator protein, 2-5A. The net result would be a reduction in the activation potential of RNase L followed by a subsequent drop in its antiviral/ apoptotic capabilities. This would therefore account for the reduced cell death in C33AE6 cells observed 24 hrs post-transfection with RNase L. Six hour lopinavir treatment was initially shown to cause a mild reduction in the ABCE1/ RNase L interaction in C33AE6 transfected cells (Figure 6.17). However, in cells treated with a fixed dose of lopinavir over a 24 hr period, the reduction in RNase L associated with ABCE1 was noticeably reduced, demonstrating a linear relationship between lopinavir incubation and signal strength. The membrane was re-probed with ABCE1 and demonstrated constant ABCE1 protein levels regardless of lopinavir incubation time.

6.6. Further work

The most important result arising from the work in this chapter centres around the observation that the presence of the HPV type 16 E6 protein confers a survival advantage on C33A cells transiently transfected with RNase L. Furthermore, in addition to the potential weaknesses in this assay, highlighted in section 6.5, it is also important to further characterise the cell death induced following the re-introduction of RNase L into the C33A test cells. The 'ApoAlert' Annexin-V-FITC apoptosis detection kit available from Sigma Aldrich (http://www.sigmaaldrich.com/etc/medialib/docs/Sigma/Bulletin/apoafbul.Par.0001.File.tmp/apoafbu

l.pdf) would be utilised to assess RNase L induced cell death. However, in contrast to classical TUNEL staining (reviewed in [323]), the ApoAlert kit will allow for detection of apoptosis at an earlier stage than in addition to allowing differentiation of apoptotic cells from viable and necrotic cells.

Further to this, it was demonstrated that in E6 expressing cells, the interaction between RNase L and its endogenous inhibitor ABCE1 was noticeably stronger (Figure 6.16 and Figure 6.17), and was destabilised in the presence of lopinavir. Co-immunoprecipitation reactions would be repeated using cell samples in which RNase L is expressed endogenously, namely SiHa and Caski cells, both of which express full HPV genomes, along with endogenous RNase L protein, as demonstrated previously. CaSKi cells, derived from a small bowel mesentery metastasis originating from an epidermoid carcinoma in a 40 yr old Caucasian female [324] also contain integrated HPV16. However, in contrast to SiHa cells which contain 1-2 copies per cell [186], CaSKi cells are known to contain 400 – 600 HPV16 copies per cell [311]. Previous work has demonstrated that CaSKi cells are relatively resistant to lopinavir treatment [131] and if, as suggested by the current findings, E6 plays a role in augmenting the RNase L/ ABCE1 interaction leading to a reduction in lopinavir toxicity, the increased E6 expression in CaSKi cells will in theory explain the decreased sensitivity to lopinavir.

7. Discussion

Of the estimated 529,409 new cases of cervical cancer occurring worldwide in 2008, more than 80% were shown to occur in developing countries. Those developing countries within Africa, in particular, suffer a disproportionately high burden [10]. In a region where HIV and poverty exacerbate the problems associated with cervical malignancy, and where HPV vaccination and effective cervical screening programmes are both limited and potentially ineffective, it is clear that a low-cost, low-technology, preferably self-applied alternative therapy for the management of HPV-related cervical malignancy is essential. We provide evidence to suggest that lopinavir, an HIV-specific antiretroviral, possesses anti-cancer activities that would make it suitable for use in the management of HPV-related pre-cancerous lesions of the cervix.

7.1. Lopinavir alters protein expression in HPV positive SiHa cells

Many viruses are known to inhibit the function of, or inappropriately degrade host cell proteins detrimental to viral persistence [226-230]. More specifically, through the synergistic actions of the viral E6 and E7 proteins, HPV is able to directly 'hijack' the ubiquitin-proteasome system (reviewed in [231]) resulting in the degradation of the p53 and Rb tumour suppressor proteins, facilitating unhindered viral replication and oncogenesis. The HIV-specific protease inhibitor lopinavir has been shown to specifically inhibit the chymotryptic-like activity of the 26S proteasome [73, 325]. It is now thought that, in conjunction with inhibition of protease function, inhibition of the proteasome plays a significant role in the anti-HIV activity of lopinavir and related compounds [326]. Proteasomal inhibition with lopinavir has been shown to limit E6-dependent degradation of p53, stabilising protein levels and selective killing of HPV type 16 E6-dependent cervical carcinoma cells *in vitro* [98]. Thus, it was hypothesised that, in addition to p53, inhibition of proteasomal degradation would lead to changes in expression levels of a range of cell proteins regulated by the proteasome. Furthermore, it was postulated that one or more of the proteins exhibiting altered expression following lopinavir treatment could potentially account for the anti-HPV activity of lopinavir. In order to address this, the protein expression profiles of lopinavir-treated and DMSO-control treated HPV positive SiHa cells were compared using the Panorama Xpress725 profiler-725 antibody microarray (Chapter 4). Lopinavir treatment of HPV positive SiHa cells lead to alterations in expression levels of 51 proteins responsible for a wide range of biological functions. It was not surprising that several known apoptosis-markers, including Annexin-5, activated Caspase-3, p63, TNF and p53 were elevated (Figures 4.6 and 4.7) since previous work demonstrated lopinavir-induced apoptosis in SiHa cells [98]. Interestingly, many of the altered proteins were shown to be targets for proteasomal degradation (Highlighted (*) in Table 7.1) indicating that lopinavir can inhibit proteasomal function to such an extent so as to allow accumulation of proteins that would otherwise be degraded. Bioinformatic analysis of all the proteins in Table 7.1 was carried out,

including a search of the Virus Molecular INTeraction (Virus MINT) database [327] for known E6 and/or E7 interacting proteins. Curiously, only p53 has previously been shown to be degraded by the action of E6.

Clearly, there are limitations to using an array such as the Panorama Xpress725 profiler-725. Whilst this allows comparative analysis of expression levels of over 700 proteins this is only a small fraction of the total number of proteins comprising the complete proteome of a mammalian cell. As such, the possibility remains that lopinavir may still alter the expression of other virally dis-regulated proteins which are not represented on the array.

Table 7.1 –Proteins with altered expression levels following exposure of SiHa cells to lopinavir

Gene	Protein name	Function/Association	Fold change
ANXA5	Annexin 5	Calcium binding protein	2.15
CTBP1 (C-terminal) *	C-Terminal binding protein 1	Transcription regulatory protein	1.87
CHEK2 *	CHK2 checkpoint homolog	Serine/Threonine kinase	1.84
RAB5A	Ras related protein Rab 5A	GTPase	1.84
RNASEL *	Ribonuclease L	Ribonuclease	1.76
ACTR3	Actin related protein 3	Cytoskeletal protein	1.73
GRB2	Growth factor receptor bound protein 2	Adapter molecule	1.73
SYNPO	Synaptopodin	Cytoskeletal associated protein	1.72
CASP3	Caspase 3 (active)	Cysteine Protease	1.69
EGF	Epidermal growth factor	Growth Factor	1.68
TP63 *	Tumour protein p63	Transcription factor	1.68
BIRC5 *	Survivin	Adapter molecule	1.67
ILK *	Integrin-linked kinase	Serine/Threonine kinase	1.59
ERK2	Mitogen activated protein kinase 1	Serine/Threonine kinase	1.56
SYNPO	Synaptopodin	Cytoskeletal associated protein	1.56
SNCA	α-Synuclein	Chaperone protein	1.56
PADI4	Peptidylarginine deiminase 4	Enzyme: Hydrolase	1.52
CHEK1 *	Cell cycle checkpoint kinase	Serine/Threonine kinase	1.52
TUB	Tubulin/ Tyrosine	Cytoskeletal associated protein	1.50
NOS1 *	Nitric oxide synthase 1	Enzyme: Synthase	1.50
CTBP1 (N-terminal) *	C-Terminal binding protein 1	Transcription regulatory protein	1.49
TNF	Tumour necrosis factor-α	Ligand	1.48
H2AFX	H2A Histone Family, member X	DNA binding protein	1.47
AKT1 *	Protein Kinase B-alpha	Serine/Threonine kinase	1.47
CHEK2 *	CHK2 checkpoint homolog	Serine/Threonine kinase	1.47
FANCD2 *	Fanconi anemia, complementation group D2	Cell cycle control protein	1.47
DIABLO *	SMAC protein	Cell cycle control protein	1.46
PAWR	PRKC, apoptosis, WT1, regulator	Transcription regulatory protein	1.45
ILK *	Integrin-linked kinase	Serine/Threonine kinase	1.45
MC3R	Melanocortin 3 receptor	Cell surface receptor	1.44
APP	Amyloid Precursor Protein	Receptor activity	1.43
MKI67 *	MKI67 (FHA domain) interacting nucleolar phosphoprotein	RNA binding protein	1.43
CFL2 *	Cofilin 2	Cytoskeletal associated protein	1.38
DMD *	Dystrophin	Structural protein	1.37
CENPE	Centromeric protein E	DNA binding protein	1.36
PTK2(pp125)	Focal adhesion kinase 2 (pp125)	Tyrosine kinase	1.35
TP53 *	Tumour protein p53	Transcription factor	1.28
DMD *	Dystrophin	Structural protein	1.25
TP53 *	Tumour protein p53	Transcription factor	1.18
GJA1 *	Connexin 43	Membrane transport protein	0.76
GFAP	Glial fibrillary acidic protein	Structural protein	0.63
GJA1 *	Connexin 43	Membrane transport protein	0.60
MTOR	Mammalian Target of Rapamycin	Kinase	0.53

(Note:- Proteins marked with * are known to be substrates for proteasomal degradation)

Of significant interest was the lopinavir-induced up regulation of RNase L, which is a major cellular antiviral protein. Based on western blot analysis, lopinavir (25 µM, 6 hrs) was shown to induce a significant ($p<0.05$) 9.5-fold increase in RNase L protein levels when compared to DMSO treated control cells (Figure 5.9). Both dose and time dependent increases in RNase L expression in lopinavir treated SiHa cells (Figures 5.7 & 5.8) were confirmed by western blot analysis. RT-PCR was then used to successfully demonstrate that this up regulation was related to an accumulation of protein, as a result of proteasomal inhibition, rather than lopinavir-induced increases in gene translation and protein synthesis (Figure 5.6).

7.2. RNase L plays a key role in the toxicity of lopinavir in SiHa cells

It has previously been demonstrated that lopinavir exerts dose dependent growth-limiting effects of lopinavir in SiHa cells ([98] and Figure 3.1 in this report), however there has been no investigation as to how this correlates with RNase L expression, or indeed, no demonstration of the true importance of RNase L in this HPV-specific toxicity. In order to ascertain the significance of RNase L in lopinavir-dependent HPV-specific toxicity, the effects of transient siRNA-mediated gene silencing of RNase L in SiHa cells in the presence of lopinavir were assessed (Figure 6.7). Interestingly the data demonstrated that lopinavir exerted comparable levels of toxicity at lower (20 µM) concentrations, regardless of siRNA treatment. In contrast to this, when exposed to 25 µM lopinavir, siRNA transfected SiHa cells demonstrated a significant growth advantage over non-transfected cells, signifying a drop in lopinavir toxicity in the absence of RNase L. This indicates that RNase L plays a key role in facilitating the toxic effects of lopinavir in this HPV positive cell system. Interestingly however, beyond 25 µM lopinavir, the selective nature was lost, with both test and control cells demonstrating comparable growth inhibition, indicating, that whilst effective, lopinavir may have a very narrow optimal therapeutic window. Significantly, these data are consistent with the growth differential observed between E6/E7 immortalised and control primary human foreskin keratinocytes (PHFKs), which was shown to be optimal at 25 µM lopinavir (Figure 3.5). Interestingly, it was also demonstrated using clonogenic analysis (Chapter 3) of control and stable E6-expressing karyotypically normal hTert-immortalised keratinocytes that lopinavir could actually promote the growth of these cells (Chapter 3). Together, these observations support a functional link between RNase L and lopinavir toxicity in HPV infected cells, and indicate that lopinavir may have an effective yet narrow therapeutic optimal concentration, which will clearly have implications for dosing practices should lopinavir be shown to be an effective HPV therapeutic *in vivo*.

7.3. A Novel mechanism of HPV-specific lopinavir toxicity

We have demonstrated that at least part of the toxicity of lopinavir in HPV positive SiHa cells is reliant on an increased expression of the antiviral protein RNase L. This implies that HPV disables the RNase L pathway in virus infected cells. Indeed, several viruses have developed strategies by

which they can circumvent the RNase L pathway [328]. For example, previous work has demonstrated that HIV-1 is able to induce the expression of ABCE1 [329], the endogenous inhibitor of RNase L, and in doing so, is able to down-regulate the activity of the RNase L antiviral pathway (RNase L pathway shown in Figure 5.1). However, at this stage, the details of mechanism by which HPV alters the RNase L pathway are unknown. In addition, the mechanism by which lopinavir restores RNase L function, inducing lopinavir-dependent toxicity, is also unknown.

As a possible explanation, it was hypothesised that HPV, like HIV, may also up-regulate ABCE1 as a means of inhibiting the RNase L pathway. Although this is an interesting concept, the current data demonstrates that lopinavir does not appear to affect ABCE1 protein levels, regardless of concentration or incubation time. This clearly indicates that HPV may be utilising an alternative mechanism(s) by which to subvert normal RNase L function. Interestingly, CaSKi cells have been shown to contain several hundred-fold greater levels of HPV type 16 E6 protein than SiHa cells. This is interesting in light of the fact that they have previously been shown to be refractory to lopinavir treatment [98]. In addition we have since demonstrated that lopinavir fails to induce an up regulation of RNase L in CaSKi cells (Figure 6.8). This suggests that the E6 protein may be directly responsible for limiting RNase L function, hence impeding lopinavir toxicity in CaSKi cells.

In order to assess the interaction between RNase L and E6, we utilised the HPV negative parental C33A cells in addition to C33A cells stably expressing the HPV type 16 E6 protein (C33A E6), as we had previously demonstrated that these cells lacked endogenous RNase L mRNA and protein (Figures 5.5 and 6.11 respectively). We demonstrated that transient re-introduction of RNase L in these cells resulted in a highly significant 4.7-fold increase in cell death in parental cells when compared to E6 expressing cells. This raised the question of how does E6 curtail RNase L-mediated cell death and confer a protective effect on C33A E6 cells? Surprisingly, western blot analysis, immunohistochemical staining and nuclear/cytoplasmic fractionation ruled out E6-mediated degradation of RNase L, E6-mediated up-regulation of ABCE1 and E6-dependent alterations in nuclear/cytoplasmic localisation of RNase L. However, co-immunoprecipitation reactions with ABCE1 and RNase L were carried out in C33A parent and E6 expressing cells following transient transfection with RNase L. Western blot analysis demonstrated that HPV type 16 E6 appeared to enhance or promote the interaction between ABCE1 and RNase L.

How would this confer a protective effect on E6 expressing cells? In theory, an enhancement of the interaction between RNase L and its endogenous inhibitor, ABCE1 would result in a reduction in the potential for interaction between RNase L and 2-5A activating molecules (see section 5.1.1). The net result would be a reduction in the activation of RNase L, limiting its antiviral and apoptotic capabilities. Indeed, this is a strategy employed by HIV-1, which is known to up regulate ABCE1 as a means to down-regulate the RNase L pathway [329]. More importantly, it was subsequently demonstrated that lopinavir was able to de-stabilise the ABCE1/RNase L interaction in E6 expressing cells (Figure 6.17), which should in theory remove the steric hindrance preventing the activation of RNase L, with subsequent enhancement of antiviral/apoptotic activities in these E6-expressing, lopinavir treated cells.

The current data support the conclusion that HPV does compromise the activity of RNase L. We demonstrate, for the first time, a prospective new mode of action of lopinavir against HPV infected cells unrelated to protease inhibition. These data suggest that, in association with the stabilisation of p53 demonstrated previously [98], the effects are partly related to an induction/ stabilisation of the antiviral protein RNase L and the ability of lopinavir to modulate the E6-mediated enhancement of the interaction between RNase L and ABCE1. Importantly, the data has also unexpectedly demonstrated the ability of lopinavir to preferentially target immortalised cells, as discussed below.

7.4. Lopinavir targets Immortalised cells regardless of immortalisation technique

Whilst a useful tool for molecular studies of HPV, SiHa cells are a fully transformed cell line, and it was intended to evaluate the potential use of lopinavir for the treatment of *pre-cancerous* cervical lesions, it was essential to also use a test system more representative of the intended target cell. Working in collaboration with Professor Ingeborg Zehbe, the effects of lopinavir (0-40 µM) on control and E6/E7 immortalised primary human foreskin keratinocytes (PHFKs) were assessed by cell proliferation assays (Figure 3.5) and western blot analysis of RNase L expression (Figure 5.12). Interestingly, whilst the growth of normal PHFKs progressed relatively uninhibited up to concentrations of 25 µM, both SiHa and E6/E7-immortalised PHFKs showed markedly reduced growth. Beyond 25 µM control cells demonstrated growth inhibition comparable to E6/E7 immortalised cells, again highlighting the narrow therapeutic window of lopinavir. Furthermore, lopinavir treatment was also shown to increase RNase L protein levels in E6/E7 transduced PHFKs, albeit over a much longer time scale than demonstrated in SiHa cells, which may reflect differences in cell growth rates, or differences in the kinetics of the lopinavir/ proteasome interaction in these particular cells. As discussed previously, the timescale of proteasomal inhibition in these cells, following exposure to lopinavir, is currently unknown. This has raised several questions:

- Is there a gradual decline in proteasomal activity?
- Does lopinavir produce a simply on/off switch in proteasome function?
- Do the kinetics of lopinavir-mediated inhibition of the proteasome differ between cell types?

We have generated SiHa cells stably expressing the pZsProSensor-1 proteasome sensor vector which uses GFP expression and detection as a surrogate marker for proteasomal activity (Chapter 2). Facilities permitting, live fluorescent imaging of these cells, in the presence of lopinavir, would provide a much more detailed overview of the lopinavir/ proteasome interaction in SiHa cells, and the system could easily be replicated using a range of cell types.

The data initially suggested that lopinavir was preferentially targeting E6-immortalised cells over mortal cells. However, in addition to the PHFK system, it was thought that the combination of parental Tert, vector control, and HPV type 16 E6 expressing cells would also constitute a model test system with which to study the interaction(s) between the E6 protein and lopinavir. Tert cells are an HPV-negative karyotypically normal telomerase-immortalised human keratinocyte cell line

that demonstrates a down regulation in the expression levels of $p16^{INK4a}$, a cyclin D/cdk inhibitor [205]. Cell proliferation assays demonstrated that in addition to E6-expressing Tert cells, both vector control and parental cells, with no E6 content, also demonstrated lopinavir dose-dependent growth inhibition (Figure 3.2) indicating that immortalised cells were specifically targeted by lopinavir. In addition, as mentioned previously, C33A cells are an HPV-negative cervical carcinoma cell line and these cells are also susceptible to lopinavir treatment [98]. Significantly, this suggests that lopinavir preferentially targets immortalised cells, regardless of the immortalisation procedure, rather than specifically targeting E6 or E6/E7 immortalised cells.

This observation was also confirmed by recent work in the laboratories of our collaborator Professor Ingeborg Zehbe. HPV type 16 E6 is an extremely multi-functional protein and is able to target a wide range of host proteins (detailed in Table 1.1). Accordingly, the E6 protein is an attractive target for HPV-specific antiviral drugs. The zinc finger domains of E6 play an important role in cell transformation and mutations in this region have been shown to inhibit the interaction between E6 and cellular targets such as E6AP and the E6 binding endoplasmic reticulum calcium-binding protein (E6BP/ERC55) (As discussed in Zehbe et al, Manuscript in preparation). Thus, it is thought that targeting the E6 zinc finger motifs may eliminate HPV positive cells and several compounds have since been developed which eject zinc atoms from the zinc finger domains, thus altering E6 protein structure and function (Zehbe et al, Manuscript in preparation). In an on-going collaboration with Professor Ingeborg Zehbe (Thunder Bay Regional Research Institute, Thunder Bay, Ontario, Canada), the anti-HPV activities of lopinavir were recently compared to known zinc finger ejector (ZFE) compounds using mortal and E6/E7-immortalised PHFK in addition to the cancer cell lines SiHa, CaSKi, HeLa, ME180 and C33A, all with differing HPV/ E6 content; SiHa and CaSKi are HPV type 16 positive, HeLa are HPV type 18 positive, ME180 cells are HPV type 39 positive whilst C33A are an HPV-negative cervical carcinoma cell line with no E6 content (Zehbe et al, Manuscript in preparation). Interestingly, while the ZFE compounds were uniformly toxic to both PHFK and cancer cell lines, lopinavir again demonstrated selective toxicity. While primary mortal PHFKs were highly resistant to lopinavir treatment as expected, all cancer and E6/E7-immortalised PHFK cell lines, with the exception of CaSKi cells, were susceptible to lopinavir treatment.

These data support the hypothesis that the specificity of lopinavir for immortalised cells is not restricted to those specifically immortalised through E6/E7 expression. Indeed our Tert cell lopinavir-toxicity data from this research project (Chapter 3) support this conclusion and has been included in this manuscript, which is currently in preparation for submission to the journal of Antiviral Research. It is again interesting that the Zehbe laboratory demonstrated that CaSKi cells were refractory to lopinavir treatment. As we have discussed previously, a possible explanation of this is related to the E6 content of these cells. In comparison to SiHa cells, CaSKi express several hundred fold more HPV type 16 E6 protein. Our data has indicated that E6 may play a role in down-regulating the RNase L pathway through enhancing the ABCE1/RNase L interaction which may offer some explanation as to the resistance observed in CaSKi cells. However, the Zehbe paper also speculates that the resistance of mortal PHFK and CaSKi cells may also be related to differences in the apoptotic pathways occurring in different cell types. Specifically, they speculate

that cell type specific differences in the activity of the *pro-apoptotic* c-Jun NH2-Terminal Kinase (JNK) may play a role in lopinavir-resistance (Zehbe et al, Manuscript in preparation). Significantly, it has recently been shown that apoptotic responses differed when comparing doxorubicin treated C33A (lopinavir-sensitive) cells and CaSKi cells (lopinavir-resistant). Doxorubicin treated CaSKi cells demonstrated decreased JNK expression when compared to C33A cells [330]. In light of this observation, it may be interesting to carry out western blot analysis of JNK protein expression levels in drug treated versus DMSO treated lopinavir-resistant cells and lopinavir-susceptible cells. The importance of JNK expression in lopinavir treated cells could be further assessed by siRNA-mediated gene silencing of JNK or exposure to JNK-specific kinase inhibitors (http://www.agscientific.com/sp600125.html) which would demonstrate, if any, the role of JNK-expression in lopinavir resistance/ toxicity. In addition to the E6 protein level differences discussed previously, variation in JNK expression will undoubtedly explain some of the lopinavir-specific resistance seen in CaSKi cells. These findings suggest that lopinavir-resistance is a multifaceted response requiring further research.

It is clear from our results that RNase L is responsible for at least part of the toxicity of lopinavir in HPV positive cells however it is obviously not the only mechanism involved. Lopinavir preferentially targets immortalised cells, regardless of the immortalisation technique, indicative of alternative mechanisms, that are, at this stage unknown. However, our data does provide further evidence strongly supporting the use of lopinavir as a treatment of pre-cancerous HPV-related lesions of the cervix**.** In order to expand on these findings, it may be interesting to assess the ability of lopinavir to target a range of immortalised cell lines, for example SV40-immortalised cells, which will provide a more complete picture of lopinavir activity.

7.5. Treatment of HPV-related pre-cancerous lesions of the cervix with lopinavir

As discussed, in addition to inhibition of HIV protease, protease inhibitors demonstrate anti-angiogenic, anti-inflammatory, anti-proliferative and anti-cancer actions (see Section 1.7.2.1) mediated through inhibition of the cellular 26S proteasome, in addition to modification of the functions of MMP2, VEGF and bFGF. Protease inhibitors are, therefore, an extremely versatile group of drugs. Indeed, lopinavir and ritonavir (Kaletra) have since been shown to be effective for the treatment of Coronavirus-related Severe Acute Respiratory Syndrome (SARS) [331, 332]. There are several on-going clinical trials investigating the use of protease inhibitors against a range of tumour types (Table 7.2), however, to date, there are no clinical trials specifically evaluating lopinavir, either as a single agent or co-formulated with ritonavir, as a means to target HPV-related pre-cancerous lesions of the cervix

Following the introduction of HAART, it was anticipated that the fall in HIV viral load and restoration of the host immune system would lead to a reduction in opportunistic infections associated with HIV. Whereas this was true for HIV-related Kaposi's sarcoma, with incidence rates dramatically falling during the HAART era, HAART was shown to have little impact on HPV-related cervical carcinoma. What could account for this apparent difference in clinical response? I now

believe that the anti-HPV effects of lopinavir are unrelated to immune restoration, occurring instead, as a result of a targeted interaction between lopinavir and the HPV infected cell. It is known that Lopinavir stabilises the p53 protein and can induce apoptosis of HPV positive cervical carcinoma cells *in-vitro,* and we now also demonstrate an up regulation of RNase L. However, these responses were shown to occur at drug concentrations approximately 15-fold higher than those generally found in cervico-vaginal secretions of women taking oral Kaletra [333]. This indicates that oral administration of HAART-PI compounds does not achieve the cervical drug concentrations required to induce the anti-HPV effects of lopinavir.

Having identified a prospective new mode of action of lopinavir against HPV infected cells, related to modification of the innate RNase L cellular antiviral pathway, we propose that lopinavir may be suitable for use in the management of HPV-related cervical carcinoma. However, we have also demonstrated the importance of lopinavir concentration in achieving these responses, and as such we propose that lopinavir will be of greatest use when used as a topically applied agent.

Table 7.2 Clinical trials investigating the use of protease inhibitors as anti-cancer agents

Trial ID	Cancer type and stage	Trial Phase	Institution	Treatment and Schedule
NCT01095094	Progressive or Recurrent High Grade Glioma	II	Cleveland Clinic Taussig Institute, Case Comprehensive Cancer Center, Ohio, USA	Oral ritonavir and lopinavir twice daily in the absence of disease progression or unacceptable toxicity
NCT00233948	Recurrent liposarcoma	I/II	City of Hope, Duarte, CA, USA	Nelfinavir orally, twice daily every 28 days
NCT00436735	Solid tumours	I	National Cancer Institute, Bethesda, MD, USA	Nelfinavir orally, twice daily every 21 days
NCT00589056	Stage IIII NSCLC	I/II	University of Pennsylvania, PA, USA	Nelfinavir orally, twice daily beginning 1-2 weeks before initiation of chemoradiotherapy and continuing until completion of radiotherapy 5 days per week for 7-8 weeks; with intravenous cisplatin intravenously on days 1, 8, 29 and 36 and etoposide intravenously days 1-5 and 29-33
NCT00705393	Locally advanced pancreatic cancer	I	University of Nebraska, Omaha, NE, USA	Nelfinavir orally twice daily concurrent with stereotactic radiotherapy after neoadjuvant gemcitabine, fl uorouracil, and calcium folinate chemotherapy,followed by surgery and adjuvant chemotherapy
NCT00704600	Rectal cancer	I/II	Maastro Clinic, Maastricht, Netherlands	Nelfinavir orally twice daily beginning 7 days before chemoradiotherapy with capecitabine 825 mg/m2 twice daily
NCT00694837	Glioblastoma	I/II	Maastricht University, Maastricht, Netherlands	Nelfinavir orally twice daily beginning 7 days before chemoradiotherapy with temozolomide

(Table Adapted from [167]).

7.5.1. Topical application of lopinavir

We have demonstrated extensive *in vitro* evidence indicating that lopinavir specifically targets and can induce apoptosis in both HPV-infected cells and non-HPV infected immortalised cells. Furthermore the data suggests that a final drug concentration of ≥25 µM is required, effectively precluding the use of oral lopinavir, instead suggesting that a topical application may be required.

The use of topical agents for application to the cervix is not a new concept. The small molecule terameprocol (tetra-*O*-methyl nordihyrdoguaiaretic acid, M4N, EM1421) was recently evaluated in a phase I/II dose-escalation clinical trial for use as a topically applied agent in women with HPV-associated CIN. The trial aimed to define the maximum tolerated dose, dose-limiting toxicities and pharmacokinetic properties [334] of terameprocol vaginal ointment. Terameprocol, derived from the plant *Larrea tridentata* demonstrates several anti-viral and anti-cancer abilities [334]:

- It selectively interferes with transcription of viral genes with Sp-1-dependent promoters, including HPV E6 and E7.
- Inhibits Sp-1-dependent Cdc2 (p34) gene expression inhibition causing G2 cell cycle arrest.
- Stimulates apoptosis by reducing mRNA levels and subsequent protein production of the cyclin-dependent kinase CDC2, resulting in the inactivation of the CDC2/cyclin B complex.
- Down regulation of the production and activation of survivin, a member of the Inhibitor of Apoptosis (IAP) family of proteins, which down regulates apoptosis through inhibition of the function of caspases [335].

Terameprocol was applied to the cervix of trial participants in 5 ml aliquots using a disposable vaginal applicator. All patients received a total of three doses of terameprocol, administered by a physician at intervals of one week. The study demonstrated that terameprocol vaginal ointment was well tolerated with a favourable safety profile, with no serious adverse events reported and only mild self-limiting adverse events. The authors did however admit some limitations to the study;

- The terameprocol vaginal ointment was formulated with white petroleum jelly, and its effects, if any, on drug bioavailability were unknown at the time of the study
- The duration of drug exposure at the cervix was anticipated to be extremely brief since patients were allowed to move around after application.
- No devices, such as diaphragms or pessaries were used to increase the contact time between drug and cervical cells.

Clearly this phase I/II study has provided sufficient justification to suggest that topical application of lopinavir on the cervix is a viable treatment option. Indeed, in the on going studies, we aim to assess the usefulness of lopinavir as a topical application, however the studies will also

aim to address the limitations highlighted in the terameprocol vaginal ointment study, in particular, the short duration of drug exposure at the cervix. As discussed, topical application of a given therapeutic agent will generally result in only a brief exposure of the target cells to the agent in question. Accordingly with any topically applied agent, improving dose duration is of great importance. The principle of direct, targeted, gynaecological drug exposure has been previously demonstrated by the NuvaRing® contraceptive drug delivery system, an oestrogen and progestin impregnated, slow release delivery system made of flexible ethylene-vinyl acetate copolymer (Figure 7.1) (http://www.nuvaring.com/Consumer/index.asp).

Figure 7.1 – Flexible, slow release gynaecological drug delivery system

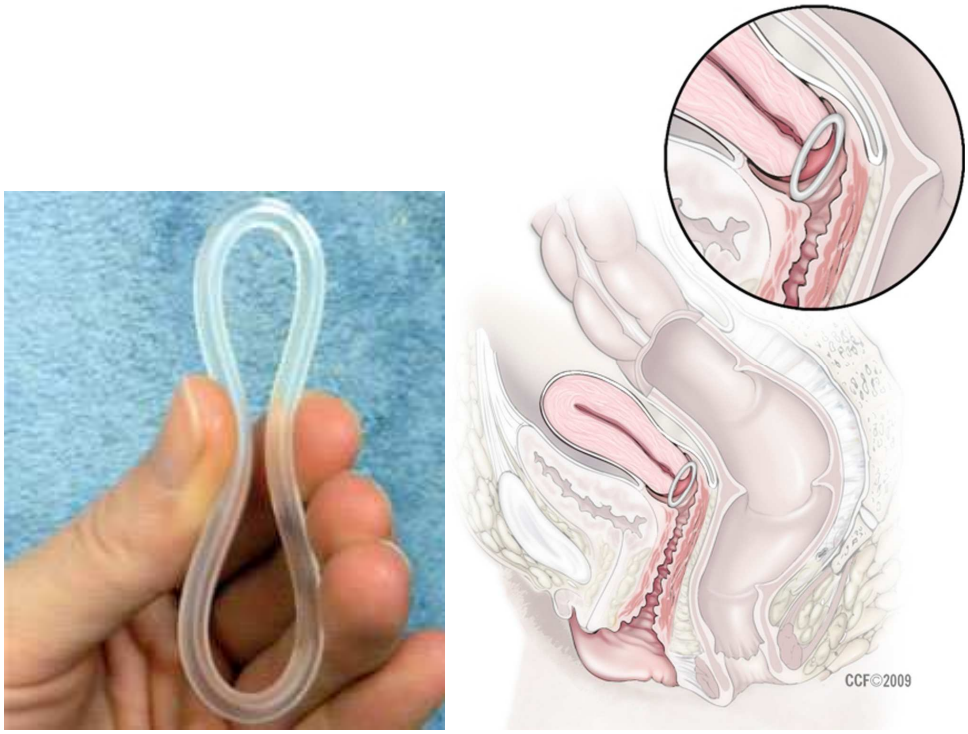

Figure 7.1. (Left) NuvaRing® vaginal flexible slow release drug delivery system and (Right) *in-situ* location proximal to the cervical transformation zone (images taken from http://women-health-info.com/173-NuvaRing.html and [336]).

This particular drug delivery system has many attributes that would make it useful for the local application of lopinavir to the cervix. Initially, the highly vascularised nature of the vaginal mucosa, in combination with the localised slow-release mechanism avoids first-pass metabolism at

the liver, allowing for sustained drug levels. In addition the NuvaRing® is extremely low-technology [336]. However, by far the most interesting attribute relates to the dosing schedule. The NuvaRing® is inserted manually, and remains in place for a period of 3 weeks, followed by a 7 day drug-free period. Subsequently, a fresh ring is inserted and so on. It has been shown that this dosing strategy improves patient compliance [336]. As discussed previously, current screening and

surgical approaches to managing HPV related cervical malignancy are hampered in low-resource regions, Africa in particular, by the lack of basic health facilities and trained personnel [337]. In a region where vaccination is not currently a viable option, and where HIV co-infection exacerbates the problems of HPV related malignancy, a low-cost, low-technology therapeutic approach which promotes patient compliance and requires minimal dosing may be particularly useful. It is thought that the system may be adapted in order to develop a slow-release system for use with lopinavir, however, whilst an extremely interesting concept, the reformulation studies of lopinavir that would be required to develop such a system will be prohibitively expensive at this stage. Fortunately however, there are several formulations of Kaletra currently available, including standard tablets, an alcohol based liquid, and a soft-gel capsule (Kaletra Drug Safety Data Sheet available from http://www.rxabbott.com/pdf/kaletratabpi.pdf).

It is anticipated that soft-gel capsules (SGC) will be the most favourable formulation for use as a topical application. While the SGC formulation has been shown to be relatively heat stable at low ambient temperatures, it has also been shown to lose structural integrity at temperatures over 35℃, while maintaining pharmacological activity [3 38]. It is anticipated that when inserted into the vagina, in close proximity to the cervix, that the combination of body temperature, vaginal secretions and patient movement, will lead to the controlled breakdown of the SGC formulation, resulting in slow, targeted release of lopinavir, directly targeting the pre-cancerous cells of the cervix. Clearly, self-application of the capsule removes both the requirement for extensive health care facilities and highly trained personnel.

8. Conclusions and Novel findings

8.1. Conclusion

The aims of this research project were to (1) To identify cellular proteins, in addition to p53, degraded by HPV that are stabilised in the presence of lopinavir and (2) To identify potential new effectors of lopinavir that account for its anti-HPV activity and to fully characterise the potential mechanism(s).

A range of proteins were stabilised in the presence of lopinavir, of most significance was the demonstration that lopinavir leads to a dose and time dependent stabilisation of the antiviral protein RNase L. It is proposed that the HPV-specific antiviral effects of lopinavir are as a result of the synergistic actions of the lopinavir stabilised proteins p53 and RNase L. The data potentially indicates that HPV can inactivate RNase L by enhancing the interaction with its endogenous inhibitor protein, ABCE1, an interaction with is subsequently de-stabilised in the presence of lopinavir. We believe the data demonstrates a previously unknown mode of action of lopinavir against HPV-infected cells that is unrelated to the ability of this compound to inhibit the HIV protease. Interestingly, the ability of lopinavir to induce apoptosis of non-HPV related immortalised cells merits further investigation since this indicates this drug may be useful for the treatment of other non HPV related pre-malignant conditions.

In view of the observation that infection with HPV can enhance the sexual transmission of HIV in both men and women, a low cost, low technology, non-surgical alternative for the management of HPV-related pre-cancerous cervical lesions will not only reduce the burden of HPV-related disease but may also reduce the health burden associated with HIV infection.

The findings support the conclusion that lopinavir may be a suitable, low-cost, self-applied topical alternative for the management of HPV-related pre-cancerous lesions of the cervix. Furthermore, it is anticipated that this agent will be of particular benefit in low-resource countries, in particular sub-Saharan Africa, which currently bears a disproportionate burden of world wide HPV-related cervical cancer cases.

8.2. Novel Findings

- Lopinavir up-regulates RNase L in HPV positive SiHa cells.
- RNase L protein is a key protein in the regulating anti-HPV activity of lopinavir.
- HPV type 16 E6 protein produces a protective effect in C33A cervical carcinoma cells, inhibiting RNase L-mediated cell death.
- HPV Type 16 E6 protein does not degrade RNase L, effect its sub-cellular localisation or up-regulate ABCE1 (RNase L inhibitor).
- The HPV type 16 E6 protein enhances the association between RNase L and ABCE1, whilst lopinavir appears to destabilise the association.

9. Future Work

9.1. Analysis of the effects of lopinavir on mTOR

The *M*ammalian *T*arget *O*f *R*apamycin (mTOR) (Figure 9.2) is the target of the drug rapamycin which, together with its derivatives, has been shown to have prolonged antitumour activity in a variety of cancers [339]. The antibody micro array analysis indicated that lopinavir induces a down-regulation of mTOR in SiHa cells (figure 4.7 & 4.8). Interestingly it has recently been shown that the mTOR pathway is constitutively activated in CIN and invasive cervical carcinoma [221] and indeed it has also been shown that HPV type 16 E6 protein activates mTORC1 signalling pathways resulting in increased protein synthesis [222]. In light of these observations we will initially treat SiHa and other cervical carcinoma cell lines (HeLa & CaSKi) with a range of concentrations and durations of exposure to lopinavir. Proteins will be extracted and the effects of this treatment on mTOR levels examined by western blotting.

Figure 9.2 – mTOR signalling pathway

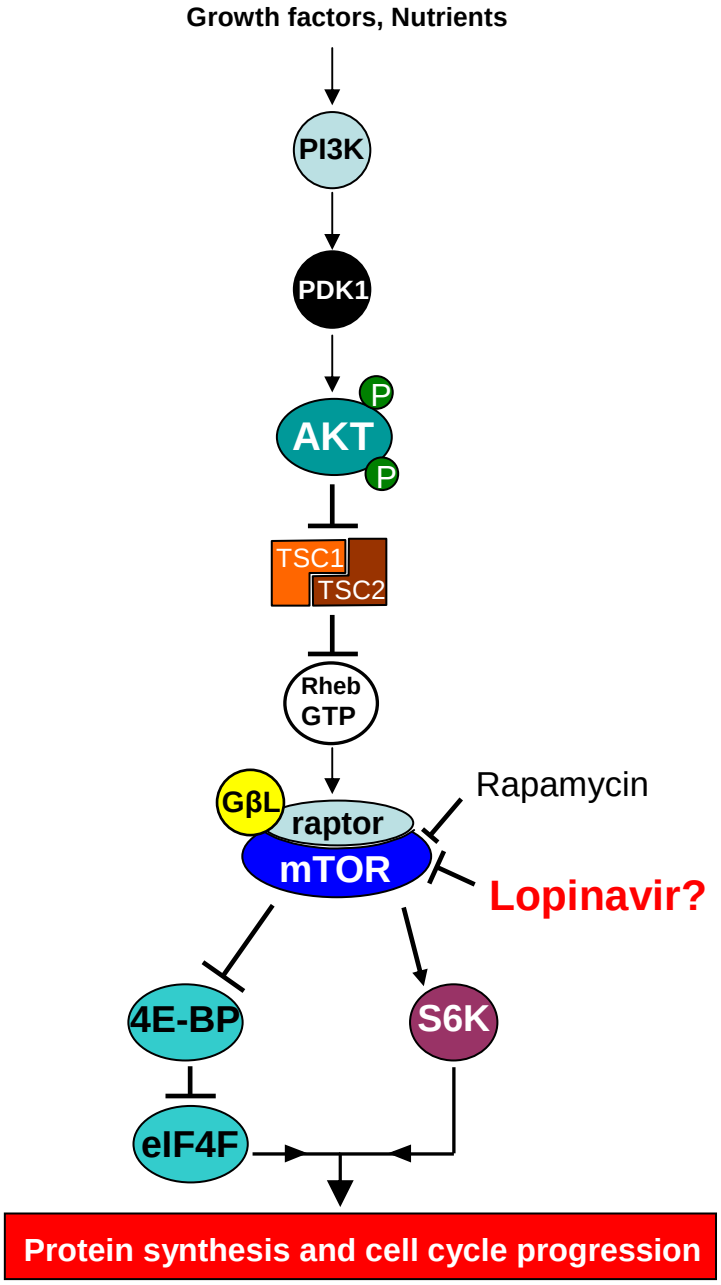

Figure 7.2 – mTOR signalling pathway. The *m*ammalian *t*arget *o*f *r*apamycin protein is an intracellular kinase that controls protein synthesis and cell cycle progression. The pathway is stimulated by growth signals and exposure to nutrients. Activation of the pathway results in active mTOR, which phosphorylates S6K and also 4E-BP. Active S6K, promotes formation of translation initiation complexes, whilst phosphorylation of 4E-BP releases eIF4F which binds to the 5' cap of mRNA, initiating cap dependent translation.
(PI3K, phosphatidylinositol 3'-kinase; PDK1, phosphoinositide-dependent kinase-1; AKT, also known as protein kinase B, PKB; TSC1 & TSC2, tuberous sclerosis complex 1 & 2, also referred to as hamartin and tuberin respectively; Rheb, Ras-homolog enriched in brain, GTP bound; GβL, also known as mLST8, Gβ-like protein; Raptor, regulatory associated protein of TOR; S6K, p70S6 kinase).

If these results confirm the lopinavir-induced down regulation of mTOR, the ability of lopinavir to synergise with rapamycin to induce apoptosis of abnormal cells will be assessed. The effects of these compounds will also be evaluated in the organotypic culture systems described in section 9.3.1. Notably in recent phase II clinical trials of endometrial cancer, mTOR inhibitors have shown promising results [340] synergising with platinum and taxane based drugs [341]. Depending of the extent of the synergism observed between lopinavir and rapamycin in the preceding experiments, the levels of lopinavir achievable by oral administration may be sufficient to attain synergistic effects with rapamycin. These data would thus support a prospective new use for this combination of drugs in the treatment of premalignant and invasive cervical carcinoma.

9.2. High Risk HPV E7 protein and lopinavir

While the current findings support a role for HPV type 16 E6 in the inhibition of RNase L-dependent cell death (Figure 6.6), the data has not yet ruled out the possibility of E7 contributing to this effect. In addition to C33A E6 cells, E7 expressing cells are available. It is planned to repeat transient RNase L transfection using cells, with cell death assessed 24 hours post transfection by trypan blue exclusion.

9.3. Topical application of lopinavir – a Phase I clinical trial

9.3.1. Drug penetration studies

Prior to commencing a planned phase I clinical study, it will be essential to evaluate the ability of lopinavir to penetrate human skin. In order to assess this, we intend to use the full-thickness *in* vitro model of human skin recently developed by Stratatech (http://www.stratatechcorp.com/products/stratatest.php). It is intended to use this cell system to assess the ability of lopinavir as a single agent, or formulated as Kaletra® to penetrate from the apical cell surface through to the basement membrane and accumulate in sufficient quantities (≥ 25 µM). Working in collaboration with the laboratories of Professor Roy Goodacre and Dr Dong-Hyun Kim (Manchester Interdisciplinary Biocentre, Manchester, UK), we have developed Fourier Transformation Infra Red spectroscopy techniques to analyse the metabolic changes occurring in lopinavir treated cervical carcinoma cells [184] and direct Raman spectroscopic imaging to identify the site of action of the drug in cells [185].

In addition, working in collaboration with Professor I. Zehbe (Lakehead University, Canada) organotypic air interface raft cultures of primary human foreskin keratinocytes that have been retrovirally transfected and immortalised with HPV16 E6/E7 cDNA (figure 7.2) will also be used to assess the cellular penetration of lopinavir in 3D cell culture systems [342]

Figure 7.2 – 3D organotypic raft cultures of human keratinocytes

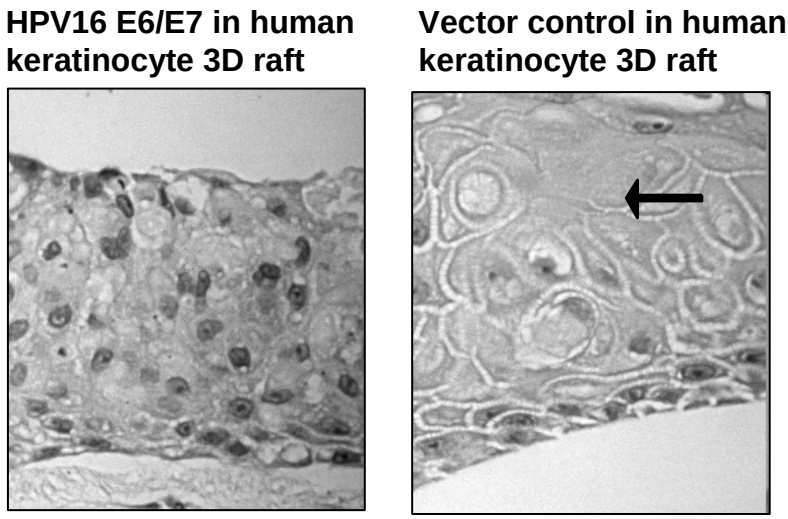

Figure 7.2 - Sections from 3D organotypic raft cultures of human keratinocytes expressing HPV type 16 E6 & E7 proteins. Vector control cells are included, demonstrating anucleated differentiated cells (arrowed).

Karyotypically normal, Telomerase immortalised keratinocytes (Tert cells) will be used to produce the same type of 3D organotypic cultures shown in figure 7.1 [343]. The ability of lopinavir, at a range of final concentrations, to penetrate into the cell will then be assessed using these cell systems. Treated and control untreated cultures will be harvested, frozen sections cut and these evaluated by H&E staining and the extent of drug penetration assessed by the techniques of Fourier transform infrared (FT-IR) spectroscopy and Raman micro-spectroscopy [185, 344].

These methods are based on vibrational spectroscopy and will be calibrated using cellular extracts where the drug levels have been quantified using HPLC-MS**.** Having determined the optimum drug dosage required to achieve biologically active concentrations of lopinavir in these homogenous cultures, organotypic raft cultures composed of mixed E6/E7 and Tert keratinocyte organotypic cultures will then be used. The effects of lopinavir treatment on these mixed cultures will then be assessed by immunohistochemical analysis of the expression of known protein markers of E6/E7 activity ($p16^{INK4a}$, p53, RNase L, mTOR). We will also use TUNEL apoptosis staining (TACS XL In situ Apoptosis Kit, R & D Systems, Minneapolis, USA) to evaluate the cytotoxic effects of these various drug treatments on homogenous and mixed culture. As we have previously demonstrate the ability of lopinavir to selectively target immortalised cells, the expected outcome will be a lopinavir dose that eliminates E6/E7-immortalised cells whilst maintaining Tert cells in mixed organotypic cultures of these cell types. All these experiments will be repeated using a 4:1 ratio of lopinavir: ritonavir since this is the commercially available HIV drug Kaletra that will be used in our planned clinical trial.

9.3.2. Phase I clinical trial

Extensive preparations have been made for a Phase I clinical trial. However, in brief, the clinical trial will be carried out at the Kenyatta National Hospital, Nairobi, Kenya, in association with Dr Innocent Maranga, a University of Manchester student predicted to obtain his PhD in early 2011. The study subjects will be recruited among patients attending the specialist colposcopy clinic at the Kenyatta National Hospital, Nairobi, Kenya. Initially, the trial will aim to recruit 30 HIV-negative CIN II/III positive women and will be in the form of a dose-escalating phase I clinical trial with three main objectives:

- To assess tolerability of the soft-gel capsule formulation
- To assess adverse side effects of lopinavir when administered as a vaginal pessary
- To gauge potential benefit of lopinavir in the treatment of pre-cancerous lesions of the cervix

Prior to commencing the trial, each participant will undergo standard Pap smear/ LBC screening to assess CIN status. The trial will use a generic soft-gel formulation of lopinavir and ritonavir, manufactured by Cipla (www.cipla.com) containing 133 mg lopinavir and 33 mg ritonavir. On commencing the trial, the 30 participants will be randomly assigned to one of 3 dosing groups:

- 1 capsule, once a day
- 1 capsule, twice a day
- 1 capsule, three times a day

All participants will receive their assigned dose for a period of 14 days, and will be assessed every two days for signs of unwanted adverse effects. In addition to the pre-trial cytological assessment, participants will also be assessed at 1 and 3 months for HPV.

As mentioned previously it is essential that any new treatment for use in a low resource country be low-cost requiring minimal expertise in applying the treatment. In light of these requirements, generic soft gel capsules, marketed as ‘lopimune’ will be used. Currently, lopimune is sold in containers of 180 capsules for $160, working out as less than $1/capsule, making vast financial improvements on the prices of the current vaccinations (£120/dose, for a 3-dose regime).

Clearly, any further clinical evaluation of lopinavir as a topical agent will depend of the information gathered as part of this phase-I clinical trial.

References

1. W.H.O, *Human Papillomavirus and Related Cancers Summary Report Update. November 15, 2010 (http://apps.who.int/hpvcentre/statistics/dynamic/ico/country_pdf/XWX.pdf?CFID=4663156&CFTOKEN=85356562)*. 2010.
2. Castellsague, X., *HPV and cervical cancer in the 2007 report.* Vaccine, 2007. **25 Suppl 3**: p. C1-230.
3. Boulet, G., et al., *Human papillomavirus: E6 and E7 oncogenes.* Int J Biochem Cell Biol, 2007. **39**(11): p. 2006-11.
4. Strauss, M.J., E.W. Shaw, and et al., *Crystalline virus-like particles from skin papillomas characterized by intranuclear inclusion bodies.* Proc Soc Exp Biol Med, 1949. **72**(1): p. 46-50.
5. zur Hausen, H., *Condylomata acuminata and human genital cancer.* Cancer Res, 1976. **36**(2 pt 2): p. 794.
6. Walboomers, J.M., et al., *Human papillomavirus is a necessary cause of invasive cervical cancer worldwide.* J Pathol, 1999. **189**(1): p. 12-9.
7. Burchell, A.N., et al., *Chapter 6: Epidemiology and transmission dynamics of genital HPV infection.* Vaccine, 2006. **24 Suppl 3**: p. S3/52-61.
8. Mejlhede, N., et al., *Multiple human papilloma virus types in cervical infections: competition or synergy?* Apmis, 2010. **118**(5): p. 346-52.
9. Mendez, F., et al., *Cervical coinfection with human papillomavirus (HPV) types and possible implications for the prevention of cervical cancer by HPV vaccines.* J Infect Dis, 2005. **192**(7): p. 1158-65.
10. Castellsague, X., *Natural history and epidemiology of HPV infection and cervical cancer.* Gynecol Oncol, 2008. **110**(3 Suppl 2): p. S4-7.
11. Yim, E.K. and J.S. Park, *Role of proteomics in translational research in cervical cancer.* Expert Rev Proteomics, 2006. **3**(1): p. 21-36.
12. Dell, G. and K. Gaston, *Human papillomaviruses and their role in cervical cancer.* Cell Mol Life Sci, 2001. **58**(12-13): p. 1923-42.
13. Gentile, G., et al., *Cervical intraepithelial neoplasia in HIV seropositive patients.* Eur J Gynaecol Oncol, 1993. **14**(3): p. 246-8.
14. Maiman, M., et al., *Human immunodeficiency virus infection and cervical neoplasia.* Gynecol Oncol, 1990. **38**(3): p. 377-82.
15. Porreco, R., et al., *Gynecologic malignancies in immunosuppressed organ homograft recipients.* Obstet Gynecol, 1975. **45**(4): p. 359-64.
16. Schneider, V., S. Kay, and H.M. Lee, *Immunosuppression as a high-risk factor in the development of condyloma acuminatum and squamous neoplasia of the cervix.* Acta Cytol, 1983. **27**(3): p. 220-4.
17. Wang, C., et al., *Rapid Rise in Detection of Human Papillomavirus (HPV) Infection Soon After Incident HIV Infection Among South African Women.* J Infect Dis, 2011.
18. Dell, G. and K. Gaston, *Human papillomaviruses and their role in cervical cancer.* Cell Mol Life Sci, 2001. **58**(12-13): p. 1923-42.
19. de Villiers, E.M., et al., *Classification of papillomaviruses.* Virology, 2004. **324**(1): p. 17-27.
20. Doorbar, J., *The papillomavirus life cycle.* J Clin Virol, 2005. **32 Suppl 1**: p. S7-15.
21. Munger, K., et al., *Mechanisms of human papillomavirus-induced oncogenesis.* J Virol, 2004. **78**(21): p. 11451-60.
22. zur Hausen, H., *Papillomavirus infections--a major cause of human cancers.* Biochim Biophys Acta, 1996. **1288**(2): p. F55-78.

23. Bernard, H.U., I.E. Calleja-Macias, and S.T. Dunn, *Genome variation of human papillomavirus types: phylogenetic and medical implications.* Int J Cancer, 2006. **118**(5): p. 1071-6.
24. Veldhuijzen, N.J., et al., *Factors affecting transmission of mucosal human papillomavirus.* Lancet Infect Dis, 2010. **10**(12): p. 862-74.
25. Berumen, J., et al., *Asian-American variants of human papillomavirus 16 and risk for cervical cancer: a case-control study.* J Natl Cancer Inst, 2001. **93**(17): p. 1325-30.
26. Ordonez, R.M., et al., *Enhanced oncogenicity of Asian-American human papillomavirus 16 is associated with impaired E2 repression of E6/E7 oncogene transcription.* J Gen Virol, 2004. **85**(Pt 6): p. 1433-44.
27. Grodzki, M., et al., *Increased risk for cervical disease progression of French women infected with the human papillomavirus type 16 E6-350G variant.* Cancer Epidemiol Biomarkers Prev, 2006. **15**(4): p. 820-2.
28. Schiffman, M., et al., *Human papillomavirus and cervical cancer.* Lancet, 2007. **370**(9590): p. 890-907.
29. Hebner, C.M. and L.A. Laimins, *Human papillomaviruses: basic mechanisms of pathogenesis and oncogenicity.* Rev Med Virol, 2006. **16**(2): p. 83-97.
30. Fehrmann, F. and L.A. Laimins, *Human papillomaviruses: targeting differentiating epithelial cells for malignant transformation.* Oncogene, 2003. **22**(33): p. 5201-7.
31. Doorbar, J., *Molecular biology of human papillomavirus infection and cervical cancer.* Clin Sci (Lond), 2006. **110**(5): p. 525-41.
32. McBride, A.A., H. Romanczuk, and P.M. Howley, *The papillomavirus E2 regulatory proteins.* J Biol Chem, 1991. **266**(28): p. 18411-4.
33. Hamid, N.A., C. Brown, and K. Gaston, *The regulation of cell proliferation by the papillomavirus early proteins.* Cell Mol Life Sci, 2009. **66**(10): p. 1700-17.
34. Chiang, C.M., et al., *Control of human papillomavirus type 11 origin of replication by the E2 family of transcription regulatory proteins.* J Virol, 1992. **66**(9): p. 5224-31.
35. Chiang, C.M., et al., *Viral E1 and E2 proteins support replication of homologous and heterologous papillomaviral origins.* Proc Natl Acad Sci U S A, 1992. **89**(13): p. 5799-803.
36. Skiadopoulos, M.H. and A.A. McBride, *Bovine papillomavirus type 1 genomes and the E2 transactivator protein are closely associated with mitotic chromatin.* J Virol, 1998. **72**(3): p. 2079-88.
37. You, J., et al., *Interaction of the bovine papillomavirus E2 protein with Brd4 tethers the viral DNA to host mitotic chromosomes.* Cell, 2004. **117**(3): p. 349-60.
38. Thierry, F. and M. Yaniv, *The BPV1-E2 trans-acting protein can be either an activator or a repressor of the HPV18 regulatory region.* Embo J, 1987. **6**(11): p. 3391-7.
39. Longworth, M.S. and L.A. Laimins, *Pathogenesis of human papillomaviruses in differentiating epithelia.* Microbiol Mol Biol Rev, 2004. **68**(2): p. 362-72.
40. Motoyama, S., et al., *The role of human papilloma virus in the molecular biology of cervical carcinogenesis.* Kobe J Med Sci, 2004. **50**(1-2): p. 9-19.
41. Modis, Y., B.L. Trus, and S.C. Harrison, *Atomic model of the papillomavirus capsid.* EMBO J, 2002. **21**(18): p. 4754-62.
42. Horvath, C.A., et al., *Mechanisms of cell entry by human papillomaviruses: an overview.* Virol J, 2010. **7**: p. 11.
43. Culp, T.D. and N.D. Christensen, *Kinetics of in vitro adsorption and entry of papillomavirus virions.* Virology, 2004. **319**(1): p. 152-61.

44. Day, P.M., D.R. Lowy, and J.T. Schiller, *Papillomaviruses infect cells via a clathrin-dependent pathway.* Virology, 2003. **307**(1): p. 1-11.
45. Giroglou, T., et al., *Human papillomavirus infection requires cell surface heparan sulfate.* J Virol, 2001. **75**(3): p. 1565-70.
46. Joyce, J.G., et al., *The L1 major capsid protein of human papillomavirus type 11 recombinant virus-like particles interacts with heparin and cell-surface glycosaminoglycans on human keratinocytes.* J Biol Chem, 1999. **274**(9): p. 5810-22.
47. Sapp, M. and M. Bienkowska-Haba, *Viral entry mechanisms: human papillomavirus and a long journey from extracellular matrix to the nucleus.* FEBS J, 2009. **276**(24): p. 7206-16.
48. Yang, R., et al., *Cell surface-binding motifs of L2 that facilitate papillomavirus infection.* J Virol, 2003. **77**(6): p. 3531-41.
49. Muratani, M. and W.P. Tansey, *How the ubiquitin-proteasome system controls transcription.* Nat Rev Mol Cell Biol, 2003. **4**(3): p. 192-201.
50. Glotzer, M., A.W. Murray, and M.W. Kirschner, *Cyclin is degraded by the ubiquitin pathway.* Nature, 1991. **349**(6305): p. 132-8.
51. DeSalle, L.M. and M. Pagano, *Regulation of the G1 to S transition by the ubiquitin pathway.* FEBS Lett, 2001. **490**(3): p. 179-89.
52. Chen, Z., et al., *Signal-induced site-specific phosphorylation targets I kappa B alpha to the ubiquitin-proteasome pathway.* Genes Dev, 1995. **9**(13): p. 1586-97.
53. Rock, K.L., et al., *Inhibitors of the proteasome block the degradation of most cell proteins and the generation of peptides presented on MHC class I molecules.* Cell, 1994. **78**(5): p. 761-71.
54. Ciechanover, A., *The ubiquitin-proteasome proteolytic pathway.* Cell, 1994. **79**(1): p. 13-21.
55. Ward, C.L., S. Omura, and R.R. Kopito, *Degradation of CFTR by the ubiquitin-proteasome pathway.* Cell, 1995. **83**(1): p. 121-7.
56. Scheffner, M., et al., *The E6 oncoprotein encoded by human papillomavirus types 16 and 18 promotes the degradation of p53.* Cell, 1990. **63**(6): p. 1129-36.
57. Werness, B.A., A.J. Levine, and P.M. Howley, *Association of human papillomavirus types 16 and 18 E6 proteins with p53.* Science, 1990. **248**(4951): p. 76-9.
58. Ciehanover, A., Y. Hod, and A. Hershko, *A heat-stable polypeptide component of an ATP-dependent proteolytic system from reticulocytes.* Biochem Biophys Res Commun, 1978. **81**(4): p. 1100-5.
59. Wilkinson, K.D., M.K. Urban, and A.L. Haas, *Ubiquitin is the ATP-dependent proteolysis factor I of rabbit reticulocytes.* J Biol Chem, 1980. **255**(16): p. 7529-32.
60. Ciechanover, A., et al., *"Covalent affinity" purification of ubiquitin-activating enzyme.* J Biol Chem, 1982. **257**(5): p. 2537-42.
61. Ciechanover, A., et al., *Activation of the heat-stable polypeptide of the ATP-dependent proteolytic system.* Proc Natl Acad Sci U S A, 1981. **78**(2): p. 761-5.
62. Hershko, A., et al., *Components of ubiquitin-protein ligase system. Resolution, affinity purification, and role in protein breakdown.* J Biol Chem, 1983. **258**(13): p. 8206-14.
63. Ciechanover, A. and A.L. Schwartz, *The ubiquitin-proteasome pathway: the complexity and myriad functions of proteins death.* Proc Natl Acad Sci U S A, 1998. **95**(6): p. 2727-30.
64. Ciechanover, A., *The ubiquitin-proteasome pathway: on protein death and cell life.* Embo J, 1998. **17**(24): p. 7151-60.

65. Goldberg, A.L., *Functions of the proteasome: from protein degradation and immune surveillance to cancer therapy.* Biochem Soc Trans, 2007. **35**(Pt 1): p. 12-7.
66. Thrower, J.S., et al., *Recognition of the polyubiquitin proteolytic signal.* Embo J, 2000. **19**(1): p. 94-102.
67. Goldberg, A.L., *Degradation of abnormal proteins in Escherichia coli (protein breakdown-protein structure-mistranslation-amino acid analogs-puromycin).* Proc Natl Acad Sci U S A, 1972. **69**(2): p. 422-6.
68. Etlinger, J.D. and A.L. Goldberg, *A soluble ATP-dependent proteolytic system responsible for the degradation of abnormal proteins in reticulocytes.* Proc Natl Acad Sci U S A, 1977. **74**(1): p. 54-8.
69. Hough, R., G. Pratt, and M. Rechsteiner, *Ubiquitin-lysozyme conjugates. Identification and characterization of an ATP-dependent protease from rabbit reticulocyte lysates.* J Biol Chem, 1986. **261**(5): p. 2400-8.
70. Arrigo, A.P., et al., *Identity of the 19S 'prosome' particle with the large multifunctional protease complex of mammalian cells (the proteasome).* Nature, 1988. **331**(6152): p. 192-4.
71. Voges, D., P. Zwickl, and W. Baumeister, *The 26S proteasome: a molecular machine designed for controlled proteolysis.* Annu Rev Biochem, 1999. **68**: p. 1015-68.
72. Voges, D., P. Zwickl, and W. Baumeister, *The 26S proteasome: a molecular machine designed for controlled proteolysis.* Annu Rev Biochem, 1999. **68**: p. 1015-68.
73. Piccinini, M., et al., *The HIV protease inhibitors nelfinavir and saquinavir, but not a variety of HIV reverse transcriptase inhibitors, adversely affect human proteasome function.* Antivir Ther, 2005. **10**(2): p. 215-23.
74. Zavrski, I., et al., *Proteasome: an emerging target for cancer therapy.* Anticancer Drugs, 2005. **16**(5): p. 475-81.
75. Kisselev, A.F., et al., *The sizes of peptides generated from protein by mammalian 26 and 20 S proteasomes. Implications for understanding the degradative mechanism and antigen presentation.* J Biol Chem, 1999. **274**(6): p. 3363-71.
76. Cole, S.T. and O. Danos, *Nucleotide sequence and comparative analysis of the human papillomavirus type 18 genome. Phylogeny of papillomaviruses and repeated structure of the E6 and E7 gene products.* J Mol Biol, 1987. **193**(4): p. 599-608.
77. Chakrabarti, O. and S. Krishna, *Molecular interactions of 'high risk' human papillomaviruses E6 and E7 oncoproteins: implications for tumour progression.* J Biosci, 2003. **28**(3): p. 337-48.
78. Harper, J.W., et al., *The p21 Cdk-interacting protein Cip1 is a potent inhibitor of G1 cyclin-dependent kinases.* Cell, 1993. **75**(4): p. 805-16.
79. Honda, R., H. Tanaka, and H. Yasuda, *Oncoprotein MDM2 is a ubiquitin ligase E3 for tumor suppressor p53.* FEBS Lett, 1997. **420**(1): p. 25-7.
80. Huibregtse, J.M., M. Scheffner, and P.M. Howley, *A cellular protein mediates association of p53 with the E6 oncoprotein of human papillomavirus types 16 or 18.* Embo J, 1991. **10**(13): p. 4129-35.
81. Huibregtse, J.M., et al., *A family of proteins structurally and functionally related to the E6-AP ubiquitin-protein ligase.* Proc Natl Acad Sci U S A, 1995. **92**(11): p. 5249.
82. Scheffner, M., et al., *The HPV-16 E6 and E6-AP complex functions as a ubiquitin-protein ligase in the ubiquitination of p53.* Cell, 1993. **75**(3): p. 495-505.

83. Huibregtse, J.M., M. Scheffner, and P.M. Howley, *Localization of the E6-AP regions that direct human papillomavirus E6 binding, association with p53, and ubiquitination of associated proteins.* Mol Cell Biol, 1993. **13**(8): p. 4918-27.
84. Mantovani, F. and L. Banks, *The human papillomavirus E6 protein and its contribution to malignant progression.* Oncogene, 2001. **20**(54): p. 7874-87.
85. Scheurer, M.E., G. Tortolero-Luna, and K. Adler-Storthz, *Human papillomavirus infection: biology, epidemiology, and prevention.* Int J Gynecol Cancer, 2005. **15**(5): p. 727-46.
86. Dyson, N., et al., *The human papilloma virus-16 E7 oncoprotein is able to bind to the retinoblastoma gene product.* Science, 1989. **243**(4893): p. 934-7.
87. Lee, W.H., et al., *Human retinoblastoma susceptibility gene: cloning, identification, and sequence.* Science, 1987. **235**(4794): p. 1394-9.
88. Lee, W.H., et al., *The retinoblastoma susceptibility gene encodes a nuclear phosphoprotein associated with DNA binding activity.* Nature, 1987. **329**(6140): p. 642-5.
89. Weinberg, R.A., *Tumor suppressor genes.* Science, 1991. **254**(5035): p. 1138-46.
90. DeCaprio, J.A., et al., *The product of the retinoblastoma susceptibility gene has properties of a cell cycle regulatory element.* Cell, 1989. **58**(6): p. 1085-95.
91. Weinberg, R.A., *The retinoblastoma protein and cell cycle control.* Cell, 1995. **81**(3): p. 323-30.
92. Chellappan, S.P., et al., *The E2F transcription factor is a cellular target for the RB protein.* Cell, 1991. **65**(6): p. 1053-61.
93. Kato, J., et al., *Direct binding of cyclin D to the retinoblastoma gene product (pRb) and pRb phosphorylation by the cyclin D-dependent kinase CDK4.* Genes Dev, 1993. **7**(3): p. 331-42.
94. Koff, A., et al., *Human cyclin E, a new cyclin that interacts with two members of the CDC2 gene family.* Cell, 1991. **66**(6): p. 1217-28.
95. Lees, J.A., et al., *The retinoblastoma protein is phosphorylated on multiple sites by human cdc2.* Embo J, 1991. **10**(13): p. 4279-90.
96. Wang, J., et al., *Both Rb and E7 are regulated by the ubiquitin proteasome pathway in HPV-containing cervical tumor cells.* Oncogene, 2001. **20**(34): p. 4740-9.
97. Butel, J.S., *Viral carcinogenesis: revelation of molecular mechanisms and etiology of human disease.* Carcinogenesis, 2000. **21**(3): p. 405-26.
98. Hampson, L., H.C. Kitchener, and I.N. Hampson, *Specific HIV protease inhibitors inhibit the ability of HPV16 E6 to degrade p53 and selectively kill E6-dependent cervical carcinoma cells in vitro.* Antivir Ther, 2006. **11**(6): p. 813-25.
99. Hampson, L., et al., *The PDZ protein Tip-1 is a gain of function target of the HPV16 E6 oncoprotein.* Int J Oncol, 2004. **25**(5): p. 1249-56.
100. Oliver, A.W., et al., *The HPV16 E6 binding protein Tip-1 interacts with ARHGEF16, which activates Cdc42.* Br J Cancer, 2011. **104**(2): p. 324-31.
101. Yim, E.K. and J.S. Park, *Role of proteomics in translational research in cervical cancer.* Expert Rev Proteomics, 2006. **3**(1): p. 21-36.
102. Fuchs, E. and S. Raghavan, *Getting under the skin of epidermal morphogenesis.* Nat Rev Genet, 2002. **3**(3): p. 199-209.
103. Denecker, G., et al., *Caspase-14 reveals its secrets.* J Cell Biol, 2008. **180**(3): p. 451-8.
104. Stubenrauch, F. and L.A. Laimins, *Human papillomavirus life cycle: active and latent phases.* Semin Cancer Biol, 1999. **9**(6): p. 379-86.

105. Schwarz, T.F. and O. Leo, *Immune response to human papillomavirus after prophylactic vaccination with AS04-adjuvanted HPV-16/18 vaccine: improving upon nature.* Gynecol Oncol, 2008. **110**(3 Suppl 1): p. S1-10.
106. Stanley, M.A., *Immune responses to human papilloma viruses.* Indian J Med Res, 2009. **130**(3): p. 266-76.
107. Isaacs, A. and J. Lindenmann, *Virus interference. I. The interferon.* Proc R Soc Lond B Biol Sci, 1957. **147**(927): p. 258-67.
108. Schiffman, M., et al., *Human papillomavirus and cervical cancer.* Lancet, 2007. **370**(9590): p. 890-907.
109. Pett, M. and N. Coleman, *Integration of high-risk human papillomavirus: a key event in cervical carcinogenesis?* J Pathol, 2007. **212**(4): p. 356-67.
110. Woodman, C.B., S.I. Collins, and L.S. Young, *The natural history of cervical HPV infection: unresolved issues.* Nat Rev Cancer, 2007. **7**(1): p. 11-22.
111. Choo, K.B., C.C. Pan, and S.H. Han, *Integration of human papillomavirus type 16 into cellular DNA of cervical carcinoma: preferential deletion of the E2 gene and invariable retention of the long control region and the E6/E7 open reading frames.* Virology, 1987. **161**(1): p. 259-61.
112. Boulet, G., et al., *Human papillomavirus: E6 and E7 oncogenes.* Int J Biochem Cell Biol, 2007. **39**(11): p. 2006-11.
113. Lee, D., et al., *Human papillomavirus E2 down-regulates the human telomerase reverse transcriptase promoter.* J Biol Chem, 2002. **277**(31): p. 27748-56.
114. Thorland, E.C., et al., *Common fragile sites are preferential targets for HPV16 integrations in cervical tumors.* Oncogene, 2003. **22**(8): p. 1225-37.
115. Jeon, S. and P.F. Lambert, *Integration of human papillomavirus type 16 DNA into the human genome leads to increased stability of E6 and E7 mRNAs: implications for cervical carcinogenesis.* Proc Natl Acad Sci U S A, 1995. **92**(5): p. 1654-8.
116. Mesri, E.A., E. Cesarman, and C. Boshoff, *Kaposi's sarcoma and its associated herpesvirus.* Nat Rev Cancer, 2010. **10**(10): p. 707-19.
117. De Vuyst, H., et al., *HIV, human papillomavirus, and cervical neoplasia and cancer in the era of highly active antiretroviral therapy.* Eur J Cancer Prev, 2008. **17**(6): p. 545-54.
118. De Vuyst, H., et al., *HIV, human papillomavirus, and cervical neoplasia and cancer in the era of highly active antiretroviral therapy.* Eur J Cancer Prev, 2008. **17**(6): p. 545-54.
119. Baay, M.F., et al., *Human papillomavirus in a rural community in Zimbabwe: the impact of HIV co-infection on HPV genotype distribution.* J Med Virol, 2004. **73**(3): p. 481-5.
120. McKenzie, N.D., et al., *Women with HIV are more commonly infected with non-16 and -18 high-risk HPV types.* Gynecol Oncol, 2010. **116**(3): p. 572-7.
121. Serraino, D., et al., *Risk of invasive cervical cancer among women with, or at risk for, HIV infection.* Int J Cancer, 1999. **82**(3): p. 334-7.
122. Palefsky, J., *Biology of HPV in HIV infection.* Adv Dent Res, 2006. **19**(1): p. 99-105.
123. Cvetkovic, R.S. and K.L. Goa, *Lopinavir/ritonavir: a review of its use in the management of HIV infection.* Drugs, 2003. **63**(8): p. 769-802.
124. Sham, H.L., et al., *ABT-378, a highly potent inhibitor of the human immunodeficiency virus protease.* Antimicrob Agents Chemother, 1998. **42**(12): p. 3218-24.

125. Sham, H.L., et al., *Synthesis and antiviral activities of the major metabolites of the HIV protease inhibitor ABT-378 (Lopinavir).* Bioorg Med Chem Lett, 2001. **11**(11): p. 1351-3.
126. Eagling, V.A., D.J. Back, and M.G. Barry, *Differential inhibition of cytochrome P450 isoforms by the protease inhibitors, ritonavir, saquinavir and indinavir.* Br J Clin Pharmacol, 1997. **44**(2): p. 190-4.
127. Kumar, G.N., et al., *Potent inhibition of the cytochrome P-450 3A-mediated human liver microsomal metabolism of a novel HIV protease inhibitor by ritonavir: A positive drug-drug interaction.* Drug Metab Dispos, 1999. **27**(8): p. 902-8.
128. Schrader, S., et al., *Significant improvements in self-reported gastrointestinal tolerability, quality of life, patient satisfaction, and adherence with lopinavir/ritonavir tablet formulation compared with soft gel capsules.* AIDS Res Ther, 2008. **5**: p. 21.
129. Piccinini, M., et al., *The HIV protease inhibitors nelfinavir and saquinavir, but not a variety of HIV reverse transcriptase inhibitors, adversely affect human proteasome function.* Antivir Ther, 2005. **10**(2): p. 215-23.
130. Piccinini, M., et al., *The human 26S proteasome is a target of antiretroviral agents.* Aids, 2002. **16**(5): p. 693-700.
131. Hampson, L., H.C. Kitchener, and I.N. Hampson, *Specific HIV protease inhibitors inhibit the ability of HPV16 E6 to degrade p53 and selectively kill E6-dependent cervical carcinoma cells in vitro.* Antivir Ther, 2006. **11**(6): p. 813-25.
132. Bratcher, L.F. and V.V. Sahasrabuddhe, *The impact of antiretroviral therapy on HPV and cervical intraepithelial neoplasia: current evidence and directions for future research.* Infect Agent Cancer, 2010. **5**: p. 8.
133. Heard, I., et al., *Highly active antiretroviral therapy enhances regression of cervical intraepithelial neoplasia in HIV-seropositive women.* Aids, 2002. **16**(13): p. 1799-802.
134. Minkoff, H., et al., *The effect of highly active antiretroviral therapy on cervical cytologic changes associated with oncogenic HPV among HIV-infected women.* Aids, 2001. **15**(16): p. 2157-64.
135. Paramsothy, P., et al., *The effect of highly active antiretroviral therapy on human papillomavirus clearance and cervical cytology.* Obstet Gynecol, 2009. **113**(1): p. 26-31.
136. Del Mistro, A., et al., *Antiretroviral therapy and the clinical evolution of human papillomavirus-associated genital lesions in HIV-positive women.* Clin Infect Dis, 2004. **38**(5): p. 737-42.
137. Dorrucci, M., et al., *Incidence of invasive cervical cancer in a cohort of HIV-seropositive women before and after the introduction of highly active antiretroviral therapy.* J Acquir Immune Defic Syndr, 2001. **26**(4): p. 377-80.
138. Heard, I., J.M. Palefsky, and M.D. Kazatchkine, *The impact of HIV antiviral therapy on human papillomavirus (HPV) infections and HPV-related diseases.* Antivir Ther, 2004. **9**(1): p. 13-22.
139. Schuman, P., et al., *Longitudinal study of cervical squamous intraepithelial lesions in human immunodeficiency virus (HIV)-seropositive and at-risk HIV-seronegative women.* J Infect Dis, 2003. **188**(1): p. 128-36.
140. Franceschi, S. and H. Jaffe, *Cervical cancer screening of women living with HIV infection: a must in the era of antiretroviral therapy.* Clin Infect Dis, 2007. **45**(4): p. 510-3.
141. Panos, G., et al., *Mortality and morbidity of HIV infected patients receiving HAART: a cohort study.* Curr HIV Res, 2008. **6**(3): p. 257-60.

142. Dal Maso, L., D. Serraino, and S. Franceschi, *Epidemiology of AIDS-related tumours in developed and developing countries.* Eur J Cancer, 2001. **37**(10): p. 1188-201.
143. Parkin, D.M. and F. Bray, *Chapter 2: The burden of HPV-related cancers.* Vaccine, 2006. **24 Suppl 3**: p. S3/11-25.
144. Boring, C.C., et al., *Cancer statistics, 1994.* CA Cancer J Clin, 1994. **44**(1): p. 7-26.
145. Pisani, P., F. Bray, and D.M. Parkin, *Estimates of the world-wide prevalence of cancer for 25 sites in the adult population.* Int J Cancer, 2002. **97**(1): p. 72-81.
146. Kitchener, H.C., et al., *ARTISTIC: a randomised trial of human papillomavirus (HPV) testing in primary cervical screening.* Health Technol Assess, 2009. **13**(51): p. 1-150, iii-iv.
147. Strander, B., et al., *Liquid-based cytology versus conventional Papanicolaou smear in an organized screening program : a prospective randomized study.* Cancer, 2007. **111**(5): p. 285-91.
148. Stanley, M., *Human papillomavirus vaccines versus cervical cancer screening.* Clin Oncol (R Coll Radiol), 2008. **20**(6): p. 388-94.
149. Denny, L., M. Quinn, and R. Sankaranarayanan, *Chapter 8: Screening for cervical cancer in developing countries.* Vaccine, 2006. **24 Suppl 3**: p. S3/71-7.
150. Jordan, J., et al., *European guidelines for clinical management of abnormal cervical cytology, part 2.* Cytopathology, 2009. **20**(1): p. 5-16.
151. Gien, L.T. and A. Covens, *Fertility-sparing options for early stage cervical cancer.* Gynecol Oncol, 2010. **117**(2): p. 350-7.
152. Mandic, A., P. Novakovic, and D. Nincic, *Surgical approaches towards fertility preservation in young patients with early invasive cervical carcinoma.* J BUON, 2009. **14**(4): p. 581-6.
153. Lima, M.I., et al., *Cervical intraepithelial neoplasia recurrence after conization in HIV-positive and HIV-negative women.* Int J Gynaecol Obstet, 2009. **104**(2): p. 100-4.
154. Spinillo, A., et al., *Cervical intraepithelial neoplasia and cervicovaginal shedding of human immunodeficiency virus.* Obstet Gynecol, 2006. **107**(2 Pt 1): p. 314-20.
155. Wright, T.C., Jr., et al., *Human immunodeficiency virus 1 expression in the female genital tract in association with cervical inflammation and ulceration.* Am J Obstet Gynecol, 2001. **184**(3): p. 279-85.
156. Smith-McCune, K.K., et al., *Type-specific cervico-vaginal human papillomavirus infection increases risk of HIV acquisition independent of other sexually transmitted infections.* PLoS One, 2010. **5**(4): p. e10094.
157. Jarrett, W.F., et al., *Studies on vaccination against papillomaviruses: the immunity after infection and vaccination with bovine papillomaviruses of different types.* Vet Rec, 1990. **126**(19): p. 473-5.
158. Stanley, M., *Prophylactic HPV vaccines: prospects for eliminating ano-genital cancer.* Br J Cancer, 2007. **96**(9): p. 1320-3.
159. Harper, D.M., et al., *Efficacy of a bivalent L1 virus-like particle vaccine in prevention of infection with human papillomavirus types 16 and 18 in young women: a randomised controlled trial.* Lancet, 2004. **364**(9447): p. 1757-65.
160. Harper, D.M., et al., *Sustained efficacy up to 4.5 years of a bivalent L1 virus-like particle vaccine against human papillomavirus types 16 and 18: follow-up from a randomised control trial.* Lancet, 2006. **367**(9518): p. 1247-55.
161. Paavonen, J., et al., *Efficacy of a prophylactic adjuvanted bivalent L1 virus-like-particle vaccine against infection with human papillomavirus types 16 and 18 in*

young women: an interim analysis of a phase III double-blind, randomised controlled trial. Lancet, 2007. **369**(9580): p. 2161-70.
162. Villa, L.L., et al., *High sustained efficacy of a prophylactic quadrivalent human papillomavirus types 6/11/16/18 L1 virus-like particle vaccine through 5 years of follow-up.* Br J Cancer, 2006. **95**(11): p. 1459-66.
163. Cuzick, J., A. Castanon, and P. Sasieni, *Predicted impact of vaccination against human papillomavirus 16/18 on cancer incidence and cervical abnormalities in women aged 20-29 in the UK.* Br J Cancer, 2010. **102**(5): p. 933-9.
164. Kling, M. and J.A. Zeichner, *The role of the human papillomavirus (HPV) vaccine in developing countries.* Int J Dermatol, 2010. **49**(4): p. 377-9.
165. Agosti, J.M. and S.J. Goldie, *Introducing HPV vaccine in developing countries--key challenges and issues.* N Engl J Med, 2007. **356**(19): p. 1908-10.
166. Cornelio, D.B., R. Roesler, and G. Schwartsmann, *Emerging therapeutic agents for cervical cancer.* Recent Pat Anticancer Drug Discov, 2009. **4**(3): p. 196-206.
167. Chow, W.A., C. Jiang, and M. Guan, *Anti-HIV drugs for cancer therapeutics: back to the future?* Lancet Oncol, 2009. **10**(1): p. 61-71.
168. Ghosh, R.K., S.M. Ghosh, and S. Chawla, *Recent advances in antiretroviral drugs.* Expert Opin Pharmacother, 2011. **12**(1): p. 31-46.
169. Monini, P., et al., *Antitumour effects of antiretroviral therapy.* Nat Rev Cancer, 2004. **4**(11): p. 861-75.
170. Bower, M., et al., *Highly active anti-retroviral therapy (HAART) prolongs time to treatment failure in Kaposi's sarcoma.* AIDS, 1999. **13**(15): p. 2105-11.
171. Lebbe, C., et al., *Clinical and biological impact of antiretroviral therapy with protease inhibitors on HIV-related Kaposi's sarcoma.* Aids, 1998. **12**(7): p. F45-9.
172. Sgadari, C., et al., *HIV protease inhibitors are potent anti-angiogenic molecules and promote regression of Kaposi sarcoma.* Nat Med, 2002. **8**(3): p. 225-32.
173. Gialeli, C., A.D. Theocharis, and N.K. Karamanos, *Roles of matrix metalloproteinases in cancer progression and their pharmacological targeting.* FEBS J, 2011. **278**(1): p. 16-27.
174. Sgadari, C., et al., *Use of HIV protease inhibitors to block Kaposi's sarcoma and tumour growth.* Lancet Oncol, 2003. **4**(9): p. 537-47.
175. Andre, P., et al., *An inhibitor of HIV-1 protease modulates proteasome activity, antigen presentation, and T cell responses.* Proc Natl Acad Sci U S A, 1998. **95**(22): p. 13120-4.
176. Schubert, U., et al., *Proteasome inhibition interferes with gag polyprotein processing, release, and maturation of HIV-1 and HIV-2.* Proc Natl Acad Sci U S A, 2000. **97**(24): p. 13057-62.
177. Schmidtke, G., et al., *How an inhibitor of the HIV-I protease modulates proteasome activity.* J Biol Chem, 1999. **274**(50): p. 35734-40.
178. Gaedicke, S., et al., *Antitumor effect of the human immunodeficiency virus protease inhibitor ritonavir: induction of tumor-cell apoptosis associated with perturbation of proteasomal proteolysis.* Cancer Res, 2002. **62**(23): p. 6901-8.
179. Pajonk, F., et al., *The human immunodeficiency virus (HIV)-1 protease inhibitor saquinavir inhibits proteasome function and causes apoptosis and radiosensitization in non-HIV-associated human cancer cells.* Cancer Res, 2002. **62**(18): p. 5230-5.
180. Kuhn, D.J., et al., *Targeted inhibition of the immunoproteasome is a potent strategy against models of multiple myeloma that overcomes resistance to conventional drugs and nonspecific proteasome inhibitors.* Blood, 2009. **113**(19): p. 4667-76.

181. Dewar, R., et al., *Bortezomib treatment causes remission in a Ph+ ALL patient and reveals FoxO as a theranostic marker.* Cancer Biol Ther, 2011. **11**(6).
182. Driscoll, J.J., J. Burris, and C.M. Annunziata, *Targeting the Proteasome With Bortezomib in Multiple Myeloma: Update on Therapeutic Benefit as an Upfront Single Agent, Induction Regimen for Stem-Cell Transplantation and as Maintenance Therapy.* Am J Ther, 2011.
183. Williams, S.A. and D.J. McConkey, *The proteasome inhibitor bortezomib stabilizes a novel active form of p53 in human LNCaP-Pro5 prostate cancer cells.* Cancer Res, 2003. **63**(21): p. 7338-44.
184. Kim, D.H., Jarvis, R. M., Xu, Y., Oliver, A. W., Allwood, J. W., Hampson, L., Hampson, I. N., Goodacre, R., *Combining metabolic fingerprinting and footprinting to understand the phenotypic response of HPV16 E6 expressing cervical carcinoma cells exposed to the HIV anti-viral drug lopinavir.* Analyst, 2010. **135**: p. 1235-1244.
185. Kim, D.H., et al., *Raman chemical mapping reveals site of action of HIV protease inhibitors in HPV16 E6 expressing cervical carcinoma cells.* Anal Bioanal Chem, 2010. **398**(7-8): p. 3051-61.
186. Mincheva, A., L. Gissmann, and H. zur Hausen, *Chromosomal integration sites of human papillomavirus DNA in three cervical cancer cell lines mapped by in situ hybridization.* Med Microbiol Immunol, 1987. **176**(5): p. 245-56.
187. Pegg, A.E., *Recent advances in the biochemistry of polyamines in eukaryotes.* Biochem J, 1986. **234**(2): p. 249-62.
188. Li, X. and P. Coffino, *Distinct domains of antizyme required for binding and proteolysis of ornithine decarboxylase.* Mol Cell Biol, 1994. **14**(1): p. 87-92.
189. Rechsteiner, M., *Regulation of enzyme levels by proteolysis: the role of pest regions.* Adv Enzyme Regul, 1988. **27**: p. 135-51.
190. Elias, S., et al., *Degradation of ornithine decarboxylase by the mammalian and yeast 26S proteasome complexes requires all the components of the protease.* Eur J Biochem, 1995. **229**(1): p. 276-83.
191. Hampson, L., et al., *The HPV16 E6 and E7 proteins and the radiation resistance of cervical carcinoma.* Faseb J, 2001. **15**(8): p. 1445-7.
192. Sambrook, J., E.F. Fritsch, and T. Maniatis, *Molecular cloning: a laboratory manual. 2nd ed.* Cold Spring Harbor Laboratory
Cold Spring Harbor, N.Y., 1989.
193. Kuhn, D.J., et al., *Targeted inhibition of the immunoproteasome is a potent strategy against models of multiple myeloma that overcomes resistance to conventional drugs and nonspecific proteasome inhibitors.* Blood, 2009. **113**(19): p. 4667-76.
194. Franken, N.A., et al., *Clonogenic assay of cells in vitro.* Nat Protoc, 2006. **1**(5): p. 2315-9.
195. Brown, J.M. and L.D. Attardi, *The role of apoptosis in cancer development and treatment response.* Nat Rev Cancer, 2005. **5**(3): p. 231-7.
196. Puck, T.T. and P.I. Marcus, *Action of x-rays on mammalian cells.* J Exp Med, 1956. **103**(5): p. 653-66.
197. Chung, C.H. and M.L. Gillison, *Human papillomavirus in head and neck cancer: its role in pathogenesis and clinical implications.* Clin Cancer Res, 2009. **15**(22): p. 6758-62.
198. Corbitt, G., et al., *Human papillomavirus (HPV) genotypes associated with laryngeal papilloma.* J Clin Pathol, 1988. **41**(3): p. 284-8.

199. Lin, H.W., et al., *Malignant transformation of a highly aggressive human papillomavirus type 11-associated recurrent respiratory papillomatosis.* Am J Otolaryngol, 2009.
200. Mounts, P., K.V. Shah, and H. Kashima, *Viral etiology of juvenile- and adult-onset squamous papilloma of the larynx.* Proc Natl Acad Sci U S A, 1982. **79**(17): p. 5425-9.
201. Ragin, C.C., F. Modugno, and S.M. Gollin, *The epidemiology and risk factors of head and neck cancer: a focus on human papillomavirus.* J Dent Res, 2007. **86**(2): p. 104-14.
202. Zarod, A.P., J.D. Rutherford, and G. Corbitt, *Malignant progression of laryngeal papilloma associated with human papilloma virus type 6 (HPV-6) DNA.* J Clin Pathol, 1988. **41**(3): p. 280-3.
203. Stamataki, S., et al., *Juvenile recurrent respiratory papillomatosis: still a mystery disease with difficult management.* Head Neck, 2007. **29**(2): p. 155-62.
204. Donne, A.J., et al., *Cidofovir induces an increase in levels of low-risk and high-risk HPV E6.* Head Neck, 2009. **31**(7): p. 893-901.
205. Farwell, D.G., et al., *Genetic and epigenetic changes in human epithelial cells immortalized by telomerase.* Am J Pathol, 2000. **156**(5): p. 1537-47.
206. Donne, A.J., et al., *Potential risk factors associated with the use of cidofovir to treat benign human papillomavirus-related disease.* Antivir Ther, 2009. **14**(7): p. 939-52.
207. Donne, A.J., et al., *Cidofovir induces an increase in levels of low-risk and high-risk HPV E6.* Head Neck, 2009. **31**(7): p. 893-901.
208. Coller, H.A., L. Sang, and J.M. Roberts, *A new description of cellular quiescence.* PLoS Biol, 2006. **4**(3): p. e83.
209. Smith, E.J., et al., *The accumulation of an E2F-p130 transcriptional repressor distinguishes a G0 cell state from a G1 cell state.* Mol Cell Biol, 1996. **16**(12): p. 6965-76.
210. Wilkins, M.R., et al., *From proteins to proteomes: large scale protein identification by two-dimensional electrophoresis and amino acid analysis.* Biotechnology (N Y), 1996. **14**(1): p. 61-5.
211. Anderson, N.L. and N.G. Anderson, *Proteome and proteomics: new technologies, new concepts, and new words.* Electrophoresis, 1998. **19**(11): p. 1853-61.
212. Kopf, E. and D. Zharhary, *Antibody arrays--an emerging tool in cancer proteomics.* Int J Biochem Cell Biol, 2007. **39**(7-8): p. 1305-17.
213. Zhu, H., M. Bilgin, and M. Snyder, *Proteomics.* Annu Rev Biochem, 2003. **72**: p. 783-812.
214. Alam, S.L., J.F. Atkins, and R.F. Gesteland, *Programmed ribosomal frameshifting: much ado about knotting!* Proc Natl Acad Sci U S A, 1999. **96**(25): p. 14177-9.
215. Griffin, T.J. and R. Aebersold, *Advances in proteome analysis by mass spectrometry.* J Biol Chem, 2001. **276**(49): p. 45497-500.
216. Gygi, S.P., et al., *Correlation between protein and mRNA abundance in yeast.* Mol Cell Biol, 1999. **19**(3): p. 1720-30.
217. Haab, B.B., M.J. Dunham, and P.O. Brown, *Protein microarrays for highly parallel detection and quantitation of specific proteins and antibodies in complex solutions.* Genome Biol, 2001. **2**(2): p. RESEARCH0004.
218. Ernst, L.A., et al., *Cyanine dye labeling reagents for sulfhydryl groups.* Cytometry, 1989. **10**(1): p. 3-10.
219. Cleveland, D.W., et al., *Peptide mapping by limited proteolysis in sodium dodecyl sulfate and analysis by gel electrophoresis.* J Biol Chem, 1977. **252**(3): p. 1102-6.

220. Chatr-aryamontri, A., et al., *VirusMINT: a viral protein interaction database.* Nucleic Acids Res, 2009. **37**(Database issue): p. D669-73.
221. Feng, W., et al., *Morphoproteomic evidence of constitutively activated and overexpressed mTOR pathway in cervical squamous carcinoma and high grade squamous intraepithelial lesions.* Int J Clin Exp Pathol, 2009. **2**(3): p. 249-60.
222. Spangle, J.M. and K. Munger, *The human papillomavirus type 16 E6 oncoprotein activates mTORC1 signaling and increases protein synthesis.* J Virol, 2010. **84**(18): p. 9398-407.
223. Tang, G., Z. Xu, and J.E. Goldman, *Synergistic effects of the SAPK/JNK and the proteasome pathway on glial fibrillary acidic protein (GFAP) accumulation in Alexander disease.* J Biol Chem, 2006. **281**(50): p. 38634-43.
224. Bisbal, C. and R.H. Silverman, *Diverse functions of RNase L and implications in pathology.* Biochimie, 2007. **89**(6-7): p. 789-98.
225. Silverman, R.H., *A scientific journey through the 2-5A/RNase L system.* Cytokine Growth Factor Rev, 2007. **18**(5-6): p. 381-8.
226. Conticello, S.G., R.S. Harris, and M.S. Neuberger, *The Vif protein of HIV triggers degradation of the human antiretroviral DNA deaminase APOBEC3G.* Curr Biol, 2003. **13**(22): p. 2009-13.
227. Feng, Z., et al., *The VP35 protein of Ebola virus inhibits the antiviral effect mediated by double-stranded RNA-dependent protein kinase PKR.* J Virol, 2007. **81**(1): p. 182-92.
228. Minakshi, R., et al., *The SARS Coronavirus 3a protein causes endoplasmic reticulum stress and induces ligand-independent downregulation of the type 1 interferon receptor.* PLoS One, 2009. **4**(12): p. e8342.
229. Munakata, T., et al., *Hepatitis C virus induces E6AP-dependent degradation of the retinoblastoma protein.* PLoS Pathog, 2007. **3**(9): p. 1335-47.
230. Schwartz, R.A., et al., *Distinct requirements of adenovirus E1b55K protein for degradation of cellular substrates.* J Virol, 2008. **82**(18): p. 9043-55.
231. Banks, L., D. Pim, and M. Thomas, *Viruses and the 26S proteasome: hacking into destruction.* Trends Biochem Sci, 2003. **28**(8): p. 452-9.
232. Goodbourn, S., L. Didcock, and R.E. Randall, *Interferons: cell signalling, immune modulation, antiviral response and virus countermeasures.* J Gen Virol, 2000. **81**(Pt 10): p. 2341-64.
233. Sadler, A.J. and B.R. Williams, *Interferon-inducible antiviral effectors.* Nat Rev Immunol, 2008. **8**(7): p. 559-68.
234. Sadler, A.J. and B.R. Williams, *Interferon-inducible antiviral effectors.* Nat Rev Immunol, 2008. **8**(7): p. 559-68.
235. Silverman, R.H., *Viral encounters with 2',5'-oligoadenylate synthetase and RNase L during the interferon antiviral response.* J Virol, 2007. **81**(23): p. 12720-9.
236. Sarkar, S.N., et al., *Enzymatic characteristics of recombinant medium isozyme of 2'-5' oligoadenylate synthetase.* J Biol Chem, 1999. **274**(3): p. 1848-55.
237. Dong, B. and R.H. Silverman, *2-5A-dependent RNase molecules dimerize during activation by 2-5A.* J Biol Chem, 1995. **270**(8): p. 4133-7.
238. Silverman, R.H., *Viral encounters with 2',5'-oligoadenylate synthetase and RNase L during the interferon antiviral response.* J Virol, 2007. **81**(23): p. 12720-9.
239. Zhou, A., B.A. Hassel, and R.H. Silverman, *Expression cloning of 2-5A-dependent RNAase: a uniquely regulated mediator of interferon action.* Cell, 1993. **72**(5): p. 753-65.
240. Li, J., A. Mahajan, and M.D. Tsai, *Ankyrin repeat: a unique motif mediating protein-protein interactions.* Biochemistry, 2006. **45**(51): p. 15168-78.

241. Liang, S.L., D. Quirk, and A. Zhou, *RNase L: its biological roles and regulation.* IUBMB Life, 2006. **58**(9): p. 508-14.
242. Ramakrishnan, C., V.S. Dani, and T. Ramasarma, *A conformational analysis of Walker motif A [GXXXXGKT (S)] in nucleotide-binding and other proteins.* Protein Eng, 2002. **15**(10): p. 783-98.
243. Tanaka, N., et al., *Structural basis for recognition of 2',5'-linked oligoadenylates by human ribonuclease L.* Embo J, 2004. **23**(20): p. 3929-38.
244. Cox, J.S., C.E. Shamu, and P. Walter, *Transcriptional induction of genes encoding endoplasmic reticulum resident proteins requires a transmembrane protein kinase.* Cell, 1993. **73**(6): p. 1197-206.
245. Henry, K.A., et al., *The unfolded protein response is not necessary for the G1/S transition, but it is required for chromosome maintenance in Saccharomyces cerevisiae.* PLoS One, 2010. **5**(9): p. e12732.
246. Bork, P. and C. Sander, *A hybrid protein kinase-RNase in an interferon-induced pathway?* FEBS Lett, 1993. **334**(2): p. 149-52.
247. Dong, B. and R.H. Silverman, *Alternative function of a protein kinase homology domain in 2', 5'-oligoadenylate dependent RNase L.* Nucleic Acids Res, 1999. **27**(2): p. 439-45.
248. Bisbal, C., et al., *Cloning and characterization of a RNAse L inhibitor. A new component of the interferon-regulated 2-5A pathway.* J Biol Chem, 1995. **270**(22): p. 13308-17.
249. Short, A.L., *Viral evasion of interferon stimulated genes.* Bioscience Horizons, 2009. **2**: p. 212-224.
250. Sanchez, R. and I. Mohr, *Inhibition of cellular 2'-5' oligoadenylate synthetase by the herpes simplex virus type 1 Us11 protein.* J Virol, 2007. **81**(7): p. 3455-64.
251. Kwong, A.D., J.A. Kruper, and N. Frenkel, *Herpes simplex virus virion host shutoff function.* J Virol, 1988. **62**(3): p. 912-21.
252. Cayley, P.J., et al., *Activation of the ppp(A2'p)nA system in interferon-treated, herpes simplex virus-infected cells and evidence for novel inhibitors of the ppp(A2'p)nA-dependent RNase.* Eur J Biochem, 1984. **143**(1): p. 165-74.
253. Saunders, L.R. and G.N. Barber, *The dsRNA binding protein family: critical roles, diverse cellular functions.* Faseb J, 2003. **17**(9): p. 961-83.
254. Nowotny, M. and W. Yang, *Structural and functional modules in RNA interference.* Curr Opin Struct Biol, 2009. **19**(3): p. 286-93.
255. Barber, G.N., *The NFAR's (nuclear factors associated with dsRNA): evolutionarily conserved members of the dsRNA binding protein family.* RNA Biol, 2009. **6**(1): p. 35-9.
256. Yang, J.D. and L.R. Roberts, *Hepatocellular carcinoma: A global view.* Nat Rev Gastroenterol Hepatol, 2010. **7**(8): p. 448-58.
257. Taguchi, T., et al., *Hepatitis C virus NS5A protein interacts with 2',5'-oligoadenylate synthetase and inhibits antiviral activity of IFN in an IFN sensitivity-determining region-independent manner.* J Gen Virol, 2004. **85**(Pt 4): p. 959-69.
258. Enomoto, N., et al., *Comparison of full-length sequences of interferon-sensitive and resistant hepatitis C virus 1b. Sensitivity to interferon is conferred by amino acid substitutions in the NS5A region.* J Clin Invest, 1995. **96**(1): p. 224-30.
259. Enomoto, N., et al., *Mutations in the nonstructural protein 5A gene and response to interferon in patients with chronic hepatitis C virus 1b infection.* N Engl J Med, 1996. **334**(2): p. 77-81.

260. Gale, M., Jr., et al., *Control of PKR protein kinase by hepatitis C virus nonstructural 5A protein: molecular mechanisms of kinase regulation.* Mol Cell Biol, 1998. **18**(9): p. 5208-18.
261. Gale, M.J., Jr., et al., *Evidence that hepatitis C virus resistance to interferon is mediated through repression of the PKR protein kinase by the nonstructural 5A protein.* Virology, 1997. **230**(2): p. 217-27.
262. Francois, C., et al., *Expression of hepatitis C virus proteins interferes with the antiviral action of interferon independently of PKR-mediated control of protein synthesis.* J Virol, 2000. **74**(12): p. 5587-96.
263. Han, J.Q. and D.J. Barton, *Activation and evasion of the antiviral 2'-5' oligoadenylate synthetase/ribonuclease L pathway by hepatitis C virus mRNA.* Rna, 2002. **8**(4): p. 512-25.
264. Lingappa, J.R., et al., *Basic residues in the nucleocapsid domain of Gag are required for interaction of HIV-1 gag with ABCE1 (HP68), a cellular protein important for HIV-1 capsid assembly.* J Biol Chem, 2006. **281**(7): p. 3773-84.
265. Zimmerman, C., et al., *Identification of a host protein essential for assembly of immature HIV-1 capsids.* Nature, 2002. **415**(6867): p. 88-92.
266. Martinand, C., et al., *RNase L inhibitor is induced during human immunodeficiency virus type 1 infection and down regulates the 2-5A/RNase L pathway in human T cells.* J Virol, 1999. **73**(1): p. 290-6.
267. Silverman, R.H., *Implications for RNase L in prostate cancer biology.* Biochemistry, 2003. **42**(7): p. 1805-12.
268. Steinberg, G.D., et al., *Family history and the risk of prostate cancer.* Prostate, 1990. **17**(4): p. 337-47.
269. Smith, J.R., et al., *Major susceptibility locus for prostate cancer on chromosome 1 suggested by a genome-wide search.* Science, 1996. **274**(5291): p. 1371-4.
270. Ostrander, E.A. and J.L. Stanford, *Genetics of prostate cancer: too many loci, too few genes.* Am J Hum Genet, 2000. **67**(6): p. 1367-75.
271. Stanford, J.L. and E.A. Ostrander, *Familial prostate cancer.* Epidemiol Rev, 2001. **23**(1): p. 19-23.
272. Goode, E.L., et al., *Clinical characteristics of prostate cancer in an analysis of linkage to four putative susceptibility loci.* Clin Cancer Res, 2001. **7**(9): p. 2739-49.
273. Carpten, J., et al., *Germline mutations in the ribonuclease L gene in families showing linkage with HPC1.* Nat Genet, 2002. **30**(2): p. 181-4.
274. Li, H. and B.C. Tai, *RNASEL gene polymorphisms and the risk of prostate cancer: a meta-analysis.* Clin Cancer Res, 2006. **12**(19): p. 5713-9.
275. Meyer, M.S., et al., *Genetic variation in RNASEL associated with prostate cancer risk and progression.* Carcinogenesis, 2010. **31**(9): p. 1597-603.
276. Robbins, C.M., et al., *Association of HPC2/ELAC2 and RNASEL non-synonymous variants with prostate cancer risk in African American familial and sporadic cases.* Prostate, 2008. **68**(16): p. 1790-7.
277. Shook, S.J., et al., *Association of RNASEL variants with prostate cancer risk in Hispanic Caucasians and African Americans.* Clin Cancer Res, 2007. **13**(19): p. 5959-64.
278. Wiklund, F., et al., *Genetic analysis of the RNASEL gene in hereditary, familial, and sporadic prostate cancer.* Clin Cancer Res, 2004. **10**(21): p. 7150-6.
279. Xiang, Y., et al., *Effects of RNase L mutations associated with prostate cancer on apoptosis induced by 2',5'-oligoadenylates.* Cancer Res, 2003. **63**(20): p. 6795-801.
280. Casey, G., et al., *RNASEL Arg462Gln variant is implicated in up to 13% of prostate cancer cases.* Nat Genet, 2002. **32**(4): p. 581-3.

281. Devanur, L.D. and J.R. Kerr, *Chronic fatigue syndrome.* J Clin Virol, 2006. **37**(3): p. 139-50.
282. Avellaneda Fernandez, A., et al., *Chronic fatigue syndrome: aetiology, diagnosis and treatment.* BMC Psychiatry, 2009. **9 Suppl 1**: p. S1.
283. Suhadolnik, R.J., et al., *Changes in the 2-5A synthetase/RNase L antiviral pathway in a controlled clinical trial with poly(I)-poly(C12U) in chronic fatigue syndrome.* In Vivo, 1994. **8**(4): p. 599-604.
284. Suhadolnik, R.J., et al., *Upregulation of the 2-5A synthetase/RNase L antiviral pathway associated with chronic fatigue syndrome.* Clin Infect Dis, 1994. **18 Suppl 1**: p. S96-104.
285. Urisman, A., et al., *Identification of a novel Gammaretrovirus in prostate tumors of patients homozygous for R462Q RNASEL variant.* PLoS Pathog, 2006. **2**(3): p. e25.
286. Urisman, A., et al., *Identification of a novel Gammaretrovirus in prostate tumors of patients homozygous for R462Q RNASEL variant.* PLoS Pathog, 2006. **2**(3): p. e25.
287. Dong, B., et al., *An infectious retrovirus susceptible to an IFN antiviral pathway from human prostate tumors.* Proc Natl Acad Sci U S A, 2007. **104**(5): p. 1655-60.
288. Dunn, G.P., et al., *IFN unresponsiveness in LNCaP cells due to the lack of JAK1 gene expression.* Cancer Res, 2005. **65**(8): p. 3447-53.
289. Rennert, H., et al., *A novel founder mutation in the RNASEL gene, 471delAAAG, is associated with prostate cancer in Ashkenazi Jews.* Am J Hum Genet, 2002. **71**(4): p. 981-4.
290. Stieler, K., et al., *Host range and cellular tropism of the human exogenous gammaretrovirus XMRV.* Virology, 2010.
291. Hong, S., et al., *Fibrils of prostatic acid phosphatase fragments boost infections with XMRV (xenotropic murine leukemia virus-related virus), a human retrovirus associated with prostate cancer.* J Virol, 2009. **83**(14): p. 6995-7003.
292. Schlaberg, R., et al., *XMRV is present in malignant prostatic epithelium and is associated with prostate cancer, especially high-grade tumors.* Proc Natl Acad Sci U S A, 2009. **106**(38): p. 16351-6.
293. Knouf, E.C., et al., *Multiple integrated copies and high-level production of the human retrovirus XMRV (xenotropic murine leukemia virus-related virus) from 22Rv1 prostate carcinoma cells.* J Virol, 2009. **83**(14): p. 7353-6.
294. Lombardi, V.C., et al., *Detection of an infectious retrovirus, XMRV, in blood cells of patients with chronic fatigue syndrome.* Science, 2009. **326**(5952): p. 585-9.
295. Mikovits, J.A., et al., *Distribution of xenotropic murine leukemia virus-related virus (XMRV) infection in chronic fatigue syndrome and prostate cancer.* AIDS Rev, 2010. **12**(3): p. 149-52.
296. Metzger, M.J., et al., *The prostate cancer-associated human retrovirus XMRV lacks direct transforming activity but can induce low rates of transformation in cultured cells.* J Virol, 2009. **84**(4): p. 1874-80.
297. Dirks, C., et al., *Mechanism of cell entry and transformation by enzootic nasal tumor virus.* J Virol, 2002. **76**(5): p. 2141-9.
298. Liu, S.L. and A.D. Miller, *Transformation of madin-darby canine kidney epithelial cells by sheep retrovirus envelope proteins.* J Virol, 2005. **79**(2): p. 927-33.
299. Liu, S.L. and A.D. Miller, *Oncogenic transformation by the jaagsiekte sheep retrovirus envelope protein.* Oncogene, 2007. **26**(6): p. 789-801.
300. Nishigaki, K., et al., *Friend spleen focus-forming virus transforms rodent fibroblasts in cooperation with a short form of the receptor tyrosine kinase Stk.* Proc Natl Acad Sci U S A, 2005. **102**(43): p. 15488-93.

301. Wootton, S.K., C.L. Halbert, and A.D. Miller, *Sheep retrovirus structural protein induces lung tumours.* Nature, 2005. **434**(7035): p. 904-7.
302. Menendez-Arias, L., *Evidence and controversies on the role of XMRV in prostate cancer and chronic fatigue syndrome.* Rev Med Virol, 2010.
303. Erlwein, O., et al., *Failure to detect the novel retrovirus XMRV in chronic fatigue syndrome.* PLoS One, 2010. **5**(1): p. e8519.
304. Groom, H.C., et al., *Absence of xenotropic murine leukaemia virus-related virus in UK patients with chronic fatigue syndrome.* Retrovirology, 2010. **7**: p. 10.
305. Switzer, W.M., et al., *Absence of evidence of xenotropic murine leukemia virus-related virus infection in persons with chronic fatigue syndrome and healthy controls in the United States.* Retrovirology, 2010. **7**: p. 57.
306. van Kuppeveld, F.J., et al., *Prevalence of xenotropic murine leukaemia virus-related virus in patients with chronic fatigue syndrome in the Netherlands: retrospective analysis of samples from an established cohort.* Bmj, 2010. **340**: p. c1018.
307. Hue, S., et al., *Disease-associated XMRV sequences are consistent with laboratory contamination.* Retrovirology, 2010. **7**(1): p. 111.
308. Robinson, M.J., et al., *Mouse DNA contamination in human tissue tested for XMRV.* Retrovirology, 2010. **7**(1): p. 108.
309. Sato, E., R.A. Furuta, and T. Miyazawa, *An endogenous murine leukemia viral genome contaminant in a commercial RT-PCR Kit is amplified using standard primers for XMRV.* Retrovirology, 2010. **7**(1): p. 110.
310. Smith, R.A., *Contamination of clinical specimens with MLV-encoding nucleic acids: implications for XMRV and other candidate human retroviruses.* Retrovirology, 2010. **7**(1): p. 112.
311. Kozuka, T., et al., *Enhancer-promoter activity of human papillomavirus type 16 long control regions isolated from cell lines SiHa and CaSki and cervical cancer biopsies.* Jpn J Cancer Res, 2000. **91**(3): p. 271-9.
312. Towbin, H., T. Staehelin, and J. Gordon, *Electrophoretic transfer of proteins from polyacrylamide gels to nitrocellulose sheets: procedure and some applications.* Proc Natl Acad Sci U S A, 1979. **76**(9): p. 4350-4.
313. Pyrko, P., et al., *HIV-1 protease inhibitors nelfinavir and atazanavir induce malignant glioma death by triggering endoplasmic reticulum stress.* Cancer Res, 2007. **67**(22): p. 10920-8.
314. Elbashir, S.M., et al., *Duplexes of 21-nucleotide RNAs mediate RNA interference in cultured mammalian cells.* Nature, 2001. **411**(6836): p. 494-8.
315. Rand, T.A., et al., *Argonaute2 cleaves the anti-guide strand of siRNA during RISC activation.* Cell, 2005. **123**(4): p. 621-9.
316. Kawamata, T. and Y. Tomari, *Making RISC.* Trends Biochem Sci, 2010.
317. Tolia, N.H. and L. Joshua-Tor, *Slicer and the argonautes.* Nat Chem Biol, 2007. **3**(1): p. 36-43.
318. Rao, D.D., et al., *siRNA vs. shRNA: similarities and differences.* Adv Drug Deliv Rev, 2009. **61**(9): p. 746-59.
319. Jarve, A., et al., *Surveillance of siRNA integrity by FRET imaging.* Nucleic Acids Res, 2007. **35**(18): p. e124.
320. Phizicky, E.M. and S. Fields, *Protein-protein interactions: methods for detection and analysis.* Microbiol Rev, 1995. **59**(1): p. 94-123.
321. Paunesku, T., et al., *Proliferating cell nuclear antigen (PCNA): ringmaster of the genome.* Int J Radiat Biol, 2001. **77**(10): p. 1007-21.

322. Kwara, A., et al., *Antiretroviral drug concentrations and HIV RNA in the genital tract of HIV-infected women receiving long-term highly active antiretroviral therapy.* Clin Infect Dis, 2008. **46**(5): p. 719-25.
323. Loo, D.T., *In situ detection of apoptosis by the TUNEL assay: an overview of techniques.* Methods Mol Biol, 2011. **682**: p. 3-13.
324. Pattillo, R.A., et al., *Tumor antigen and human chorionic gonadotropin in CaSki cells: a new epidermoid cervical cancer cell line.* Science, 1977. **196**(4297): p. 1456-8.
325. Piccinini, M., et al., *The human 26S proteasome is a target of antiretroviral agents.* Aids, 2002. **16**(5): p. 693-700.
326. Klinger, P.P. and U. Schubert, *The ubiquitin-proteasome system in HIV replication: potential targets for antiretroviral therapy.* Expert Rev Anti Infect Ther, 2005. **3**(1): p. 61-79.
327. Chatr-aryamontri, A., et al., *VirusMINT: a viral protein interaction database.* Nucleic Acids Res, 2009. **37**(Database issue): p. D669-73.
328. Short, A.L., *Viral evasion of interferon stimulated genes.* Bioscience Horizons, 2009. **2**: p. 212-224.
329. Martinand, C., et al., *RNase L inhibitor is induced during human immunodeficiency virus type 1 infection and down regulates the 2-5A/RNase L pathway in human T cells.* J Virol, 1999. **73**(1): p. 290-6.
330. Suh, D.S., et al., *Differential apoptotic response in HPV-infected cancer cells of the uterine cervix after doxorubicin treatment.* Oncol Rep, 2010. **23**(3): p. 751-6.
331. Chen, F., et al., *In vitro susceptibility of 10 clinical isolates of SARS coronavirus to selected antiviral compounds.* J Clin Virol, 2004. **31**(1): p. 69-75.
332. Chu, C.M., et al., *Role of lopinavir/ritonavir in the treatment of SARS: initial virological and clinical findings.* Thorax, 2004. **59**(3): p. 252-6.
333. Min, S.S., et al., *Protease inhibitor and nonnucleoside reverse transcriptase inhibitor concentrations in the genital tract of HIV-1-infected women.* J Acquir Immune Defic Syndr, 2004. **37**(5): p. 1577-80.
334. Khanna, N., et al., *Phase I/II clinical safety studies of terameprocol vaginal ointment.* Gynecol Oncol, 2007. **107**(3): p. 554-62.
335. Chiou, S.K., M.K. Jones, and A.S. Tarnawski, *Survivin - an anti-apoptosis protein: its biological roles and implications for cancer and beyond.* Med Sci Monit, 2003. **9**(4): p. PI25-9.
336. Wieder, D.R. and L. Pattimakiel, *Examining the efficacy, safety, and patient acceptability of the combined contraceptive vaginal ring (NuvaRing).* Int J Womens Health, 2010. **2**: p. 401-9.
337. Denny, L., M. Quinn, and R. Sankaranarayanan, *Chapter 8: Screening for cervical cancer in developing countries.* Vaccine, 2006. **24 Suppl 3**: p. S3/71-7.
338. Pau, A.K., et al., *Instability of lopinavir/ritonavir capsules at ambient temperatures in sub-Saharan Africa: relevance to WHO antiretroviral guidelines.* AIDS, 2005. **19**(11): p. 1233-4.
339. Faivre, S., G. Kroemer, and E. Raymond, *Current development of mTOR inhibitors as anticancer agents.* Nat Rev Drug Discov, 2006. **5**(8): p. 671-88.
340. Delmonte, A. and C. Sessa, *Molecule-targeted agents in endometrial cancer.* Curr Opin Oncol, 2008. **20**(5): p. 554-9.
341. Shafer, A., et al., *Rapamycin potentiates the effects of paclitaxel in endometrial cancer cells through inhibition of cell proliferation and induction of apoptosis.* Int J Cancer, 2009. **126**(5): p. 1144-54.

342. Rader, J.S., et al., *In vitro differentiation of epithelial cells from cervical neoplasias resembles in vivo lesions.* Oncogene, 1990. **5**(4): p. 571-6.
343. Dickson, M.A., et al., *Human keratinocytes that express hTERT and also bypass a p16(INK4a)-enforced mechanism that limits life span become immortal yet retain normal growth and differentiation characteristics.* Mol Cell Biol, 2000. **20**(4): p. 1436-47.
344. Kim, D.H., et al., *Combining metabolic fingerprinting and footprinting to understand the phenotypic response of HPV16 E6 expressing cervical carcinoma cells exposed to the HIV anti-viral drug lopinavir.* Analyst, 2010. **135**(6): p. 1235-44.

Appendix 1 - Vector Information

pZsProsensor-1 Vector – Proteasome Sensor Vector

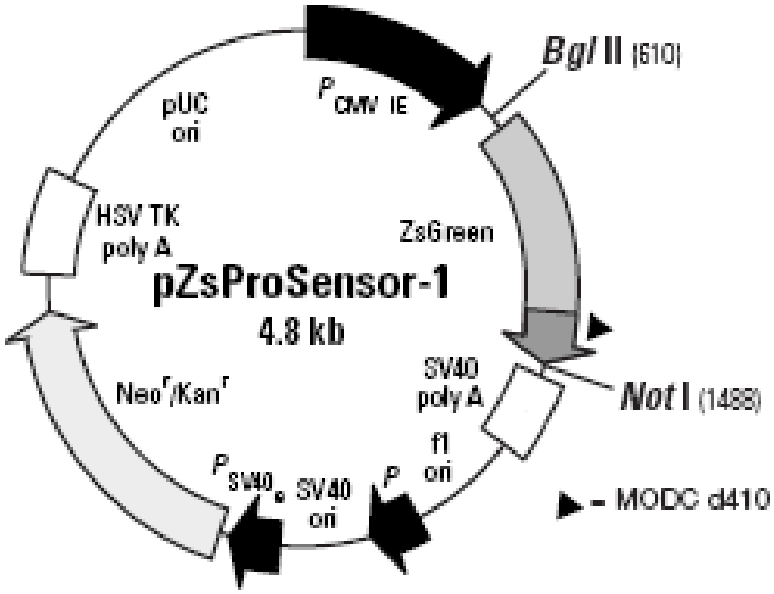

www.clontech.com/images/pt/PT3712-5.pdf

pReceiver-M02 – Mammalian RNase L Expression Vector

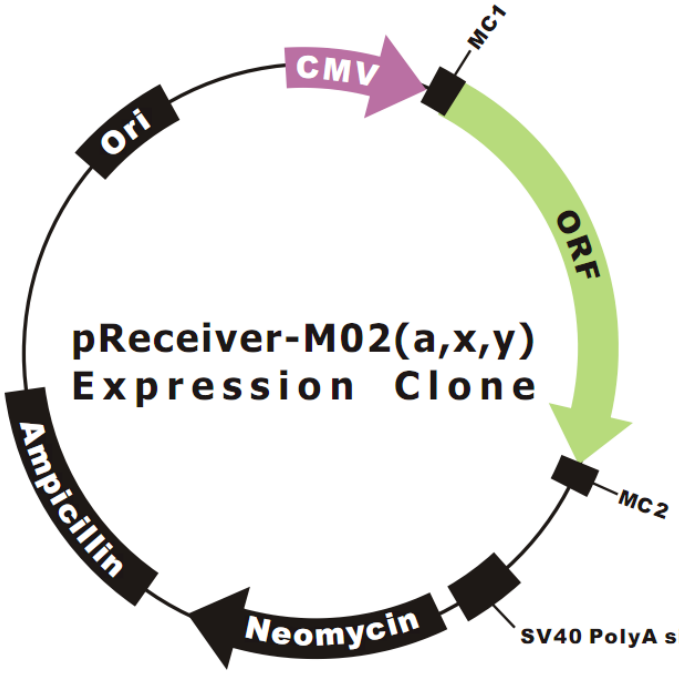

Vector Features

Promoter	CMV
Host Cell	Mammalian
Bacterial selection antibiotic	Ampicillin
Mammalian selection marker	Yes
Tag	N/A

http://www.genecopoeia.com/tech/omicslink/pReceiver-M02.pdf

Appendix 2

Solutions

All solutions were prepared using sterile filtered water and autoclaved for 11 minutes at 121℃ using a Prestige Medical 2100 seri es bench top autoclave (Prestige Medical, Blackburn, UK)

1x Phosphate Buffered Saline (PBS)

2 PBS tablets dissolved in 400ml distilled water (autoclaved for sterile 1 x PBS)

10x TAE buffer (1L)

Tris base	48.4g
Acetic acid	11.4ml
EDTA (0.5M) (pH8)	20ml

Made up to 1L with distilled water

1x TE Buffer

Tris base	0.12g
EDTA (0.5M)	200µl

Made up to 100ml with distilled water

10x Laemmli Buffer

Tris base	15.2g
Glycine	72.1g

Made up to 500ml with distilled water

Bioline PCR BioMix™ Red

BIOTAQ DNA Polymerase	
dNTPs	2mM
$(NH_2)_2SO_4$	32mM
Tris HCl (pH 8.8 at 25℃)	125mM
Tween 20	0.02%
$MgCl_2$	4mM
Stabiliser	
Inert Dye	

1% Agarose

1g Agarose dissolved in 100ml 1x TAE buffer and microwaved until dissolved

Luria Bertani (LB) media

Sodium chloride	10g
Select peptone/ tryptone	10g
Select yeast extract	5g

Made up to 1L with distilled water

LB Agar
As for LB media with added 1.5% Agar

B-Galactosidase reporter gene staining solution

Magnesium chloride (200mM)	10µl
Potassium Ferricyanide (400mM)	10µl
Potassium Ferrocyanide (400mM)	10µl
X-Gal solution (20mg/ml)*	50µl
1xPBS	920µl

*****Lab stock of 100mg/ml X-Gal (5-bromo-4-chloro-3-indolyl-β-D-galactopyranoside) solution diluted 1/5 with N-N-Dimethylformamide

Western Blotting Solutions

10x Laemmle running Buffer (500ml)

Tris	15.2g
Glycine	72.1g

Made up to 500ml with distilled water – for 1x running buffer add SDS to 0.1% (i.e. 5ml in 500ml)

Transfer Buffer (500ml)

2.9g Tris base	2.9g
1.5g Glycine	1.5g
Dissolve the above in 200ml distilled water	
Methanol	200ml

1M Tris pH 6.8 (100ml)

Tris	12.1g
Distilled water	100ml

pH to 6.8 with HCl

1.5M Tris pH 8.8 (100ml)

Tris	18.1g
Distilled water	100ml

pH to 8.8 with HCl

2 x Loading Buffer (Laemmle)

Tris (pH 6.8)	0.6 ml (60 mM Final)
10% SDS	2 ml
Bromophenol Blue (0.05%)	To colour
Glycerol (50%)	1 ml
Dithiothreitol (DTT) (0.1M)	1ml
sdH_20	5.4 ml

Stacking Gel

distilled Water	2.7ml
Acrylamide Mix	0.67ml
Tris (pH 6.8)	0.5ml
SDS (10%)	0.04ml
APS (10%)	0.04ml
TEMED[a]	0.004ml

[a] – N, N, N[I], N[I]-Tetramethylethylenediamine

Resolving/ Separating Gel (15ml of 12% Gel Solution)

distilled water	5ml
Acrylamide mix	6ml
Tris (0.5M) pH 8.8	3.8ml
SDS (10%)	0.15ml
APS (10%)	0.15ml
TEMED[a]	0.006ml

[a] – N, N, N[I], N[I]-Tetramethylethylenediamine

Preparation of Competent XL-1 Blue *E.coli*

TFB-1

Potassium acetate	0.59g
Calcium chloride	0.294g
Manganese chloride	1.98g
Rubidium chloride	2.42g
Glycerol	15%

Filter Sterilise

Made up to 200ml with distilled water and pH to 5.8 with 1M acetic acid

TFB - 2

MOPS	0.23g
Calcium chloride	1.1g
Rubidium chloride	0.121g
Glycerol	15%

Filter Sterilise
Made up to 100ml with distilled water and pH to 6.5 with potassium hydroxide

Plasmid Preparation Solutions

Solution 1

Glucose	4.51g
Tris (1M)	12.5ml
EDTA (0.5M)	10ml

Made up to 50ml with distilled water

Solution 2

Sodium Hydroxide (10M)	400µl
10% Sodium dodeycl sulphate (SDS)	2ml

Made up to 20ml with distilled water – Made fresh every time.

Solution 3

Potassium acetate	147.2g
Acetic acid	57.5ml

Made up to 500ml with distilled water

Appendix 3 - PCR primers and thermal cycling conditions

β-Actin-F	5'-TCC-ATC-ATG-AAG-TGT-GAC-GT-3'	55.3ºC
β-Actin-R	5'-TCA-GGA-GCA-ATG-ATC-TT-3'	55.3ºC
Product Length	161bp	

Stage	Temp (℃)	Time	N° Cycles
Denature	95	5min	1
Denature	94	25sec	
Anneal	53	25sec	32
Extend	72	25sec	
Extend	72	5 min	1
Hold	4		

		Tm
ZsG-F	5'-ATC-TTG-TCC-GCC-GCC-TTC-AAC-TA-3'	62.4ºC
ZsG-R	5'-TTC-ACG-CCG-TAG-AAC-TTG-GAC-T-3'	60.3ºC
Product Length	212bp	

Stage	Temp (℃)	Time	N° Cycles
Denature	95	5min	1
Denature	94	25sec	
Anneal	57	25sec	32
Extend	72	25sec	
Extend	72	5 min	1
Hold	4		

		Tm
GAPDH-F	5'-CATTGACCTCAACTACATGGT-3'	62.4ºC
GAPDH-R	5'-TCGCTCCTGGAAGATGGTGAT-3'	60.3ºC
Product Length	130bp	

Stage	Temp (℃)	Time	N° Cycles
Denature	95	5min	1
Denature	94	25sec	
Anneal	58	25sec	30
Extend	72	25sec	
Extend	72	5 min	1
Hold	4		

RNASEL-F	5’-AGC-AGA-CTC-TGG-AAG-CGT-GTT-3’	60.3ºC
RNASEL-R	5’-TGC-CAG-GTG-AGC-AGC-TTT-CTT-3’	60.3ºC
Product Length	194bp	

Stage	Temp (℃)	Time	Nº Cycles
Denature	95	5min	1
Denature	94	25sec	30
Anneal	56	25sec	
Extend	72	25sec	
Extend	72	5 min	1
Hold	4		

PLA-F	5'-AAGTTCTTGATCCCCAATGCT-3'	56ºC
PLA-R	5'-GCAACCAACACATCCTATCAGAC-3'	54ºC
Product Length	196bp	

Stage	Temp (℃)	Time	Nº Cycles
Denature	95	5min	1
Denature	94	25sec	33
Anneal	54	25sec	
Extend	72	25sec	
Extend	72	5 min	1
Hold	4		

Appendix 4 – RNase L-specific siRNA sequences

Four different RNase L-specific siRNA oligonucleotides (siRNA 1-4) plus ALLSTARS (sequence unpublished) and MAPK control oligonucleotides with no significant off-target homology were designed by and obtained from Qiagen (Flexitube siRNA system, Qiagen, West Sussex, UK)

siRNA-1	**5'**	**CCA-GAC-TAC-ACT-AGT-CCA-TAA**	**3'**
siRNA-2	**5'**	**CAA-GTG-GAC-GAC-TAA-GAT-TAA**	**3'**
siRNA-3	**5'**	**CAG-GAA-GTC-AAG-AGA-GAT-CTA**	**3'**
siRNA-4	**5'**	**CCC-TAT-GAT-TGG-CAA-ACT-CAA**	**3'**

Original article

Lopinavir up-regulates expression of the antiviral protein ribonuclease L in human papillomavirus-positive cervical carcinoma cells

Gavin Batman[1], Anthony W Oliver[1], Ingeborg Zehbe[2], Christina Richard[3], Lynne Hampson[1†], Ian N Hampson[1†]*

[1]Gynaecological Oncology Laboratories, School of Cancer & Enabling Sciences, University of Manchester, St Mary's Hospital, Manchester, UK
[2]Probe Development & Biomarker Exploration, Regional Research Institute, Thunder Bay, ON, Canada
[3]Regional Cancer Care, Thunder Bay, Thunder Bay Regional Health Sciences Centre, Thunder Bay, ON, Canada

*Corresponding author e-mail: ian.hampson@manchester.ac.uk
†These authors are joint senior authors

Background: We have previously shown that the HIV protease inhibitor lopinavir has selective toxicity against human papillomavirus (HPV)-positive cervical carcinoma cells via an unknown mechanism.
Methods: SiHa cervical carcinoma cells were stably transfected with the proteasome sensor vector pZsPro-Sensor-1 to confirm lopinavir inhibits the proteasome in these cells. The Panorama Xpress profiler 725 antibody array was then used to analyse specific changes in protein expression in lopinavir-treated versus control untreated SiHa cells followed by PCR and western blotting. Colorimetric growth assays of lopinavir-treated E6/E7 immortalised versus control human keratinocytes were performed. Targeted small interfering RNA gene silencing followed by growth assay comparison of lopinavir-treated/untreated SiHa cells was also used.
Results: Lopinavir induced an increase in the fluorescence of pZsProSensor-1 transfected SiHa cells, indicative of proteasomal inhibition. Ribonuclease L (RNASEL) protein was shown to be up-regulated in lopinavir-treated SiHa cells, which was confirmed by PCR and western blot. Targeted silencing of RNASEL reduced the sensitivity of SiHa cells to lopinavir. Selective toxicity against E6/E7 immortalised keratinocytes versus control cells was also seen with lopinavir and was associated with up-regulated RNASEL expression.
Conclusions: These data are consistent with the toxicity of lopinavir against HPV-positive cervical carcinoma cells being related to its ability to block viral proteasome activation and induce an up-regulation of the antiviral protein RNASEL. This is supported by the drug's selective toxicity and up-regulation of RNASEL in E6/E7 immortalised keratinocytes combined with the increased resistance to lopinavir observed in SiHa cells following silencing of RNASEL gene expression.

Introduction

Human papillomavirus (HPV) has been unequivocally implicated as a causative agent in the development of cervical cancer [1,2] with >490,000 women worldwide diagnosed every year and >273,000 deaths per annum. Although there are over 100 subtypes of HPV, 70% of cervical cancer cases are attributed to infection with just two high-risk types, 16 and 18 [3,4].

There are currently large differences in the incidence of this disease between developed and developing countries, mainly due to the implementation of effective screening strategies in the former [5]. For example, in the UK, cervical cancer now rates as the 11th most common women's malignancy, whereas in Africa it remains the most prevalent. Lack of screening is not the only contributory factor here, as many African nations also carry the additional burden of HIV infection, which is known to predispose to HPV-related cervical neoplasia [6]. Whilst surgery remains the current treatment of choice for HPV-related pre-cancerous lesions, this is not generally advocated for low-grade disease for which a 'wait and see' approach is usually adopted. Unfortunately for HIV-positive women, surgery is far less effective and recurrence rates of cervical cancer are much higher in these women than those with a negative HIV status [7]. Surgical intervention for cervical cancer in HIV-positive women can also lead to a massive post-

operative increase in vaginal fluid HIV titre, thereby greatly increasing the chances of sexual transmission of the virus [8,9].

The production of an HPV vaccine has prompted many developed countries to implement anti-HPV vaccination programmes which aim to target females prior to their first sexual exposure [10]. However, this will still leave large numbers of already infected women at risk, in addition to those infected with high-risk types of HPV not covered by the current vaccines. In developing areas like Africa the cost of such a vaccination programme, even with subsidies, is likely to be prohibitively expensive. Furthermore, there is also evidence to indicate that vaccination will be less effective in HIV-positive women [11,12].

For the foreseeable future it is clear that development of a non-surgical, preferably self-applied, treatment for HPV-related cervical dysplasia would be extremely valuable. This would have particular impact and benefit in low-resource settings where high levels of HIV infection can aggravate this condition.

We previously investigated the ability of HIV protease inhibitors to combat HPV infection and demonstrated that the antiretroviral drug lopinavir could stabilise the p53 protein and induce apoptosis of HPV-positive cervical carcinoma cells *in vitro*, albeit at higher doses than those achieved by oral administration [13]. These data indicated that lopinavir could potentially be used topically as an anti-HPV therapeutic. Prior to a clinical trial to test this new indication, we set out to further characterise how lopinavir works against HPV. In this regard we have used Fourier Transformation Infra Red spectroscopy to analyse the metabolic changes occurring in lopinavir-treated cervical carcinoma cells [14] and direct Raman spectroscopic imaging to identify the site of action of the drug in cells [15]. We now provide evidence to further support our initial observations and present data on the specific molecular mechanisms by which lopinavir works against HPV.

Methods

Cell culture

HPV16-positive SiHa and CaSki cells derived from cervical carcinoma were obtained from the American Type Culture Collection (Manassas, VA, USA) and were cultured at 37°C in a humidified atmosphere containing 5% CO_2 in RPMI-1640 medium (Invitrogen, Paisley, UK) supplemented with 10% fetal bovine serum (Sigma–Aldrich, Dorset, UK) and 2 mM L-glutamine (Sigma–Aldrich). Primary human foreskin keratinocytes (PHFKs) immortalised by retrovirally transducing with HPV16 E6 and E7 genes were grown in serum-free keratinocyte medium as recently described [16].

Protease inhibitor

Lopinavir was provided as a kind gift by Abbott Laboratories (Abbott Park, IL, USA). A 20 mM working stock solution of lopinavir was prepared in DMSO (Sigma–Aldrich).

Derivation and use of pZsProSensor-1 transfected SiHa cells

The pZsProSensor-1 proteasome sensor vector (Clontech, Mountain View, CA, USA) was used to assess the ability of lopinavir to induce proteasomal inhibition and thus alter cellular protein levels. Linearised vector was used to stably transfect SiHa cells using Lipofectamine-2000 according to the manufacturer's recommendations (Invitrogen). Successfully transfected cells were selected using G-418-sulphate (Geneticin; Invitrogen).

pZsProSensor-1 transfected SiHa cells were seeded in duplicate wells of an eight-well slide flask (BD Biosciences, Bedford, UK). At 70% confluency, the growth medium was aspirated and replaced with growth medium supplemented with the non-specific proteasome inhibitor MG-132 as a positive control (Merck [Calbiochem], Nottingham, UK) at a final concentration of 10 μM for 4 h or lopinavir at a final concentration of 25 μM for 6 h. DMSO-treated control cells were also included. Following the incubation, cells were fixed in 2% paraformaldehyde and counter stained for 10 min using Hoechst nuclear stain at 0.5 μg/ml (Sigma–Aldrich). Expression of the green fluorescence reef coral protein (GFP) was detected through a standard FITC filter using an Olympus widefield microscope (Olympus, Southend-on-Sea, UK). Images were acquired using the Metavue software package (Metavue, Downington, PA, USA).

Analysis of changes in protein expression using antibody microarrays

The Panorama XPRESS Profiler-725 antibody microarray was used according to the manufacturer's instructions (Sigma–Aldrich; Additional file 1). In brief, HPV-positive SiHa cells were grown to 80% confluency before being treated for 6 h with either 25 μM lopinavir or DMSO control. Cells were harvested and total protein extracts from lopinavir and control DMSO-treated SiHa cells were fluorescently labelled with Cy3 fluorophore. The levels of expressed proteins were compared by immunoprobing duplicate antibody microarrays and scanning with a Perkin Elmer ProScanArray fluorescent scanner (PerkinElmer, Waltham, MA, USA). Although Affymetrix full expression profile microarrays require multiple-comparison statistical analysis, the Panorama XPRESS Profiler-725 antibody microarray compares protein expression levels using duplicate antibody spots, combined with a variety of antibodies against house keeping protein for signal normalisation. The

accompanying PerkinElmer ProScanArray fluorescent scanner software was used to convert scan intensities into numerical values and treated versus control cell values plotted for each protein. This analysis produces a ratio rendering the data quantitative. More traditional protein quantitation techniques, such as western blotting were used to validate antibody array results.

RT-PCR

All reverse transcription (RT)-PCR work was carried out using an Applied Biosystems GeneAmp PCR System 2700 (Applied Biosystems, Carlsbad, CA, USA). The 'Cells-to-cDNA™ II Kit' (Invitrogen) was used according to the manufacturer's recommendations to synthesise complementary DNA (cDNA) from SiHa cells treated with either lopinavir (6 h at 25 μM) or DMSO control as previously described [13]. PCR was carried out in a 20 μl reaction volume containing 10 μl Biomix red (Bioline, London, UK), 0.5 μl each of ribonuclease L (RNASEL) forward primer (5′-AGC-AGA-CTC-TGG-AAG-CGT-GTT-T-3′) and reverse primer (5′-TGC-CAG-GTG-AGC-AGC-TTT-CTT-A-3′), and 2 μl cDNA sample. Cycle parameters were as follows: denaturing at 94°C for 5 min, followed by amplification for 32 cycles with denaturing at 94°C for 25 s, annealing at 53–57°C for 25 s, extension at 72°C for 25 s for 33 cycles followed by a final extension period of 3 min at 72°C. HPV16 E6 forward (5′-AAT-GTT-TCA-GGA-CCC-ACA-GG-3′) and reverse (5′-CAT-ACA-GCA-TAT-GGA-TT-CC-C-3′) test primers were used and GAPDH control PCR was carried out using the forward primer (5′- CAT-TGA-CCT-CAA-CTA-CAT-GGT-3′) and reverse primer (5′-TCG-CTC-GTG-GAA-GAT-GGT-GAT-3′).

Western blotting and antibodies used

Protein lysates were prepared from duplicate flasks treated with either lopinavir or DMSO control. Briefly, the growth medium was aspirated, and cells were washed with 1× phosphate-buffered saline (PBS) and detached from the culture flask using pre-warmed trypsin/EDTA (0.25%; Invitrogen) with incubation at 37°C/5% CO_2. Trypsin was then neutralised by addition of 10 ml complete RPMI-1640 medium containing fetal bovine serum. A cell count was carried out and 5×10^5 cells were pelleted by centrifugation at 295 × g. Total protein from 5×10^5 cells, was lysed with 2× Laemmli sample buffer, and separated by 12% SDS PAGE for 2 h. Following this, proteins were transferred onto Hybond C Extra nitrocellulose membranes (Amersham Biosciences, Buckinghamshire, UK) using a semi-dry blotter (Whatman Biometra, Goettingen, Germany). Immunoprobing was carried out as described previously [13], with the following primary antibodies, both supplied by Abcam (Cambridge, UK), polyclonal rabbit anti-RNASEL (ab32307) 1:500 in 1×PBS overnight at +4°C and mouse monoclonal anti-GAPDH (ab9484), 1:1,500 in 1×PBS, 1.5 h at room temperature. This was followed by washing and incubation with appropriate horse radish peroxidase-conjugated secondary antibodies at 1:2,000 in 5% milk powder in PBS for 2 h at room temperature. Swine anti-rabbit and rabbit anti-mouse horse radish peroxidase conjugated secondary antibodies were obtained from Dako, Cambridge, UK. Proteins were visualised using ECL and exposure to hyperfilm (Amersham Biosciences).

Analysis of growth and RNASEL expression in lopinavir-treated E6/E7 immortalised and control PHFKs

Stable E6/E7 immortalised PHFKs were treated with lopinavir at concentrations between 5 μM and 40 μM and cell growth assessed at 72 h by means of the CellTitre 96® AQ_{ueous} One Solution Cell Proliferation Assay (AQ-96 assay; Promega, Southampton, UK). RNASEL protein levels were determined in lopinavir-treated E6/E7 immortalised PHFKs by western blotting as described.

siRNA silencing of RNASEL expression

Four different RNASEL-specific siRNA oligonucleotides (siRNA 1-4) plus AllStars and MAPK control oligonucleotides with no significant off-target homology were designed and obtained from Qiagen (Flexitube siRNA system; West Sussex, UK; siRNA-1, 5′-CCA-GAC-TAC-ACT-AGT-CCA-TAA-3′; siRNA-2, 5′-CAA-GTG-GAC-GAC-TAA-GAT-TAA-3′; siRNA-3, 5′-CAG GAA-GTC-AAG-AGA-GAT-CTA-3′; siRNA-4, 5′-CCC-TAT-GAT-TGG-CAA-ACT-CAA-3′). These were transiently transfected into SiHa cells using Lipofectamine-2000 reagent according to the manufacturer's instructions (Invitrogen). RNASEL down-regulation was assessed by western blot 24 h post-transfection following 6 h of treatment with 25 μM lopinavir. SiHa cells were seeded in 96-well plates and transfected with siRNA-1 or the AllStars negative control as described above. Twenty four h post-transfection the growth medium was aspirated and replaced with fresh medium and initial cell viability determined by means of the AQ-96 assay. Growth medium in the remaining wells was supplemented with lopinavir to final concentrations of 20 μM, 25 μM, 30 μM or DMSO control. AQ-96 assay was then used to assess cell viability at each lopinavir concentration at 24, 48 and 72 h. Every data point was the result of three separate assays from three separately transfected wells.

Results

Lopinavir inhibits proteasome activity

Our previous studies have shown that lopinavir-treated cervical cancer cell culture lysates have decreased

Figure 1. Lopinavir inhibits the proteasome in SiHa cells

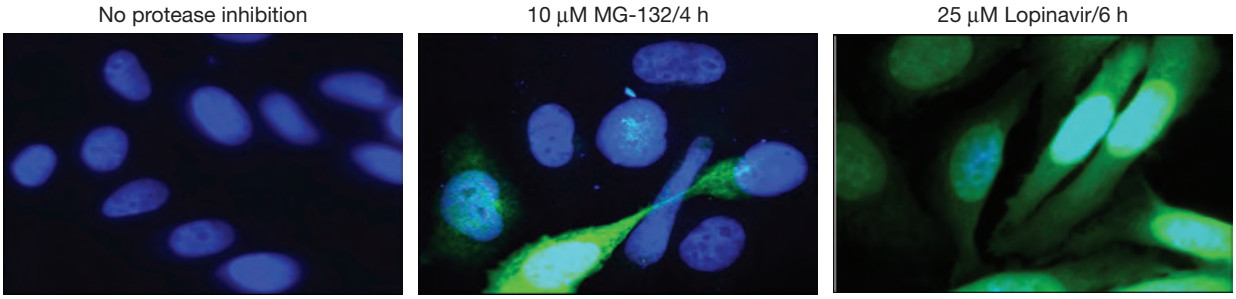

Fluorescent microscopy analysis of stable transfected SiHa cells expressing the proteasome sensor vector pZsProSensor-1. Cells were treated with either lopinavir or MG-132 at final concentrations of 25 μM and 10 μM, respectively. Control cells were treated with DMSO. Green fluorescent protein (GFP) was visualised using a fluorescein isothiocyanate filter on an Olympus Heinrich widefield microscope. MG-132- and lopinavir-treated cells demonstrated high levels of GFP when compared to control DMSO-treated transfected cells.

proteasome activity [13]. In order to verify this finding *in vivo* the SiHa HPV-positive cervical cancer cell line was stably transfected with the pZsProSensor-1 vector. This allows real-time monitoring of the proteasome in living cells, whereby addition of proteasome-inhibiting drugs results in accumulation of the fluorescent rapidly degraded proteasome target ZS-Green(GFP)/murine ornithine decarboxylase fusion protein encoded by the vector. The pZsProSensor-1 transfected SiHa cells were treated with lopinavir, the known proteasome inhibitor MG132 or a DMSO control. Lopinavir and MG132 produced a marked increase in detectable GFP levels when compared to DMSO-treated cells (Figure 1), demonstrating that, in a similar fashion to MG132, lopinavir has the ability to inhibit proteasomal activity. As the proteasome is a major cellular mechanism for regulating the concentration of a wide range of proteins, it follows that treatment of SiHa cells with lopinavir will result in changes in the cellular protein expression profile. Antibody microarray screening was therefore utilised in order to assess the extent of these changes on a number of proteins.

Lopinavir induces specific changes in protein expression in SiHa cells

Of the 725 proteins on the antibody array representing a wide range of biological pathways, 38 showed altered expression levels after lopinavir treatment (Table 1). Only three showed a reduction in levels whilst the remaining proteins all showed a drug-induced increase. A detailed discussion of the potential significance of all of these changes is beyond the scope of this communication. However, for information, we have tabulated the main functions currently ascribed to these proteins based on published literature searches. Significantly, several classical apoptosis-related proteins were up-regulated such as annexin 5, tumour necrosis factor, active caspase 3, Tp63 and Tp53. This finding was relevant as it substantiated our previous work where we demonstrated apoptotic cell death in HPV-positive SiHa cells following lopinavir treatment. Of particular interest, however, was the upregulation of the interferon-induced RNASEL since it had previously been reported to have antiviral activity [17,18]. Figure 2A highlights the differential RNASEL antibody array protein signal we obtained from lopinavir versus control DMSO-treated SiHa cells. This was confirmed by immuno-probing a western blot of proteins isolated from these cells where a significant up-regulation of RNASEL was observed (Figure 2B). Since RT-PCR demonstrated no obvious difference in the RNASEL messenger RNA levels between replicate DMSO-treated control and lopinavir-treated SiHa cells (Figure 2C) these data support the hypothesis that lopinavir inhibits proteasomal degradation of the RNASEL protein and this was prioritised for further study.

Lopinavir induces both dose- and time-dependent changes in RNASEL protein levels in SiHa cells but has no effect on CaSki cells

To further investigate the association between lopinavir treatment of SiHa cells and variations in RNASEL protein levels, both dose- and time-dependent effects were assessed. Lopinavir produced a clear dose-dependent increase in RNASEL levels over a range of concentrations tested (Figure 3A). This was repeated on a second HPV-positive cervical carcinoma cell line, CaSki, which we had previously reported as refractory to lopinavir treatment [13]. No evidence of RNASEL up-regulation was observed in CaSki cells, which is interesting in light of the fact that they express much higher

Table 1. Summary of proteins with altered expression levels following exposure of SiHa cells to lopinavir

Gene	Protein name	Function/association	Fold change
ANXA5	Annexin 5	Calcium-binding protein	2.15
CTBP1 (C-terminal)[a]	C-Terminal binding protein 1	Transcription regulatory protein	1.87
CHEK2[a]	CHK2 checkpoint homolog	Serine/threonine kinase	1.84
RAB5A	Ras related protein Rab 5A	GTPase	1.84
RNASEL[a]	Ribonuclease L	Ribonuclease	1.76
ACTR3	Actin related protein 3	Cytoskeletal protein	1.73
GRB2	Growth factor receptor bound protein 2	Adapter molecule	1.73
SYNPO	Synaptopodin	Cytoskeletal-associated protein	1.72
CASP3	Caspase 3 (active)	Cysteine protease	1.69
EGF	Epidermal growth factor	Growth factor	1.68
TP63[a]	Tumour protein p63	Transcription factor	1.68
BIRC5[a]	Survivin	Adapter molecule	1.67
ILK[a]	Integrin-linked kinase	Serine/threonine kinase	1.59
ERK2	Mitogen-activated protein kinase 1	Serine/threonine kinase	1.56
SYNPO	Synaptopodin	Cytoskeletal-associated protein	1.56
SNCA	α-Synuclein	Chaperone protein	1.56
PADI4	Peptidylarginine deiminase 4	Enzyme: hydrolase	1.52
CHEK1[a]	Cell cycle checkpoint kinase	Serine/threonine kinase	1.52
TUB	Tubulin/tyrosine	Cytoskeletal-associated protein	1.50
NOS1[a]	Nitric oxide synthase 1	Enzyme: synthase	1.50
CTBP1 (N-terminal)[a]	C-Terminal binding protein 1	Transcription regulatory protein	1.49
TNF	Tumour necrosis factor-α	Ligand	1.48
H2AFX	H2A Histone Family, member X	DNA binding protein	1.47
AKT1[a]	Protein kinase B-alpha	Serine/threonine kinase	1.47
CHEK2[a]	CHK2 checkpoint homolog	Serine/threonine kinase	1.47
FANCD2[a]	Fanconi anemia, complementation group D2	Cell cycle control protein	1.47
DIABLO[a]	SMAC protein	Cell cycle control protein	1.46
PAWR	PRKC, apoptosis, WT1, regulator	Transcription regulatory protein	1.45
ILK[a]	Integrin-linked kinase	Serine/threonine kinase	1.45
MC3R	Melanocortin 3 receptor	Cell surface receptor	1.44
APP	Amyloid precursor protein	Receptor activity	1.43
MKI67[a]	MKI67 (FHA domain) interacting nucleolar phosphoprotein	RNA-binding protein	1.43
CFL2[a]	Cofilin 2	Cytoskeletal-associated protein	1.38
DMD[a]	Dystrophin	Structural protein	1.37
CENPE	Centromeric protein E	DNA-binding protein	1.36
PTK2(pp125)	Focal adhesion kinase 2 (pp125)	Tyrosine kinase	1.35
TP53[a]	Tumour protein p53	Transcription factor	1.28
DMD[a]	Dystrophin	Structural protein	1.25
TP53[a]	Tumour protein p53	Transcription factor	1.18
GJA1[a]	Connexin 43	Membrane transport protein	0.76
GFAP	Glial fibrillary acidic protein	Structural protein	0.63
GJA1[a]	Connexin 43	Membrane transport protein	0.60

Different antibodies against the same protein are represented more than once on the array. Since fold changes shown are based on duplicate data points, statistical significance has not yet been assigned. Thus, other than RNASEL, these results require immunoblot confirmation. [a]These proteins are known to be subject to proteasomal degradation.

levels of HPVT16 E6 (Figure 3B). SiHa cells were then tested further by treating with a fixed concentration of lopinavir (25 μM) and RNASEL levels assessed at various time points (Figure 3C). There was a clear time-dependent increase of RNASEL protein over the 2 h intervals up to 12 h of treatment. This was followed by drop in level at 24 h. However, as the housekeeping GAPDH control signal also dropped at 24 h this was likely due to the previously reported toxic effects of 25 μM lopinavir at this time point [13].

Lopinavir induces selective toxicity against E6/E7 immortalised PHFKs with an associated up-regulation of RNASEL

The SiHa cervical carcinoma cell line has proved itself as a useful laboratory tool and has been used

extensively by many groups over the last 40 years. It is, however, a fully transformed cell line and if lopinavir is to be used as a topical treatment for the *pre*-cancerous target cells that are present in HPV-related cervical dysplasia, then cells more representative of the intended cell type should also be tested. For this reason it was decided to investigate the effects of lopinavir against HPV16 E6/E7 immortalised primary human foreskin keratinocytes (PHFKs) and control PHFKs which were treated over a 72 h period using a dose range of 5–40 μM (Figure 4A). This demonstrated greatly increased toxicity of lopinavir for E6/E7-expressing PHFKs when compared to normal (non-transduced) PHFKs. While the growth of normal PHFKs progressed relatively uninhibited up to concentrations of 25 μM, both SiHa and E6/E7 PHFKs showed markedly reduced growth. Furthermore, RNASEL protein levels in E6/E7 transduced PHFKs also increased, albeit at a slower rate than was observed in SiHa cells (Figure 4B). While 25 μM lopinavir treatment caused a peak RNASEL signal in SiHa cells after 8 h and a subsequent drop after 24 h (Figure 3B), E6/E7-expressing PHFKs peaked at 48 h followed by a subsequent drop after 72 h (Figure 4B).

siRNA-targeted silencing of RNASEL reduces the toxicity of lopinavir in SiHa cells

An extensive reduction in RNASEL protein level was seen following transfection with four different RNASEL targeting siRNAs and siRNA oligonucleotide 1 (siRNA-1) was found to be the most effective (Figure 5A) and was used in subsequent experiments. The effects of transfection with siRNA-1, or the AllStar negative control on SiHa cell growth in the presence of DMSO control or different concentrations of lopinavir was assessed. Both AllStar and siRNA-1 transfected cells treated with DMSO control showed steady growth over the whole 72 h period (Figure 5B) although siRNA-1 transfected cells had a modest growth advantage. Exposure of identically transfected cells to 20, 25 and 30 μM concentrations of lopinavir demonstrated a dose-dependent inhibition of growth over 72 h (Figure 5C, 5D and 5E).

Figure 2. Lopinavir induces an up-regulation of the RNASEL protein in SiHa cells

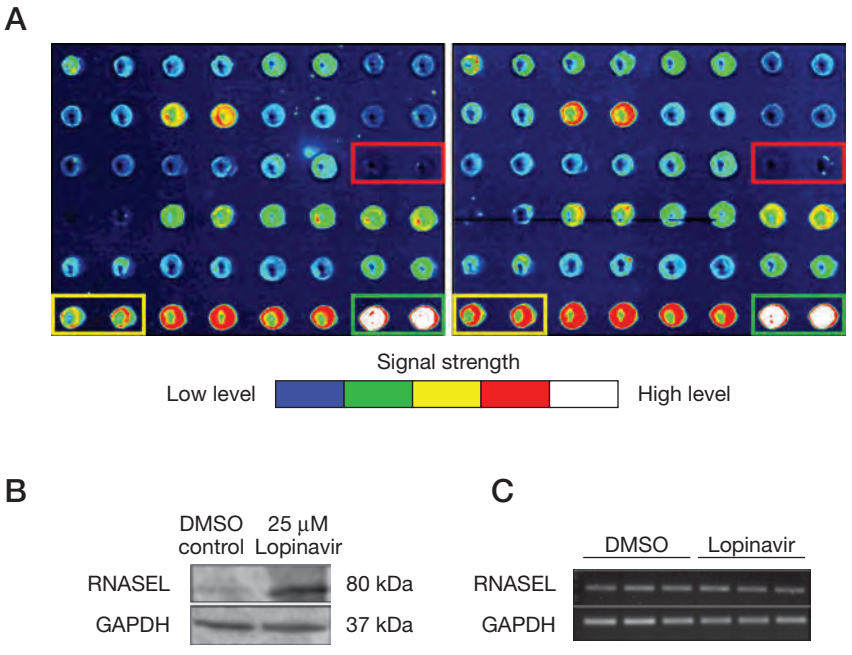

(A) The antibody array Cy3 fluorophore signal obtained for ribonuclease L (RNASEL). Protein levels are colour coded from low expression in blue, through to high protein expression in white. The left and right panels represent the untreated and treated protein lysates, respectively. The red boxed pair, on each panel, represents an internal negative control in duplicate, whilst the green boxes represent the positive control. The yellow boxed pair of signals represents duplicate spots of the RNASEL antibody which have increased signals following lopinavir treatment. **(B)** Western blot of protein lysates prepared from duplicate lopinavir-treated and DMSO control SiHa cells as used for the antibody microarray. These were immunoprobed with rabbit anti-RNASEL using anti-GAPDH as loading control. Lopinavir treatment caused an increase in the levels of RNASEL protein, when compared to DMSO-treated control cells. **(C)** Agarose gel electrophoresis of RNASEL primer specific reverse transcription-PCR products derived from messenger RNA isolated from lopinavir or DMSO-treated SiHa cells. No significant increase in RNASEL messenger RNA was found following lopinavir treatment when compared to DMSO-treated control cells.

Figure 3. Lopinavir induces a dose- and time-dependent increase in levels of the RNASEL protein in SiHa but not CaSki cells

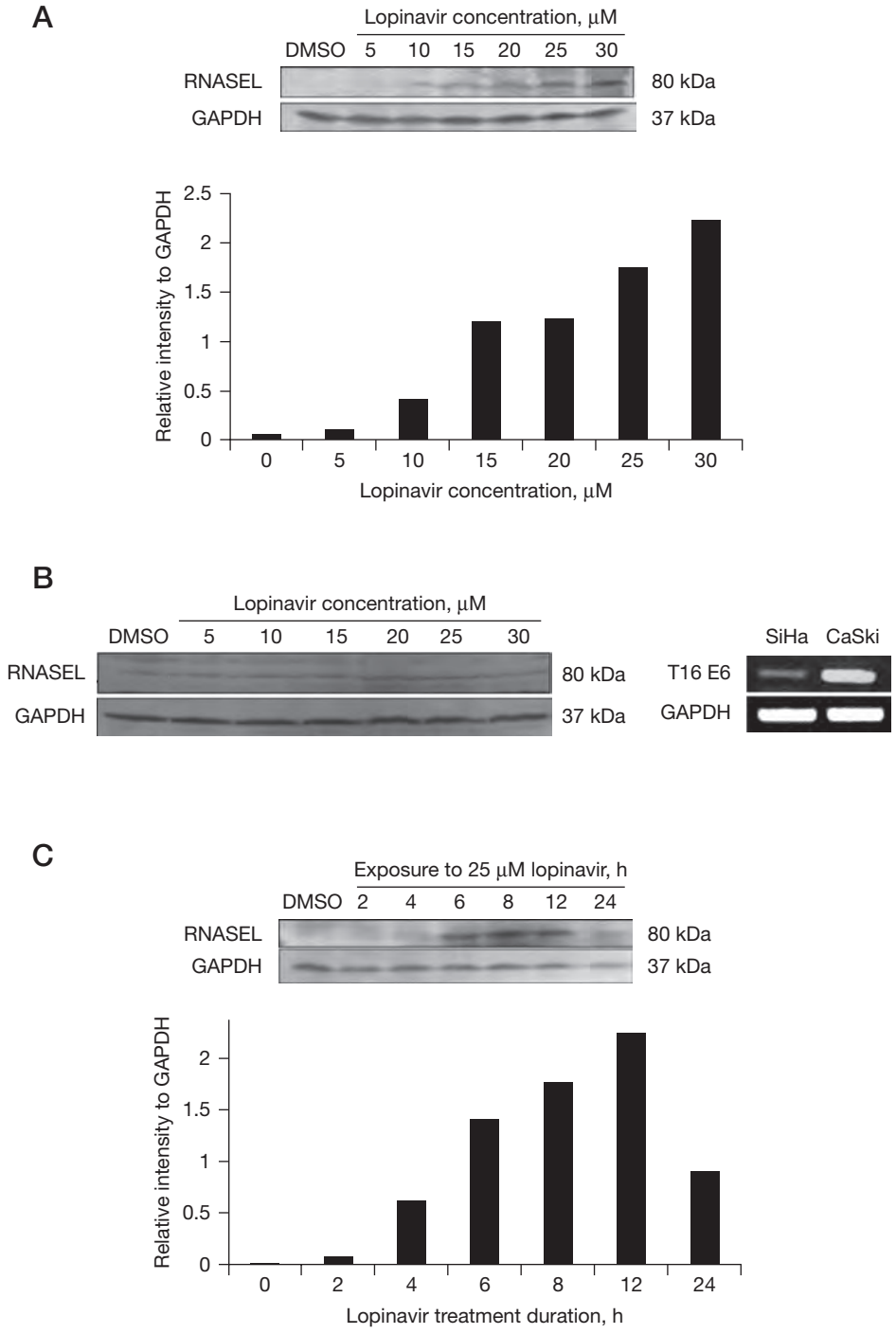

(A) Western blot and quantitative densitometry of proteins isolated from SiHa cells treated with increasing doses of lopinavir and immunoprobed with ribonuclease L (RNASEL) and GAPDH antibodies. Lopinavir produced a clear dose-dependent increase in RNASEL protein levels. **(B)** Western blot of proteins isolated from CaSki cells treated with increasing doses of lopinavir and immunoprobed with RNASEL and GAPDH antibodies. Lopinavir did not increase the levels of RNASEL in these cells. Reverse transcription-PCR analysis of T16 E6 and GAPDH expression showing much higher levels of E6 messenger RNA are present in CaSki than in SiHa cells. **(C)** Western blot and quantitative densitometry of SiHa cells treated with DMSO or lopinavir at a final concentration of 25 μM. Cells were harvested at the times indicated and immuno-probed with RNASEL and GAPDH antibodies. Lopinavir produced a time-dependent increase in RNASEL protein levels, with a peak occurring after approximately 12 h incubation with lopinavir. This peak was followed by a decrease in protein levels observed at 24 h.

At a 25 μM concentration of lopinavir, siRNA-1 transfected cells showed a significant ($P<0.05$ at 72 h) growth advantage over AllStar transfected cells (Figure 5D), whereas at 30 μM there was equivalent growth inhibition (Figure 5E). This finding is consistent with the observed toxic effects of lopinavir on E6/E7 immortalised and control PHFKs shown in Figure 4A where the growth of normal PHFKs was unaffected at concentrations up to 25 μM lopinavir, whereas at 30 μM they were inhibited by this treatment. The data from the RNASEL silencing experiments thus provides strong evidence that this protein plays a role in the observed selective toxicity of lopinavir in HPV E6/E7 cells up to an optimum concentration of 25 μM.

Discussion

Our data are the first to show that the HIV protease inhibitor lopinavir induces an increase in the levels of the RNASEL protein in HPV-positive cervical carcinoma cells and in stable HPV16 E6/E7 transfected human keratinocytes. Lopinavir was also shown to have enhanced toxicity against E6/E7 immortalised PHFKs when compared to normal PHFKs and our results are consistent with RNASEL contributing to this selective toxicity.

In agreement with the results shown in Figure 1, other groups have shown lopinavir can induce selective inhibition of the proteasome and this ability is thought to play a significant role in the anti-HIV effects of this, and other related compounds [19–22]. In addition to HIV, many viruses including HPV, have been shown to subvert/hijack the activity of the host proteasome in order to eliminate proteins that would be detrimental to viral persistence [23]. In HPV-infected cells the E6 and E7 oncoproteins are largely responsible for this activity, whereby they signal the destruction of selected cellular proteins (for example, p53 and Rb) in order to execute the viral life cycle [24].

Based on these observations, we opted to use antibody array screening of lopinavir-treated SiHa cells to analyse changes in protein expression following this treatment. This identified a whole range of cellular

Figure 4. Lopinavir shows selective toxicity against E6/E7 immortalised versus normal control PHFK cells with an associated increase in RNASEL

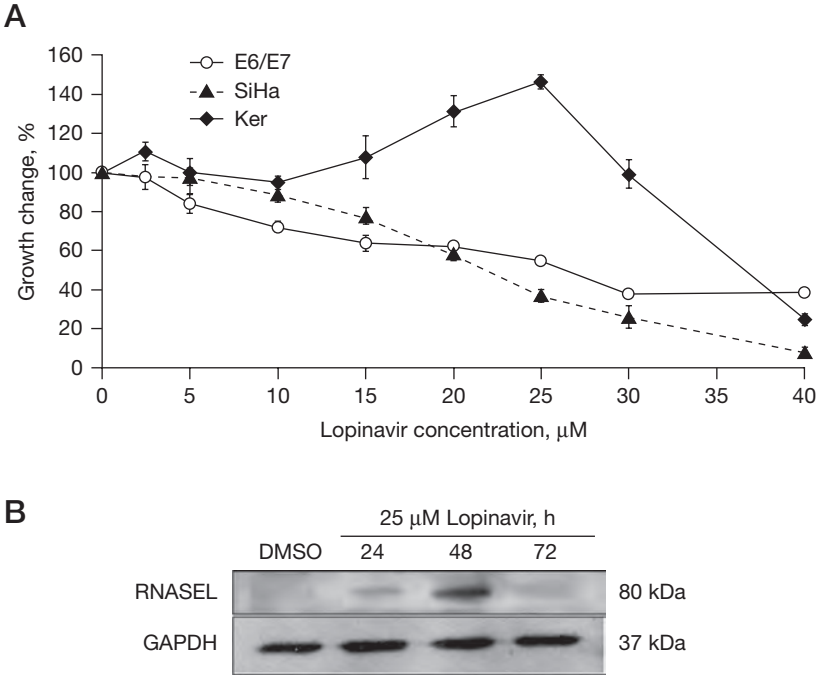

(A) E6/E7 immortalised primary human foreskin keratinocytes (PHFKs), normal PHFKs (Ker) and SiHa cells were treated for 72 h with lopinavir over a dose range of 5–40 μM. Cell growth was assessed and expressed in terms of percentage growth change when compared to untreated control cells. Mean values ± standard deviations were based on triplicate data points which were calculated in Microsoft Excel 2003 (Microsoft, Redmond, WA, USA). **(B)** Western blot of proteins isolated from E6/E7 immortalised PHFKs treated from 24 to 72 h with 25 μM lopinavir immunoprobed with ribonuclease L (RNASEL) and GAPDH antibodies. A time-dependent increase in RNASEL was observed which peaked at 48 h of incubation.

Figure 5. siRNA-mediated gene silencing of RNASEL reduces the toxicity of lopinavir in SiHa cells

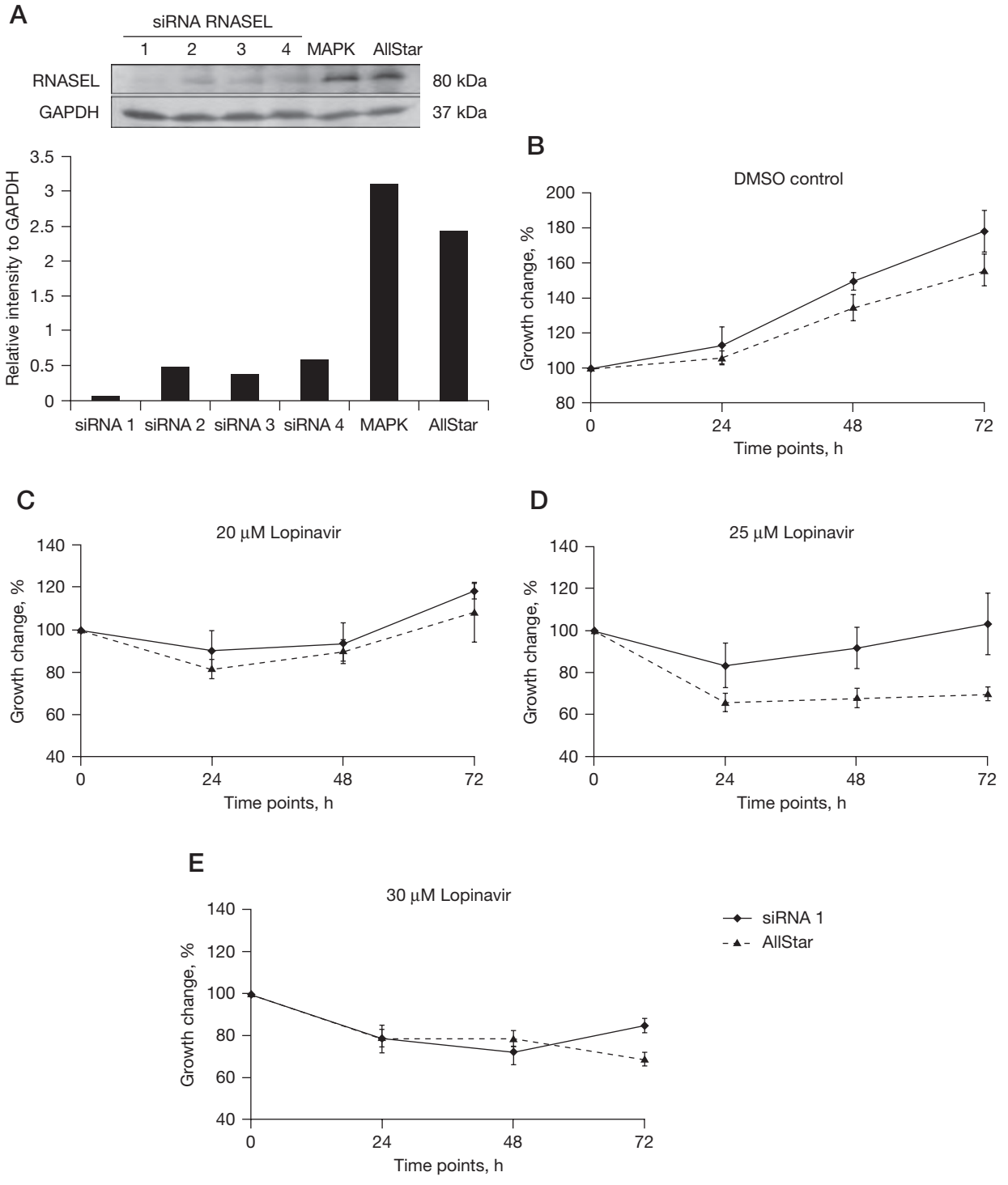

(A) Western blot and quantitative densitometry of ribonuclease L (RNASEL) expression in proteins isolated from lopinavir-treated (25 μM for 6 h) SiHa cells transiently transfected with RNASEL small interfering RNAs (siRNAs; 1–4) in addition to AllStar and mitogen activated protein kinase (MAPK) siRNA controls. **(B–E)** 72-h cell proliferation assays were carried out 24 h after RNASEL siRNA 1 or control AllStar siRNA transfection of SiHa cells. Cells were treated with DMSO, or 20 μM, 25 μM or 30 μM concentrations of lopinavir respectively, and cell proliferation recorded over 72 h. Mean values ± standard deviations were based on triplicate data points and were calculated in Microsoft Excel 2003 (Microsoft, Redmond, WA, USA). A Student *t*-test was performed using Microsoft Excel 2003 (Microsoft) and *P*-values <0.05 were considered significant.

proteins that were up-regulated (Table 1), including Tp53 which is consistent with our previously reported findings [13]. Indeed, as we have discussed, lopinavir induced changes in the levels of several other apoptosis-related proteins and it is also significant that the majority of the proteins listed in Table 1 are known to be regulated by proteasomal degradation. On this point, an interesting finding was the observed lopinavir-induced down-regulation of GFAP which is known to be capable of inhibiting the proteasome [25]. Since p53 is a target of high-risk HPV E6, we searched the Virus Molecular INTeraction (VirusMINT) database [26] for any other known E6 and E7 targeted proteins which are affected by lopinavir treatment (Table 1). At this time, only Tp53 is a confirmed target of high-risk HPV.

Given that SiHa cells are a fully malignant cell type, we opted to investigate the toxicity of lopinavir against E6/E7 immortalised and normal control PHFKs. This showed that at a concentration of 25 μM, lopinavir up-regulated RNASEL expression in the E6/E7 cells which were much more susceptible to lopinavir-induced cell death than control PHFKs. At higher concentrations of drug, this selectivity was lost and these data indicate that lopinavir has a good therapeutic index for E6/E7 PHFKs at concentrations up to 25 μM. Since these cells are not transformed it is most likely that this is due to the ability of lopinavir to activate apoptotic antiviral systems which are suppressed by E6/E7.

Curiously, it is known that HIV patients receiving oral lopinavir as part of HAART do not show enhanced clearance of HPV-related lesions [27]. On this point, it is noteworthy that the concentration of lopinavir found in the vaginal fluid of HIV patients taking oral Kaletra is <2 μM [28], which has been discussed in our previous study [13].

In order to address the issue of whether the observed HPV-specific toxicity of lopinavir is related to its ability to block RNASEL degradation by E6/E7, siRNA RNASEL gene silencing experiments were carried out in lopinavir-treated SiHa cells. These experiments showed that, at the optimum therapeutic dose range of 25 μM, lopinavir had much reduced toxicity in RNASEL siRNA transfected SiHa cells when compared to the same cells transfected with AllStar control siRNA. These results support the hypothesis that the selective toxicity of lopinavir in HPV E6/E7 expressing cells is at least in part mediated by up-regulated expression of the RNASEL protein.

It is also notable that our results support the conclusion that HPV can compromise the antiviral activity of RNASEL. The observation that CaSki cells are insensitive to lopinavir [13] and do not up-regulate RNASEL is significant since CaSki cells express much higher levels of E6 than do SiHa (Figure 3B). Indeed, investigation of the effects of E6 on RNASEL toxicity is the subject of our continued work.

Thus, the logical conclusion from these observations is that inactivation of the RNASEL response by HPV infection of the cervix could lower host antiviral defences and increase the likelihood of infection with other viruses. This is highly significant when considered with the previously discussed findings that genital HPV infections can predispose to increased risk of HIV transmission in both men and women [29,30].

In conclusion, our data support the potential use of lopinavir as a topical, self-administered treatment for HPV-related cervical dysplasia. If successful, this treatment would be particularly useful in low-resource countries which lack cytology screening and surgical services, and where HIV infection is often a significant additional complication. With current pricing strategies, anti-HPV vaccines are not an option in such settings, and as previously discussed, they will most likely have reduced efficacy in HIV-positive women. Furthermore, in view of the observation that infection with HPV can enhance the sexual transmission of HIV in both men and women [29,30], this clearly indicates that a simple, non-surgical treatment for HPV-related precancerous lesions may not only reduce the burden of cervical cancer but may also reduce the chances of HIV transmission.

Acknowledgements

This work was primarily funded by the Humane Research Trust, Stockport, UK. Work in the Gynaecological Oncology labs is also supported by the Cancer Prevention Research Trust and the Caring Cancer Research Trust. AO is the Humane Research Trust Monica Lumsden post doctoral fellow. The IZ laboratories are funded by the National Science and Engineering Council Canada. AWO and IZ both contributed equally to this work.

Disclosure statement

The authors declare no competing interests.

Additional file

Additional file 1: An antibody array schematic can be found at http://www.intmedpress.com/uploads/documents/AVT-10-OA-1889_Batman_Add_file1.pdf

References

1. zur Hausen H. Papillomavirus infections – a major cause of human cancers. *Biochim Biophys Acta* 1996; **1288:**F55–F78.
2. Walboomers JM, Jacobs MV, Manos MM, *et al*. Human papillomavirus is a necessary cause of invasive cervical cancer worldwide. *J Pathol* 1999; **189:**12–19.

3. Castellsagué X. Natural history and epidemiology of HPV infection and cervical cancer. *Gynecol Oncol* 2008; **110:**S4–S7.
4. Muñoz N, Bosch FX, de Sanjose S, *et al*. Epidemiologic classification of human papillomavirus types associated with cervical cancer. *N Engl J Med* 2003; **348:**518–527.
5. Peto J, Gilham C, Fletcher O, Matthews FE. The cervical cancer epidemic that screening has prevented in the UK. *Lancet* 2004; **364:**249–256.
6. Ellerbrock TV, Chiasson MA, Bush TJ, *et al*. Incidence of cervical squamous intraepithelial lesions in HIV-infected women. *JAMA* 2000; **283:**1031–1037.
7. Lima MI, Tafuri A, Araujo AC, de Miranda Lima L, Melo VH. Cervical intraepithelial neoplasia recurrence after conization in HIV-positive and HIV-negative women. *Int J Gynaecol Obstet* 2009; **104:**100–104.
8. Heard I, Palefsky JM, Kazatchkine MD. The impact of HIV antiviral therapy on human papillomavirus (HPV) infections and HPV-related diseases. *Antivir Ther* 2004; **9:**13–22.
9. Wright TC, Jr., Subbarao S, Ellerbrock TV, *et al*. Human immunodeficiency virus 1 expression in the female genital tract in association with cervical inflammation and ulceration. *Am J Obstet Gynecol* 2001; **184:**279–285.
10. Garland SM, Smith JS. Human papillomavirus vaccines: current status and future prospects. *Drugs* 2010; **70:**1079–1098.
11. Ali-Risasi C, Praet M, Van Renterghem L, *et al*. [Human papillomavirus genotype profile in Kinshasa, Democratic Republic of the Congo: implications for vaccination]. *Med Trop (Mars)* 2008; **68:**617–620. French.
12. McKenzie ND, Kobetz EN, Hnatyszyn J, Twiggs LB, Lucci JA, III. Women with HIV are more commonly infected with non-16 and -18 high-risk HPV types. *Gynecol Oncol* 2010; **116:**572–577.
13. Hampson L, Kitchener HC, Hampson IN. Specific HIV protease inhibitors inhibit the ability of HPV16 E6 to degrade p53 and selectively kill E6-dependent cervical carcinoma cells *in vitro*. *Antivir Ther* 2006; **11:**813–825.
14. Kim DH, Jarvis RM, Xu Y, *et al*. Combining metabolic fingerprinting and footprinting to understand the phenotypic response of HPV16 E6 expressing cervical carcinoma cells exposed to the HIV anti-viral drug lopinavir. *Analyst* 2010; **135:**1235–1244.
15. Kim DH, Jarvis RM, Allwood JW, *et al*. Raman chemical mapping reveals site of action of HIV protease inhibitors in HPV16 E6 expressing cervical carcinoma cells. *Anal Bioanal Chem* 2010; **398:**3051–3061.
16. Richard C, Lanner C, Naryzhny SN, *et al*. The immortalizing and transforming ability of two common human papillomavirus 16 E6 variants with different prevalences in cervical cancer. *Oncogene* 2010; **29:**3435–3445.
17. Bisbal C, Silverman RH. Diverse functions of RNase L and implications in pathology. *Biochimie* 2007; **89:**789–798.
18. Sadler AJ, Williams BR. Interferon-inducible antiviral effectors. *Nat Rev Immunol* 2008; **8:**559–568.
19. Piccinini M, Rinaudo MT, Chiapello N, *et al*. The human 26S proteasome is a target of antiretroviral agents. *AIDS* 2002; **16:**693–700.
20. Klinger PP, Schubert U. The ubiquitin-proteasome system in HIV replication: potential targets for antiretroviral therapy. *Expert Rev Anti Infect Ther* 2005; **3:**61–79.
21. Piccinini M, Rinaudo MT, Anselmino A, *et al*. The HIV protease inhibitors nelfinavir and saquinavir, but not a variety of HIV reverse transcriptase inhibitors, adversely affect human proteasome function. *Antivir Ther* 2005; **10:**215–223.
22. Parker RA, Flint OP, Mulvey R, *et al*. Endoplasmic reticulum stress links dyslipidemia to inhibition of proteasome activity and glucose transport by HIV protease inhibitors. *Mol Pharmacol* 2005; **67:**1909–1919.
23. Banks L, Pim D, Thomas M. Viruses and the 26S proteasome: hacking into destruction. *Trends Biochem Sci* 2003; **28:**452–459.
24. Moody CA, Laimins LA. Human papillomavirus oncoproteins: pathways to transformation. *Nat Rev Cancer* 2010; **10:**550–560.
25. Tang G, Perng MD, Wilk S, Quinlan R, Goldman JE. Oligomers of mutant glial fibrillary acidic protein (GFAP) inhibit the proteasome system in alexander disease astrocytes, and the small heat shock protein alphaB-crystallin reverses the inhibition. *J Biol Chem* 2010; **285:**10527–10537.
26. Chatr-aryamontri A, Ceol A, Peluso D, *et al*. VirusMINT: a viral protein interaction database. *Nucleic Acids Res* 2009; **37:**D669–D673.
27. De Vuyst H, Lillo F, Broutet N, Smith JS. HIV, human papillomavirus, and cervical neoplasia and cancer in the era of highly active antiretroviral therapy. *Eur J Cancer Prev* 2008; **17:**545–554.
28. Kwara A, Delong A, Rezk N, *et al*. Antiretroviral drug concentrations and HIV RNA in the genital tract of HIV-infected women receiving long-term highly active antiretroviral therapy. *Clin Infect Dis* 2008; **46:**719–725.
29. Smith-McCune KK, Shiboski S, Chirenje MZ, *et al*. Type-specific cervico-vaginal human papillomavirus infection increases risk of HIV acquisition independent of other sexually transmitted infections. *PLoS ONE* 2010; **5:**e10094.
30. Smith JS, Moses S, Hudgens MG, *et al*. Increased risk of HIV acquisition among Kenyan men with human papillomavirus infection. *J Infect Dis* 2010; **201:**1677–1685.

Accepted 19 January 2011; published online 3 May 2011

Anal Bioanal Chem (2010) 398:3051–3061
DOI 10.1007/s00216-010-4283-6

ORIGINAL PAPER

Raman chemical mapping reveals site of action of HIV protease inhibitors in HPV16 E6 expressing cervical carcinoma cells

Dong-Hyun Kim · Roger M. Jarvis · J. William Allwood · Gavin Batman · Rowan E. Moore · Emma Marsden-Edwards · Lynne Hampson · Ian N. Hampson · Royston Goodacre

Received: 17 August 2010 / Revised: 28 September 2010 / Accepted: 29 September 2010 / Published online: 19 October 2010

Abstract It has been shown that the HIV protease inhibitors indinavir and lopinavir may have activity against the human papilloma virus (HPV) type 16 inhibiting HPV E6-mediated proteasomal degradation of p53 in cultured cervical carcinoma cells. However, their mode and site of action is unknown. HPV-negative C33A cervical carcinoma cells and the same cells stably transfected with E6 (C33AE6) were exposed to indinavir and lopinavir at concentrations of 1 mM and 30 μM, respectively. The intracellular distribution of metabolites and metabolic changes induced by these treatments were investigated by Raman microspectroscopic imaging combined with the analysis of cell fractionation products by liquid chromatography–mass spectrometry (LC-MS). A uniform cellular distribution of proteins was found in drug-treated cells irrespective of cell type. Indinavir was observed to co-localise with nucleic acid in the nucleus, but only in E6 expressing cells. Principal components analysis (PCA) score maps generated on the full Raman hypercube and the corresponding PCA loadings plots revealed that the majority of metabolic variations influenced by the drug exposure within the cells were associated with changes in nucleic acids. Analysis of cell fractionation products by LC-MS confirmed that the level of indinavir in nuclear extracts was approximately eight-fold greater than in the cytoplasm. These data demonstrate that indinavir undergoes enhanced nuclear accumulation in E6-expressing cells, which suggests that this is the most likely site of action for this compound against HPV.

Keywords HPV · Indinavir · Lopinavir · Raman chemical mapping · LC-MS

Electronic supplementary material The online version of this article (doi:10.1007/s00216-010-4283-6) contains supplementary material, which is available to authorized users.

D.-H. Kim · R. M. Jarvis · J. W. Allwood · R. Goodacre
School of Chemistry, Manchester Interdisciplinary Biocentre,
The University of Manchester,
131 Princess Street,
Manchester M1 7DN, UK

G. Batman · L. Hampson · I. N. Hampson
Gynaecological Oncology Laboratories,
School of Cancer & Enabling Sciences, St Mary's Hospital,
The University of Manchester,
Manchester M13 9WL, UK

R. E. Moore · E. Marsden-Edwards
Waters Corporation,
Atlas Park, Simonsway,
Manchester M22 5PP, UK

R. Goodacre (✉)
Manchester Centre for Integrative Systems Biology (MCISB),
Manchester Interdisciplinary Biocentre,
The University of Manchester,
131 Princess Street,
Manchester M1 7DN, UK
e-mail: roy.goodacre@manchester.ac.uk

Introduction

Globally, an estimated 493,000 women are affected by cervical cancer resulting in a staggering 273,500 deaths each year (National Cervical Cancer Coalition; www.nccc-online.org). Indeed, in many low-resource countries, it is the greatest cause of women's cancer-related mortality. Human papilloma virus (HPV) is the major cause of cervical cancer [1], and there are >120 different types of HPV associated with a variety of clinical lesions [2]. There are approximately 13 so-called high-risk types which are associated with cervical cancers [1, 3], although HPV16

and 18 are the most prevalent high-risk types, accounting for >60% of cases [4, 5].

Surgery is currently the treatment of choice for HPV-related pre-cancerous cervical intraepithelial neoplasia [4, 6]. However, since it carries an increased risk of infertility, this is restricted to high-grade disease [7].

Many countries are implementing prophylactic anti-HPV vaccination programmes, yet these primarily protect against types 16 and 18 only, which leaves a significant proportion of high-risk HPV-related disease unprotected. Furthermore, vaccination is most effective when given to women prior to HPV infection, and it is expensive. Thus, since cervical cancer can take from 10 to 20 years to develop, persistently infected women will still be at risk for many years, particularly in low-resource countries that cannot afford vaccination. It is also notable that such countries do not have routine cervical screening services. Thus, it is clear that a low-cost, self-applied treatment for HPV-related disease would have many benefits, particularly in low-resource settings.

The E6 and E7 viral oncoproteins from high-risk types of HPV are responsible for their oncogenic properties, and their continued expression is essential for the growth and survival of HPV transformed cells [8]. We have previously shown that the anti-HIV protease inhibitors (HIV PIs) indinavir and lopinavir inhibit E6-mediated proteasomal degradation of p53 and selectively kill E6-dependant cervical carcinoma cells *in vitro* [9]. We have also recently shown that these compounds cause very specific alterations in the metabolism of cultured E6-expressing cervical carcinoma cells [10]. Indeed, anti-HIV drugs are now becoming increasingly recognised as having significant off-target antineoplastic properties [11]. However, the site and mode of action of this type of drug with respect to HPV is unknown. In order to address this question, we used Raman microspectroscopic imaging to investigate changes in the intracellular distribution of metabolites and macromolecules, and the subcellular location of indinavir and lopinavir in control cervical carcinoma cells treated with these compounds.

Materials and methods

Cell line and culture medium

HPV-negative human C33A cervical carcinoma cells were maintained in RPMI 1640 (Invitrogen, Paisley, UK) supplemented with 10% foetal bovine serum and 2 mM L-glutamine (Sigma-Aldrich Company Ltd., Dorset, UK; complete medium) at 37 °C, 5% CO_2. C33A cells stably transfected with HPV16 E6 (termed "C33AE6") and the pcDNA3.1 control vector (termed "C33AV") were derived and cultured as previously described [12].

Protease inhibitor

Indinavir was obtained through the NIH AIDS Research and Reference Reagent Program (Division of AIDS, NIAID, NIH): indinavir sulphate (8145). Lopinavir was provided as a generous gift from Abbott Laboratories (Park Road, Abbott Park, IL 60064-6187, USA). Indinavir and lopinavir were dissolved in sterile distilled water and DMSO (Sigma-Aldrich Company Ltd.), respectively, at a working stock concentration of 20 mM.

Raman sample preparation

Each 1×10^6 of C33AV and E6 cells was seeded in T75 culture flasks with 20 mL of the complete medium and then incubated at 37 °C, 5% CO_2. Prior to confluence, the medium was removed and the cells were detached by trypsinisation for 3 min at 37 °C, 5% CO_2. Following this, 2×10^4 cells were seeded onto a single CaF_2 disc (Crystran Plc, Dorset, UK, 20-mm diameter×2-mm thickness) in 3 mL of the complete medium in a six-well culture dish and allowed to adhere overnight at 37 °C, 5% CO_2. Previous work [9] reported dose-dependent experiments on the HIV protease inhibitors indinavir and lopinavir to inhibit the degradation of p53 promoted by E6. Based on this study, cells were then treated with either 1 mM of indinavir, 30 μM of lopinavir, water or DMSO (as controls) and incubated for 24 h at 37 °C, 5% CO_2. The cells were subsequently fixed in ice-cold methanol for 4 min at −20 °C, then washed and stored in phosphate-buffered saline (PBS) at 4 °C until use.

Raman microspectroscopy and data analysis

Raman point spectra for the chemical maps were obtained on a Renishaw System 2000 Raman microscope (Renishaw Plc., Old Town, Wotton-under-Edge, Gloucestershire, UK), and spectra were recorded directly on single CaF_2 disc mounted cells. All cells were mounted in PBS under coverslips during the acquisition of spectra to avoid desiccation. An 830-nm NIR diode laser was used for excitation, with laser power of ~5 mW at the sample using a ×50 microscope objective, with 0.95 NA which resulted in ~0.75-μm lateral spatial resolution. At each location (or pixel), a Raman spectrum was acquired over the region from 400 to 2,000 cm^{-1}. The stage was then moved in 1-μm steps for each acquisition, with the overall result generating a 3D hypercube over the single cell of dimensions X *vs.* Y *vs.* Raman spectra (see Electronic supplementary material (ESM) Fig. S1). Spectral acquisition was performed using GRAMS WiRE software (Galactic Industries Corp., Salem, NH, USA) and data processing was carried out with Matlab 7 (The MathWorks, Inc., Natick, MA, USA). Chemical

image maps were generated against a variety of univariate metrics, including peak area and S/N ratios with the full process illustrated in Fig. 1.

Matlab was also used to perform principal components analysis (PCA) using the NIPALS (nonlinear iterative partial least squares) algorithm [13]. PCA is a multivariate technique that is used widely to reduce the dimensionality of complex spectroscopic data from many wavenumber assignments to a few principal components (PCs), which retain the majority of variance within the data [14, 15]. Upon collection, the individual spectral data cubes were concatenated to produce a single large dataset within Matlab which was subjected to PCA. The first few PCs were extracted as these explained the majority of the variance and lower ones are likely to contribute only noise. Image maps were constructed from plotting each of the PC scores individually. The data cube was reshaped (in order to plot each PC as a function of X and Y) and PC scores false colour coded to generate chemical maps; the corresponding PC loadings were plotted for the first few scores.

Subcellular fractionation of C33AE6 cells

C33AE6 cells were treated with 0.3 mM of indinavir for 24 h and detached as described in "Raman sample preparation". These were resuspended in complete medium and washed twice with PBS. Cytoplasmic and nuclear extracts were prepared by the use of the NE-PER kit (Pierce, USA) according to the manufacturer's protocols.

Western immunoblotting of sub-fractionated samples

Western immunoblotting was carried out as described in [9, 16] loading 25 μg of each extract per track. Anti-histone deacetylase (HDAC1, Cell Signalling Technology, UK) was used at 1:800 and GAPDH (Abcam, UK) at 1:1,000. Following washing, membranes were incubated with 1:2,000 of HRP-conjugated secondary antibody and visualised with ECL and Hyperfilm (GE Healthcare Life Sciences, Buckinghamshire, UK).

LC-MS analysis of cell sub-fractions

Yields of 1,055 μL of cytoplasmic and 500 μL nuclear fractions were obtained, which reflect the nucleus/cytoplasmic ratio for these cell lines. Aliquots (25 μL) of these extracts were treated with 5 volumes of cold acetone for 1 h at −20 °C, centrifuged at 14,500×*g* for 15 min and the supernatant recovered. These were then dried by speed vacuum concentration for approximately 1 h at 45 °C to reduce the samples to their original volume of ~25 μL.

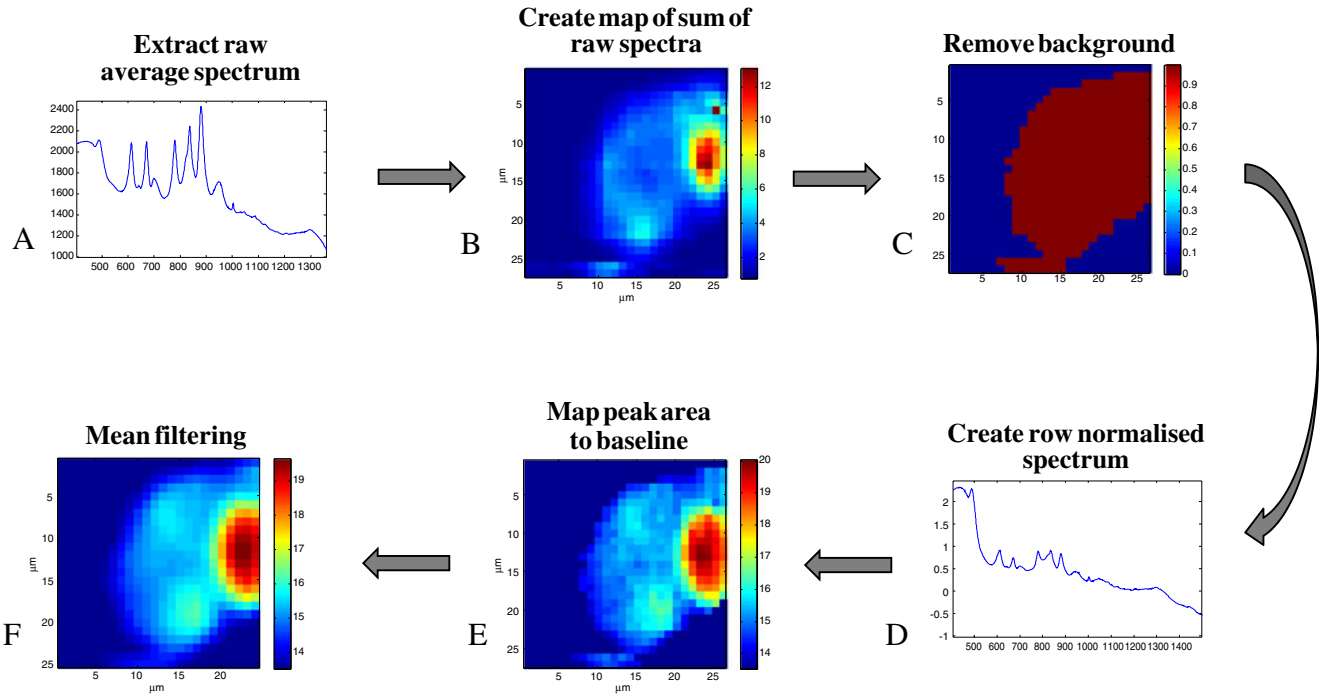

Fig. 1 Process of the generation of chemical image maps. **a** The average spectrum is plotted by the mapping function so that peaks can be selected interactively. **b** Taking the total area under the spectrum and plotting as a 2D image map allows the identification of the cell against the substrate background. **c** A simple threshold is then applied to select pixels/spectra from the map that represent the cell position. **d** The data are reanalyzed minus the background substrate spectra. **e** This can be performed through the integration of peak areas, PCA mapping or alternative algorithms. **f** The resultant image can be further smoothed by applying a 2D moving filter window

A 10-min LC methodology using 10 mM ammonium formate, pH 9, as mobile phase A and acetonitrile as mobile phase B was performed with an Acquity UPLC™ (Waters Ltd., Manchester, UK). A 2-μL sample injection was made onto a 2.1×10-mm HSS T3 (C18) Acquity column held at 45 °C; the mobile phase flow rate was 0.6 mL/min. The following gradient elution was employed (time (min), %B): (0, 2), (8, 98), (8.6, 100), (9.1, 2).

A Xevo™ QTof (Waters Ltd.) MS instrument was used in electrospray ionisation (ESI) positive ionisation mode. Prior to sample analysis, the instrument was calibrated with sodium formate following the instrument setup wizards. Sample data were acquired in MS^E mode [17, 18] with a 0.05-s scan time; the lockspray standard applied was leucine enkephalin (Leu Enk) and two points were employed for lockmass: *m/z* 556.2771 and a fragment ion from Leu Enk *m/z* 120.0813. ESI was operated using an extraction cone voltage of +3 V, a sampling cone voltage of +45 V, and the capillary voltage was set at +3 kV. The source and desolvation temperatures were 120 and 400 °C, respectively, and the cone and desolvation gas flow rates were 20 and 800 Lh^{-1}, respectively. Data were acquired over the *m/z* range 50–1,000 with six biological replicate samples to account for analytical variability.

Results

Raman analysis of C33AV control cells

A representative population of C33AV cells exposed to 1 mM of indinavir or 30 μM of lopinavir were imaged by Raman microspectroscopy. The average spectra for drug-treated and control untreated cells are shown in Fig. 2, which also shows peak centres. Cellular components such as proteins, lipids, nucleic acids and carbohydrates all contribute to this type of analysis, as illustrated in Table 1. As can be seen in Fig. 2 and Table 1, the band at 1,004 cm^{-1} originates from the aromatic ring vibration of phenylalanine and is characteristically observed in biological samples.

Chemical maps of drug-treated C33AV and untreated control cells were employed to analyse and visualise the biochemical distribution of the above intracellular components. White light images, which were used to provide information on the cell shape, and the Raman chemical image maps of cells are shown in Fig. 3. In order to enhance the detection of relevant biological information, CaF_2 substrate background removal was carried out before the image maps were generated (as illustrated in the schematic in Fig. 1). These chemical maps were generated with a spatial resolution of 1 μm from the peak area to baseline of each band within the Raman spectra acquired

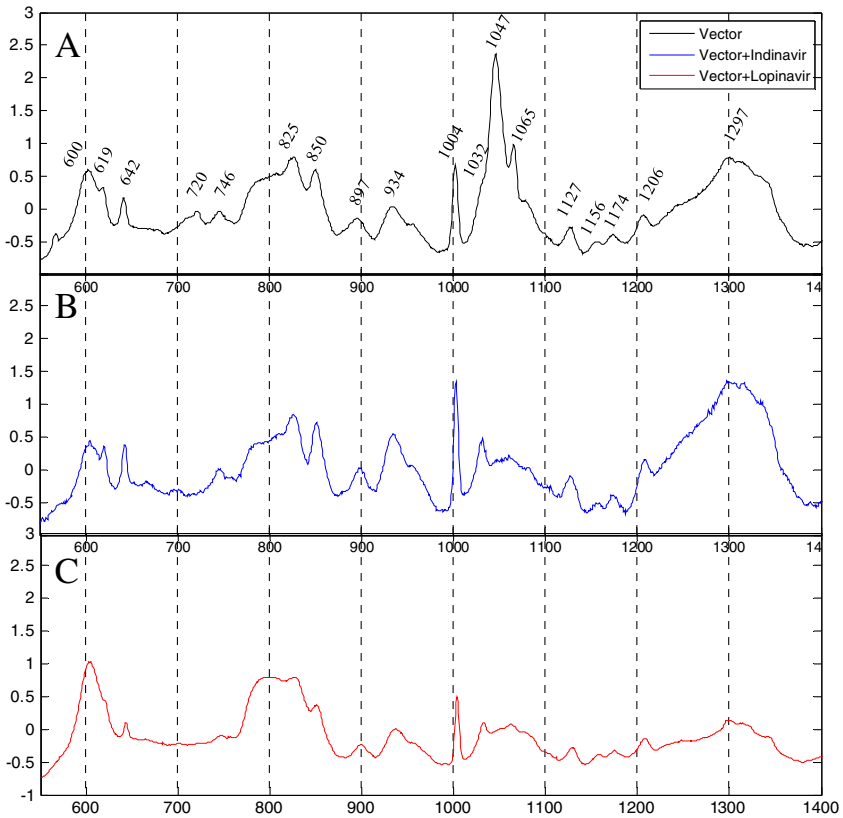

Fig. 2 Mean normalised Raman spectra from vector control cell (C33AV) (**a**) and vector cells exposed to indinavir (**b**) and lopinavir (**c**)

Table 1 Tentative Raman band assignments for the C33A cells

Wavenumber (cm^{-1})	Assignment	Raman vibrational modes
642	Tyr (643)	C–C twist
670	T, G (669)	
680	G	
712	Unidentified	
746	T	
780	C, U, T (782)	
792	C, T	n: (O–P–O) backbone
825		n: (O–P–O) backbone (828)
836	(O-P-O), Tyr (834)	n: RP; n: (O–P–O)
850		p: (C–CH) aromatic def. (852)
890		n: (O–P–O) backbone (898)
		p: (C–C) skeletal modes (898)
934		p: (C–C) backbone str. (937)
948	Deoxyribose (950)	
1003-4	Phe	(C–C) aromatic ring str.
1032	Phe	protein: (C–N) str.
1047	Carbohydrate (1049)	(C–O) str.
1063		p: (C–N) str.; l: chain (C–C) str.
1086		n: (O–P–O) backbone (1088); p: (C–C) skeletal modes (1086)
1109		n: (O–P–O) backbone (1106)
1128, 1133		p: (C–N) str.; l: chain (C–C) str. (1129)
1156		p: (C–C/C–N) str. (1158)
1172, 1174	Tyr, Phe (1175)	(C–C) str. (1172)
1206	Phe, Tyr, Amide III (1209)	
1256	Amide III(1254); C, A (1255)	
1297		(CH_2) def.
1341	A, G (1342)	p: (CH) def. (1342)

Parenthesised numbers, original Raman shifts from [33, 37, 38]

Tyr tyrosine, *Phe* phenylalanine, *A* adenine, *T* thymine, *G* guanine, *C* cytosine, *U* uracil, *RP* reverse primer, *str.* stretching, *def.* deformation, *p* protein, *l* lipid, *n* nucleotide

from the cell and surrounding area. The intense red regions indicate a higher concentration of a chemical constituent(s) relative to the low-intensity signal recorded from the CaF_2 disc substrate, which is represented by blue-coloured pixels.

Raman analysis of C33AE6 cells

The average spectra of C33AE6 and drug-exposed C33AE6 cells are shown in Fig. 4a–c. Since the expression of HPV16 E6 subverts the function of the 26S proteasome to degrade the p53 tumour suppressor and other cellular proteins [1, 3, 19, 20], it is predicted that the intracellular composition of C33AE6 cells will be different from those of the vector cells. As expected, the average spectrum obtained from untreated C33AE6-expressing cells show significant variations relating to increased and decreased peak intensities when compared to C33AV control cells (Fig. 4d). In Fig. 4a–c, several large changes were observed between the spectra of C33AE6 cells exposed to either indinavir (E6I) or lopinavir (E6L) when compared to untreated control cells. No peaks were seen at 670, 680, 746, 780 and 825 cm^{-1} in the spectrum of the C33AE6 cell, whereas the resulting spectra of these cells following the treatment with both compounds revealed marked signals at these wavenumber shifts. Interestingly, the peaks at 670, 780 and 825 cm^{-1} for E6I, and 680, 746 and 825 cm^{-1} for E6L, correspond to peaks typically ascribed to nucleic acids (Table 1). In contrast, no clear bands are observed at 1,063, 1,132 and 1,172 cm^{-1} in drug-treated C33AE6 cells, but which are very prominent in untreated C33AE6 cells. This also suggests an additional phenotypic effect as these can be attributed to the reduction in proteins, lipids and aromatic amino acids (Table 1). These spectral differences between the C33AE6 and drug-treated C33AE6 cells are

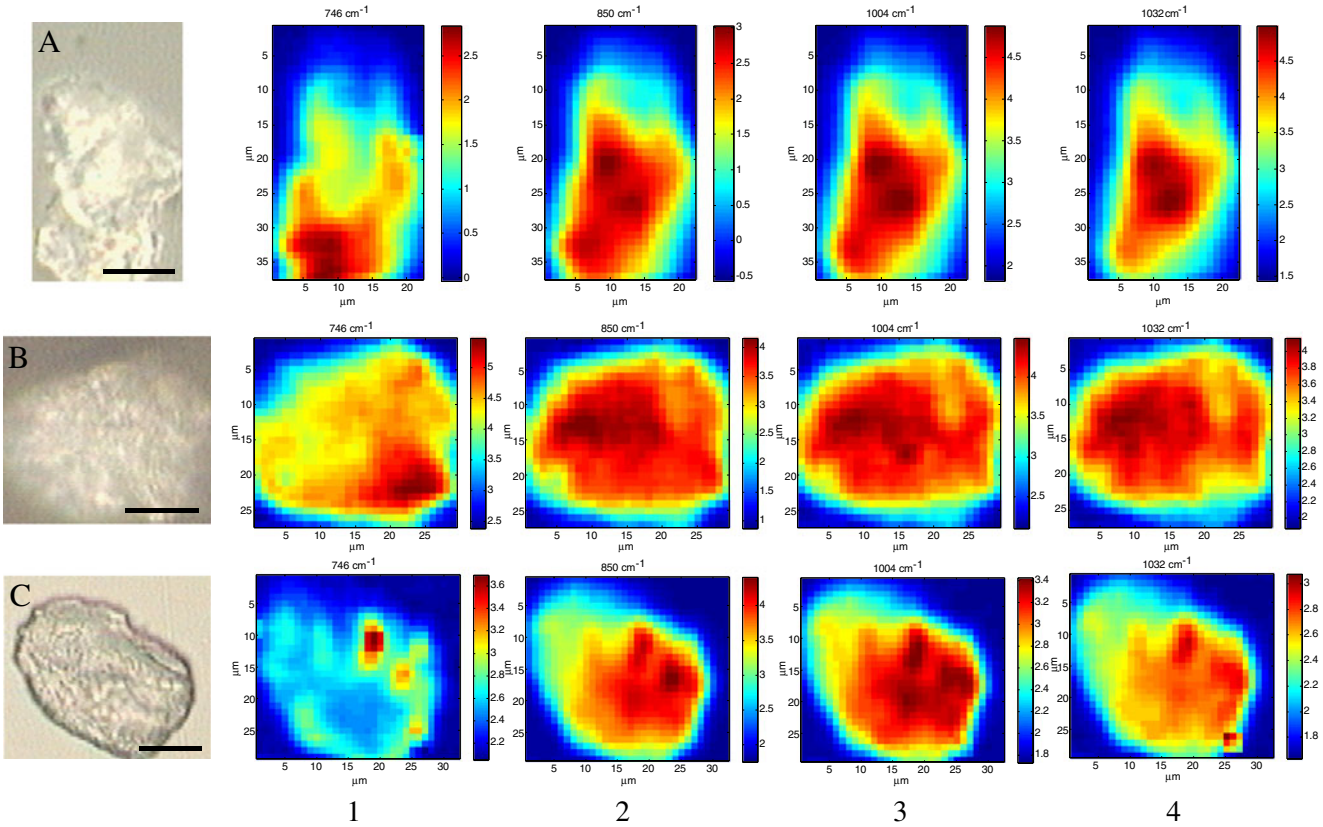

Fig. 3 White light images of C33A vector control cell (**a**), vector cell exposed to indinavir (**b**) and vector cell exposed to lopinavir (**c**). *Scale bar*, 10 μm. Raman chemical mean filtered maps of each of these cells are also shown based on the results from each band of a mean row normalised spectrum with a spatial resolution of 1 μm: *1* 746 cm^{-1} (thymine); *2* 850 cm^{-1} (protein); *3* 1,004 cm^{-1} (phenylalanine); *4* 1,032 cm^{-1} (protein). The *rainbow maps* indicate the concentration of each cellular component inside the cell, *red* showing high and *blue* showing low concentration of molecules

not from the sample matrix effects as we have recently shown that the drugs cause changes in the levels of p53 protein [9] and intracellular metabolites [10] in cultured C33AE6, but not in C33AV cells. In addition, a very interesting feature of the E6I spectra is the band at 880 cm^{-1}. By comparing the spectrum of E6I to that of the drug itself (Fig. 4e), this was deduced to be a peak originating from indinavir itself. No discernible signal was observed associated with chemical detection of lopinavir within the cells.

White light and Raman spectra chemical image maps of untreated C33AE6 and drug-treated cells were acquired using the same instrumental conditions as those applied to C33AV cells (Fig. 5). As shown previously, vibrations arising from proteins are uniformly distributed throughout both E6I (642 cm^{-1}, 5B1; 1,003 cm^{-1}, 5B4; 1,088 cm^{-1}, 5B5) and E6L (1,003 cm^{-1}, 5 C4; 642 cm^{-1}, 5 C1; 850 cm^{-1}, 5B3). The chemical image maps of the drug-exposed C33AE6 cells show very interesting features in terms of the spatial distribution of nucleic acids. Unlike C33AV (Fig. 3) and untreated C33AE6 cells (Fig. 5a), there are clear localisations from 780 cm^{-1} for E6I to 747 cm^{-1} for E6L, as shown in 2 of Fig. 5b, c, respectively. Also, the maps from 670 to 825 cm^{-1} for E6I and 680 cm^{-1} for E6L show the same distinct localisations as 780 and 747 cm^{-1}, respectively (data not shown). Interestingly, all these wavenumbers which have distinct distributions are assigned to nucleic acids (Table 1).

LC-MS analysis of subcellular localisation of drug

LC-MS is a commonly used analytical approach within the metabolomics field [21] and was applied here to quantify the level of indinavir within nuclear and cytoplasmic extracts from indinavir-treated C33AE6 cells. Immunoprobing Western blots of these extracts with GAPDH and HDAC1 antibodies demonstrated minimal nuclear/cytoplasm cross-contamination (Fig. 6). Six biological replicates were analysed in triplicate by LC-MS for both nuclear and cytoplasmic extracts (Table 2). White light microscopy was used to determine the average relative volume of the cytoplasm *vs.* nucleus of indinavir-treated C33AE6 cells and was calculated as 11.6.

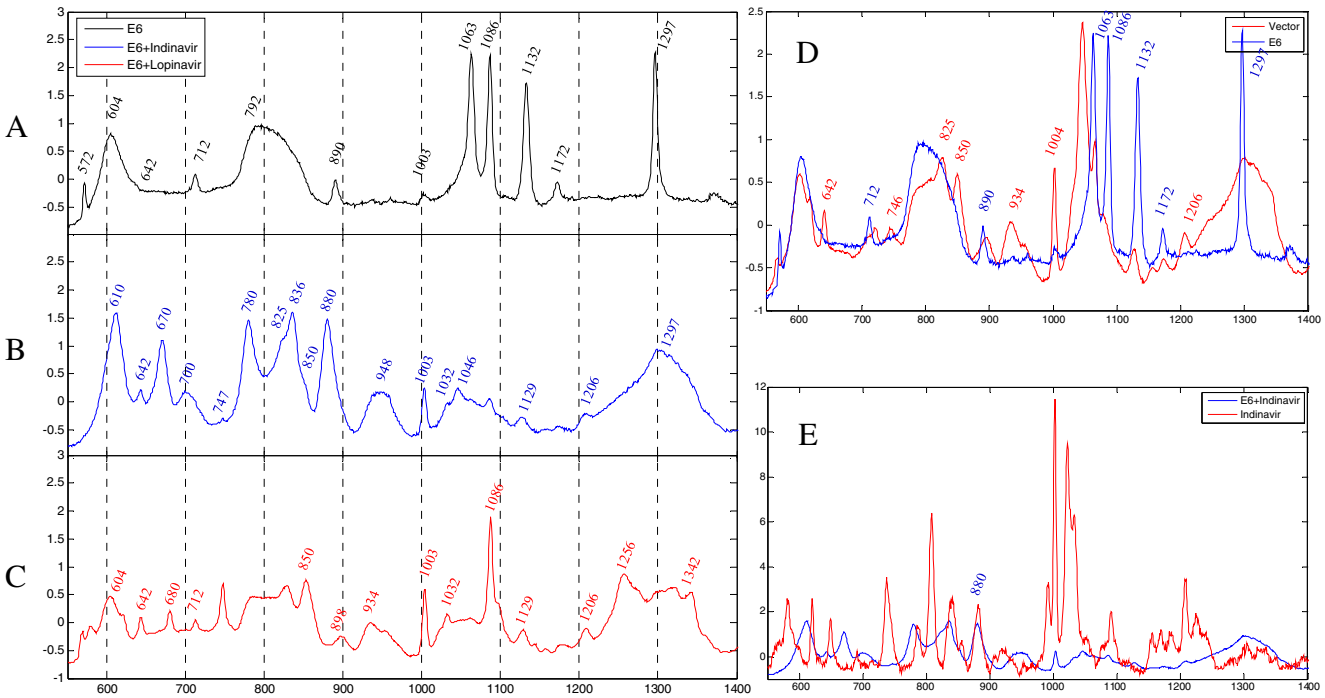

Fig. 4 Mean normalised spectra from C33AE6 cell (**a**) and E6 cells exposed to indinavir (**b**) and lopinavir (**c**). **d** Comparison of average Raman spectrum from E6 cell with that from vector control cell. **e** Comparison of average Raman spectra from indinavir exposed E6 cell with that from indinavir itself

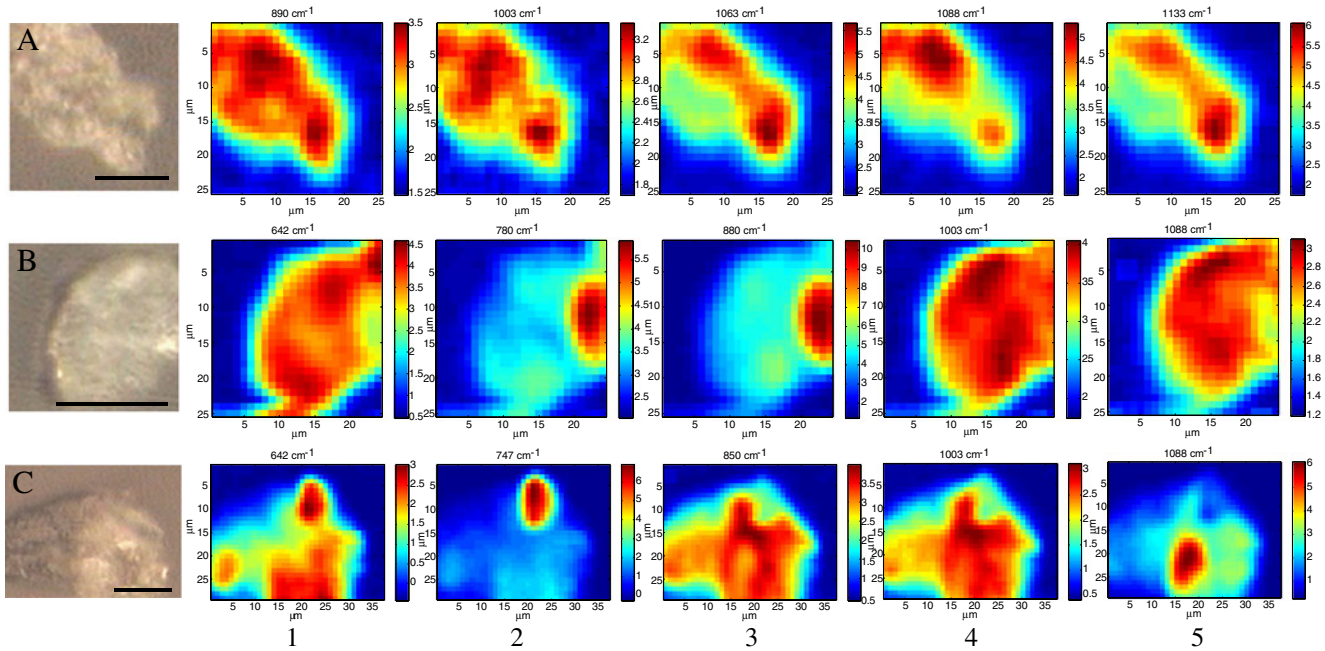

Fig. 5 White images of C33A E6 cell (**a**), E6 cell exposed to indinavir (**b**) and E6 cell exposed to lopinavir (**c**). *Scale bar*, 10 μm. Raman chemical mean filtered maps of each of these cells are also shown based on the results from each band of a mean row normalised spectrum with a spatial resolution of 1 μm. **a** *1* 890 cm^{-1} (nucleotide); *2* 1,003 cm^{-1} (phenylalanine); *3* 1,063 cm^{-1} (protein); *4* 1,088 cm^{-1} (nucleotide, protein); *5* 1,133 cm^{-1} (protein, lipid). **b** *1* 642 cm^{-1} (tyrosine); *2* 780 cm^{-1} (nucleotide); *3* 880 cm^{-1}; *4* 1,003 cm^{-1}; *5* 1,088 cm^{-1}. **c** *1* 642 cm^{-1}; *2* 747 cm^{-1} (nucleotide); *3* 850 cm^{-1} (protein); *4* 1,003 cm^{-1}; *5* 1,086 cm^{-1}. The *rainbow maps* indicate the concentration of each cellular component inside the cell, *red* showing high and *blue* showing low concentration of molecules

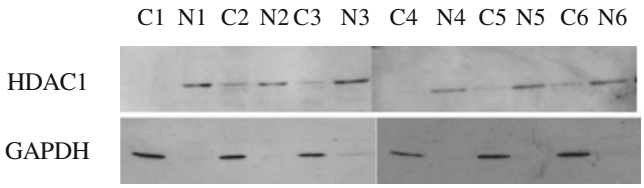

Fig. 6 Western blot of sub-fractionated samples from C33A E6-transfected cells exposed to indinavir and immunoprobed with a HDAC1 (nuclear marker) and GAPDH loading control antibodies. Sub-fractionation of drug-treated C33AE6 cells was carried out successfully with only minimal cross-contamination. *C* cytoplasm, *N* nuclear, *1–6* biological replicates

Discussion

Based on our previous studies of the effects of HIV PIs on the survival and metabolism of cultured cervical carcinoma cells [9, 10], we initially analysed the Raman spectra of HPV-negative C33A cells exposed to these drugs.

Raman spectroscopy is an optical approach in which a laser is used to irradiate a sample. Molecules within the sample vibrate, and this results in a change in energy of the light that can be measured and displayed as a Raman spectrum. This spectrum relates directly to the chemical composition of the sample [22].

The chemical mapping approach of Raman microspectroscopy involves coupling an optical microscope with a Raman spectrometer, and it is a powerful tool for analysing the chemical distribution of metabolites present at any point and the response of metabolic and physical stresses in cells or tissues [23]. Subtle changes in chemical composition and distribution on cells or tissues can be monitored using this Raman spectroscopic approach. This chemical mapping technique not only enables visualisation of spatially resolved chemical information but can also be used to detect small chemical changes in order to understand abiotic perturbations to biological systems. Thus, Raman spectroscopy has emerged as a promising diagnostic tool for disease detection in the biomedical field. Various diseases have been detected by comparing the differences of Raman spectra between normal and diseased cells or tissues because disease progression results in changes of the composition and abundance of metabolites [24–27]. The biomedical application of spectroscopy for cancer detection and disease diagnosis has been thoroughly reviewed in [22, 28, 29]. Finally, in order to develop effective chemotherapeutic agents and assess combinations of various drugs against serious diseases, the response to chemotherapy and the distribution of drugs inside cells or tissues have also been investigated [30, 31].

As can be seen in Fig. 2a–c, the differences between the spectra of drug-treated and control untreated C33AV cells are very subtle, apart from a large 1,047 cm^{-1} carbohydrate signal (see Table 1) which was reduced after incubation with either of the compounds. Although C33AV cells treated with lopinavir do not proliferate [9], the spectral differences from the level changes in intracellular components such as lipid, protein, DNA and RNA caused by proliferation are very subtle [32]. Therefore, the spectral changes between drug-challenged and non-drug-challenged control C33AV cells were not observed by visual analysis of vibrational bands in the Raman spectra.

Using these Raman spectral assignments, we next employed chemical mapping of drug-treated and control untreated C33AV cells in order to analyse intracellular distribution of internal components within the cells (Fig. 3). It is well known that biological molecules are not homogeneously distributed inside cells with localised and specific activities being related to their spatial distribution [33]. Raman chemical maps obtained from the average spectra of untreated and drug-treated C33AV cells show that the concentrations of different molecules show subcellular variation. Single cell image maps of proteins at 850, 1,004 and 1,032 cm^{-1} show a uniform distribution throughout the whole cell, whereas, as expected, the 746 cm^{-1} nucleic acid signal shows a more concentrated intracellular localisation that is consistent with specific nuclear compartmentalisation. Curiously, no Raman spectral bands that could be directly attributed to either of the drug compounds were observed in C33AV cells.

Following on from this, we investigated whether the expression of the E6 protein caused any discernible effects on the Raman spectral analysis. It is well known that E6, in association with E6AP, can facilitate the proteasomal destruction of numerous proteins, such as p53, that are detrimental to viral persistence [19]. Yet it is also known that the levels of other cellular proteins are increased by indirect effects of E6 and other viral proteins in HPV-infected cells [34, 35]. What is clear is that infection with

Table 2 Biological replicates of indinavir-treated C33E6 cells analysed in triplicate by LC-MS for both nuclear and cytoplasmic extracts

Fraction[a]	Cytoplasm abundance[b]	Nucleus abundance	Nucleus: cytoplasm
1	19.2	149.9	7.8
2	19.7	204.6	10.4
3	20.8	191.8	9.2
4	18.4	156.8	8.5
5	24.7	126.6	5.1
6	27.0	171.7	6.3
Mean			7.9

[a] Each fraction was analysed in triplicate (2 μL injected into LC-MS) and means are shown

[b] Abundance is the extracted ion chromatogram for the identified indinavir peak following scaling factors due to extraction volume differences and cytoplasm-to-nucleus volume

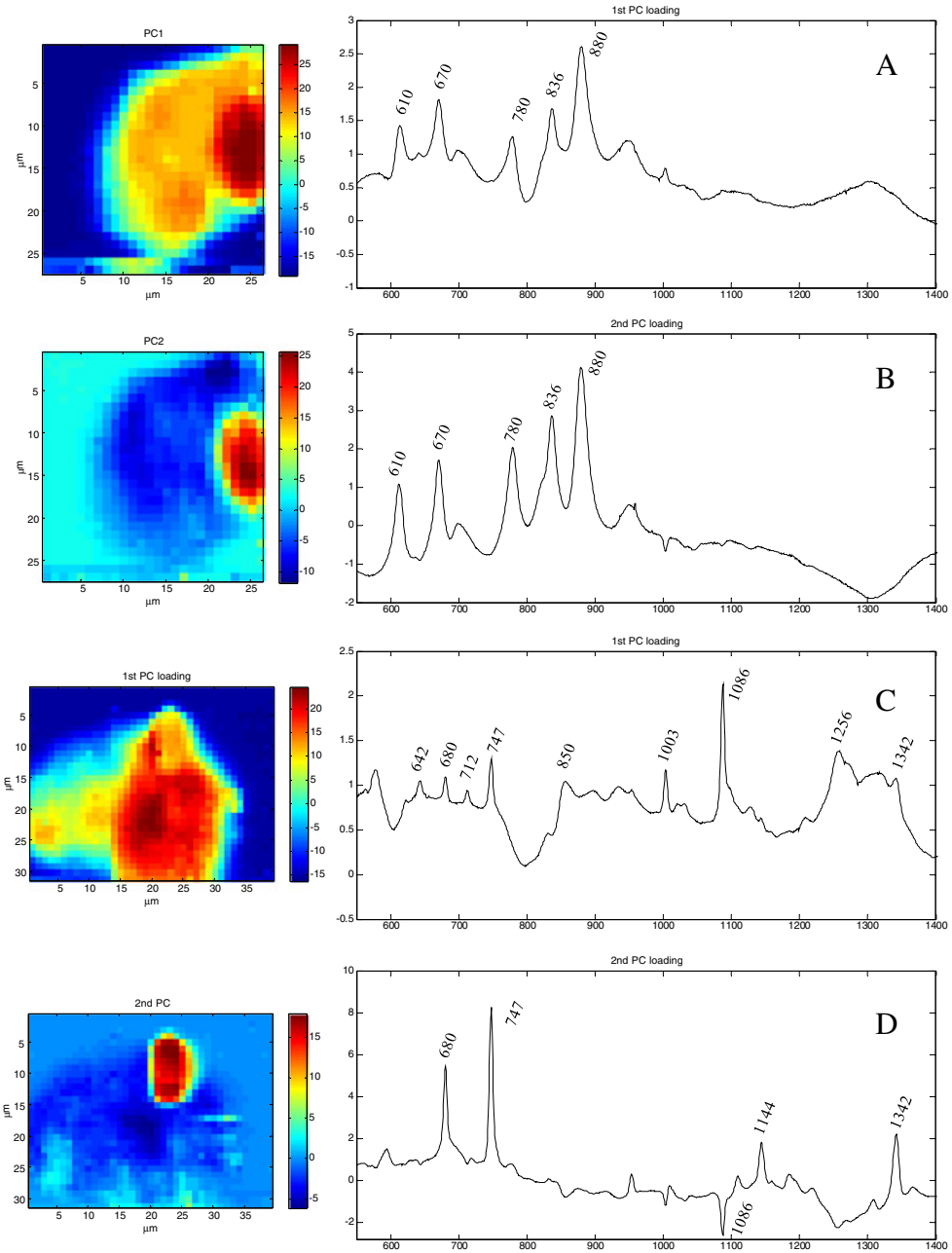

Fig. 7 PCA chemical maps constructed from PC scores with the corresponding loadings plots. E6-transfected cell exposed to indinavir showing PC1 (78.5%) (**a**) and PC2 (14.4%) (**b**) and E6-transfected cell exposed to lopinavir showing PC1 (85.6%) (**c**) and PC2 (6.5%) (**d**)

high-risk HPV produces multifactorial effects generally aimed at targeting and perturbing the function of a variety of cellular "hub" proteins. Thus, the spectral comparison of C33AV and E6 cells shown in Fig. 4d represents a snapshot of some of these effects which reflect the changes in the levels of cellular components. Indeed it is noteworthy that we have previously shown the biological properties of these two cell types to be very different. For example, xenografted experimental tumours derived from C33AE6 cells are highly resistant to radiotherapy when compared to tumours derived from C33AV cells [12], and more recently, we have used the complementary vibration technique of FT-IR spectroscopy to elucidate gross phenotypic differences between control C33A cells and those expressing E6 [10].

If lopinavir or indinavir can specifically target the biological effects of E6, we hypothesised that treatment of C33AE6 cells with these compounds may induce associated alterations in the Raman spectra. Indeed, we found large variations in the spectra between untreated and drug-treated C33AE6 cells (Fig. 4) which corresponded to peaks arising from nucleic acids and other components such as proteins, lipids and aromatic amino acids. With regard to the function of E6, it could be speculated that these drugs might increase

the level of specific types of nucleic acids in cells, and it is intended to continue work on this effect by the use of metabolic profiling [36].

To determine whether there was any difference between drug-treated and untreated C33AE6 cells in terms of the biochemical distribution of intracellular components, Raman chemical maps of these cells were generated. As can be seen in Fig. 5, although proteins are uniformly distributed within both untreated and drug-treated E6 cells, distinct localisation of nucleic acids was observed in drug-treated C33AE6 cell. Based upon the comparison of the spatial co-localisation of nucleic acids with that of the prospective indinavir signal at 880 cm^{-1}, it is possible that the metabolic activity of this drug against E6 may occur in the nucleus.

In order to investigate this hypothesis further, PCA of drug-exposed (E6I and E6L) cells was conducted. PCA provides the most compact representation of all the variations within the multivariate datasets by visualising and mining information from an XY data matrix containing the large number of Raman-detected variables (in the *Z*-axis in this spectral hypercube). Thus, in order to investigate which spatial region is the most variable and which spectral band is related to the area, PCA was carried out as described above. PCA chemical maps and their loadings plots are shown in Fig. 7. The maps and loadings plots from the PCA allow for the selection of significant variables associated with the drug activities from the spectrum of each cell. For C33AE6 cell exposed to indinavir, 78.5% of the total explained variance was recovered in the first PC and 14.4% in the second PC, whilst for C33AE6 cell exposed to lopinavir, PC1 accounted for 85.6% and PC2 6.5%. For these indinavir and lopinavir exposures, the total for the first two PCs was 92.9% and 92.1%, respectively, which highlights the efficient dimensionality reduction that PCA has achieved. On the basis of chemical image maps and loadings plots from PC1 to PC2 (representing the largest and second largest variations, respectively), many of the important variations occurring in E6I cells are found to be associated with peaks at 670, 780 and 836 cm^{-1} corresponding to nucleic acids (Fig. 7a, b). Furthermore, the large variation of the band at 880 cm^{-1} indicates that the drug location is related to changes in the levels of nucleic acids which may occur in the nucleus. For both E6I and E6L, it was found that the largest variations (PC1) were derived from nucleic acids, although a large contribution was also made by proteins. The second largest variations (PC2) mostly occurred at the position corresponding to peaks arising from the following nucleic acid signals: 680, 747 and 1,432 cm^{-1} (Fig. 7c, d).

In order to support the hypothesis that indinavir localises to the nucleus, we evaluated its levels in drug-treated sub-fractionated C33AE6 cells by the use of LC-MS. After taking into account the difference between the volume of the cytoplasm compared to the nucleus, LC-MS indicated that the concentration of indinavir was approximately eight-fold greater in the nucleus than in the cytoplasm of these cells (Table 2). Clearly, this orthogonal analytical technique definitively confirms the findings from Raman chemical mapping that indinavir is being localised to the nucleus of E6-expressing cells, and this is presumably the site of action for this antiviral drug.

Conclusions

We have used Raman chemical image mapping to compare the distribution of intracellular components within human C33A cervical cancer cells and the same cells expressing the HPV16 E6 oncoprotein. Significant variations were observed between the spectra of these two cell types, which indicates that the expression of E6 induces gross phenotypic changes which are consistent with our previous FT-IR spectroscopy-based study [10]. Finally, we also have unequivocal evidence that the HIV antiviral drug indinavir is specifically targeted to the nucleus of HPV16 E6-expressing cervical carcinoma cells. This unexpected finding will facilitate the analysis of potential drug targets for this prospective novel use of this class of compound.

Acknowledgements This research was funded by an ORS award to D-H.K. R.M.J. is very thankful to the UK BBSRC for funding. J.W. A., E.M.-E. and R.G. are grateful to the EU-funded project, Metabolomics for Plants Health and OutReach (META-PHOR: FOOD-CT-2006-036220), for financial support. R.G. is grateful to both the UK BBSRC and EPSRC for financial support of the MCISB. The authors also acknowledge the support of the Humane Research Trust, the Caring Cancer Research Trust and Cancer Research UK.

Disclosure statement The authors have no conflict of interest

References

1. zur Hausen H (1996) Papillomavirus infections—a major cause of human cancers. Biochim Biophys Acta 1288:55–78
2. de Villiers EM (1989) Heterogeneity of the human papillomavirus group. J Virol 63:4898
3. Scheffner M, Werness BA, Huibregtse JM, Levine AJ, Howley PM (1990) The e6 oncoprotein encoded by human papillomavirus types 16 and 18 promotes the degradation of p53. Cell 63:1129–1136
4. Harper DM, Franco EL, Wheeler C, Ferris DG, Jenkins D, Schuind A, Zahaf T, Innis B, Naud P, De Carvalho NS, Roteli-Martins CM, Teixeira J, Blatter MM, Korn AP, Quint W, Dubin G (2004) Efficacy of a bivalent l1 virus-like particle vaccine in prevention of infection with human papillomavirus types 16 and 18 in young women: a randomised controlled trial. Lancet 346:1757–1765
5. Munoz N, Bosch FX, de Sanjose S, Herrero R, Castellsague X, Shah KV, Snijders PJF, Meijer CJLM (2003) Epidemiologic

classification of human papillomavirus types associated with cervical cancer. N Engl J Med 348:518–527
6. Villa LL, Costa RLR, Petta CA, Andrade RP, Ault KA, Giuliano AR, Wheeler CM, Koutsky LA, Malm C, Lehtinen M, Skjeldestad FE, Olsson SE, Steinwall M, Brown DR, Kurman RJ, Ronnett RM, Stoler MH, Ferenczy A, Harper DM, Tamms GM, Yu J, Lupinacci L, Railkar R, Taddeo FJ, Jansen KU, Essser MT, Sings HL, Saah AJ, Barr E (2005) Prophylactic quadrivalent human papillomavirus (types 6, 11, 16, and 18) l1 virus-like particle vaccine in young women: a randomised double-blind placebo-controlled multicentre phase II efficacy trial. Lancet Oncol 6:271–278
7. Kyrgiou M, Koliopoulos G, Martin-Hirsch P, Arbyn M, Prendiville W, Paraskevaidis E (2006) Obstetric outcomes after conservative treatment for intraepithelial or early invasive cervical lesions: systematic review and meta-analysis. Lancet 367:489–498
8. zur Hausen H (2000) Papillomaviruses causing cancer: evasion from host-cell control in early events in carcinogenesis. J Natl Cancer Inst 92:690–698
9. Hampson L, Kitchener HC, Hampson IN (2006) Specific HIV protease inhibitors inhibit the ability of hpv16 e6 to degrade p53 and selectively kill e6-dependent cervical carcinoma cells in vitro. Antivir Ther 11:813–825
10. Kim D-H, Jarvis RM, Xu Y, Oliver AW, Allwood JW, Hampson L, Hampson IN, Goodacre R (2010) Combining metabolic fingerprinting and footprinting to understand the phenotypic response of hpv16 e6 expressing cervical carcinoma cells exposed to the hiv anti-viral drug lopinavir. Analyst 135:1235–1244
11. Chow WA, Jiang C, Guan M (2009) Anti-HIV drugs for cancer therapeutics: back to the future? Lancet Oncol 10:61–71
12. Hampson L, El Hady E, Moore JV, Kitchener H, Hampson IN (2001) The HPV16 e6 and e7 proteins and the radiation resistance of cervical carcinoma. FASEB J 15:1445–1447
13. Wold H (1966) Multivariate analysis. Academic, New York
14. Jolliffe IT (1986) Principal component analysis. Springer, New York
15. Sumner LW, Mendes P, Dixon RA (2003) Plant metabolomics: large-scale phytochemistry in the functional genomics era. Phytochemistry 62:817–836
16. Laemmli UK (1986) Cleavage of structural proteins during the assembly of the head of bacteriophage T4. Nature 227:680–685
17. Wrona M, Mauriala T, Bateman KP, Mortishire Smith RJ, O'Connor D (2005) All-in-one analysis for metabolite identification using liquid chromatography/hybrid quadrupole time-of-flight mass spectrometry with collision energy switching. Rapid Commun Mass Spectrom 19:2597–2602
18. Bateman KP, Castro-Perez J, Wrona M, Shockcor JP, Yu K, Oballa R, Nicoll-Griffith DA (2007) Ms^e with mass defect filtering for in vitro and in vivo metabolite identification. Rapid Commun Mass Spectrom 2:1485–1496
19. Banks L, Pim D, Thomas M (2003) Viruses and the 26S proteasome: hacking into destruction. Trends Biochem Sci 28:452–459
20. Mantovani F, Banks L (1999) The interaction between p53 and papillomaviruses. Semin Cancer Biol 9:387–395
21. Allwood JW, Goodacre R (2010) An introduction to liquid chromatography–mass spectrometry instrumentation applied in plant metabolomic analyses. Phytochem Anal 21:33–47
22. Ellis DI, Goodacre R (2006) Metabolic fingerprinting in disease diagnosis: biomedical applications of infrared and Raman spectroscopy. Analyst 131:875–885
23. Clark D, Sasic S (2006) Chemical images: technical approaches and issues. CytometryA 69a:815–824
24. Buschman HP, Deinum G, Morz JT, Fizmaurice M, Kramer JR, van der Laarse A, Bruschke AV, Feld MS (2001) Raman microspectroscopy of human coronary atherosclerosis: biochemical assessment of cellular and extracellular morphologic structures in situ. Cardiovasc Pathol 10:69–82
25. Harris AT, Lungari A, Needham CJ, Smith SL, Lones MA, Fisher SE, Yang XB, Cooper N, Kirkham J, Smith DA, Martin-Hirsch DP, High AS (2009) Potential for Raman spectroscopy to provide cancer screening using a peripheral blood sample. Head Neck Oncol 1:34–41
26. Hawi SR, Campbell WB, Balla AK, Murphy R (1996) Characterization of normal and malignant human hepatocytes by Raman microspectroscopy. Cancer Lett 110:35–40
27. Shafer-Peltier KE, Haka AS, Fitzmaurice M, Crowe J, Myles J, Dasari RR, Feld MS (2002) Raman microspectroscopic model of human breast tissue: implications for breast cancer diagnosis in vivo. J Raman Spectrosc 33:552–563
28. Ellis EI, Dunn WB, Griffin JL, Allwood JW, Goodacre R (2007) Metabolic fingerprinting as a diagnostic tool. Pharmacogenomics 8:1243–1266
29. Mahadevan-Jansen A, Richards-Kortum R (1997) Raman spectroscopy for cancer detection: a review. Conf Proc IEEE Eng Med Biol Soc 6:2722–2728
30. Beljebbar A, Sockalingum GD, Morjani H, Manfait M (1999) Raman and sers microspectroscopy on living cells: a promising tool towards cellular-drug response and medical diagnosis. Proc SPIE 3608:175–184
31. Kang E, Wang H, Kwon IK, Robinson J, Park K, Cheng JX (2006) In situ visualization of paclitaxel distribution and release by coherent anti-stokes Raman scattering microscopy. Anal Chem 78:8036–8043
32. Short KW, Carpenter S, Freyer JP, Mourant JR (2005) Raman spectroscopy detects biochemical changes due to proliferation in mammalian cell cutures. Biophys J 88:4274–4288
33. Uzunbajakava N, Lenferink A, Kraan Y, Willekens B, Vrensen G, Greve J, Otto C (2003) Nonresonant raman imaging of protein distribution in single human cells. Biopolymers 72:1–9
34. Wan F, Miao X, Quraishi I, Kennedy V, Creek KE, Pirisi L (2008) Gene expression changes during HPV-mediated carcinogenesis: a comparison between an in vitro cell model and cervical cancer. Int J Cancer 123:32–40
35. Martin CM, Astbury K, McEvoy L, O'Toole S, Sheils O, O'Leary JJ (2009) Gene expression profiling in cervical cancer: identification of novel markers for disease diagnosis and therapy. Meth Mol Biol 511:333–359
36. Goodacre R, Vaidyanathan S, Dunn WB, Harrigan GG, Kell DB (2004) Metabolomics by numbers: acquiring and understanding global metabolite data. Trends Biotechnol 22:245–252
37. Faolain EO, Hunter MB, Byrne JM, Kelehan P, Byrne HJ, Lyng FM (2005) The potential of vibrational spectroscopy in the early detection of cervical cancer: an exciting emerging field. Proc SPIE 5826:25–36
38. Notingher IN, Verrier S, Haque S, Polak JM, Hench LL (2003) Spectroscopic study of human lung epithelial cells (a549) in culture: living cells versus dead cells. Biopolymers 72:230–240